1127-3

146

RADIO ENGINEERING and ELECTRONIC PHYSICS

English Edition of

РАДИОТЕХНИКА И ЭЛЕКТРОНИКА

Published by the American Institute of Electrical Engineers
with the aid of a grant from the National Science Foundation

No.7 July 1961

Translated and Produced by Royer and Roger, Inc.

AMERICAN INSTITUTE OF ELECTRICAL ENGINEERS

Established 1884

345 East Forty-Seventh Street
New York 17, N. Y.

Warren H. Chase, President
N.S. Hibshman, Executive Secretary
C.E. Dean, Technical Vice President, Communications
W.F. Denkhaus, Director of Publications
L.G. Abraham, Chairman, Communications Division

The English edition of RADIO ENGINEERING AND ELECTRONIC PHYSICS is published by the American Institute of Electrical Engineers with the aid of a grant from the National Science Foundation. 1961 by American Institute of Electrical Engineers. Also published under the same arrangement are the Russian electronic journals RADIO ENGINEERING and TELECOMMUNICATIONS.

RADIO ENGINEERING AND ELECTRONIC PHYSICS

(РАДИОТЕХНИКА И ЭЛЕКТРОНИКА)

Publication of the Institute of Radio Engineering and Electronic Physics,
Academy of Sciences of the USSR

Translated and Produced
by
Royer and Roger, Inc.

Translation Editor: Leonard S. Schwartz

AIEE REVIEW COMMITTEE FOR RADIO ENGINEERING AND ELECTRONIC PHYSICS
Leonard S. Schwartz
New York University College of Engineering
Chairman

A.W. Bickley
W.P. Birkemeier
T.T.W. Bucher
J.L. Callahan
G.R. Cooper
W.A. Depp
R.S. Enticknap
A. Burr Fontaine
F.E. Froelich
Paul H. Gleichauf
G.S. Glinski
Bernard Harris
R.K. Hellmann
D.E. Higginbotham
B.A. Lengyel
W. Miller
Harry Rowe Mimno
W.W. Peterson
B. Reiffen
W.G. Schmidt
Herbert Sherman
D.L. Solomon
C.A. Stutt
G.C. Sziklai
Joseph Vogelman
G.M. White
F.B. Wood
H.L. Yudkin

Subscriptions to Radio Engineering and Electronic Physics should be sent to AIEE
Special Subscription Department
41 East 28th Street, New York 16, New York

1961 Subscription rates:

	$	£
Individuals	28.50	10
Libraries, institutes, govt. agencies	57.00	20

12 issues per annum comprising approximately 1900 pages

PROBLEMS IN THE STATISTICS OF AUTOMATIC PATTERN RECOGNITION BY MULTIFRAME SCANNING

A. E. Basharinov

The statistical indices of automatic pattern recognition equipment used in multiframe scanning are examined. Relations for the calculation of computer memory capacity of the electronic computer are derived in the stationary state for algorithms of random duration. It is noted that the memory capacity may be reduced by using selection precedures with two thresholds.

1. The principles of construction of apparatus for automatic pattern recognition are treated in [1] and [2].

In the system with a finite number of cells, the pattern to be recognized represents a given state of a group of cells (in binary quantization each cell has two states).

To be definite we will consider the case of a two-dimensional cell.

Limitation of the memory storage capacity does not as a rule permit us to realize a parallel treatment of data for all cells and therefore, a consecutive method is used, in which the cells are alternately commuted during the frame time, and only cells with a "nonzero" state are sampled.

Wax [3] considered the pattern as a track of recognition distorted by noise. When the patterns are distorted by noise, high fidelity reproduction may, nonetheless, be obtained by the simultaneous acquisition of data from several frames. The methods of data comparison depend on the properties of the pattern and, in particular, on the stability of the picture in time. In the simplest case the pattern consists of "individual" points, the position of which remains stable during observation (the zeroth order pattern).

The case of a linear shift of the dots over an interval of several frames of the pattern is described by an equation of the first order. In the more general case, when the pattern can be described by an n-th order equation, one may speak of an n-th order pattern.

2. The apparatus for pattern recognition selects signal impulses in a background of noise pulses which arise at the output of the switching system scanning the cells frame by frame.

Selection of the signal sequence is made by a comparison of the data for several frames with a logical selection according to an assumed criterion. The selection process can be represented as consisting of waiting times relative to the processing of data connected with the appearance of separate patterns (real or false). The duration of the waiting time is a random variable with a distribution law depending only on the chosen selection algorithm*.

The selection algorithms may differ in the character of the dependence of the number of memory cells on the duration of the waiting time, as an algorithm with a fixed memory load during the waiting time and as an algorithm with an increasing memory load during the waiting time.

3. Let us consider the loading characteristics of the memory capacity for the selection of algorithms, which use a fixed number of memory cells in the course of the waiting time.

---

* In contrast with cases characterizing the technique of mass servicing, the distribution function of the duration of waiting time has a nonexponential character.

The number of cells n occupied at an arbitrary moment is a random variable defined by the relation*

$$N(n)=\sum_{s=s_0}^{n}\sum_{k=0}^{\nu_s}\varepsilon_k(n,s) \tag{1}$$

where ϵ_k (n, s) is a random variable equal to zero or unity depending on the load state in the n-th frame, occupied for the first time in the s-th frame (the moments of time are considered discretely); ν_s is a random variable designating the number of pulses in a frame.

The average value of the number of occupied cells is determined from Eq. (1):

$$\overline{N(n)}=\sum_{s=s_0}^{n}\overline{\left[\sum_{k=0}^{\nu_s}\varepsilon_k(n,s)\right]}. \tag{2}$$

Using the Wald theorem concerning the average value of the sum of random variables in the case of a random number of summands [8], we obtain

$$\overline{\sum_{k=0}^{\nu_s}\varepsilon_k(n,s)}=\bar{\nu}_s\,\overline{\varepsilon_k(n,s)}, \tag{3}$$

$$\overline{\varepsilon_k(n,s)}=1-F(n-s), \tag{4}$$

where F(n-s) represents a distribution function of the duration of test.

The limiting value of the magnitude $\overline{N(n)}$ when $S_0 \to \infty$ denotes the average memory capacity load in the stationary regime:

$$\lim_{s_0\to-\infty}\overline{N(n)}=\sum_{s=-\infty}^{n}\bar{\nu}_s\,[1-F(n-s)]=\sum_{l=0}^{\infty}\bar{\nu}_l\,[1-F(l)]. \tag{5}$$

In the case of stationary flow

$$\bar{\nu}_l=\text{const}.$$

Changing to continuous time, we obtain

$$\bar{\nu}_l\sum_{l=0}^{\infty}[1-F(l)]\to\frac{\bar{\nu}_l}{\Delta t}\int_0^{\infty}[1-F(t)]\,dt, \tag{6}$$

i.e., in the stationary regime

$$\bar{N}=\bar{\varkappa}\,\bar{t}, \tag{7}$$

where $\bar{\varkappa}=\bar{\nu}_l/\Delta t$ is the average input flow density; $\bar{t}$ is the average duration of the test.

Let us consider the memory capacity due to the noise input flow**.

In this case ν_l = mp_n and $\bar{N}$ = $mp_n\bar{n}$; thus, the average number of memory cells occupied in the steady-state regime is determined by the product of the average noise flow density and the average duration of the waiting time (in the case of an arbitrary law of distribution of durations)***.

4. The magnitude of the variance of the memory load capacity the gate probability can be determined on the basis of relations obtained in the theory of mass servicing. Let us substitute for the flow, arising in the circuit under consideration at the output of the commuting device, a Poisson flow with an equivalent average number of pulses per unit time.

Khinchin [4] showed that with an infinite memory storage capacity in the case of a Poisson input flow for an arbitrary distribution law of duration of processing, the probability of loading k cells in the steady-state regime is determined by Poisson's law:

---

* It is assumed that the absence of marks in all the elements is an unlikely occurrence.

** The input flow is characterized by the probability of the appearance of noise pulses P_m and signal pulses P_{sig}.

*** The results of a calculation of the memory load capacity by the method of finite difference equations, given in [3] agree satisfactorily with calculations in accordance with (7) (see [9], [10]).

$$p_k = \frac{(\overline{\nu}\,\overline{n})^k}{k!} e^{-(\overline{\nu}\,\overline{n})}. \tag{8}$$

The average number of occupied cells equals the variance

$$\overline{N} = \sigma_N^2 = \overline{\nu}\,\overline{n}. \tag{9}$$

When calculating the load memory capacity of a limited size (number of cells equals M) one may use the Sevast'yanov [5] theorem, which tells us that in the case of a Poisson flow and an arbitrary distributionlaw for the duration of processing, k cells is determined by the Erlang formula

$$p_k = \frac{\dfrac{(\overline{\nu}\,\overline{n})^k}{k!}}{\sum\limits_{s=1}^{M} \dfrac{(\overline{\nu}\overline{n})^s}{s!}}. \tag{10}$$

When $(\nu\overline{n}) \gg 1$, which is the case, as a rule*, Eq. (10) can be approximately presented in the form

$$p_k \simeq \frac{e^{-\frac{1}{2}\left(\frac{k}{\sqrt{\overline{\nu}\,\overline{n}}} - \sqrt{\overline{\nu}\,\overline{n}}\right)^2}}{\int\limits_{\sqrt{-\overline{\nu}\,\overline{n}}}^{\frac{M}{\sqrt{\overline{\nu}\,\overline{n}}} - \sqrt{\overline{\nu}\,\overline{n}}} e^{-\frac{x^2}{2}}\, dx}. \tag{11}$$

As in the case of a device with infinite memory capacity, the average value and variance of number of occupied cells are determined by Eq. (9).

The small magnitude of the relative standard deviation in the case of a large average value of the number of occupied cells is characteristic:

$$\frac{\sigma_N}{\overline{N}} \ll 1 \text{ when } \overline{N} = (\overline{\nu}\,\overline{n}) \gg 1. \tag{12}$$

5. With the use of algorithms that require a load of increasing number of cells in the duration of the waiting time, we may take, as an index of the increase in the number of occupied cells, the integral function f(s*) of an argument indicating the flow of time after the initial waiting time.

The number of occupied cells in the system is determined analogously to Eq. (1) by the relation

$$N(n) = \sum_{s=1}^{n} f(n-s) \sum_{k=1}^{\nu_s} \varepsilon_k(n, s), \tag{13}$$

where ε_k (n, s) as before is a random variable, equal to zero or unity, depending on the state of the cells in the n-th frame, occupied first in the s-th frame.

By means of transformations similar to (4) and (6), we obtain a relation for calculating the average number of memory cells, occupied in the steady-state regime, in the form

$$\overline{N} = \overline{\varkappa} \int_0^\infty f(t)\,[1 - F(t)]\, dt, \tag{14}$$

where F(t) is the distribution function of duration of tests in all the cells, occupied during the waiting time, at the moment t after the beginning of the waiting time.

The average number of memory cells, obtainable from (14) can for example be calculated in the case $f(s) = s^k$.

Using the following relation

$$\int_0^\infty t^k\,[1 - F(t)]\, dt = \frac{1}{k+1}\,\overline{t^{k+1}}, \tag{15}$$

** The number of memory cells M is 10^3–10^4.

we find that the average number of cells in the stationary state is determined by the relation

$$\lim_{n\to\infty} \overline{N(n)} = \frac{1}{k+1} m p_{\mathrm{m}} \overline{n^{k+1}}. \tag{16}$$

In contrast with the case of an algorithm with a fixed memory load and waiting time, the use of an algorithm with an increasing number of occupied cells leads to dependence of the memory load capacity on the higher moments of the distribution function for the duration of the tests.

6. With the choice of pattern selection algorithms, one must take into account the indices of detection reliability, the required memory capacity, the complexity of realization, etc.

Algorithms can be constructed with the use of single-threshold and dual-threshold [8] criteria.

A characteristic feature of the statistically optimum algorithms is the necessity of retaining data in the memory element during the entire time of waiting, which leads to a loading of an appreciable volume of the memory capacity. With use of nonoptimal algorithms, data storage at the entire time of the process is not required, and it is not possible to carry out an analysis of a series of pulses of a single channel (or a group of channels after several frames).

Let us consider the case of pattern recognition of zeroth order. The optimum selection algorithm for the data of n frames consists of a comparison of the number of thresholds exceeded with the critical value (selection according to the test "k from n"). Nonoptimum algorithms may be based on the tests "j from e", where $l < n$.

The simplest method of selection of zeroth order frames is selection according to a single passage of a threshold (use of the test "one from n").

In the case of frame recognition of the first, second, etc., orders the use of optimum algorithms is found to be hampered by virtue of the complexity of the process, and tests of the type "j from e" are found to be natural. With the selection of first order frames, for example, we may use the criteria "3 from 3", "3 from 4", etc.

The first two markers are used to form a frame contour (track) after which we examine the hit of the third marker on the feed of one of the marked tracks.

An analogous method can be used in the selection of second order frames (here one may use the criteria "4 from 4", "4 from 5", etc.).

Markers in three frames are used to form a frame contour (track) after which we examine the hit of the fourth marker on the track feed.

The efficiency of various suboptimum algorithms of selection was compared earlier [3, 7] and is not the purpose of the present work.

One may note the appreciable economy in the loading of memory capacity, attainable with the use of dual-threshold sequential analysis in comparison with a single-threshold selection procedure (see appendix).

APPENDIX

Comparison of the average duration of test in single-threshold and dual-threshold selection.

In the case of a classical single-threshold algorithm with a sufficient process duration n, when one may use for accumulation values the standard law

$$n_0 = \frac{(|\lambda_F| + |\lambda_D|)^2}{\rho^2},$$

where (I)

$$\rho^2 = \frac{(p_{\mathrm{n_s}} - p_{\mathrm{n}})^2}{p_{\mathrm{n}}(1 - p_{\mathrm{n}})};$$

λ_D is the quantum value of the probability of distortionless reproduction D; λ_F is the quantizer of the probability of a flase marking F.

When $F \ll D$ $|\lambda_F| \gg |\lambda_D|$; $|\lambda_F| \simeq \sqrt{2|\ln F|}$. According to (I) we obtain

$$n_0 \simeq \frac{2p_{\mathrm{n}}(1 - p_{\mathrm{n}})}{(p_{\mathrm{n_s}} - p_{\mathrm{n}})^2} |\ln F|. \tag{II}$$

In the case of a dual-threshold algorithm the approximate expressions for the average times of analysis are given in [6]. When $(p_{\mathrm{n_s}} - p_{\mathrm{n}}) \ll p_{\mathrm{n}}$

$$\bar{n}_{\mathrm{ns}} \simeq \frac{2Dp_{\mathrm{n}}(1-p_{\mathrm{n}})}{(p_{\mathrm{ns}}-p_{\mathrm{n}})^2}\,|\ln F|, \quad \text{(III)}$$

$$\bar{n}_{\mathrm{n}} \simeq \frac{2p_{\mathrm{n}}(1-p_{\mathrm{n}})}{(p_{\mathrm{ns}}-p_{\mathrm{n}})^2}\,|\ln(1-D)|. \quad \text{(IV)}$$

Using (II)-(IV), we obtain the ratios of the average times of analysis for a sequential algorithm to the time of analysis for a single threshold observation:

$$\xi_{\mathrm{ns}} = \frac{\bar{n}_{\mathrm{ns}}}{n_0} \simeq D, \quad \text{(V)}$$

$$\xi_{\mathrm{n}} = \frac{\bar{n}_{\mathrm{n}}}{n_0} \simeq \frac{\ln(1-D)}{\ln F}. \quad \text{(VI)}$$

Eqs. (V) and (VI) show, in the case of an asymmetrical requirement for the admissible probabilities of passage and false detection, economy in the test duration, and consequently economy in the memory capacity with the use of sequential dual-threshold algorithms in comparison with single-threshold observation.

LITERATURE

1. A. A. Kharkevich, The principles of construction of reading machines, Radiotekhnika, 1960, 15, 2,3.
2. V. S. Fayn, The principles of construction of a machine for pattern recognition, Radiotekhnika, 1960, 15, 3, 13.
3. N. Wax, Signal-to-noise improvement in the statistics of track population, J. Appl. Phys., 1955, 26, 5, 586.
4. A. Ya. Khinchin, Mathematical methods of the theory of mass service, Trudy Matem. Inst. AN SSSR, 1955, 49.
5. B. A. Sevast'yanov, Ergodic theorem for Markov processes and its application to telephone systems with operational failures, Teoriya Veroyat. i Primen., 1957, 2, 1, 106.
6. A. E. Basharinov, B. S. Fleyshman and M. A. Samokhina, Binary storage systems with dual-threshold analyzers, Radiotekhnika i Elektronika, 1959, 4, 9, 1419.
7. M. Schwartz, A coincidence procedure for signals detection, IRE Trans, 1956, IT-2, 4, 135.
8. A. Wald, Sequential Analysis, N.Y., 1947.
9. B. S. Fleyshman, Nonstationary regime of filling the memory of a cybernetic statistical pattern recognition devices, Radiotekhnika i Elektronika, 1961, 6, 7, 1041.
10. V. A. Zyatitskiy, Modelling the filling of a memory of a control device by a method of self-analysis, Radiotekhnika i Elektronika, 1961, 6, 7, 1049.

Submitted to editors 15 June 1960

NONSTATIONARY METHOD FOR LOADING THE MEMORY OF A CONTROL DEVICE WITH STATISTICAL PATTERN RECOGNITION

B. S. Fleyshman

An expression is obtained for the generating function giving the number of occupied memory cells of a control device which services the flow of calls. A calculation is made of the nonstationary method of loading the memory of such a device. From the resulting relations, we obtain, as a special case, the well-known relations of the theory of mass service. We demonstrate the generality of the distribution of the number of tests in the case of sequential analysis of alternative hypotheses and give curves of memory cell load in this case.

In connection with the operation of control devices for recognizing signals and patterns against a noise background [1,2,3,4] along with statistical problems, a number of problems arise from the theory of mass service. Usually, the flow at the input of such a control device consists of either a flow of "noise" calls, or a flow consisting of a mixture of noise and "signal" calls. Thus, various problems of filter discrimination of signal calls from noise calls emerge. When the control device has a limited memory size, it is not possible to find the solution of such problems by the usual optimum methods of mathematical statistics (the Neyman-Pearson or the sequential analysis method). The general optimum principles of solution are not formulated here. However, one of the special problems of greatest practical significance is the study of the probability of loading the memory storage of a control device, when, this memory being limited, it is not desirable to fill it. In the stationary regime the solution of this problem is contained in [4]. In [1] a system of finite difference equations is given for calculation of the average number of occupied storage locations in the nonstationary regime. In [1] with certain broad assumptions we obtain the average variance, and the distribution of the number of occupied storage locations are obtained for the nonstationary case.

1. Let a flow of calls enter the input of a control device with an infinite number $M = \infty$ of storage locations. We will characterize it by a random function $\varkappa(s)$ equal to the number of calls entering during the time interval $t\,(s < t \leqslant s + h)$, where $h > 0$ is a discrimination time step. We will assume that $\varkappa(s)$ and $\varkappa(s')$ are independent random variables for an arbitrary $s \neq s' \geqslant 10$. Let each moment s be related to the random function $\nu(s)$ designating the service time of a call, if it entered at the moment s, reckoned from its moment of birth up until termination of service. We will assume that $\nu(s)$ does not depend on $\varkappa(s')$ for any s and $s' \geqslant$ and has a distribution function

$$P\,(\nu(s) < t) = F_s(t). \tag{1}$$

Let us first consider the case of discrete observation of a real continuous flow of calls $s = jh$, $\nu(s) = ih$ $(i,\ j = 0, 1, 2, \ldots,\ h = \text{const} > 0)$, when the moments of birth of the calls and of termination of service are indistinguishable, if they are located within the time interval $t\,(s < t \leqslant s + h)$ and they are identified, for example, with $s + h$.

Suppose each birth of calls is serviced (statistically analyzed) in a separate storage location of the control device up to the moment of the final statistical decision concerning its noise or signal character, after which the storage location is cleared and other calls can be received. Under these conditions the number $\mu(t)$ of occupied storage locations of a control device at moment t is a random integer function. One must find its distribution $T(\mu(t) = m)$ from the preassigned distributions $P(\varkappa(s) = k)$ and $P(\nu(s) < t) = F_S(t)$. We introduce the generating functions

$$g_s(x) = \sum_{k=0}^{\infty} P\,(\varkappa(s) = k)\,x^k \tag{2}$$

and

$$G_t(x) = \sum_{m=0}^{\infty} P(\mu(t) = m)\, x^m. \tag{3}$$

It can be shown (see Appendix 1) that $G_t(x)$ has the following representation basic for further discussion

$$G_t(x) = \prod_{s=h}^{t} g_s\{1 + [1 - F_s(t-s)](x-1)\}. \tag{4}$$

Differentiating (4) with respect to x, we obtain expressions for $E\mu(t)$ and the dispersion $D\mu(t)$:

$$E\mu(t) = G_t'(1) = \sum_{s=h}^{t} E\varkappa(s)\,[1 - F_s(t-s)], \tag{5}$$

$$\begin{aligned} D\mu(t) &= G_t''(1) + G_t'(1) - [G_t'(1)]^2 = \\ &= E\mu(t) + \sum_{s=h}^{t} [D\varkappa(s) - E\varkappa(s)]\,[1 - F_s(t-s)]^2, \end{aligned} \tag{6}$$

which have meaning for finite $E\varkappa(s)$ and $D\varkappa(s)$, respectively.

If $\varkappa(s)$ has a Poisson distribution with parameter $\lambda(s) = E\varkappa(s) = D\varkappa(s)$

$$P(\varkappa(s) = k) = P_{\lambda(s)}(k) = \frac{\lambda^k(s)}{k!}e^{-\lambda(s)},$$

then $\mu(t)$ also has a Poisson distribution

$$P(\mu(t) = m) = P_{\Lambda(t)}(m)$$

with the parameter

$$\Lambda(t) = E\mu(t) = D\mu(t) = \sum_{s=h}^{t} E\varkappa(s)\,[1 - F_s(t-s)], \tag{7}$$

in which it is easy to verify by a substitution of the appropriate values of the generating function in this case $g_s(x) = e^{(x-1)\lambda(s)}$ into Eq. (4).

If in this case the number of storage locations of the control device is finite, $M = \text{const} \gg \Lambda(\infty)$, then as can be shown $\mu(t)$ has a Poisson distribution averaged over M to

$$P(\mu(t) = m) = P_{\Lambda(t),M}(m) = \begin{cases} \dfrac{\Lambda^m(t)}{m!} \Big/ \displaystyle\sum_{r=0}^{M} \frac{\Lambda^r(t)}{r!} & \text{when } 0 \leqslant m \leqslant M, \\ 0 & \text{when } m > M. \end{cases} \tag{8}$$

Eq. (8) indicates that the Erlang formula [5] holds both in a discrete nonstationary Poisson flow and in an arbitrary distribution of the time of service; the probability of reloading the storage corresponds to the probability of refusal [5, 6, 11].

2. In practice the case of greatest interest is the homogeneous one in which the distributions $\varkappa(s) = \varkappa$ and $\nu(s) = \nu$ do not depend on time.

In this case Eq. (5), (6) and (7) are markedly simplified. We have

$$E\mu(t) = E\varkappa \sum_{s=h}^{t} [1 - F(s)] \leqslant E\varkappa\, E\nu, \tag{9}$$

since $\sum_{s=h}^{\infty} [1 - F(s)] = E\nu$,

and

$$D\mu(t) = E\mu(t) + (D\varkappa - E\varkappa)\sum_{s=h}^{t} [1 - F(s)]^2 \leqslant E\mu(t) + |D\varkappa - E\varkappa|\, E\nu, \tag{10}$$

since $\sum_{s=h}^{t} [1 - F(s)]^2 \leqslant \sum_{s=h}^{t} [1 - F(s)] \leqslant E\nu$.

In the case of a homogeneous Poisson flow $\mu(t)$ has a Poisson distribution with the parameter

$$\Lambda(t) = E\mu(t) = D\mu(t) = E\varkappa \sum_{s=h}^{t} [1 - F(s)] \leqslant \Lambda(\infty) = E\varkappa E\nu. \tag{11}$$

Often in practice $\Lambda(t)$ is rather large ($\Lambda(t) \geqslant 100$) and then in the case of a Poisson distribution changes to a normal distribution (with an average $\Lambda(t)$ and standard deviation $\sqrt{\Lambda(t)}$) close to a δ-distribution.

Under these circumstances, when $\Lambda(t) \leqslant \Lambda(t) + u\sqrt{\Lambda(t)} \leqslant M = \text{const}$, the difference between the cases $m = \text{const}$ and $M = \infty$ has no practical meaning, and the probability of reloading the storage equal to $\frac{1}{\sqrt{2\pi}}\int_{u}^{\infty} e^{-\frac{z^2}{2}}$ relative to a small diminution $\Lambda(t) = M - u\sqrt{M}$ in comparison with M can be made conveniently close to zero at $u > 3$.

When $\Lambda(t) < 100$ the probability of reloading the storage can be evaluated on the basis of tables given in [11].

If we carry out a discrete analysis of $N \geqslant M$ elements of phase space with probabilities of p_s and p_n of the appearance of pulses in the signal and noise elements respectively, $\varkappa$ has a Poisson distribution with parameter

$$\lambda = E\varkappa = N\,[\theta\, p_s + (1 - \theta)\, p_n],$$

where θ and $1 - \theta$ denote the fractions of the signal and noise elements in phase space.

3. Let us consider the case of large $\Lambda(t)$ when the δ-distribution $\mu(t)$ is defined by a single parameter $\Lambda(t)$. In this case $\Lambda(t)$ can be expressed in compact form. Indeed, let us introduce the time scale $\bar{t} = t/E\nu$, $\bar{s} = s/E\nu$ and designate [see (11)]

$$a(t) = \frac{\Lambda(\bar{t}E\nu)}{\Lambda(\infty)} = \frac{1}{E\nu}\sum_{s=h}^{\bar{t}E\nu} [1 - F(\bar{s}E\nu)] \leqslant 1. \tag{12}$$

Then, using Eq. (12) and assuming $F(\overline{s}E\nu) = W(s)$, we will have at $\bar{t} = \text{const}$ and $E\nu \to \infty$

$$a(\bar{t}) = \int_0^{\bar{t}} [1 - W(\bar{s})]\, d\bar{s} \leqslant 1. \tag{13}$$

Let us consider the special cases of Eq. (13).

a) Case of a constant time of service (Neyman-Pearson test). Here

$$W(\bar{s}) = \begin{cases} 0 & \text{when } 0 \leqslant \bar{s} < 1, \\ 1 & \text{when } \bar{s} \geqslant 1, \end{cases} \tag{14}$$

Substituting into (13), we will have

$$a(\bar{t}) = \begin{cases} \bar{t} & \text{when } 0 \leqslant \bar{t} < 1, \\ 1 & \text{when } \bar{t} \geqslant 1. \end{cases}$$

b) Case of an exponential time of service, characteristic for telephone applications. In this case

$$W(\bar{s}) = 1 - e^{-\bar{s}} \tag{15}$$

and substituting (15) into (13), we will have

$$a(\bar{t}) = 1 - e^{-\bar{t}}.$$

c) Wald distribution [7] of the time of service

$$W(\bar{s}) = W_C(\bar{s}) = \sqrt{\frac{C}{2\pi}} \int_0^{\bar{s}} x^{-3/2} \exp\left[-\frac{C}{2}(x + x^{-1} - 2)\right] dx, \tag{16}$$

where

$$C = (E\nu)^2/D\nu \tag{17}$$

(see Appendix 2), and

$$a(\bar{t}) = a_C(\bar{t}) = \bar{t}\,[1 - W_C(\bar{t})] + 1 - W_C(1/\bar{t}). \tag{18}$$

Eq. (18) is obtained by integration by parts of Eq. (13) with the use of the identity

$$\int_0^y x W_C'(x)\, dx \equiv \int_0^{1/y} W_C'(x)\, dx.$$

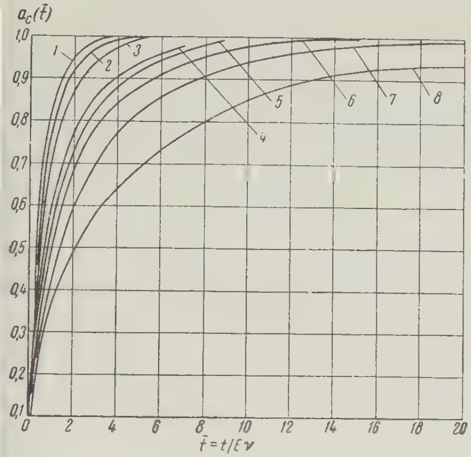

Family of normalized curves $a_c(t)$ for different values of $C = (E\nu)^2/D\nu$:
1—C = 3.0; 2—C = 2.0; 3—C = 1.0; 4—C = 0.5; 5—C = 0.4; 6—C = 0.3; 7—C = 0.2; 8—C = 0.1.

Distribution (16) was obtained by Wald [7] for the case of a choice between hypotheses concerning the magnitude of the average value of the normal distribution. One may show, however, that it has a general character (see Appendix 2) for the case of a selection between two similar hypotheses (detection of a signal with a small signal-to-noise ratio) in the case of asymmetrical thresholds. These facts justify the tabulation of $W_c(s)$ and the numerical calculation of $a_c(t)$.

The family of normalized curves $a_c(t)$, calculated from tables of the functions $W_c(\bar{s})$ at different C = 0.1; 0.2; 0.3; 0.4; 0.5; 1.0; 2.0 and 3.0 are given in the figure. But the average number of occupied storage locations at moment t is calculated according to the formula

$$E\mu(t) \simeq E\varkappa E\nu a_C(t/E\nu), \tag{19}$$

where C is determined from Eq. (17).

Comparison of curves $a_c(t)$ with analogous curves calculated by means of a calculating machine from the system of finite-difference equations [1], points to good agreement (see [10]).

4. In conclusion let us consider the case of a continuous observation of a flow of calls, when $h \to 0$ and the flow is ordinary [5], i.e.,

$$P(\varkappa(s) = 1) = \lambda(s)h + o(h),$$

$$P(\varkappa(s) > 1) = o(h),$$

whence,

$$P(\varkappa(s) = 0) = 1 - \lambda(s)h + o(h),$$

$$g_s(x) = e^{(x-1)\lambda(s)h + o(h)}.$$

In this case the generating function $\mu(t)$, where t = jh = const ($j = t/h \to \infty$), as it is easy to show has the form

$$\widetilde{G}_t(x) = \lim_{h\to 0} G_t(x) = e^{(x-1)\widetilde{\Lambda}(t)}, \tag{20}$$

where

$$\widetilde{\Lambda}(t) = \int_0^t \lambda(s)\,[1 - F_s(t-s)]\,ds, \tag{21}$$

i.e., $\mu(t)$ is a Poisson distribution with parameter $\widetilde{\Lambda}(t)$.

From Eq. (21) there follow results obtained for $F_s(t) = F(t) = 1 - e^{-t}$ ([5], p. 78) and $\lambda(s) = \lambda$, $F_s(t) = F(t)$ ([5], p. 80). For the finite number $M \gg \Lambda(t)$ the storage locations $\mu(t)$ is a Poisson distribution with a parameter $\widetilde{\Lambda}(t)$, averaged over M. In this case when $t \to \infty$, $\lambda(s) = \lambda$ and $F_s(t) = F(t)$, when $\widetilde{\Lambda}(\infty) = E\varkappa E\nu$ we obtain the result [6].

APPENDIX I

Derivation of the fundamental expression for the generating function $G_t(x)$.

Let us fix the factor $S = (s_1, s_2, \ldots, s_r)$ of the moments when at least one call appears $(0 \leqslant r \leqslant n = t/h)$. It is easy to see that the random function $\mu_S(t)$, denoting the number of occupied storage locations at the instant t, for a fixed S has the form

$$\mu_S(t) = \sum_{s \in S} \sum_{k_s = 1}^{\varkappa(s)} \varepsilon_{k_s}(s, t), \qquad (I)$$

where $\epsilon_{k_S}(s,t)$ is a random function determined by the k_s-th call which entered at the instant $s[1 \leqslant k_s \leqslant \varkappa(s)]$, which takes tha value zero, if the k_s-th call is serviced at the moment t, and the value unity otherwise.

In other words, the random function

$$\varepsilon_{k_s}(s, t) = \begin{pmatrix} 0 & 1 \\ F_s(t-s) & 1 - F_s(t-s) \end{pmatrix}$$

is a generating function

$$h_{s,t}(x) = F_s(t-s) + [1 - F_s(t-s)]\, x = 1 + [1 - F_s(t-s)]\,(x-1).$$

For fixed s and t and different $k_S \epsilon\, k_S(s,t)$ are independent, of the same distributions of random variables which also do not depend on $\varkappa(s)$. Therefore, for the inner sum of (I) one may use the iteration property of the corresponding generating functions during the formation of a complex distribution [9]. For the outer sum of (I) can be used by the multiplicative property of the generating functions during the formation of composition of the corresponding distributions, because $\varkappa(s)$ are independent at different s.

In accordance with the above-mentioned generating function $\mu_S(t)$ has the form

$$G_{t,S}(x) = \prod_{s \in S} \tilde{g}_s\{1 + [1 - F_s(t-s)]\,(x-1)\}, \qquad (II)$$

where

$$\tilde{g}_s(x) = \sum_{k=1}^{\infty} P(\varkappa(s) = k)\, x^k / [1 - P(\varkappa(s) = 0)] =$$

$$= [g_s(x) - P(\varkappa(s) = 0)] / [1 - P(\varkappa(s) = 0)] \qquad (III)$$

is the generating function of the distribution $\varkappa(s)$ under the condition that $\varkappa(s) > 0$.

It is easy to show that the generating function $\mu(t)$ has the representation

$$G_t(x) = \sum_{S \in R_n} \prod_{s \in S} [1 - P(\varkappa(s) = 0)] \prod_{s \in \bar{S}} P(\varkappa(s) = 0)\, G_{t,S}(x), \qquad (IV)$$

where the summation is carried out over S, ranging over all the possible 2^n sets $\{s_1, s_2, \ldots$ $\ldots, s_r\} = R_n$, and $\bar{S}$ designates the complement of S to R_n. Substituting the explicit expression $G_{t,S}(x)$ (II) in Eq. (IV), after simple transformations taking into consideration (III) we obtain finally

$$G_t(x) = \prod_{s=h}^{t} g_s\{1 + [1 - F_s(t-s)]\,(x-1)\}.$$

APPENDIX II

Proof of the generality of the distribution $W_c(x)$ for the case of alternative hypotheses.

Suppose we are required to make a choice between the two hypotheses $H_0\,(a = a_0)$ and H_1 $(a = a_1 > a_0)0$ value of the parameter of a one-parameter family of probability densities $f_a(x)$ of the random variable ξ with probability errors of the first and second kind in α and β respectively. With the use of sequential analysis for the solution of the stated problem, the number of tests ν before making the final decision is found to be a random variable. If $f_a(x) = \frac{1}{\sqrt{2\pi}} \exp\left[-\frac{1}{2}(x-a)^2\right]$, $\nu/E\nu$ has the distribution (16) (see [7]). Let us consider the of alternative hypotheses, when $\Delta_1 = a_1 - a_0 \sim |\Delta| = |a - a_0| \to 0$, under the condition of a greater order of smallness of α than β ($\alpha = o(\beta)$, $\beta \to 0$). Suppose at all values of x at which the random variable is defined, in the neighborhood of the values $a = a_0$ and $a = a_1$, $f_a(x) \geqslant \epsilon > 0$, $f_a(x)$ and its partial derivatives with respect to a up to the third order inclusively are continuous, and $[\ln f_a(x)]k$ ($k = 1, 2, 3$) with its derivatives with respect to a up to the third order inclusively are uniformly integrable over all x.

Then, using the Taylor formula, one may show that

$$E_a\zeta = \int_{-\infty}^{\infty} f_a(x) \ln (f_{a_0}(x) / f_{a_0}(x))\, dx = \Delta_1 \left(\frac{\Delta}{\Delta_1} - 0{,}5\right) J_2(a_0) + O(\Delta_1^3), \tag{V}$$

$$D_a\zeta = \Delta_1^2 J_2(a_0) + O(\Delta_1^3), \tag{VI}$$

$$E_a |\zeta - E_a\zeta|^3 = \Delta_1^3 J_3(a_0) + O(\Delta_1^4), \tag{VII}$$

where

$$\zeta = \ln (f_{a_1}(\xi) / f_{a_0}(\xi));$$

$$J_k(a_0) = \int_{-\infty}^{\infty} \left| \frac{\partial \ln f_a(x)}{\partial a} \right|_{a=a_0}^{k} f_{a_0}(x)\, dx > 0 \quad (k = 2,\ 3);$$

using also the results of [7] and [8], (V) and (VI), we will have, respectively,

$$E_a\nu = \frac{\ln \frac{1}{\beta} + O(\alpha)}{|E_a\zeta|} \sim \frac{\ln \frac{1}{\beta} + O(\alpha)}{\Delta_1^2 \left| \frac{\Delta}{\Delta_1} - 0{,}5 \right| J_2(a_0)}, \tag{VIII}$$

$$D_a\nu = \frac{D_a\zeta}{|E_a\zeta|^3} \left[\ln \frac{1}{\beta} + O(\alpha) \right] \sim \frac{\ln \frac{1}{\beta} + O(\alpha)}{\Delta_1^4 \left| \frac{\Delta}{\Delta_1} - 0{,}5 \right| J_2^2(a_0)} \tag{IX}$$

under the assumption $\Delta < 0.5\ \Delta_1$.

Using the Chebyshev inequality and Eqs. (VIII) and (IX), we easily obtain an estimate of the probability

$$P\left[\nu = O\left(\Delta_1^{-2} \ln \frac{1}{\beta}\right)\right] > 1 - O\left(\frac{1}{\ln \beta}\right). \tag{X}$$

Let us now proceed directly to a proof of the generality of distribution (16) for the case of alternative hypotheses. A sequential procedure of selection between the hypotheses H_0 ($a = a_0$) and H_1 ($a = a_1 > a_0$) is based on a dual-threshold analysis of the coefficient of likelihood

$$l_\nu = \sum_{i=1}^{\nu} \zeta_i, \tag{XI}$$

where $\zeta_i = \ln (f_{a_1}(x_i)/f_{a_0}(x_i))$ is a function of the i-th selective value of x_i.

Let us introduce new variables

$$\tilde{\zeta}_j = \sum_{i=s(j-1)+1}^{sj} \zeta_i.$$

Then (XI) can be written in the form

$$l_\nu = \sum_{j=1}^{\nu} \tilde{\zeta}_j + \sum_{i=s\tilde{\nu}+1}^{\nu} \zeta_i, \tag{XII}$$

where $\tilde{\nu} = [\nu/s]$ is the integral part of the number ν/s. Suppose the rate of growth of $s = 0\left[\left(\Delta_1^{-2} \sqrt{\ln \frac{1}{\beta}}\right)^{1-\eta}\right]$, where η ($0 < \eta < 1$) is arbitrarily small. Then the Lyapunov relation [see (VI) and (VII)] has the form

$$\sqrt{sD_a\zeta} \Big/ \sqrt[3]{sE_a|\zeta - E_a\zeta|^3} \sim \sqrt{J_2(a_0)} \Big/ \sqrt[3]{J_3(a_0)}\sqrt[6]{s} \to 0,$$

which ensures the asymptotic normality of $\tilde{\zeta}_j$. At the same time, if $\nu = 0\left(\Delta_1^{-2} \ln \frac{1}{\beta}\right)$, one may show that when $\Delta_1 \to 0$ the distribution of l_2 is determined only by the first random sum relation (XII). Let us now define the sequential procedure of selection between the two hypotheses

$$H_0^*\left(a^* = a_0^* = \frac{a_0 + a_1}{2} - \Delta_1 \frac{E_{a_0}\zeta}{D_{a_0}\zeta}\right) \text{ and } H_1^*\left(a^* = a_1^* = \frac{a_0 + a_1}{2} + \Delta_1 \frac{E_{a_1}(\zeta)}{D_{a_1}\zeta}\right)$$

relative to the average value

$$a^* = \frac{a_0 + a_1}{2} + \Delta_1 \frac{E_a\zeta}{D_a\zeta}$$

of a normally distributed random variable ξ^*, having the probability density

$$f_{a^*}^*(x) = \frac{1}{\sqrt{2\pi}\sigma} \exp\left[-\frac{1}{2\sigma^2}(x - a^*)^2\right]$$

with a certain variance $\sigma^2 = \Delta_1^2 / sD_a\zeta$.

It is easy to show that the corresponding elementary logarithm of the coefficient of likelihood has the form

$$\zeta^* = \ln\left(f_{a_1^*}^*(\zeta^*) / f_{a_0^*}^*(\xi^*)\right) = \frac{\Delta_1}{\sigma^2}\left(\xi^* - \frac{a_0 + a_1}{2}\right)$$

and it is again normalized by $(sE_a\zeta,\ sD_a\zeta)$.

Thus, the random variables ζ and ζ^* are asymptotically and identically normally distributed. Hence, we clearly find the same asymptotic distribution of the number ν and ν^* of tests for the termination of both procedures. But according to [7] ν^* has the distribution (16). From this it follows that ν also has the same distribution. We note that our assertion was made under the assumption that $\nu = O\left(\Delta^{-2} \ln \frac{1}{\beta}\right)$. Thus it holds good only with a probability (X), close to unity. If $\Delta > 0.5\,\Delta_1$, by exchanging α and β in all the preceding discussions, we reach an analogous conclusion.

LITERATURE

1. N. Wax, Signal-to-noise improvement and the statistics of track populations, J. Appl. Phys., 1955, 26, 5, 586.
2. A. A. Kharkevich, The principles of construction of reading machines, Radiotekhnika, 1960, 15, 2,3.
3. V. S. Fayn, The principles of construction of a machine for pattern recognition, Radiotekhnika, 1960, 15, 3, 13.
4. A. E. Basharinov, Problems of statistics of automatic pattern recognition using multiframe observation, Radiotekhnika i Elektronika, 1961, 6, 7, 1035.
5. A. Ya. Khinchin, Mathematical methods of the theory of mass service, Trudy Matem. Inst. AN SSSR, 1955, 49.
6. B. A. Sevast'yanov, Ergodic theorem for Markov processes and its application to telephone systems with operational failures, Teoryia Veroyat. i Primen., 1957, 2, 1, 106.
7. A. Wald, Sequential Analysis, N.Y., 1947.
8. A. E. Basharinov and B. S. Fleyshman, Application of the method of sequential analysis to binary systems with Rayleigh fluctuation of the signal intensity, Radiotekhnika i Elektronika, 1959, 4, 2, 155.
9. W. Feller, Introduction to the Theory of Probability [Russian trans.], IL, 1952.
10. V. A. Zyatitskiy, Modelling of the memory load of a control device by the method of self-analysis, Radiotekhnika i Elektronika, 1961, 6, 7, 1049.
11. G. P. Basharin, The limiting distribution of a fully available line beam, Teoriya Veroyat. i Primen., 1960, 5, 2, 246.

MODEL OF THE MEMORY LOADING OF A CONTROL DEVICE BY THE METHOD OF SELF-ANALYSIS

V. A. Zyanitskiy

A direct method is presented for the sequential analysis of the memory loading of an electronic computer (EC) contained in a control device—the method of self-analysis—for binary quantization of data fed to the input of this device.

We give an algorithmic description of the method, a block diagram of the algorithm (the operating technique can be used in any EC). We introduce the programming parameters with which the calculation was carried out.

One of the basic parameters restricting the feasibility of pattern recognition by a control device is the storage space of an electronic digital computer contained in this device [1,2].

In [1] a calculation is given of the memory for the stationary case, and in [2] for the nonstationary. In [3] a system of finite-difference equations is given for calculation of the average number of occupied storage locations of a computer in the nonstationary case for binary quantization (the equations are solved using the computer). In the present paper we propose a direct method of analysis of the loading of the computer memory—a method of self-analysis, which can be used in a number of cases not considered in [2,3]; we compare curves of the memory load calculated by methods given in [2] and [3], and we also compare the curves of [2] with those obtained by the method of self-analysis.

1. Let us consider a phase space R consisting of a large but finite number of N elements: $R = \{r_1, r_2, \ldots, r_i, \ldots, r_N\}$. In the elements r_i on the general noise background of patterns the appearance of patterns consisting of separate signals is expected. The signals either remain stationary in time, or move from element to element. When the pattern is recognized element by element, in contrast with identification of the pattern as a whole, consideration of the geometric configuration of the pattern does not leave any essential meaning for the determination of the memory loading; the only essential is the overal fraction of signal elements from R entering into the expected pattern.

Separation of signal elements from R creates a control device having an electronic computer with a memory space of M locations. The case when $M \ll N$ is interesting.

When we speak of a call on element r_i, we understand by that the appearance of a signal in the r_i-th element of the phase space (in the case of binary quantization, this means the heightening of the intensity of a certain threshold in the element).

Let us consider the operation of the control device. It repeats many times the scanning of elements r_i $(i = 1, 2, \ldots, N)$* and determines a fixed relation between an incoming call and a free cell in the memory of the computer (for brevity we shall call it simply a cell). At the same time a fixed number f_1—the initial characteristic of the element—is transported to the cell. In the course of time, data accumulates at the cell, giving a flow characteristic of element f from R. As soon as the control device determines the noise or signal character of the f-element, the memory cell corresponding to this element is cleared and can be used below. Our problem is to make a calculation of the memory loading of the electronic computer.

2. Let us consider the case of sequential analysis of data in the case of binary quantization. This corresponds to the following algorithm [3], equivalent to an algorithm of sequential analysis.

After each call from a given element (with an intensity exceeding the first threshold X_1) at the corresponding storage locations, there is accumulated the random number $f = f_\nu$ ("weight" according to the terminology of [3]):

---

* The period of single examination is used as a unit of discrete time.

$$f_\nu = f_1 + \sum_{i=1}^{\nu} [\xi_i l - (1 - \xi_i)], \tag{1}$$

where ξ_i is a random variable taking the value one or zero, respectively, when the intensity of the second threshold X_2 is exceeded or not exceeded during the i-th examination of the indicated cell of phase space R (the value l cm in (9), $f_1 > 0$ cm in (8)). The cell is cleared if the noise ($f \leqslant 0$) or signal ($f \geqslant f_A$) character of the cell, where f_A cm in (7). When $0 < f < f_A$ the test is continued, i.e., at a subsequent instant we change f according to Eq. (1) and apply anew our test.

3. Let us proceed to a description of the direct mechanical realization of the algorithm [2], with which the computer analyzes its own memory (self-analysis).

3-1. Solving the problem concerning loading of the memory of an electronic computer, we must determine the number of cells containing the number $0 < f < f_A$, where f is the flow characteristic of the element registered in the computer memory.

3-2. Thus, it is immaterial to us how the actual relation between the element and cell which stores f is realized.

3-3. Section 3-2 enables us to reject the requirement of a rigid relation between the element and the corresponding fixed cell (see para. 1) and allows us to hypothesize the existence of, on the contrary, a rather flexible relation (see 3-6 and 3-6-2).

3-4. For realization, of 3-1 under the assumptions of 3-3, let us require that all the computer cells, where the numbers f are stored, be positioned one after the other, without a lapse.

3-5. We also assume that all the "births" of calls will have manifested themselves by the end of the examination.

Suppose $\mu^*[(t-1)]$ cells remain in the computer memory with the numbers f at the end of the (t-1)-th examination, and let $\varkappa(t-1)$ new calls enter the control device. Then we send each of the $\varkappa[(t-1)]$ numbers f_1 to cells with the numbers

$$\mu^*[(t-1)] + 1,\ \mu^*[(t-1)] + 2,\ \ldots,\ \mu^*[(t-1)] + \varkappa[(t-1)].$$

Well before the beginning of the t-th examination, the following $\mu(t)$ cells were occupied by numbers f:

$$\begin{gathered} \mu(t) = \mu^*[(t-1)] + \varkappa[(t-1)], \\ \mu^*(0),\ f = f_j(t-1), \end{gathered} \tag{2}$$

where j is the number of cells containing f; <j> is the number existing in the cell j ($\varkappa(t)$ in the general case is subject to the Poisson law [2]).

3-6. Suppose the i-th examination of phase space R be made, i.e., in accordance with Eq. (1) we develop the flow characteristics f, which are stored in the computer memory.

As a result of the process of <j> = $f_j(t-1)$, we obtain <j> = $f_j(t)$. We assume that, at a given stage of the process, d numbers of f exist (d is the number of the cell storing f):

$$\mu^*(t) \leqslant d \leqslant \mu(t) \tag{3}$$

Let us show how requirement 3-4 is realized depending on the obtained value of <j> = $f_j(t)$ (3-6-2: $j < d$).

3-6-1. If $f_j(t) \leqslant 0$ or $f_j(t) \geqslant f_A$, we send into the j cell the number $f_d(t-1)$*, i.e., again we apply formula (1) to <j> = $f_d(t-1)$.

3-6-2. If $0 < f_j(t) < f_a$, we pass on to the processing of quantity <j+1> = $f_{j+1}(t-1)$.

3-7. If d = j, then after processing <d> according to Eq. (1) the processing is concluded and $\mu^*(t)$ equals

$$\mu^*(t) = \begin{cases} d & 0 < f_d(t) < f_A, \\ d - 1 & f_d(t) \leqslant 0,\ f_d(t) \geqslant f_A. \end{cases} \tag{4}$$

3-8. Figure 1 gives a block diagram of a program used to realize a miniature-scale operation. A program interpreting the method of self-analysis requires 50 cells for a command; 5 more cells are occupied by a constant and 6 cells are auxiliaries (one for the address

---

* The number of cells with the number $0 < f < f_A$ is decreased in this way to unity.

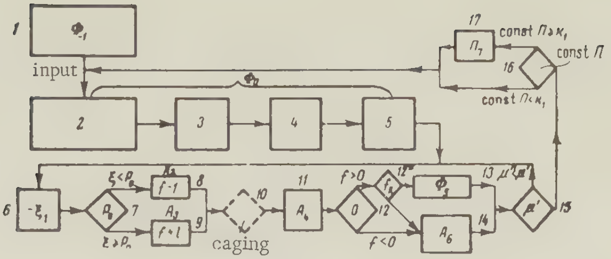

Figure 1. Block diagram of the program, by means of miniature-scale operation was realized.
1 - clearing of memory, construction of the program from data r; 2 - formation of dispatch commands of r numbers f_1; 3 - fixing of a given length of a block L; 4 - calculation of the total number of examined cells; 5 - remembering of commands and clearing of the flow computer series; 6 - ξ-meter of random numbers distributed according to a uniform law; 7 - comparison with p_0; 8 - decrease of the flow weight of f by a unit; 9 - increase of the flow weight of f by l; 10 - stop; 11 - fixing of the number of examined series of cells where f > 0; 12 - comparison with the threshold zero; 12* - comparison with the threshold f_A; 13 - formation of commands to passing to the next cell; 14 - decrease of the block length by a unit and dispatch of f of latter to the site f< 0; 15 - comparison with μ' —the number of nonzero elements of the series; 16 - comparison with the constant, regulating the printing frequency; 17 - control of printing frequency and printing.

substitution of a constant and 5 commands for restoration of used commands); as operating cells we used the entire remaining operative memory of the electronic-computer cell distribution in a block program: block I, 7 cells; block II, 3 cells; blocks III - IV, 8 cells; block V, 3 cells; block VI, 9 cells; block VII, 1 cell; block VIII, 2 cells; block IX, 1 cell; block XI, 1 cell; block XII, 1 cell; block XIII, 5 cells; block XIV, 5 cells; block XV, 1 cell; block XVI, 1 cell; block XVII, 2 cells. The numbers introduced in the program were in the form of binary normalized numbers. Taking into account the design features of the BESM-1, we included group operations in the program and the address substitution constants were taken from a DZU.

To obtain the random numbers an algorithm introduced by G. A. Osokov was used.

It is noteworthy that ~3 min were required to obtain the results by the self-analysis method, and ≃20 min for identical results according to [3].

3-9. The memory load curve μ(t) is obtained on a BESM by the method stated in 3-1 to 3-7. For simplicity we took $\varkappa(t) = \varkappa = E\varkappa = \text{const}$. Having normalized time t and μ(t), we obtain

$$\bar{t}_t = \frac{t}{E\nu}, \quad a_C^*(\bar{t}) = \frac{\mu(\bar{t}E\nu)}{E\nu\, E\varkappa} \tag{5}$$

{the value Eν is [see (10)] the average shut-down time of f = fv within limits $0<f<f_A$, and $E\varkappa$ is the average number of newly entering calls}. Let us compare the following curve with $a_C^*(\bar{t})$

$$a_C(\bar{t}) = \bar{t}\,[1 - W_C(\bar{t})] + 1 - W_C\left(\frac{1}{\bar{t}}\right) \tag{6}$$

(see [2]), where $W_C(t)$ is the Wald function (see Figure 2). It can be seen that satisfactory agreement is obtained. This in practice is experimental verification of the theory developed in [1,2].

4. Let us compare the results obtained by methods [2] and [3]. Designating α - the probability of an error of the first kind; β - the probability of an error of the second kind; p_1 - the probability of exceeding the first threshold in the signal element; p_0 — the same probability in the noise element, one can obtain the parameters [3] when

$$f_A = \frac{\ln \frac{1-\beta}{\alpha\beta}}{\ln \frac{1-p_0}{1-p_1}}, \tag{7}$$

$$f_1 = \frac{-\ln \beta}{\ln \frac{1-p_0}{1-p_1}}, \tag{8}$$

$$l = \frac{\ln \frac{p_0}{p_1}}{\ln \frac{1-p_0}{1-p_1}} \tag{9}$$

and the parameters [1, 2]

$$E\nu = \frac{f_1}{1-p_0-lp_0}, \tag{10}$$

$$C = \frac{(E\nu)^2}{D\nu} = \frac{f_1^2}{E\nu(1-l)^2 p_0 (1-p_0)}, \tag{11}$$

$$E\mu(\infty) = E\varkappa E\nu = Np_n E\nu, \tag{12}$$

where p_n is the probability of a call from the noise element ($p_n \ll p_0$, and $X_1 > X_2$; it is assumed that the number of signal elements R is small in comparison with the noise elements.

By inverse transformations it is easy to obtain α, β, p_1 in terms of the parameters [3], assigning an additional p_0. The random number $\mu(t)$ of occupied memory cells at a discrete moment of time t is represented in [3] in the form

$$\mu(t) = \sum_{f=1}^{f_A} \mu_f(t), \tag{13}$$

where $\mu_f(t)$ is the random number of occupied cells in which $f_\nu = f$. For normalized average values

$$\frac{E\mu_f(t)}{E\mu(\infty)} = m(t, f), \qquad \frac{E\mu(t)}{E\mu(\infty)} = m(t) \tag{14}$$

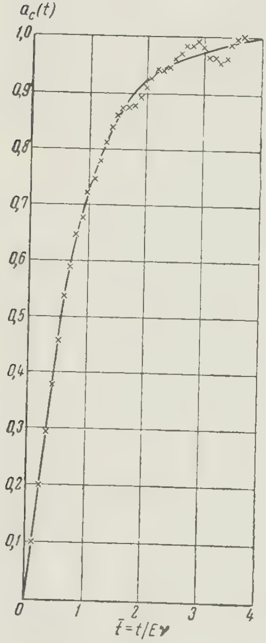

Figure 2

Figure 2. Curve $a_C(\bar{t})$ at C = 1.5625. The points of the curve $a_C^*(\bar{t})$ are plotted as crosses ($\alpha = 0.8995 \cdot 10^{-6}$; $\beta = 0.1$; $p_0 = 0.2$; $p_1 = 0.2825$; $E\nu = 100$; $f_1 = 20$; $l = 3$; $f_A = 100$; $\varkappa = E\varkappa = 9$).

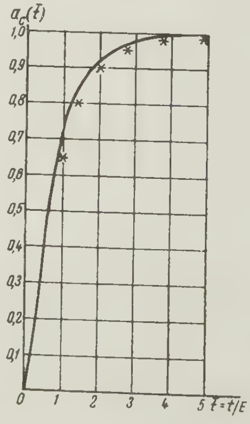

Figure 3

Figure 3. Curve $a_C(\bar{t})$ at C = 2.02. The points of the curve m(t) are plotted as crosses ($\alpha = 10^{-6}$; $\beta = 0.1$; $p_0 = 10^{-2}$; $p_1 = 0.04641589$; $E\nu = 105.84155$; $f_1 = 61$; $l = 41$; $f_A = 427$).

of the recurrent system, introduced in [3] on the basis of algorithm A.2, one may give the following compact form (parameter Q-1, [3])

$$\left.\begin{aligned} m(t, f) &= m^*(t, f), \\ m(t, f_1) &= m^*(t, f_1) + \frac{1}{E\nu} - p_0 m\,[(t-1)], \\ m(t, f_A) &= p_0 \sum_{f=f_A-l}^{f_A} m(t-1, f), \end{aligned}\right\} \tag{15}$$

$$m(t) = \sum_{f=1}^{f_A} m(t, f), \tag{16}$$

wherein

$$m^*(t, f) = (1 - p_0)\, m(t-1, f+1) + p_0 m(t-1, f-l), \tag{17}$$

where on the right-hand side $m(t-1, x) = 0$ for $x \leq 0$. A calculation of the curve m(t) was made on the BESM-1; after normalization of time $\bar{t} = t/E\nu$ it was compared with the corresponding curve (6). This comparison showed good agreement (see Figure 3). However, repetition of the calculation according to [3] leads to accumulation during the computation of errors, which possibly also was manifest in an error in counting the points of the curve (Figure 1 in [3]) when $p = 1/4$, $Q = 1/2$ (actually the curve lies lower than in [3]).

In conclusion we mention that miniature-scale operation by the method of self-analysis of the memory load does not give rise to difficulties even in the more complicated situation of moving models {see [1], (13)} in which a theoretical calculation of the nonstationary state is analytically exceedingly complex.

The author expresses his gratitude to. E. E. Fleyshman, under whose guidance this work was completed, and to A. E. Basharinov, who took part in discussions of the work.

REFERENCES

1. A. E. Basharinov, Problems of statistics of automatic recognition of patterns using multiframe observation, Radiotekhnika i Elektronika, 1961, 6, 7, 1035.
2. B. S. Fleyshman, Nonstationary regime of the memory load of a control device with statistical pattern recognition, Radiotekhnika i Elektronika, 1961, 6, 7, 1041.
3. N. Wax, Signal-to-noise improvement in the statistics of track populations, J. Appl. Phys., 1955, 26, 5, 586.

Submitted to editors 15 June 1960

THE THEORY OF OPTIMAL DETECTION OF A COMPOUND SIGNAL WITH CORRELATED NOISE

V.F. Nesteruk

This article deals with the problem of detecting a signal whose components are a random function and a deterministic function on the background of normal correlated noise. An expression for the likelihood factor is established. Detection characteristics are considered for a number of specific cases.

INTRODUCTION

The statistical problem of detecting a useful signal on a background of fluctuation noise is formulated as follows: the input signal s(t) arriving at the receiver consists of a useful signal M(t) and the noise n(t). Thus,

$$s(t) = M(t) + n(t). \tag{1}$$

It will be assumed known that the noise represents a random function of time with a given multidimensional distribution function of the probability density of order H. With regard to the function M(t), it is assumed that it depends on a number of known and unknown parameters. Let the intervals of the observation time be T. In a time T, the receiver must provide an answer as to whether or not there is a useful signal, if the signal at the input is s(t).

A number of works [1-6] have been devoted to the solution of this problem with different conditions placed on the functions M(t) and n(t). According to the general theory, an optimal receiver which will provide a maximum probability of detection D for a given probability of false alarm F and a given observation time T must be designed in such a way that the likelihood factor at the output is

$$l(s) = \int \ldots \int \frac{P_{M+n}(s)}{P_n(s)} P(M_1, \ldots, M_k)\, dM_1 \ldots dM_k, \tag{2}$$

where $P_{M+n}(s)$ is the probability function of the occurrence of s when a useful signal M(t) and noise n(t) arrive at the receiver; $P_n(s)$ is the probability function of the occurrence of s when only noise n(t) arrive at the receiver; and finally, $P(M_1, \ldots, M_k)$ is the density function of the unknown parameters of the useful signal.

The probability coefficient l(s) must be compared with the threshold value l_0, Then

$$\begin{aligned} &\text{if } l \geqslant l_0, \text{ it follows that } s = M + n \\ &\text{if } l < l_0, \text{ it follows that } s = n \end{aligned} \tag{3}$$

In this article, the problem of detection is solved using the following assumptions: n(t) is a stationary random Gaussian function, and the useful signal M(t) is compound,* i.e.,

$$M(t) = m(t) + \mu(t), \tag{4}$$

where m(t) is a function of time with completely known parameters, and μ(t) is a stationary random Gaussian function with a given multidimensional distribution function of the probability density. Moreover, it is assumed that the random functions n(t) and μ(t) are statistically independent and that their average values are equal to zero.

Thus, in terms of the classification given in [3], we are solving a problem of a complex detection of a compound signal (4) on the background of correlated noise.

1. THE PROBABILITY COEFFICIENT

We shall assume that in the observation time T, H measurements of the instantaneous values of the random function s(t) are made at discrete moments of time $t_k = k\Delta t$ ($k = 1, 2, \ldots, H$; $H\Delta t = T$).

Let us define the sampling $s(t_k) = s_k$; $n(t_k) = n_k$; $m(t_k) = m_k$; $\mu(t_k) = \mu_k$. Considering Eq. (4), we can write Eq. (1) for a sampling in the form

$$s_k = n_k + m_k + \mu_k. \tag{5}$$

Let us define the correlation functions

$$\overline{n(t)\, n(t+\tau)} = R^n(\tau), \quad \overline{\mu(t)\, \mu(t+\tau)} = R^{\mu}(\tau) \tag{6}$$

and the corresponding correlation matrices and their inverse

$$R^n,\ R^{\mu},\ D^n = [R^n]^{-1}, \quad D^{\mu} = [R^{\mu}]^{-1}. \tag{7}$$

Because of the statistical independence of the random functions n(t) and μ(t), the correlation matrix $R^{n+\mu}$ of the sum n(t) + μ(t) will be equal to the sum of the correlation matrices of n(t) and μ(t), i.e.,

$$R^{n+\mu} = R^n + R^{\mu}. \tag{8}$$

To compute l(s), let us substitute into Eq. (2) the explicit expresssion for all the functions under the integral

$$\begin{gathered} P_{M+n}(s) = \frac{1}{(2\pi)^{\frac{H}{2}}\ \mathrm{Det}\,[R^n]^{\frac{1}{2}}} \exp\left\{-\frac{1}{2}\sum_{i,k=1}^{H} D_{ik}^{n}(s_i - M_i)(s_k - M_k)\right\}, \\ P_n(s) = P_{M+n}(s) \quad \text{when } M = 0, \\ P(\mu_1, \ldots, \mu_H) = \frac{1}{(2\pi)^{\frac{H}{2}}\ \mathrm{Det}\,[R^{\mu}]^{\frac{1}{2}}} \exp\left\{-\frac{1}{2}\sum_{i,\,k=1}^{H} D_{ik}^{\mu}\mu_i\mu_k\right\}. \end{gathered} \tag{9}$$

As a result of this substitution and some transformations, Eq. (2) becomes

$$l(s) = \Lambda_1(s)\, \Lambda_2(s - m), \tag{10}$$

where

$$\Lambda_1(s) = \exp\left\{\sum_{i,\,k=1}^{H} D_{ik}^{n} s_i m_k - \frac{1}{2}\sum_{i,\,k=1}^{H} D_{ik}^{n} m_i m_k\right\} \tag{11}$$

---

*The term "compound signal" has a different meaning in [1].

is the probability coefficient when M(t) equal m(t), i.e., for the case of simple detection on the background of correlated noise [3], and

$$\Lambda_2(\eta) = \frac{1}{(2\pi)^{\frac{H}{2}} \operatorname{Det}[R^{\mu}]^{\frac{1}{2}}} \int_{-\infty}^{\infty} \cdots \int \exp\left\{ \sum_{i,\,k=1}^{H} D^{n}_{ik} \eta_i \mu_k - \frac{1}{2} \sum_{i,\,k=1}^{H} (D^{n}_{ik} + D^{\mu}_{ik}) \mu_i \mu_k \right\} \times \times d\mu_1 \ldots d\mu_H \tag{12}$$

is the probability coefficient for detection of a signal of random shape, i.e., when M(t) = μ(t). For our case, η = s-m. To compute Eqs. (10), (11) and (12), let us define new variables from the rule

$$\mu_k = \sum_{\alpha=1}^{H} b_{k\alpha} \theta_\alpha. \tag{13}$$

Since the matrices R^n and R^{μ}, and consequently the matrices D^n and D^{μ}, are positively defined, it follows from the theory [7] that there exists a nonsingular matrix D with elements $b_{k\alpha}$ such that the following equations are satisfied:

$$B^{*} D^{n} B = E = [1, 1, \ldots, 1], \tag{14}$$

$$B^{*} D^{\mu} B = U = [u_1, \ldots, u_H], \tag{15}$$

where the numbers u_k are roots of the characteristic equation

$$\operatorname{Det}[D^{\mu} - U D^{n}] = 0 \tag{16}$$

and B* is the transposed matrix of B.

Using the notation

$$D^{n} B = [B^{*}]^{-1} = C; \quad D^{n} = CC^{*} \tag{17}$$

and performing the necessary computations, let us find the final expression for the probability coefficient

$$l(s) = \frac{\operatorname{Det}[R^{n}]^{\frac{1}{2}}}{\operatorname{Det}[R^{\mu}]^{\frac{1}{2}} \prod_{\alpha=1}^{H} \sqrt{1 + u_\alpha}} \times \times \exp \frac{1}{2} \left\{ \sum_{\alpha=1}^{H} \left(\frac{x_\alpha}{\sqrt{1 + u_\alpha}} + \frac{u_\alpha}{\sqrt{1 + u_\alpha}} \nu_\alpha \right)^2 - \sum_{\alpha=1}^{H} \nu_\alpha^2 u_\alpha \right\}, \tag{18}$$

where

$$x_\alpha = \sum_{i=1}^{H} C_{i\alpha} s_i; \quad \nu_\alpha = \sum_{i=1}^{H} C_{i\alpha} m_i. \tag{19}$$

From Eq. (19) for ν_α, it follows that ν_α does not depend on the input signal s(t). From Eq. (18) it follows that l(s) increases monotonically with the quantity

$$\varphi = \sum_{\alpha=1}^{H} W_\alpha^{2}, \tag{20}$$

where

$$W_\alpha = \frac{1}{\sqrt{1 + u_\alpha}} (x_\alpha + u_\alpha \nu_\alpha). \tag{21}$$

Eqs. (20) and (21) determine the structure of an optimal receiver for detecting a compound signal. It follows from these equations that the optimal procedure for processing the input signal s(t) in the given case consists of both linear and nonlinear operations, the linear operations occurring both before detection and after detection. It is known that for optimal detection of a signal with a given shape, linear processing alone is sufficient. From Eq. (21), it follows that the presence of a determined component (ν_α) affects the general scheme of processing by introducing the additional linear operation of summing χ_α with the quantities $u_\alpha v_\alpha$ before detection. Let us also note that Eqs. (20) and (21) can be transformed, so as to retain only terms depending on s;

$$\varphi'(s) = \sum_{\alpha=1}^{H} \frac{x_\alpha^2}{1+u_\alpha} + 2\sum_{\alpha=1}^{H} \frac{u_\alpha x_\alpha v_\alpha}{1+u_\alpha}. \qquad (22)$$

The first term determines the structure of an optimal receiver in the detection of a single signal of random shape. The second, a correlation term, determines the additional linear elements of an optimal receiver in detecting a compound signal.

For the subsequent discussion, it is necessary to study the statistical properties of the random quantities W_α and φ.

2. NUMERICAL CHARACTERISTICS OF THE QUANTITIES W_α AND φ.

The random quantities χ_α are normal because they are formed linearly from the normal random quantities s_i in Eq. (19). Consequently, the quantities formed from Eqs. (21) are also normal.

1) The numerical characteristics W_α and φ in the case where the input signal is $s(t) = n(t) + m(t) = \mu(t)$.

The average value of W_α is

$$\overline{W}_\alpha = v_\alpha \sqrt{1+u_\alpha}. \qquad (23)$$

Let us now find the correlation function of the quantity W_α and φ.

$$\overline{\Delta W_\alpha \Delta W_\beta} = \begin{cases} \overline{(\Delta W_\alpha)^2} = \dfrac{1}{u_\alpha} & \text{for } \beta = \alpha, \\ 0 & \text{for } \beta \neq \alpha. \end{cases} \qquad (24)$$

From Eqs. (23) and (24), it directly follows that

$$a_1 = \bar{\varphi} = \sum_{\alpha=1}^{H} \overline{W_\alpha^2} = \sum_{\alpha=1}^{H} \left[\frac{1}{u_\alpha} + v_\alpha^2 (1+u_\alpha)\right], \qquad (25)$$

$$\sigma_1^2 = \overline{(\varphi - \bar{\varphi})^2} = 2\sum_{\alpha=1}^{H} \left[\frac{1}{u_\alpha^2} + 2v_\alpha^2 \frac{1+u_\alpha}{u_\alpha}\right]. \qquad (26)$$

2) The numerical characteristics W_α and φ in the case where the input signal $s(t) = n(t)$.

The average value of W_α is

$$\overline{W}_\alpha = \frac{v_\alpha u_\alpha}{\sqrt{1+u_\alpha}}. \qquad (27)$$

The correlation function of the quantities W_α and W_β is

$$\overline{\Delta W_\alpha \Delta W_\beta} = \begin{cases} \overline{(\Delta W_\alpha)^2} = \dfrac{1}{1+u_\alpha} & \text{for } \beta = \alpha, \\ 0 & \text{for } \beta \neq \alpha. \end{cases} \qquad (28)$$

On the basis of (27) and (28), we obtain

$$a_2 = \bar{\varphi} = \sum_{\alpha=1}^{H} \overline{W_\alpha^2} = \sum_{\alpha=1}^{H} \left[\frac{1}{1+u_\alpha} + \frac{u_\alpha^2 v_\alpha^2}{1+u_\alpha} \right], \tag{29}$$

$$\sigma_2^2 = \overline{(\varphi - \bar{\varphi})^2} = 2 \sum_{\alpha=1}^{H} \left[\frac{1}{(1+u_\alpha)^2} + 2 \frac{u_\alpha^2 v_\alpha^2}{(1+u_\alpha)^2} \right], \tag{30}$$

From Eqs. (24) and (28), it follows that the random quantities W_α are uncorrelated, and, consequently, since they are normal, they are all independent.

3. CHARACTERISTICS OF DETECTION IN SPECIAL CASES

According to Eqs. (18), (20) and (21), an optimal receiver can determine the presence or absence of the useful signal according to the following scheme:

if $\varphi \geq \varphi_0$, then, $s = M + n$

if $\varphi < \varphi_0$, then, $s = n$

where φ_0 is the threshhold value of φ.

1. We shall regard H as a large number and use Gauss's law as an approximation with the distribution function of φ on the basis of Lyapunov's theorem and (20), (24) and (28). The number H is determined in works [8] for given values of the probability of detection D, the probability of false alarm F, and the quantities a_1, a_2, σ_1^2, and σ_2^2, when a normal distribution is used to approximate the distribution law of φ (these distribution laws being necessary to distinguish hypotheses). Let us note that a normal distribution is a fairly accurate approximation of the true distribution function only in the region of φ close to $\bar{\varphi}$. This gives rise to difficulties in computing the probability of false alarm F, which assumes small values (10^{-6} - 10^{-4}) in practice.* At the same time, it can be assumed that $H \simeq 20$ [9]. with an accuracy within 10% for values of $D = 0.9$. Considering that the value of the distribution function changes slowly in the region of small values of F and confining ourselves to the above-mentioned accuracy, we obtain

$$F \quad \frac{1}{\sqrt{2\pi}} \int_{\frac{\varphi_0 - a_2}{\sigma_2}}^{\infty} e^{-\frac{t^2}{2}} dt, \tag{31}$$

where α_2 and σ_2 are computed from Eqs. (29) and (30), and

$$D = \frac{1}{\sqrt{2\pi}} \int_{\frac{\varphi_0 - a_1}{\sigma_1}}^{\infty} e^{-\frac{t^2}{2}} dt, \tag{32}$$

where α_1 and σ_1 are computed from Eqs. (25) and (26). Eliminating the parameter φ_0 from (31) and (32), we find the characteristic of the detection of a compound signal, this characteristic depending on 2 H parameters in the general case,

$$D = D\,(F;\, u_1, \ldots, u_H;\, v_1, \ldots, v_H). \tag{33}$$

In many practical cases, the number of parameters of Equation (33) can be reduced. Indeed, if it is assumed that $\sigma_1^2 \simeq \sigma_2^2$, there exists a single parameter which plays the role of the effective signal-to-noise ratio

---

*A considerable amount of attention is devoted to the approximation of actual distribution functions by Gauss' law in [5].

$$d = \frac{[a_1 - a_2]^2}{\sigma_1^2} \simeq \frac{[a_1 - a_2]^2}{\sigma_2^2}. \tag{34}$$

Equation (34) is easily obtained from Eqs. (31) and (32) for $\sigma_1^2 \simeq \sigma_2^2$.

On the basis of Equations (26) and (30), we conclude that the condition $\sigma_1^2 \simeq \sigma_2^2$ implies the requirements

$$u_{\min} \gg 1, \tag{35}$$

where $u_{\min}$ is the smallest root of Equation (16).

To explain the physical meaning of this requirement, let us assume that the matrices R^n and R^μ commute, and let $\nu_\alpha{}^n$ and $\nu_\alpha{}^\mu$ be their characteristic numbers ($\nu_\alpha{}^n > 0$, $\nu_\alpha{}^\mu > 0$). Then

$$u_\alpha = \frac{\nu_\alpha^n}{\nu_\alpha^\mu}, \quad \alpha = 1, 2, \ldots, H. \tag{36}$$

Let us consider the trace of the matrices R^n and R^μ:

$$SpR^n = HN = \sum_{\alpha=1}^{H} \nu_\alpha^n, \quad SpR^\mu = HP = \sum_{\alpha=1}^{H} \nu_\alpha^\mu,$$

where N and P are the average power of the noise n(t) and the average power of the signal component $\mu(t)$, respectively. Hence, it follows that

$$N = \sum_{\alpha=1}^{H} \left(\frac{\nu_\alpha^n}{H}\right), \quad P = \sum_{\alpha=1}^{H} \left(\frac{\nu_\alpha^\mu}{H}\right). \tag{37}$$

Equations (37) show that the average power of the noise and the average power of the random component of the signal are sums of the "partial powers" belonging to one "degree of freedom".

Equation (36) gives the ratio of the partial powers of the noise to the partial powers of the components of the useful signal $\mu(t)$. Thus, the assumption of the condition $\sigma_1^2 \simeq \sigma_2^2$ means that we are considering the case where any of the partial signal-to-noise ratios is much smaller than unity, i.e., on the basis of (37), the ratio $P/N \ll 1$ (the threshhold signal). In practice the above conditions are realized, when, for instance, an object is detected in the presence of random reflections from a "cloud of reflectors" [5]. The small volume of the cloud of reflectors is absorbed by the object, and the reflections which take place during this process must be related to the useful signal rather than to the noise. Since the volume of the part of the cloud of reflectors producing the useful signal is small relative to the volume producing the noise, it is natural to assume that $P/N \ll 1$.

We emphasize that all we have said holds only for the $\mu(t)$ component of the useful signal. No restrictions are placed on the signal component m(t).

Substituting the values of a_1, a_2 and $\sigma_1^2 \simeq \sigma_2^2$ into (34), and considering (35), we can simplify Equation (34):

$$d = r + \rho,$$

$$r = \frac{1}{2} \sum_{\alpha=1}^{H} \frac{1}{u_\alpha^2}; \quad \rho = \sum_{i,k=1}^{H} D_{ik}^n m_i m_k. \tag{38}$$

We note that the quantity r depends only on the properties of the random functions $\mu(t)$ and n(t), while the quantity ρ depends wholly on the properties of the random function n(t) and the deterministic function m(t).

If the deterministic part of the useful signal predominates, i.e., $M(t) \simeq m(t)$, then obviously, $r \ll \rho$ and from Eq. (38) it follows that $d = \rho$. The quantity ρ was defined in article [3] and is called the generalized signal-to-noise ratio in simple detection.*

---

*In article [3], the quantity ρ is denoted by the letter μ.

If the random component of the useful signal predominates, i.e., $M(t) \simeq \mu(t)$ and $r \gg \rho$, we will have

$$d = r = \frac{1}{2} \sum_{\alpha=1}^{H} \frac{1}{u_\alpha^2}. \tag{39}$$

Thus, the quantity r can be called the "effective signal-to-noise ratio" in the detection of a random signal on a background of correlated noise.

Equation (38) shows that, under the assumption of the above conditions, effective signal-to-noise ratios of the components of the useful signal can be added.

2. Within the framework of the practical examples described above, it is natural to regard the energy spectra of the random functions $\mu(t)$ and $n(t)$ as similar to one another:

$$G^\mu(\omega) = \gamma G^n(\omega), \tag{40}$$

where $\gamma = 0$.

The assumption of this condition is based on the fact that the nature of the random function $\mu(t)$ and $n(t)$ is identical, i.e., they are produced by different parts of the same cloud of reflection.

When condition (4) is satisfied, the matrices R^n and R^μ commute, and it is easily shown that as a result, we have

$$\frac{1}{u_1} = \cdots = \frac{1}{u_H} = \gamma = \frac{P}{N}. \tag{41}$$

On the basis of Eqs. (24) and (28), we conclude that the dispersion of the random quantities W_α will be identical for $\alpha = 1, 2, \ldots, H$. This makes it possible to abandon a normal approximation of the distribution function of φ. To find the probabilities of D and F we shall use the function $\psi = \varphi^{1/2}$ as an adequate approximation. The distribution function of ψ is given in work [10]. On the basis of [10] in Eq. (41), we have

$$F = \frac{(1+\gamma)\exp\left[-\frac{A_2^2(1+\gamma)}{2\gamma}\right]}{\gamma A_2^{\frac{H-2}{2}}} \int_{\psi_0}^{\infty} Z^{\frac{H}{2}} e^{-\frac{Z^2(1+\gamma)}{2\gamma}} I_{\frac{H-2}{2}}\left[\frac{(1+\gamma)ZA_2}{\gamma}\right] dZ, \tag{42}$$

$$D = \frac{\exp\left[-\frac{A_1^2}{2\gamma}\right]}{\gamma A_1^{\frac{H-2}{2}}} \int_{\psi_0}^{\infty} Z^{\frac{H}{2}} e^{-\frac{Z^2}{2\gamma}} I_{\frac{H-2}{2}}\left(\frac{ZA_1}{\gamma}\right) dZ, \tag{43}$$

where ψ_0 is the threshhold value of ψ, $I_n(Z)$ is a modified Bessel function of order n, and the quantity A is

$$A = \left[\sum_{\alpha=1}^{H} \overline{W}_\alpha^2\right]^{\frac{1}{2}}. \tag{44}$$

On the basis of (23), (27), (41) and (44), we obtain

$$A_1 = \left[\frac{1+\gamma}{\gamma}\rho\right]^{\frac{1}{2}}, \quad A_2 = \left[\frac{\rho}{\gamma(1+\gamma)}\right]^{\frac{1}{2}}. \tag{45}$$

It is easily seen that the detection characteristic for this case will have three parameters

$$D = D(F; \gamma; \rho; H). \tag{46}$$

If there is no deterministic component of the useful signal, the probabilities D and F are computed from the distribution of χ^2 with H degrees of freedom.

CONCLUSION

The theory of optimal detection of a compound signal in the presence of correlated noise is considered. The components of the compound signal can be represented separately by signals having maximum and minimum probabilities of correct detection [4]. In special cases, the equations giving the probability of correct detection, the probability of false alarm and the effective signal-to-noise ratio are found. Equation (10) is still correct when it is assumed that the function m(t) has unknown parameters. Thus it is possible to generalize Eq. (18) without any special difficulty to cases in which the initial phase of m(t) is unknown or in which one of the samplings m_k ($k = 1, 2, 3 \ldots H$) is random.

The author uses this opportunity to thank N.N. Porfir'yeva and V.A. Sokolova for their help.

BIBLIOGRAPHY

1. V.A. Kotel'nikov. Theory of Potential Noise, GEI, 1956.
2. V. Peterson, T. Birdsal and B. Fawkes. Theory of signal detection. Information Theory and its Application, edited by A.A. Kharkevich, GIFML, 1959.
3. V.D. Zubakov. Optimal detection in the presence of correlated noise. Radiotekhnika i Elektronika, 1958, 3, 12, 1441.
4. V.A. Kotel'nikov, Signals with maximum and minimum probabilities of detection. Radiotekhnika i Elektronika, 1959, 4, 3, 354.
5. L.A. Vaynshteyn and V.D. Zubakov. The detection of signals on the background of random noise. Izd. Soviet Radio, 1960.
6. V.G. Sragovich. The optimal detection of signals on the background of correlated Gaussian noise. Radiotekhnika i Elektronika, 1959, 4, 5, 745.
7. V.I. Smirnov. Course in Higher Mathematics, Vol. 3, Part 1, GITTL, 1951.
8. A.A. Petrov. Verification of statistical hypothesis on the nature of a distribution from small samplings. Theory of Probability and Applications, 1956, 1, 2, 248
9. Threshhold Signals. Trans. from English under edit. A.P. Sivers, 1952.
10. K.S. Miller, R.I. Bernstein, L.E. Blumenson, Generalized Rayleigh processes, Quart. Appl. Math., 1958, 16, 2, 137.

Submitted on November 14, 1959

OPTIMAL RECEPTION OF A NARROWBAND SIGNAL OF UNKNOWN FREQUENCY ON A BACKGROUND OF NOISE

R. L. Stratonovich

The a posteriori probability distribution function for the frequency of a narrowband signal distorted by noise is found. A differential equation for the optimal nonlinear filter discrimination is found and a tracking system providing optimal processing of the received signal is proposed.

INTRODUCTION

Narrowband signals of the form $s(t) = A \cos(\omega t + \varphi)$ are used very frequently in radio engineering. The useful information in these signals is contained in the values of the amplitude A, the phase φ or the frequency ω. When the observer receives a total signal $r(t) = = s(t) + n(t)$, distorted by noise $n(t)$, the problem of optimal separation of the useful signal $s(t)$ arises. Here, a large number of different special cases is possible, since the signal parameters can be unknown or partly known and constant or unconstant, while the noise can be Gaussian or non-Gaussian and white or correlated. In some of the most simple cases, the problem of optimal filter discrimination is solved by the use of well-known, so-called "classical" methods. When the frequency ω is known and the "Cartesian coordinates" $\chi = A \cos \varphi$ and $y = -A \sin \varphi$ represent Gaussian random quantities or processes in the presence of Gaussian noise, the Wiener-Kolmogorov theory of linear discrimination is sufficient. However, it is sufficient to assume that the amplitude A is also known a priori, i.e., that it has a delta-type distribution function rather than a Rayleigh distribution function for the linear theory to be insufficient. The equations for nonlinear filter discrimination corresponding to this special case are considered in [1]. In the general case where all three parameters, $A\varphi$, and ω of the useful signal present an interest to the observer and must be determined, the problem can be solved by obtaining analogs of the system of equations for optimal nonlinear filter discrimination described in [1, 2].

In this article, we shall consider the case where the observer is chiefly interested in the frequency of the useful signal. Of course, in this case as well it is possible to obtain analogs of the system of equations for all three parameters at once, and then to use only the value of the frequency. However, the optimal system in this case will be fairly complicated. Therefore, we shall indicate another way of solving the problem, subjecting the theory of [1] to modifications which are convenient for the special case.*

---

*In article [5] which was published after this article had been typeset, it is assumed that the rate of change of the frequency is constant. Thus, the case of variable frequency reduces to the case of constant parameters considered in [2].

To separate a narrowband signal with an unknown frequency from noise, reception with synchronization is sometimes used. The received signal is fed to an oscillator operating in a locking regime, as a result of which the frequency of the oscillator is approximately the same as the frequency of the useful signal. However, this method of receiving is not optimal. This follows from the mere fact that the parameters of the system (the oscillator) are taken to be independent of the intensity of the noise and the velocity of the a priori changes in frequency.

In this article, optimal receiving systems designed according to a different principle are proposed, namely according to the principle of tracking of the most probable value of the frequency. For this tracking, a frequency discriminator controlled by back coupling can be used. The optimal back coupling can be computed theoretically from the equation for optimal filtered discrimination. It is variable in accordance with the fact that the significance of the received information is not constant in time. The other distinguishing feature of the system is the fact that the mismatching Δ of the natural frequencies of the discriminator circuits is not directly related to the time of the a priori variation in frequency and to the attenuation of the circuits. The system will operate correctly when the mismatching Δ is smaller than the difference between the estimated frequency and the true frequency.

The proposed system is characterized by certain difficulties connected with the initial time of work, since the initial time of the estimated frequencies may be far from the true frequencies and at first the system will operate in a nonoptimal regime. We shall not consider these difficulties. We shall assume that for the initial detection of the signal and rough estimation of its frequency, one of the already known systems is used, for instance, the system of parallel circuits [3]. The system proposed by us is then connected to improve the value of the frequency and to follow its changes. The system will operate in a nonstationary regime. Our principle of tracking the frequency is to some extent an echo of the previously expressed idea of tracking tuning [4]. However, the resemblance is rather superficial. The system of [4] is nonoptimal, since it does not make use of data on the noise intensity and the rate of change of the frequency. In the light of our recommendations, the idea of tracking tuning acquired fundamentally new significance.

1. A POSTERIORI PROBABILITY DENSITY FOR THE FREQUENCY

The problem of filter discrimination of a narrowband signal will be most complicated in the case where its frequency will be a priori unknown. In the future we shall confine ourselves to this case, assuming in addition that the phase of the signal has a uniform distribution and that it does not carry any information, and thus presents no interest. To start with, until specially specified, we shall assume that the signal parameters, are constant, having an a priori distribution density

$$w_{\rm pr}(A, \varphi, \omega) = \frac{1}{2\pi} w_{\rm pr}(A)\, w_{\rm pr}(\omega). \tag{1}$$

Suppose that the distorted signal $r(t) = s(t) + n(t)$ during a time signal $0 < t < T$. After the reception the frequency ω remains a random quantity described by the a posteriori distribution density $w_{\rm ps}(\omega, T)$, which must be determined.

If the noise $n(t)$ is a Markov process, it corresponds to a probability functional $W[n(t)]$ [2], which will be used to find the a posteriori distribution. Considering the statistical independence between the signal and the noise, we can write the joint distribution of the noise and the signal parameters, A, φ, and ω in the form

$$\text{const}\, w_{\rm pr}(A, \varphi, \omega)\, W\,[n(t)].$$

Substituting $n(t) = r(t) - s(t)$ into this, we find the a posteriori distribution of the signal parameters from the inverse probability theorem:

$$w_{\rm ps}(A, \varphi, \omega) = \text{const}\, w_{\rm pr}(A, \varphi, \omega)\, W\,[r(t) - A\cos(\omega t + \varphi)]. \tag{2}$$

To obtain the a posteriori distribution of the function, it is still necessary to consider (1) and to integrate Eq. (2) over A and φ. Let us consider separate special cases.

1. Let A, φ, and ω be constant, and let $n(t)$ be white noise with a correlation function

Then

$$W\,[n\,(t)] = \exp\left\{-\frac{1}{N_0}\int_0^T n^2(t)\,dt\right\}. \tag{3}$$

In this case Eq. (2) gives

$$w_{\text{ps}}\,(A,\,\varphi,\,\omega) = \text{const}\;w_{\text{pr}}\,(A,\,\varphi,\,\omega)\,\exp\left\{-\frac{A^2}{N_0}\int_0^T \cos^2(\omega t+\varphi)\,dt + \right.$$
$$\left. + 2\,\frac{A}{N_0}\int_0^T \cos\,(\omega t+\varphi)\,r\,(t)\,dt\right\}. \tag{4}$$

Using the narrowband condition, the integral $\int_0^T \cos^2(\omega t+\varphi)\,dt$ can be replaced by T/2 for $\omega T \gg 1$. After this we obtain (4)

$$w_{\text{ps}}\,(\omega) = \text{const}\;w_{\text{pr}}\,(\omega)\left\langle \exp\left\{-\frac{A^2T}{2N_0} + 2\,\frac{A}{N_0}\int_0^T \cos\,(\omega t+\varphi)\,r\,(t)\,dt\right\}\right\rangle, \tag{5}$$

where the skew brackets indicate the average over the a priori distribution of the amplitude and the phase. This equation leads to the following results.

a) When the amplitude A = A is known, only the integral over φ remains in (5). This integral is expressed in terms of a Bessel function with an imaginary argument $I_0(z) = J_0(iz)$, according to the well-known formula. Therefore,

$$w_{\text{ps}}\,(\omega) = \text{const}\;w_{\text{pr}}\,(\omega)\;I_0\left(2\,\frac{A_0}{N_0}\,E_T\,(\omega)\right), \tag{6}$$

where

$$E_T^2\,(\omega) = \left(\int_0^T \cos\,\omega t\,r\,(t)\,dt\right)^2 + \left(\int_0^T \sin\,\omega t\,r\,(t)\,dt\right)^2 =$$
$$= \int_0^T\!\!\int_0^T \cos\,\omega\,(t-t')\,r\,(t)\,r\,(t')\,dt\,dt'. \tag{7}$$

Under the conditions $\overline{A^2}T/N_0 \gg 1$, which can be called the conditions for good filter discrimination, the argument of the Bessel function is considerably greater than unity, and it is impossible to use the well-known asymptotic expression for the Bessel function. This gives

$$w_{\text{ps}}\,(\omega) = \text{const}\;w_{\text{pr}}\,(\omega)\;e^{2\,\frac{2A_0}{N_0}E_T\,(\omega)}. \tag{8}$$

b) Let χ = A cos φ and y = -A sin φ be independent random Gaussian quantities with a variance σ^2. This corresponds to a Rayleigh distribution of the amplitude ($\overline{A^2} = 2\sigma^2$). Equation (5) can be written in the form

$$w_{\text{ps}}\,(\omega) = \text{const}\;w_{\text{pr}}\,(\omega)\left\langle \exp\left\{-\frac{T}{2N_0}\,(x^2+y^2) + \frac{2x}{N_0}\int_0^T \cos\,\omega t\,r\,(t)\,dt + \right.\right.$$
$$\left.\left. + \frac{2y}{N_0}\int_0^T \sin\,\omega t\,r\,(t)\,dt\right\}\right\rangle. \tag{9}$$

If we take the integral

$$\frac{1}{\sqrt{2\pi}\sigma}\int_{-\infty}^{\infty}\exp\left\{-\frac{x^2}{2\sigma^2}-\frac{T}{2N_0}x^2+ux\right\}dx=\left(1+\frac{\sigma^2T}{N_0}\right)^{-1/2}\exp\left[\frac{u^2\sigma^2}{2\left(1+\frac{\sigma^2T}{N_0}\right)}\right],$$

we obtain

$$w_{\text{ps}}(\omega)=\text{const}\, w_{\text{pr}}(\omega)\exp\left[\frac{2\sigma^2E_T^2(\omega)}{N_0(\sigma^2T+N_0)}\right]. \tag{10}$$

In the special case where the a priori spread of amplitude is large ($\sigma^2T \gg N_0$) we have

$$w_{\text{ps}}(\omega)=\text{const}\, w_{\text{pr}}(\omega)\exp\left[\frac{2E_T^2(\omega)}{N_0T}\right]. \tag{11}$$

c) These results can be generalized to the case of a correlated Gaussian noise n(t). In Appendix 1, it is shown that if the time of observation T is considerably greater than the correlation time of the noise, $T \gg \tau_{\text{cor}}$, the equations retain the same form. The only change consists of replacing N_0 by a spectral density

$$S_n(\omega)=2\int_{-\infty}^{\infty}e^{i\omega\tau}\langle nn_\tau\rangle\,dt, \tag{12}$$

which is nonuniform in the range of possible values of the frequency. In particular, Eq. (11) becomes

$$w_{\text{ps}}(\omega)=\text{const}\, w_{\text{pr}}(\omega)\exp\left[\frac{2E_T^2(\omega)}{S_n(\omega)T}\right]. \tag{13}$$

2. Let us now consider the case of a priori nonconstant amplitude of phase, or in other words the case of variable $\chi = A\cos\varphi$ and $y = A\sin\varphi$. Suppose that the latter quantities are independent stationary Gaussian processes whose average values are zero and whose correlation function is

$$\langle xx_\tau\rangle=\langle yy_\tau\rangle=k_0(\tau)=\sigma^2R\,(\tau). \tag{14}$$

We note that the correlation function of the useful signal for this case is expressed by the equation

$$\langle ss_\tau\rangle=k_s(\tau)=k_0(\tau)\cos\omega\tau. \tag{15}$$

If n(t) is white noise, we obtain for the a posteriori distribution of the frequency, the equation

$$w_{\text{ps}}(\omega)=\text{const}\, w_{\text{pr}}(\omega)\left\langle\exp\left\{-\frac{1}{2N_0}\int_0^T(x^2+y^2)\,dt+\right.\right.$$
$$\left.\left.+\frac{2}{N_0}\int_0^T x(t)\cos\omega t\, r(t)\,dt+\frac{2}{N_0}\int_0^T y(t)\sin\omega t\, r(t)dt\right\}\right\rangle, \tag{16}$$

which serves as a generalization of Eq. (9). Here the average is taken over the random functions x(t) and y(t).

The computation of the mean in (16) according to the method shown in Appendix 2, leads to the result

$$w_{\mathrm{ps}}(\omega) = \mathrm{const}\, w_{\mathrm{pr}}(\omega) \times$$
$$\times \exp\left\{\frac{2}{N_0^2}\int_0^T\int_0^T k_1(t,\, t')\cos\omega\,(t-t')\, r(t)\, r(t')\, dt\, dt'\right\}. \tag{17}$$

Here, in the case of intervals T considerably larger than the correlation time τ_a of the fluctuations in amplitude and phase, k_1 is determined from the equation

$$k_1(t,\, t') = \frac{1}{4\pi}\int_{-\infty}^{\infty} e^{-i\omega(t-t')} S_1(\omega)\, d\omega;\;\; S_1(\omega) = \frac{S_0(\omega)}{1+\dfrac{S_0(\omega)}{2N_0}} \tag{18}$$

$$\left(S_0(\omega) = 2\int_{-\infty}^{\infty} e^{i\omega\tau} k_0(\tau)\, d\tau\right).$$

For small intervals $T \ll \tau_a$, the variations of the amplitude and the phase have no effect and Eq. (10) can be used. For intermediate values $T \sim \tau_a$, there is a transition from $k_1 = \left(\frac{T}{N_0} + \frac{1}{\sigma_2}\right)^{-1}$ to Eq. (18), $k_1(t,\, t')$ being found as a solution of integral equation XII in Appendix 2. In the special case where $k_0(\tau) = \sigma^2 e^{-\gamma|\tau|}$ we find, using (18)

$$S_1(\omega) = \frac{4\gamma\sigma^2}{\omega^2+\gamma^2+\dfrac{2\gamma\sigma^2}{N_0}},$$

$$k_1(\tau) = \sigma_1^2 e^{-\gamma_1|\tau|},$$

$$\gamma_1 = \sqrt{\gamma^2 + \frac{2\gamma\sigma^2}{N_0}},$$

$$\sigma_1^2 = \frac{\gamma}{\gamma_1}\sigma^2. \tag{19}$$

3. So far, we have regarded the frequency ω as an a priori constant quantity. The opposite case, where the frequency is variable, is more difficult to analyze. To avoid complications connected with accurately accounting for variations in frequency, and yet in order to still take into account the finiteness of the time intervals with the duration of the order of $\tau_\omega = 1/\beta$, during which ω remains approximately constant, it is necessary to take the integration in the previously found equations over the interval $T - \tau_\omega < t < T$ rather than over the entire integral $0 < t < T$. The finiteness of τ_ω can also be taken into account by introducing a "cutoff" factor $e^{-\beta(T-t)}$, which describes the decrease of the role of the previous values of the signal in the determination of the frequency. Then, in all the corresponding equations, it is necessary to substitute, in place of Eq. (7)

$$E_T^2(\omega) = \int_0^T\int_0^T e^{-\beta(T-t)-\beta(T-t')}\cos\omega\,(t-t')\, r(t)\, r(t')\, dt dt' \equiv X^2 + Y^2, \tag{20}$$

where

$$X = \int_0^T e^{-\beta(T-t)}\cos\omega\,(T-t)\, r(t)\, dt;$$

$$Y = \int_0^T e^{-\beta(T-t)}\sin\omega\,(T-t)\, r(t)\, dt. \tag{21}$$

For $T \gg 1/\beta$, the lower limit of integration can be extended to $-\infty$. In this case, the following equation can be used instead of (11):

$$w_{ps}(\omega) = \text{const}\, w_{pr}(\omega) \exp\left[\frac{2}{N_0}\frac{2\beta}{1-e^{-2\beta T}} E_T^2(\omega)\right]. \tag{22}$$

2. THE EQUATION FOR OPTIMAL FILTER DISCRIMINATION. OPTIMAL SYSTEMS

1. Our discussion has shown that it is possible to obtain an analytic expression for the a posteriori distribution of the parameter with which we are concerned as a result of theoretical study. This expression is conveniently written in the form

$$w_{ps}(\omega) = \text{const}\, e^{\Phi(\omega,\, T)} \tag{23}$$

and it can be used for the computation and designing of systems with optimal filter discrimination. The results already obtained give various examples of equations $\Phi(\omega, T)$. Thus, if we specifically select Eq. (11), we obtain

$$\Phi(\omega, T) = \ln \omega_{pr}(\omega) + \frac{2}{N_0 T} E_T^2(\omega). \tag{24}$$

The second term, which depends on the received signal, generally has a much sharper maximum than the first term, which corresponds to a priori data. The condition of the form $\overline{A^2}T/N_0 \gg 1$ under which this occurs can be called the condition for noise which in relative terms is not too large. This condition must be satisfied in cases where filter discrimination of good quality and satisfactory work of the entire system are required. When it is satisfied, the a priori data do not play an important role and it is not necessary to take them into account. Let us note that, when this condition is satisfied, there is no longer any point in an accurate selection of the criterion for optimal operations, since different criteria will lead to practically the same results. To be specific in our calculations, we shall use the criterion of maximum probability.

After reception of the signal r(t) in the integral $0 < t < T$, it is necessary to indicate the estimated value of the frequency corresponding to the form of the signal r(t). This value of the frequency depends on T, and we shall denote it by $\omega_0 T$. If we determine this frequency from the condition of the extrema of Eq. (23), we have

$$\frac{\partial \Phi(\omega, T)}{\partial \omega} = 0 \text{ when } \omega = \omega_0(T). \tag{25}$$

With increasing time T, the value of $\omega_0(T)$ changes, since our a posteriori information is changed and improved. An optimal system, which in the last analysis operates according to the principle of the tracking system, must follow these changes. Differentiating Eq. (25) with respect to T, we obtain the differential equation

$$\frac{d\omega_0(T)}{dT} = \alpha(T)\, \frac{\partial^2 \Phi(\omega_0(T), T)}{\partial \omega \partial T} \tag{26}$$

where

$$\frac{1}{\alpha(T)} = a(T) = -\frac{\partial^2 \Phi(\omega_0(T), T)}{\partial \omega^2}. \tag{27}$$

The quantity α(T) [or a(T)] has a direct physical meaning. It describes the a posteriori inacurracy of $\Delta\omega$ in the determination of the parameter $\omega(\Delta\omega = \sqrt{\alpha(T)})$. By differentiating (27) with respect to T, it is possible to obtain an equation for α(T):

$$\frac{d}{dT}\left(\frac{1}{\alpha}\right) = \frac{da}{dT} = -\frac{\partial^3 \Phi(\omega_0, T)}{\partial \omega^2 \partial T} \tag{28}$$

where the term $\frac{\partial^3\Phi}{\partial\omega^3}\frac{\partial\omega_0}{\partial T}$ .has been neglected.

Equations (26) and (28) represent the equation for optimal filter discrimination in the Gaussian approximation. They are derived in [1, 2] by another method. An optimal system must be designed in accordance with these equations. The right member of (26) shows that the extremum of ω_0, which gives the maximum of the derivative $\partial\Phi/\omega T$ is followed. The mismatch signal in this process is proportional to $\partial^2\Phi/\partial\omega\partial T$. The corresponding transfer constant $\alpha(T)$ depends on time. The exact value of this coefficient and its dependence on r(t) do not play a fundamental role in the tracking process. In this respect an optimal system in the type we are considering is flexible. It is only important that the following orders of magnitude be maintained:

$$\alpha(T) \sim (\Delta\omega)^2. \tag{29}$$

The lack of sensitivity with respect to $\alpha(T)$ makes it possible to simplify the problem of designing optimal systems. Indeed, it is necessary to consider only Eq. (26) rather than both Eqs. (26) and (28), since an exact determination of $\alpha(T)$ is not necessary and from average values

$$\frac{1}{\alpha(T)} = -\frac{\overline{\partial^2\Phi(\omega_0, T)}}{\partial\omega^2}. \tag{30}$$

can be taken instead of (27).

2. Here, $\Phi(\omega, T)$ should be taken to represent the specific equations obtained in the previous section. For example, (24), Eq. (26) has the form

$$\frac{d\omega_0}{dT} = \frac{2\alpha}{N_0T}\frac{\partial}{\partial\omega}\left[E_T\frac{\partial E_T}{\partial T} + E_T T\frac{\partial}{\partial T}\left(\frac{E_T}{T}\right)\right]. \tag{31}$$

Analysis shows that the first term in this equation is of crucial importance in filter discrimination. Therefore, we shall consider the problem of obtaining the analog of the optimal filter-discrimination equation on the basis of the very simple equation

$$\frac{d\omega_0}{dT} = \frac{2\alpha}{N_0T}\frac{\partial}{\partial\omega}\left(E_T\frac{\partial E_T}{\partial T}\right), \tag{32}$$

where, according to (30)

$$\frac{N_0T}{2\alpha} = \frac{1}{\lambda} = -\frac{\partial^2}{\partial\omega^2}\overline{E_T^2}. \tag{33}$$

In the case of more complicated expressions of $\Phi(\omega, T)$ and more complicated filter-discrimination equations, the problem is solved in basically the same way, but there may be additional complications in the filter-discriminating system.

Using Eq. (7) and defining

$$X = \int_0^T \cos\omega_0(T-t)\,r(t)\,dt,\quad Y = \int_0^T \sin\omega_0(T-t)\,r(t)\,dt, \tag{34}$$

we have

$$E_T^2 = X^2 + Y^2,\quad \frac{\partial(E_T^2)}{\partial T} = 2rX. \tag{35}$$

Therefore, Eq. (32) becomes

$$\frac{\partial\omega_0}{\partial T} = \lambda\frac{\partial}{\partial\omega_0}(rX). \tag{36}$$

From (34), it follows that X = X(T) is a solution of the differential equation

$$\frac{d^2X(t)}{dt^2} + \omega_0^2 X(t) = \frac{dr(t)}{dt}. \tag{37}$$

This equation includes the quantities $\omega_0 = \omega_0(T)$ and X(t), which refer to different moments of time. Therefore, the process of obtaining the analog of this equation entails additional difficulties, since a time lag is required. When $\omega_0(T)$ is a relatively slowly changing quantity, Eq. (37) can be transformed to

$$\frac{d^2X(t)}{dt^2} + \omega_0^2(t)\, X(t) = \frac{dr(t)}{dt}, \tag{38}$$

for which an analog is much easier to obtain. The error connected with the substitution is fully justified by the simplification of the optimal system.

To obtain the equation from which the analog will be directly obtained, it is still necessary to remove the derivative with respect to ω_0 in (36). This can be done in two different ways. The first involves consideration of the two signals X and X_Δ. These are defined by the equation

$$\begin{aligned} &\ddot{X} + \omega_0^2(t)\, X = \dot{r}, \\ &\ddot{X}_\Delta + [\omega_0(t) - \Delta]^2\, X_\Delta = \dot{r}, \end{aligned} \tag{39}$$

which correspond to a constant separation Δ. Equation (36) becomes for this case

$$\omega_0 = \frac{\lambda}{\Delta} r[X - X_\Delta]. \tag{40}$$

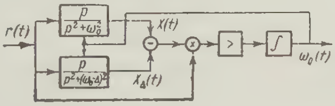

r(t)
$\frac{p}{p^2+\omega_0^2}$
X(t)
$\frac{p}{p^2+(\omega_0-\Delta)^2}$
$X_\Delta(t)$
x
>
∫
$\omega_0(t)$

Fig. 1. Block diagram of a system with parallel circuits.

The separation Δ can be taken to be arbitrary and sufficiently small (smaller than the attenuation of the circuits and the other constants of the system).

The system corresponding to Eqs. (39) and (40) can be called a parallel-circuit system. A block diagram of the system is given in Fig. 1. The difference of the voltages $X - X_\Delta$ attained at the output of the two oscillatory circuits which have a mistuning Δ, is multiplied by r(t), amplified, and fed to an integrating unit, which corrects the resonance frequency of the circuits through feedback. It is also possible to use heterodyning with control of the frequency of the heterodyne.

There is another version of the parallel-circuit system, in which the frequency of the circuits is controlled by the difference of the amplitudes $E_T - E_{T\Delta}$ of the oscillation X(t) and $X_\Delta(t)$ at the output of the circuit, rather than by $r[X - X_\Delta]$. In this version of the system, the signals X(t) and $X_\Delta(t)$ are first detected and then subtracted. The question of the most advantageous version of the system can be solved experimentally, although in our opinion the first version is more flexible, since it is based on the theory given above.*

The other method of removing the derivative in (36) consists of the following. As can be seen from (37), the signal X can be written in operator form as

$$X = \frac{p}{p^2 + \omega_0^2}\, r\left(p = \frac{d}{dt}\right). \tag{41}$$

Direct differentiation gives

$$\frac{\partial X}{\partial \omega_0} = -2\omega_0 \frac{p}{(p^2 + \omega_0^2)^2}\, r. \tag{42}$$

---

*The second version corresponds to a filter-discrimination equation of the form $d\omega_0/dT = a\,\partial\Phi/\partial\omega$.

If we define

$$Z = \frac{\omega_0 p}{(p^2 + \omega_0^2)^2}\, r = \frac{\omega_0}{p^2 + \omega_0^2}\, X, \tag{43}$$

(36) will become

$$\dot{\omega}_0 = -2\lambda r Z, \tag{44}$$

and from (43)

$$\begin{aligned} \ddot{Z} + \omega_0^2 Z &= \omega_0 X, \\ \ddot{X} + \omega_0^2 X &= \dot{r}. \end{aligned} \tag{45}$$

The block diagram of the system which is the analog of these equations is shown in Fig. 2. It has two oscillating circuits in series, tuned to the same resonance frequency, which is controlled by feedback.

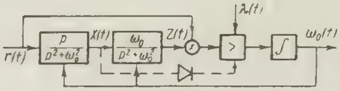

Fig. 2. Block diagram of the series-circuit system.

3. In the case of absolutely constant parameters, A, φ and ω, the oscillatory circuits in the optimal system must have a small (theoretically zero) attenuation. In practice, this means that the attenuation must be smaller than 1/T*. If the nonconstant nature of the parameters is taken into account, a finite attenuation is obtained. Let us consider the case of nonconstant amplitude and phase for $T \gg \tau_a$. If we suppose that $k_1(\tau)$ has the form of (19) in Eq. (17), we obtain

$$\Phi(\omega, T) = \frac{2\sigma_1^2}{N_0^2}\, \widetilde{E}_T^2, \tag{46}$$

where

$$\widetilde{E}_T^2 = \int_0^T \int_0^T e^{-\gamma_1|t-t'|} \cos \omega\, (t - t')\, r\,(t)\, r\,(t')\, dt\, dt'.$$

The filter-discrimination equation (26) has the form

$$\frac{d\omega_0}{dT} = \lambda \frac{\partial^2}{\partial\omega\partial T}\, \widetilde{E}_T^2 \left(\frac{1}{\lambda} = \frac{N_0^2}{2\alpha\sigma_1^2} \sim - \overline{\frac{\partial^2 \widetilde{E}_T^2}{\partial\omega^2}}\right), \tag{47}$$

in which

$$\frac{\partial \widetilde{E}_T^2}{\partial T} = 2r\,(T) \int_0^T e^{-\gamma_1(T-t)} \cos \omega\, (T - t)\, r\,(t)\, dt = 2r\,(T)\, X_1(T). \tag{48}$$

The signal X_1 which appears here satisfied the equation

$$[(p + \gamma_1)^2 + \omega_0^2]\, X_1 = pr. \tag{49}$$

---

*This result is connected with the special properties of the nonstationary regime.

Comparing (49) with (38), we see that, as a consequence of the finiteness of the time of variation $\tau_a \sim 1/\gamma$, the selective binomial $p^2 + \omega_0^2$ must be replaced by the trinomial $p^2 + 2\gamma_1 p + \omega_0^2$ corresponding to finite attenuation of the circuit (we assume that $\gamma_1 \ll \omega_0$).

If the time of variation of the frequency $\tau_\omega = 1/\beta$ is considered, an analogous result is obtained. In this case, Eqs. (34) are replaced by Eqs. (21). From the first of Eqs. (21), we obtain

$$X = \frac{p}{p^2 + 2\beta p + \omega_0^2}\, r. \tag{50}$$

The function E_T, appearing in the filter-discrimination equation

$$\frac{d\omega_0}{dT} = \lambda \frac{\partial}{\partial\omega} \frac{\partial (E_T^2)}{\partial T}$$
$$\left(\frac{1}{\lambda} = \frac{1 - e^{-2\beta T}}{4\alpha\beta} N_0 \sim - \overline{\frac{\partial^2 E_T^2}{\partial\omega^2}} \right), \tag{51}$$

is the amplitude of the signal (50). Instead of the equation $\partial(E_T^2)/\partial T = 2rX$ it now satisfies the equation

$$\frac{\partial (E_T^2)}{\partial T} = - 2\beta E_T^2 + 2rX. \tag{52}$$

This produces some modifications in the optimal system, although its principle remains the same. Thus, defining $\partial(E_T^2)/\partial\omega = U$, we now have the system of equations

$$\begin{gathered} (p^2 + 2\beta p + \omega_0^2) X = pr, \quad (p + 2\beta) U = - 4rZ, \\ (p^2 + 2\beta p + \omega_0^2) Z = \omega_0 X, \quad p\omega_0 = \lambda p U, \end{gathered} \tag{53}$$

for which the analog must be found.

4. We still have to consider the value of the amplification coefficient α or γ, which appears in Eqs. (26), (32), (44), and (51) and which corresponds to the amplification unit in Figs. 1 and 2.

As we have already noted, the fluctuation change of this coefficient is not very important, and after the average is taken, Eq. (27) can be replaced by Eq. (30). We shall illustrate the method of determining λ or α on the basis of Eqs. (32), (33), (44) and (51). In computing the right member of (33), let us fix the true unknown value of the frequency $\omega = \omega^*$ of the signal. Taking the average over the remaining random quantities and considering that the fluctuations of the noise of the signal are independent, we obtain

$$\overline{E_T^2} = \frac{1}{2} \overline{A^2} \frac{1 - \cos (\omega - \omega^*) T}{(\omega - \omega^*)^2} + \frac{1}{2} N_0 T \tag{54}$$

and consequently

$$\frac{N_0}{\overline{A^2} T} = \alpha T^2 f((\omega - \omega^*) T), \quad f(z) = - \frac{d^2}{dz^2} \frac{1 - \cos z}{z^2}. \tag{55}$$

It it is considered that $\omega - \omega^*$ is of the same order of magnitude as the error $\Delta\omega$ [connected with α by Eq. (29)] in the determination of the frequency, we obtain $\alpha T^2 \sim [(\omega - \omega^*)T]^2$. Moreover, we have already given and used the condition for good filter discrimination, which has the form

$$\frac{N_0}{\overline{A^2} T} \ll 1 \quad \text{when} \quad \frac{N_0 \beta}{\overline{A^2}} \ll 1$$
$$\text{or} \tag{56}$$

(the latter form holding for a nonconstant signal frequency). When this condition is satisfied, (55) leads to the inequality

$$|\omega - \omega^* | \ll 1. \tag{57}$$

But since $f(z) = 1/12 - z^2 \ldots$, it follows that

$$\alpha = 12 \frac{N_0}{\overline{A^2} T^3}, \; \lambda = \frac{24}{\overline{A^2}} \frac{1}{T^4} \cdot \tag{58}$$

If we consider the more general case of nonconstant frequency, it is necessary to turn to Eq. (51) and to use Eq. (20). Taking the average of Eq. (51), differentiating with respect to ω, and using (57), we find

$$\frac{1}{\lambda} = -\frac{\partial^2 \overline{E_T^2}}{\partial \omega^2} = \frac{A^2}{2\beta^4} [1 - (2 + \beta^2 T^2) e^{-\beta T} + e^{-2\beta T}]. \tag{59}$$

For $\beta T \ll 1$, this equation transforms to (58), while for $\beta T \gg 1$ it transforms to the constant $\lambda_\infty = 2\beta^2/\overline{A^2}$. When the optimal system operates in a stationary regime, (for instance, in prolonged reception of a frequency-modulated signal), the amplification coefficient can be maintained constant. At the start of the work or in the reception of a pulse-type signal it is advisable to use a variable amplification coefficient in accordance with (58) and (59).

To avoid the necessity of solving for a signal which clearly is a special function of time, it is convenient to regulate the amplification by means of the signal which would in any event exist in the circuit. For this, it is advisable to use the average value of the square of the signal

$$Z = -\frac{1}{2} \frac{\partial X}{\partial \omega} = -\frac{1}{2} \int_0^T (T - t) e^{-\beta(T-t)} \sin \omega (T - t) r(t)\, dt.$$

If we compute the average $\overline{Z}^2$, taking into account (56) and (57), we obtain

$$\overline{Z^2} = \frac{1}{32} \frac{\overline{A^2}}{\beta^4} [1 - (1 + \beta T) e^{-\beta T}]^2, \tag{60}$$

which coincides with (59) in terms of the order of magnitude and the nature of its variation as a function of βT. Therefore, it is convenient to set $\lambda = (16\,\overline{Z^2})^{-1}$. This method of controlling the amplification coefficient by the signal Z is noted in Fig. 2 by a dotted line.

In conclusion, let us note that the system we have described is not fully optimal for two reasons; first of all, Eqs. (26) and (29) are approximate, since they are only the first equations of a more complicated system. The error arising in this connection is smaller the greater the accuracy of the a posteriori estimate of the frequency. The second approximation was made in the transition from (37) to (38). As a consequence of these approximations, there will be less than optimal performance in the system, especially during the initial moments of time when a small amount of a posteriori information is accumulated. Therefore, it is necessary to make a special examination of the method of putting the given system into operation.

The author avails himself of this opportunity to thank Yu. B. Kobzarev and A. Ye. Basharinov, who joined in discussing the work.

APPENDIX I

A posteriori probabilities for the case of correlated noise

Let us consider the case of correlated noise when n(t) is a stationary normal random process whose average value is zero and whose correlation function is $\overline{nn_\tau} = k(\tau)$. As known, the probability function for a process of this type has the form

$$W[n(t)] = \exp\left\{-\frac{1}{2}\int_0^T \int_0^T n(t')\, a(t', t)\, n(t)\, dt' dt\right\}, \tag{I}$$

where a is the inverse kernel of k, i.e.,

$$\int a(t', t)\, k(t - t'')\, dt = \delta(t' - t'') \quad (0 \leqslant t', t'' \leqslant T). \tag{II}$$

We shall restrict ourselves to the cases where the duration of the observation time T is considerably greater than the correlation time of the noise τ_{cor}. As a rule, this condition is satisfied in all practical cases. Then, for the vast majority of values t' and t (everywhere with the exception of the boundary region $t' \sim \tau_{\mathrm{cor}}$, $t \sim \tau_{\mathrm{cor}}$, $T - t' \sim \tau_{\mathrm{cor}}$, and $T - t \sim \tau_{\mathrm{cor}}$), the function a (t', t) is a function of the difference between the variables a(t', t) = a (t' - t). This function is found from an equation which is analogous to (II):

$$\int a(t' - t)\, k(t - t'')\, dt = \delta(t' - t''), \tag{III}$$

which, however, is taken over the entire infinite straight line $-\infty < t < \infty$. This last equation is solved by a Fourier transformation. For the transforms

$$\alpha(\omega) = \int\limits_{-\infty}^{\infty} e^{i\omega\tau} a(\tau)\, d\tau, \tag{IV}$$

$$\frac{1}{2} S_n(\omega) = \int\limits_{-\infty}^{\infty} e^{i\omega\tau} k(\tau)\, d\tau \tag{V}$$

we obtain from (III) the equation

$$\alpha(\omega) = \frac{2}{S_n(\omega)}. \tag{VI}$$

Equation (2) becomes in this case

$$w_{\mathrm{ps}}(A, \varphi, \omega) = \mathrm{const}\, w_{\mathrm{pr}}(A, \varphi, \omega) \times$$
$$\times \exp\left\{-\frac{1}{2}\int\limits_0^T\int\limits_0^T s(t')\, a(t', t)\, s(t)\, dt dt' + \int\limits_0^T\int\limits_0^T s(t')\, a(t', t)\, r(t)\, dt dt'\right\}. \tag{VII}$$

But

$$\int\limits_0^T s(t')\, a(t', t)\, dt' = \int\limits_0^T A\cos(\omega t' + \varphi)\, a(t' - t)\, dt',$$

since a(t', t) = a (t'-t). In addition, as a consequence of the condition $T \gg \tau_{\mathrm{cor}}$, this last integral scarcely differs from the corresponding integral with infinite limits of integration, which is expressed in terms of the spectrum of (IV)

$$A\int\limits_{-\infty}^{\infty} \cos(\omega t' + \varphi)\, a(t' - t)\, dt' = \frac{A}{2} e^{i\omega t + i\varphi} \alpha(\omega) + \frac{A}{2} e^{-i\omega t - i\varphi} \alpha(-\omega)$$
$$(\alpha(\omega) = \alpha(-\omega))$$

or, on the basis of (VI), in terms of the spectral noise

$$A\int\limits_{-\infty}^{\infty} \cos(\omega t + \varphi)\, a(t' - t)\, at' = \frac{2}{S_n(\omega)} s(t). \tag{VIII}$$

Thus, Eq. (VII) is transformed into the form

$$w_{ps}(A, \varphi, \omega) = \text{const}\, w_{pr}(A, \varphi, \omega) \exp\left\{-\frac{1}{S_n(\omega)} \int_0^T s^2(t)\, dt + \right.$$

$$\left. + \frac{2}{S_n(\omega)} \int_0^T s(t)\, r(t)\, dt\right\}, \tag{IX}$$

which is analogous to (4). The only difference is that N_0 has been replaced by the spectral density $S_n(\omega)$, which is nonuniform in the range of possible values of the frequency. All of the previously derived equations (6) - (11) remain correct when the corresponding substitution of $S_n(\omega)$ for N_0 is made.

APPENDIX 2

A posteriori probability for the case of fluctuating amplitude and phase

To compute the probability (16), let us find the mean

$$m = \left\langle \exp\left\{-\frac{1}{2N_0} \int_0^T x^2(t)\, dt + \int_0^T x(t)\, u(t)\, dt\right\}\right\rangle \tag{X}$$

$$\left(u(t) = \frac{2}{N_0} r(t) \cos \omega t\right)$$

and the analogous mean for y(t) and $v(t) = \dfrac{2}{N_0}\, r(t) \sin \omega t$. Here x(t) and y(t) are Gaussian processes (14). In matrix form, (X) becomes

$$m = \frac{M[u]}{M[0]},$$

$$M[u] = \text{const} \int \cdots \int \exp\left[-\frac{1}{2} x \left(k_0^{-1} + \frac{1}{N_0}\right) x + xu\right] \Pi dx(t).$$

Using the well-known general formula, we obtain

$$M[u] = \text{const} \exp\left[\frac{1}{2} u \left(k_0^{-1} + \frac{1}{N_0}\right)^{-1} u\right].$$

Consequently,

$$m = e^{\frac{1}{2} u k_1 u},$$

where

$$k_1 = \left(k_0^{-1} + \frac{1}{N_0}\right)^{-1} = \left(1 + \frac{k_0}{N_0}\right)^{-1} k_0 \tag{XI}$$

is the kernel satisfying the equation $\left(1 + \dfrac{k_0}{N_0}\right) k_1 = k_0$, i.e.,

$$k_1(t', t'') + \frac{1}{N_0} \int_0^T k_0(t' - t)\, k_1(t, t'')\, dt = k_0(t' - t'')$$

$$(0 < t,\ t' < T). \tag{XII}$$

When the interval $0 < t < T$ can be replaced by the infinite interval $-\infty < t - \infty$ (for $T \gg \tau_a$), Eq. (XII) can be solved by the method of the Fourier transformation. Since k_0 and k_1 are $\frac{1}{2} S_0(\omega)$, $\frac{1}{2} S_1(\omega)$ in the spectral representation, we obtain (XI) from (18).

REFERENCES

1. R.L. Stratonovich. Application of the theory of Markov processes to optimal filter discrimination of signals, Radiotekhnika i Elektronika, 1960, 5, 11, 1751.
2. P.L. Stratonovich. Optimal nonlinear systems for separating a signal with constant parameters from noise. Izv. Vuzov MVO SSSR (Radiofizika), 1959, 2, 6, 892.
3. Yu.B. Chernyak. The detection of a signal with a frequency at an arbitrary initial phase on the background of white noise. Radiotekhnika i Elektronika, 1960, 5, 3, 366.
4. D.V. Ageyev, Ya.R. Rodionov. Frequency-modulated radio reception with tracking tuning, GEI, 1958.
5. P. Bello. Joint estimation of delay, Doppler and Doppler rate, IRE Trans., 1960, T-6, 3, 330.

Department of Physics,
M.V. Lomonosov Moscow State University

Submitted on April 28, 1960

THE SPECTRUM OF AN OSCILLATION WHOSE FREQUENCY PASSES THROUGH ZERO

M.I. Dorman

The properties of the spectrum of an oscillation whose frequency changes according to a linear function are studied. Special attention is devoted to cases where the oscillation frequency passes through the zero value. On the basis of this spectral approach, the nature of the effect of an operation of this type on the selective system is determined.

A large amount of literature has been devoted to the analysis of a frequency-modulated oscillation and its effect on linear systems (the work of I.F. Gonorovskiy, A.A. Kharkevich, and others is generally known).

In different specific problems, the usual initial assumption is that the change of the instantaneous frequency of the oscillation always takes place in an interval at a considerable distance from zero.* However, in many cases which are important in practice, in particular in the heterodyning of frequency-modulated signals, the oscillation frequency can pass through zero. The special nature and a number of characteristic features of processes of this type were pointed out in one of the works of I.S. Gonorovskiy [1], and subsequently in article [2].

The purpose of the present study is to shed more light on certain properties of frequency-modulated signals.

Let us consider a very simple frequency-modulated oscillation

$$u(t) = U_0 \cos \int \Omega(t)\, dt \tag{1}$$

---

*Variations from this restriction have sometimes led to misunderstanding (see article of S.M. Khlytchiyev [4] and the discussion relating to it [5].

with a constant amplitude U_0 and an instantaneous frequency $\Omega(t)$ changing during the interval $[-T/2,\ T/2]$ according to the equation

$$\Omega(t) = \Omega_0 + 2\beta t \tag{2}$$

or according to equation

$$\Omega(t) = \Omega_0 + 2\beta |t|, \tag{3}$$

where $\Omega_0 = \text{const}$; $\beta = \Delta\omega_d/T$ and $\Delta\omega_d$ is the variation of the frequency during the time T/2 (see Fig. 1).

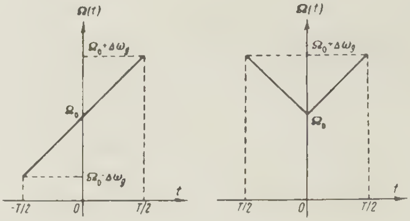

Fig. 1. The functions giving the frequency variations.

The voltage u(t) can be obtained as a result of multiplication (heterodyning) of two oscillations with subsequent separation of the different components. Let us determine the deformation of the oscillation spectrum when the parameters Ω_0 and $\Delta\omega_d$ change for the two types of variations of the frequency (2) and (3).

If $\Omega(t)$ is given by Eq. (2), then

$$u(t) = U_0 \cos(\beta t^2 + \Omega_0 t + \Phi_0), \tag{4}$$

where Φ_0 is the initial phase of the oscillation at t = 0.

The spectrum of the oscillation

$$G(\omega) = U_0 \int_{-\frac{T}{2}}^{\frac{T}{2}} \cos(\beta t^2 + \Omega_0 t + \Phi_0)\, e^{-i\omega t}\, dt$$

can be expressed in terms of Fresnel integrals

$$S(x) = \int_0^x \sin\frac{\pi}{2} t^2\, dt \quad \text{и} \quad C(x) = \int_0^x \cos\frac{\pi}{2} t^2\, dt,$$

namely,

$$\begin{aligned} G(\omega) = \frac{U_0}{2}\sqrt{\frac{\pi}{2\beta}} \Big\{ & e^{i\psi_1}\left[C\left(\frac{\Delta\omega_d + \Omega_0 - \omega}{\sqrt{2\pi\beta}}\right) + C\left(\frac{\Delta\omega_d - \Omega_0 + \omega}{\sqrt{2\pi\beta}}\right)\right] + \\ & + e^{-i\psi_2}\left[C\left(\frac{\Delta\omega_d + \Omega_0 + \omega}{\sqrt{2\pi\beta}}\right) + C\left(\frac{\Delta\omega_d - \Omega_0 - \omega}{\sqrt{2\pi\beta}}\right)\right] + \\ & + ie^{i\psi_1}\left[S\left(\frac{\Delta\omega_d + \Omega_0 - \omega}{\sqrt{2\pi\beta}}\right) + S\left(\frac{\Delta\omega_d - \Omega_0 + \omega}{\sqrt{2\pi\beta}}\right)\right] - \\ & - ie^{-i\psi_2}\left[S\left(\frac{\Delta\omega_d - \Omega_0 - \omega}{\sqrt{2\pi\beta}}\right) + S\left(\frac{\Delta\omega_d + \Omega_0 + \omega}{\sqrt{2\pi\beta}}\right)\right]\Big\}, \end{aligned} \tag{5}$$

where

$$\psi_1 = \Phi_0 - \frac{(\Omega_0 - \omega)^2}{4\beta};$$

$$\psi_2 = \Phi_0 - \frac{(\Omega_0 + \omega)^2}{4\beta}.$$

First of all let us consider the case where

$$\Omega_0 \gg \Delta\omega_d > 0.$$

In this case, for $\omega > 0$

$$C\left(\frac{\Delta\omega_d + \Omega_0 + \omega}{\sqrt{2\pi\beta}}\right) + C\left(\frac{\Delta\omega_d - \Omega_0 - \omega}{\sqrt{2\pi\beta}}\right) \simeq 0,$$

$$S\left(\frac{\Delta\omega_d + \Omega_0 + \omega}{\sqrt{2\pi\beta}}\right) + S\left(\frac{\Delta\omega_d - \Omega_0 - \omega}{\sqrt{2\pi\beta}}\right) \simeq 0,$$

while for $\omega < 0$

$$C\left(\frac{\Delta\omega_d + \Omega_0 + |\omega|}{\sqrt{2\pi\beta}}\right) + C\left(\frac{\Delta\omega_d - \Omega_0 - |\omega|}{\sqrt{2\pi\beta}}\right) \simeq 0,$$

$$S\left(\frac{\Delta\omega_d + \Omega_0 + |\omega|}{\sqrt{2\pi\beta}}\right) + S\left(\frac{\Delta\omega_d - \Omega_0 - |\omega|}{\sqrt{2\pi\beta}}\right) \simeq 0.$$

If this is considered, it can be easily shown that the modulus of the spectral density is

$$|G(\omega)| \simeq \frac{U_0}{2}\sqrt{\frac{\pi}{2\beta}}\sqrt{C_1^2 + S_1^2}, \tag{6}$$

while the phase is

$$\Theta(\omega) \simeq \operatorname{arc\,tan} \frac{S_1 + C_1 \operatorname{tg}\left[\Phi_0 - \frac{(\Omega_0 - |\omega|)^2}{4\beta}\right]}{C_1 - S_1 \operatorname{tg}\left[\Phi_0 - \frac{(\Omega_0 - |\omega|)^2}{4\beta}\right]},$$

where

$$S_1 = S\left(\frac{\Delta\omega_d + \Omega_0 - |\omega|}{\sqrt{2\pi\beta}}\right) + S\left(\frac{\Delta\omega_d - \Omega_0 + |\omega|}{\sqrt{2\pi\beta}}\right),$$

$$C_1 = C\left(\frac{\Delta\omega_d + \Omega_0 - |\omega|}{\sqrt{2\pi\beta}}\right) + C\left(\frac{\Delta\omega_d - \Omega_0 + |\omega|}{\sqrt{2\pi\beta}}\right).$$

Let us note that $|G(\omega)|$ does not depend on the initial phase of oscillation Φ_0 and that it cannot have zero values for finite values of ω.

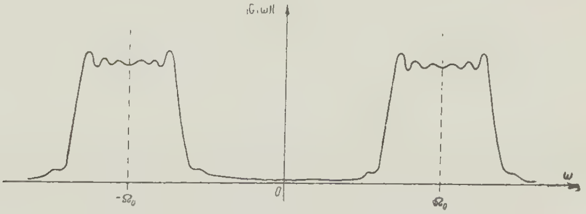

Fig. 2. Spectrum of a frequency-modulated oscillation for $\Delta\omega_d \ll \Omega_0$.

Because the Fresnel integrals are odd, it is obvious that

$$\lim_{|\omega|\to\infty} |G(\omega)| = 0.$$

Moreover, for large rates of change of the frequency ($\Delta\omega_d/\sqrt{2\pi\beta} \ll 1$), the spectral density near the zero frequency is extremely small. Let us also note that the function is symmetric with respect to the frequency $\omega = \Omega_0$ (see Fig. 2). Indeed, it is easily seen that

$$G\,[\pm(\Omega_0 \pm \Delta\omega_d)]| = \frac{U_0}{2}\sqrt{\frac{\pi}{2\beta}}\sqrt{C^2\left(\Delta\omega_d\sqrt{\frac{2}{\pi\beta}}\right) + S^2\left(\Delta\omega_d\sqrt{\frac{2}{\pi\beta}}\right)}.$$

If $\Delta\omega_d \to \infty$, it follows from (5) that (see Fig. 3)

$$|G(\omega) = U_0\sqrt{\frac{\pi}{\beta}}\left|\cos\left(\frac{\Omega_0^2+\omega^2}{4\beta} - \Phi_0 - \frac{\pi}{4}\right)\right|. \tag{7}$$

Hence, it is seen that as $\Delta\omega_d$* increases, the envelope becomes increasingly more uniform, while the spectral density passes through its minimum (zero) values at the frequency

$$\omega_k = \sqrt{\beta\,[\pi(4k+3) + 4\Phi_0] - \Omega_0^2},\ k = 0, 1, 2, \ldots.$$

An important property of the spectrum given by (7) is its dependence on the initial phase Φ at all rates of change of frequency.

Let us return to the initial equations (5) and (6). As Ω_0 decreases, both "humps" of the spectral function, which are located in the region of positive and negative frequencies, draw closer to one another. For $\Omega_0 < \Delta\omega_d$ the instantaneous frequency $\Omega(t)$ passes through the zero value, i.e., "zero beats" are formed. When $\Omega(t) = 0$, the frequency $\Omega(t)$ is an odd function of time [2], and the spectral density of the zero is

$$G(\omega) = U_0\sqrt{\frac{\pi}{2\beta}}\left\{\cos\left(\frac{\omega^2}{4\beta} - \Phi_0\right)\left[C\left(\frac{\Delta\omega_d+\omega}{\sqrt{2\pi\beta}}\right) + C\left(\frac{\Delta\omega_d-\omega}{\sqrt{2\pi\beta}}\right)\right] + \right.$$
$$\left. + \sin\left(\frac{\omega^2}{4\beta} - \Phi_0\right)\left[S\left(\frac{\Delta\omega_d+\omega}{\sqrt{2\pi\beta}}\right) + S\left(\frac{\Delta\omega_d-\omega}{\sqrt{2\pi\beta}}\right)\right]\right\}. \tag{8}$$

Obviously, in this case as well, $\lim_{|\omega|\to\infty} G(\omega) = 0$ and

$|\omega|\to\infty$

$$G(0) = U_0\sqrt{\frac{2\pi}{\beta}}\left[\cos\Phi_0 C\left(\frac{\Delta\omega_d}{\sqrt{2\pi\beta}}\right) - \sin\Phi_0 S\left(\frac{\Delta\omega_d}{\sqrt{2\pi\beta}}\right)\right]. \tag{9}$$

As the frequency variation $\Delta\omega_d$ increases, the shape of the spectrum $G(\omega)$ resembles more and more the initial oscillation (1). Indeed, if $\Delta\omega_d \to \infty$ in (7) or (8), it is easily seen that

$$G(\omega) = U_0\sqrt{\frac{\pi}{\beta}}\cos\left(\frac{\omega^2}{4\beta} - \Phi_0 - \frac{\pi}{4}\right). \tag{10}$$

Let us consider an operation spectrum whose frequency is an even function of time. In this case

$$u(t) = \begin{cases} U_0\cos(\beta t^2 - \Omega_0 t - \Phi_0), & -\frac{T}{2} \leqslant t \leqslant 0, \\ U_0\cos(\beta t^2 + \Omega_0 t + \Phi_0), & 0 \leqslant t \leqslant \frac{T}{2}. \end{cases}$$

---

*For a constant rate of change of the frequency, this means an increase of the duration of the oscillation.

Let us also express the spectrum $G(\omega)$ which we are determining in terms of Fresnel integrals:

$$\begin{aligned} G(\omega) = \frac{U_0}{2}\sqrt{\frac{\pi}{2\beta}}\Big\{&(e^{i\varphi_1} + e^{-i\psi_2})\left[C\left(\frac{\Delta\omega_d + \Omega_0 + \omega}{\sqrt{2\pi\beta}}\right) - C\left(\frac{\Omega_0 + \omega}{\sqrt{2\pi\beta}}\right)\right] + \\ &+ (e^{-i\varphi_2} + e^{i\psi_1})\left[C\left(\frac{\Delta\omega_d + \Omega_0 - \omega}{\sqrt{2\pi\beta}}\right) - C\left(\frac{\Omega_0 - \omega}{\sqrt{2\pi\beta}}\right)\right] + \\ &+ i(e^{i\varphi_1} - e^{-i\psi_2})\left[S\left(\frac{\Delta\omega_d + \Omega_0 + \omega}{\sqrt{2\pi\beta}}\right) - S\left(\frac{\Omega_0 + \omega}{\sqrt{2\pi\beta}}\right)\right] - \\ &- i(e^{-i\varphi_2} - e^{i\psi_1})\left[S\left(\frac{\Delta\omega_d + \Omega_0 - \omega}{\sqrt{2\pi\beta}}\right) - S\left(\frac{\Omega_0 - \omega}{\sqrt{2\pi\beta}}\right)\right]\Big\}, \end{aligned} \tag{11}$$

where $\varphi_1 = -\Phi_0 - \frac{(\Omega_0 + \omega)^2}{4\beta}$ and $\varphi_2 = -\Phi_0 - \frac{(\Omega_0 - \omega)^2}{4\beta}$. It can be shown that, for $\Phi_0 = k\pi$, $k = 0, \pm 1, \pm 2, \ldots$ Eq. (11) is the same as Eq. (5). If $\Omega_0 \ll \Delta\omega_d > 0$ then

$$|G(\omega)| = U_0\sqrt{\frac{\pi}{2\beta}}\sqrt{C_2^2\cos^2\frac{(\Omega_0 - |\omega|)^2}{4\beta} + S_2^2\sin^2\frac{(\Omega_0 - |\omega|)^2}{4\beta}}, \tag{12}$$

and

$$\Theta(\omega) = \begin{cases} \dfrac{C_2\tan\Phi_0 + S_2\tan\dfrac{(\Omega_0 - \omega)^2}{4\beta}}{C_2 - S_2\tan\Phi_0\tan\dfrac{(\Omega_0 - \omega)^2}{4\beta}}, & \omega \geqslant 0, \\ \dfrac{S_2\tan\dfrac{(\Phi_0 - |\omega|)^2}{4\beta} - C_2\,\mathrm{tg}\,\Phi_0}{C_2 + S_2\tan\Phi_0\tan\dfrac{(\Omega_0 - |\omega|)^2}{4\beta}}, & \omega \leqslant 0, \end{cases}$$

where

$$S_2 = S\left(\frac{\Delta\omega_d + \Omega_0 - |\omega|}{\sqrt{2\pi\beta}}\right) - S\left(\frac{\Omega_0 - |\omega|}{\sqrt{2\pi\beta}}\right);$$

$$C_2 = C\left(\frac{\Delta\omega_d + \Omega_0 - |\omega|}{\sqrt{2\pi\beta}}\right) - C\left(\frac{\Omega_0 - |\omega|}{\sqrt{2\pi\beta}}\right).$$

Without dwelling here on the properties of the spectrum given by (11), let us note only that the modulus $|G(\omega)|$ likewise does not depend on the initial phase of the oscillation Φ_0. There is a certain interest in the case where $\Omega \to 0$ and zero beats are formed whose frequency changes according to an even function $\Omega(t)$ [2]. Setting $\Omega_0 = 0$ in (11), we obtain the spectrum of zero beats

$$\begin{aligned} G(\omega) = U_0\sqrt{\frac{\pi}{2\beta}}\Big\{&e^{-i\Phi_0}\left[\cos\frac{\omega^2}{4\beta}C\left(\frac{\Delta\omega_d + \omega}{\sqrt{2\pi\beta}}\right) + \sin\frac{\omega^2}{4\beta}S\left(\frac{\Delta\omega_d + \omega}{\sqrt{2\pi\beta}}\right)\right] + \\ &+ e^{i\Phi_0}\left[\cos\frac{\omega^2}{4\beta}C\left(\frac{\Delta\omega_d - \omega}{\sqrt{2\pi\beta}}\right) + \sin\frac{\omega^2}{4\beta}S\left(\frac{\Delta\omega_d - \omega}{\sqrt{2\pi\beta}}\right)\right] + \\ &+ 2i\sin\Phi_0\left[\cos\frac{\omega^2}{4\beta}C\left(\frac{\omega}{\sqrt{2\pi\beta}}\right) + \sin\frac{\omega^2}{4\beta}S\left(\frac{\omega}{\sqrt{2\pi\beta}}\right)\right]\Big\}, \end{aligned} \tag{13}$$

which depends on the initial phase Φ_0. It is easily seen, for instance, that

$$G(0) = U_0\sqrt{\frac{2\pi}{\beta}}\cos\Phi_0 C\left(\frac{\Delta\omega_d}{\sqrt{2\pi\beta}}\right). \tag{14}$$

For $\Phi_0 = k\pi$ Eq. (14) is the same as Eq. (9), as should have been expected. Finally, let us find the spectral density for $\Delta\omega_d \to \infty$:

$$|G(\omega)| = U_0\sqrt{\frac{\pi}{\beta}}\sqrt{\cos^2\Phi_0\cos^2\left(\frac{\omega^2}{4\beta}-\frac{\pi}{4}\right)+\to\ldots}$$
$$\ldots\to\sqrt{+2\sin^2\Phi_0\left[\cos\frac{\omega^2}{4\beta}C\left(\frac{\omega}{\sqrt{2\pi\beta}}\right)+\sin\frac{\omega^2}{4\beta}S\left(\frac{\omega}{\sqrt{2\pi\beta}}\right)\right]^2}. \tag{15}$$

It is interesting to note that near the zero frequency

$$|G(\omega)| \simeq U_0\sqrt{\frac{\pi}{\beta}}\left|\cos\Phi_0\cos\left(\frac{\omega^2}{4\beta}-\frac{\pi}{4}\right)\right|,$$

while for $\omega \to \infty$

$$|G(\omega)| \simeq U_0\sqrt{\frac{\pi}{\beta}}\left|\cos\left(\frac{\omega^2}{4\beta}-\frac{\pi}{4}\right)\right|.$$

Consequently, the strong dependence of the spectral density on the initial phase holds in this case only at relatively low frequencies.

Let us determine the properties of the effect of the frequency-modulated oscillation on the selective system. Let us assume a frequency characteristic in the form of a rectangle (see Fig. 4).

$$K(\omega) = \begin{cases} 1 & |\omega-\omega_0| < \Delta\omega_0,\ \Delta\omega_0 > 0, \\ 0 & \text{outside of this interval,} \end{cases}$$

where $2\Delta\omega_0$ is the passband of the system, and ω_0 is the central frequency of the passband.

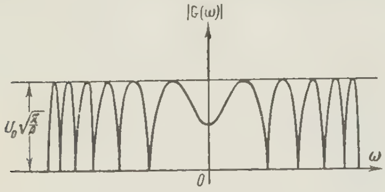

Fig. 3. Spectrum of a frequency-modulated oscillation for $\Delta\omega_d \to \infty$

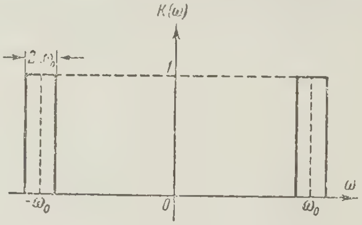

Fig. 4. Frequency characteristic of a selective system

Let us find the energy E given off by the oscillation at the output of the system in the case where the frequency variation $\Delta\omega_d$ is fairly large (7). According to Rayleigh's theorem,

$$E = \frac{U_0^2}{\beta}\int_{\omega_0-\Delta\omega_0}^{\omega_0+\Delta\omega_0}\cos^2\left(\frac{\Omega_0^2+\omega^2}{4\beta}-\Phi_0-\frac{\pi}{4}\right)d\omega.$$

Omitting the computations, we give the final expression for the energy:

$$E = \frac{U_0^2}{2}\sqrt{\frac{\pi}{\beta}}\left\{\frac{2\Delta\omega_0}{\sqrt{\pi\beta}}+\cos\left(\frac{\Omega_0^2}{2\beta}-2\Phi_0\right)\left[S\left(\frac{\omega_0+\Delta\omega_0}{\sqrt{\pi\beta}}\right)-S\left(\frac{\omega_0-\Delta\omega_0}{\sqrt{\pi\beta}}\right)\right]+\right.$$
$$\left.+\sin\left(\frac{\Omega_0^2}{2\beta}-2\Phi_0\right)\left[C\left(\frac{\omega_0+\Delta\omega_0}{\sqrt{\pi\beta}}\right)-C\left(\frac{\omega_0-\Delta\omega_0}{\sqrt{\pi\beta}}\right)\right]\right\}. \tag{16}$$

From this, it is seen that for a given amplitude at the input, the energy at the output depends on the initial phase and on the position of the passband on the frequency axis, as well as on the rate of change of the frequency of the oscillation and the passband of the system. Only in the case where $\omega_0 \gg \sqrt{\pi\beta}$ and $\Delta\omega_0 \ll \omega_0$ is

$$E \simeq \frac{\Delta\omega_0 U_0^2}{\beta}, \tag{17}$$

i.e., the energy depends neither on the initial phase, nor on ω_0.

Let us consider another limiting case. Let $\omega_0 \simeq 0$ (low-frequency filter) and $\Delta\omega_0/\sqrt{\pi\beta} \ll 1$. Then, retaining only the first terms of the Taylor series, we obtain for $S\left(\frac{\Delta\omega_0}{\sqrt{\pi\beta}}\right)$ and $C\left(\frac{\Delta\omega_0}{\sqrt{\pi\beta}}\right)$ [3].

$$E \simeq \frac{\Delta\omega_0 U_0^2}{\beta}\left[1 + \sin\left(\frac{\Omega_0^2}{2\beta} - 2\Phi_0\right)\right]. \tag{18}$$

In this case, the response energy depends strongly on Φ_0 and Ω_0, and of course, on ω_0 and $\Delta\omega_0/\sqrt{\pi\beta}$.

An examination of the other special cases leads to similar results.

From the above discussion, it follows that, in a number of cases, to find the response of a selective system, it is necessary to take into account not only the shape of the envelope, but also the "fine structure" of the effect and, in particular, the nature of the change of its phase.

REFERENCES

1. I.S. Gonorovskiy. The effect of an EMF with a rapidly changing frequency on inertial systems. Radiotekhnika i Elektronika, 1960, 5, 6, 902.
2. M.I. Dorman. The properties of oscillation phenomena when the frequency passes through zero. Radiotekhnika, 1960, 15, 10, 27.
3. Tables of Fresnel Integrals, Izd. AN SSSR, 1958.
4. S.M. Khlytchiyev. The effect of a voltage with a linearly changing frequency on linear systems. Radiotekhnika, 1956, 11, 1, 61.
5. V.A. Korneyeva, V.S. Ponkratov, Radiotekhnika, 1959, 14, 4, 76.

Submitted October 17, 1960

THE MARKOV NATURE OF THE ENVELOPE OF QUASI-HARMONIC OSCILLATIONS

V.I. Tikhonov

A differential equation is obtained for the envelope of the quasi-harmonic oscillations at the output of an oscillatory circuit with a large Q factor, when wideband noise acts on the input of a circuit. From the equation it follows that the envelope represents a Markov process. The problem of when the envelope first attains a certain level is solved.

INTRODUCTION

Recently several notes [1, 2, 3] have appeared in which various arguments are used to substantiate the supposition that the envelope of the quasi-harmonic oscillation which arise at the output of an oscillatory circuit with a high Q factor under the action of white noise on the circuit is a Markov process.

In the basic article [1], it is shown that the envelope of the oscillations at the output of an oscillatory circuit is a process without aftereffect, and the multidimensional probability densities for the envelope are expressed in terms of the one-dimensional initial distribution and the transition probability. Hence, the Markov nature of the envelope follows [4, 5].

In a note [2], a method of obtaining the Fokker-Planck equation for the envelope and of finding the transition probability is indicated by means of a transformation from Cartesian coordinates to polar coordinates. This note also expresses doubts in regard to the possibility of practical utilization of the results of [1] and proposes another method for substantiating the Markov nature of the envelope. In this connection, there arose a discussion [3] between the authors, chiefly of a methodological nature. This discussion left no doubt about the fact that the envelope of the oscillations at the output of the circuit is a Markov process.

Although this can be regarded as an established supposition, the present article is devoted to a similar question. The reason for this is that the Markov nature of the envelope can be used to solve a number of problems which are of physical and practical interest. For instance, for Markov processes, in a number of cases it is possible to solve fully the problem of the first moment of passage of the envelope to a definite level. This provides an original method for considering the problem of the effect of the envelope of quasi-harmonic oscillations on "threshhold devices" (electronic relays, triggers, etc.), [6]. For Markov processes, in principle, it is also possible to solve the problem of computing the probability that a random process will cross a given level a given number of times during a definite interval of time, [7]. This is directly related to the computation of the probability of false alarm in the theory of noise immunity.

In our study, we shall obtain the Fokker-Planck equation for the one-dimensional probability density of the envelope by two methods. The first of these methods, which is briefly indicated in note [2], consists in making a transformation to polar coordinates of the Fokker-Planck equation written in rectangular coordinates of the phase plane. In this way, it is immediately possible to obtain the corresponding Fokker-Planck equation for the envelope.

However, in this article, our basic attention will be devoted to the second method, which is more easily interpreted in terms of physics, while possessing the same degree of mathematical rigor. This method consists of first finding the differential equation for the envelope of the quasi-harmonic oscillations in the oscillatory circuit and then forming the Fokker-Planck equation for the one-dimensional probability density.

In this work, we give a steady-state solution of the Fokker-Planck equation, and compute the average time for the first passage of the envelope to some fixed value.

It appears that, apart from the quantitative results, certain aspects of the article may present a methodological interest (for instance, the computation of the correlation between the random phase and the reacting oscillations). Similar questions are encountered in other problems (for instance, in considering the effect of fluctuations on the operation of a self-oscillator) [8, 9].

1. THE FOKKER-PLANCK EQUATION FOR THE ENVELOPE

Let a fluctuation current $\xi(t)$ act on an RLC oscillatory circuit. In our discussion, we shall assume that the random function $\xi(t)$ represents a normal stationary random process whose average value is zero and whose correlation function is

$$k_{\xi}(\tau) = \sigma^2 R(\tau), \tag{1}$$

where σ^2 is the variance. The spectral density of $\xi(t)$ is regarded as approximately uniform within the limits of the amplitude-frequency characteristic of the circuit. Therefore, $\xi(t)$ can be regarded as white noise with a correlation function

$$k(\tau) = N_0 \delta(\tau), \quad N_0 = \int_{-\infty}^{\infty} k_{\xi}(\tau)\, d\tau, \tag{2}$$

where $\delta(\tau)$ is a delta function.

For the current $\eta(t)$ in the inductive branch of the oscillatory circuit, we have the following differential equation:

$$\ddot{\eta} + 2\alpha\dot{\eta} + \omega_0^2\eta = \omega_0^2\xi(t), \tag{3}$$

where

$$\omega_0^2 = \frac{1}{LC}; \qquad \alpha = \frac{R}{2L}. \tag{4}$$

Let us assume that the oscillatory circuit has a large Q-factor

$$Q = \frac{\omega_0 L}{LC} = \frac{\omega_0}{2\alpha} \gg 1. \tag{5}$$

In Eq. (3), let us transform the new variable

$$\begin{aligned} x &= \eta\cos(\omega_0 t + \varphi_0) - \frac{\dot{\eta}}{\omega_0}\sin(\omega_0 t + \varphi_0), \\ y &= \eta\sin(\omega_0 t + \varphi_0) + \frac{\dot{\eta}}{\omega_0}\cos(\omega_0 t + \varphi_0), \end{aligned} \tag{6}$$

where φ_0 is the random initial phase, which is statistically independent of $\xi(t)$

The inverse equations have the form

$$\begin{aligned} \eta &= x\cos(\omega_0 t + \varphi_0) + y\sin(\omega_0 t + \varphi_0), \\ \frac{\dot{\eta}}{\omega_0} &= -x\sin(\omega_0 t + \varphi_0) + y\cos(\omega_0 t + \varphi_0). \end{aligned} \tag{7}$$

It follows from Eqs. (6) that the coordinates x and y which describe a point on the phase plane must satisfy the following conditions:

$$\dot{x} = -\frac{\sin(\omega_0 t + \varphi_0)}{\omega_0}(\ddot{\eta} + \omega_0^2\eta), \qquad \dot{y} = \frac{\cos(\omega_0 t + \varphi_0)}{\omega_0}(\ddot{\eta} + \omega_0^2\eta).$$

Using (3) and (7), we obtain

$$\begin{aligned} \dot{x} &= -\alpha x - \omega_0\sin(\omega_0 t + \varphi^0)\,\xi(t) + \alpha x\cos 2(\omega_0 t + \varphi_0) + \alpha y\sin 2(\omega_0 t + \varphi_0), \\ \dot{y} &= -\alpha y + \omega_0\cos(\omega_0 t + \varphi_0)\,\xi(t) + \alpha x\sin 2(\omega_0 t + \varphi_0) - \alpha y\cos 2(\omega_0 t + \varphi_0). \end{aligned}$$

If we consider the selective properties of the circuit (5), and if accordingly we neglect the terms containing high-frequency factors (the frequency $2\omega_0$), we can write

$$\dot{x} = -\alpha x - \omega_0\sin(\omega_0 t + \varphi_0)\,\xi(t), \qquad \dot{y} = -\alpha y + \omega_0\cos(\omega_0 t + \varphi_0)\,\xi(t). \tag{8}$$

In a more general case, these equations can have the following form:

$$\dot{x} = X(x, y) + \xi_1(t), \qquad \dot{y} = Y(x, y) + \xi_2(t). \tag{9}$$

The corresponding Fokker-Planck equation for them is written as

$$\frac{\partial w}{\partial t} = -\frac{\partial}{\partial x}(Xw) - \frac{\partial}{\partial y}(Yw) + \frac{1}{2}N\left(\frac{\partial^2 w}{\partial x^2} + \frac{\partial^2 w}{\partial y^2}\right). \tag{10}$$

Here it is assumed that the random functions $\xi_1(t)$ and $\xi_2(t)$, which have a zero average value, can be regarded as a correlated delta function with the same coefficient of intensity N, i.e., if

$$k_1(\tau) = \langle\xi_1(t)\,\xi_1(t+\tau)\rangle, \qquad k_2(\tau) = \langle\xi_2(t)\,\xi_2(t+\tau)\rangle, \tag{11}$$

it is possible to write

$$\begin{gathered} k_1(\tau) = k_2(\tau) = N\delta(\tau), \\ N = \int_{-\infty}^{\infty}\langle\xi_1(t)\,\xi_1(t+\tau)\rangle\,d\tau = \int_{-\infty}^{\infty}\langle\xi_2(t)\,\xi_2(t+\tau)\rangle\,d\tau. \end{gathered} \tag{12}$$

Here and in the future, we shall use skew brackets to denote the statistical mean.

Let us define the potential function U(x, y) by the equation

$$\frac{\partial U}{\partial x} = -X, \qquad \frac{\partial U}{\partial y} = -Y.$$

The steady-state solution of the Fokker-Planck equation (10), satisfying the natural requirement that the probability density vanishes at infinity, can be written in the following form as is easily seen by direct substitution:

$$w(x, y) = C \exp\left[-\frac{2}{N} U(x, y)\right], \tag{13}$$

where C is the normalization constant.

With regard to our special case (8), we have

$$\begin{gathered} X = -\alpha x, \qquad Y = -\alpha y, \qquad U(x, y) = -\frac{\alpha}{2}(x^2 + y^2), \\ \xi_1(t) = -\omega_0 \sin(\omega_0 t + \varphi_0)\, \xi(t), \qquad \xi_2(t) = \omega_0 \cos(\omega_0 t + \varphi_0)\, \xi(t), \\ w(x, y) = \frac{\alpha}{\pi N} \exp\left[-\frac{\alpha}{N}(x^2 + y^2)\right]. \end{gathered} \tag{14}$$

Let us note here that if we change to polar coordinates

$$x = A \cos\varphi, \qquad y = A \sin\varphi \tag{15}$$

and use the well-known equation

$$w(x, y)\, dx\, dy = W(A, \varphi)\, A dA d\varphi,$$

we can obtain the Rayleigh function for the envelope A from Eq. (14)

$$W(A) = \frac{2\alpha}{N} A \exp\left(-\frac{\alpha}{N} A^2\right). \tag{16}$$

Let us find the coefficient of intensity N for the given example. For this, it is necessary to consider that both the random functions $\xi_1(t)$ and $\xi_2(t)$ are expressed in terms of the random function $\xi(t)$ and contain a random initial phase φ_0, which does not depend on $\xi(t)$. Therefore, in considering the statistical characteristics, it is first necessary to take over the set of observations of $\xi(t)$ and then over the random initial phase φ_0 [10]. To distinguish the second average from the first one, we shall indicate it by a subscript φ_0. We find

$$\begin{gathered} \langle \xi_1(t) \rangle = -\omega_0 \langle \sin(\omega_0 t + \varphi_0) \rangle_{\varphi_0} \langle \xi(t) \rangle = 0, \\ \langle \xi_2(t) \rangle = \omega_0 \langle \cos(\omega_0 t + \varphi_0) \rangle_{\varphi_0} \langle \xi(t) \rangle = 0, \\ k_1(\tau) = \langle\langle \xi_1(t)\, \xi_1(t + \tau) \rangle\rangle_{\varphi_0} = \frac{1}{2} \omega_0^2 k_\xi(\tau) \cos \omega_0 \tau, \\ k_2(\tau) = \langle\langle \xi_2(t)\, \xi_2(t + \tau) \rangle\rangle_{\varphi_0} = \frac{1}{2} \omega_0^2 k_\xi(\tau) \cos \omega_0 \tau, \end{gathered}$$

$$N = \frac{1}{2} \omega_0^2 \int_{-\infty}^{\infty} k_\xi(\tau) \cos \omega_0 \tau\, d\tau = \omega_0^2 \int_0^{\infty} k_\xi(\tau) \cos \omega_0 \tau\, d\tau = \frac{1}{4} \omega_0^2 S(f_0), \tag{17}$$

where $S(f_0)$ is the physically measurable spectral density of the fluctuations of $\xi(t)$ at a frequency f_0.

For the case (8) with which we are concerned, the Fokker-Planck equation (10) becomes

$$\frac{\partial w}{\partial t} = 2\alpha w + \alpha\left(x \frac{\partial w}{\partial x} + y \frac{\partial w}{\partial y}\right) + \frac{1}{2} N \left(\frac{\partial^2 w}{\partial x^2} + \frac{\partial^2 w}{\partial y^2}\right). \tag{18}$$

Let us change to polar coordinates (15) in this equation. We obtain

$$\frac{\partial w}{\partial t} = \alpha w + \frac{\partial}{\partial A}(\alpha A w) + \frac{1}{2}\frac{N}{A^2}\frac{\partial^2 w}{\partial \varphi^2} + \frac{1}{2}\frac{N}{A}\frac{\partial}{\partial A}\left(A\frac{\partial w}{\partial A}\right). \tag{19}$$

Let us find the Fokker-Planck equation for the probability density of the envelope A. Equation (19) must be solved for certain initial values A_0 and φ_0. The initial phase φ_0 can assume any value in the integral $-\pi \leq \varphi_0 \leq \pi$. Since the oscillatory circuit has a positive region $\alpha > 0$, it is clear in physical terms that there must be a steady-state probability density of the envelope which is independent of the initial values A_0 and φ_0.

Consequently, for any value of φ_0, we must obtain the same steady-state distribution for the envelope A. Therefore, the steady-state probability density for the envelope should not depend on φ at all, and in finding the equation for this density, the third term in the right member of Eq. (19) can be set equal to zero:

$$\frac{\partial w}{\partial t} = \alpha w + \frac{\partial}{\partial A}(\alpha A w) + \frac{1}{2}\frac{N}{A}\frac{\partial}{\partial A}\left(A\frac{\partial w}{\partial A}\right). \tag{20}$$

Let us note also that, while the function w(x, y) gives the probability density in rectangular coordinates, x, y in Eq. (18), in Eq. (20) the function w does not give the probability density of the envelope. The function w(x, y) characterizes the probability concentrated in the elementary area dxdy in the neighborhood of the point (x, y), while the probability density of the envelope W(A) must characterize the probability concentrated in the corresponding ring of thickness dA. Therefore,

$$W(A) = 2\pi A w(x, y). \tag{21}$$

Transforming from the function w to W in Eq. (20), we obtain the final Fokker-Planck equation for the envelope

$$\frac{\partial W}{\partial t} = \frac{\partial}{\partial A}\left[\left(\alpha A - \frac{N}{2A}\right)W\right] + \frac{1}{2}N\frac{\partial^2 W}{\partial A^2}. \tag{22}$$

It is easily seen that the stationary solution of this equation is given by Eq. (16).

Thus, the envelope of the quasi-harmonic oscillations at the output of an oscillatory circuit with a large Q-factor satisfies the Fokker-Planck equation (22), and, consequently, it is a Markov process.

2. THE DIFFERENTIAL EQUATION FOR THE ENVELOPE

Let us obtain the differential equation for the envelope. Under the assumptions previously made with regard to the oscillatory circuit, (a large Q-factor) and the fluctuations $\xi(t)$, (a uniform spectrum), the fluctuation current $\eta(t)$ can be written in the form of a quasi-harmonic oscillation

$$\eta(t) = A(t)\cos\psi(t), \qquad \psi(t) = \varphi_0 + \omega_0 t + \varphi(t), \tag{23}$$

where the envelope A(t) in the phase $\varphi(t)$ are random functions of time which are small relative to $\cos \omega_0 t$, and φ_0 is a random initial phase statistically independent of $\xi(t)$. Let us further define the envelope in the phase by the well-known equation (10) [11]

$$\dot{\eta}(t) = -\omega_0 A(t)\sin\psi(t). \tag{24}$$

From Eqs. (23) and (24), we obtain the equations for the envelope in the phase:

$$A = \left(\eta^2 + \frac{\dot{\eta}^2}{\omega_0^2}\right)^{\frac{1}{2}}, \qquad \varphi = -\varphi_0 - \omega_0 t - \operatorname{arc\,tan}\frac{\dot{\eta}}{\omega_0 \eta}. \tag{25}$$

Differentiating these equations, we obtain

$$\dot{A} = \frac{\dot{\eta}}{\omega_0^2 A}(\ddot{\eta} + \omega_0^2\eta), \quad \dot{\varphi} = -\frac{\eta}{\omega_0 A^2}(\ddot{\eta} + \omega_0^2\eta).$$

Using Eq. (3) and Eqs. (23) and (24), we can write

$$\left.\begin{aligned} \dot{A} &= -\alpha A(1 - \cos 2\psi) - \omega_0 \sin\psi\,\xi(t), \\ \dot{\varphi} &= -\alpha \sin 2\psi - \frac{\omega_0}{A}\cos\psi\,\xi(t). \end{aligned}\right\} \tag{26}$$

Let us transform in the usual way from the exact equations (26) to the simplified (approximate) equations. For this, when there are random effects, it is necessary to drop only terms containing high-frequency factors (the frequency $2\omega_0$) [12]. We obtain

$$\left.\begin{aligned} \dot{A} &= -\alpha A - \omega_0 \sin\psi(t)\,\xi(t), \\ \dot{\varphi} &= -\frac{\omega_0}{A}\cos\psi(t)\,\xi(t). \end{aligned}\right\} \tag{27}$$

We denote

$$\zeta(t) = -\sin\psi(t)\,\xi(t). \tag{28}$$

Let us find the mean value and the correlation function for $\zeta(t)$. In computing these and other statistical characteristics of $\zeta(t)$, it should be remembered that the phase $\varphi(t)$ depends statistically on the random function $\xi(t)$. This can be seen from the second of Equations (27). In the expression for the increment of the phase in some time interval Δ, there is a random function $\xi(t)$:

$$\Delta\varphi = \varphi(t) - \varphi(t - \Delta) = -\omega_0 \int\limits_{t-\Delta}^{t} \frac{1}{A(s)} \cos[\varphi_0 + \omega_0 s + \varphi(s)]\,\xi(s)\,ds =$$

$$= -\omega_0 \int\limits_{-\Delta}^{0} \frac{\xi(t - x)}{A(t + x)} \cos[\varphi_0 + \omega_0 t + \omega_0 x + \varphi(t + x)]\,dx. \tag{29}$$

To compute the above-mentioned characteristics, we shall make use of the initial assumptions. Since, according to the assumptions, the correlation time τ_k of the fluctuations $\xi(t)$ is much smaller than the time constant $\tau_c = 1/\alpha$ of the oscillatory circuit (which characterizes the rate of change of the envelope A in the phase φ), it is possible to take a time inverval Δ for which the values of the random functions $\xi(t-\Delta)$ and $\xi(t)$ will be uncorrelated and during which the change of the envelope and the phase will be insignificant. In other words, let us select $\Delta > 0$ such that the following inequalities will be satisfied simultaneously:

$$\tau_k \ll \Delta \ll \tau_c. \tag{30}$$

At the same time, the equation

$$A(t - \Delta) \simeq A(t), \quad \varphi(t - \Delta) \simeq \varphi(t). \tag{31}$$

will be satisfied approximately, and thus the phase increment $\Delta\varphi$ will be fairly small.

Let us note that the quantities $A(t-\Delta)$ and $\varphi(t-\Delta)$ which are obtained as a result of integration with the random functions $\xi(t)$ with a certain delay, for the "passed" intervals of time are statistically independent of the "future" values of $\xi(t)$. This statement is not correct when the random quantities $A(t + \Delta)$, $\varphi(t + \Delta)$ and $\xi(t)$ are considered. It can be seen on the basis of a series RC circuit. If this circuit is acted on by a noise $\xi(t)$ with a correlation function

$$k(\tau) = N_0\delta(\tau),$$

the correlation function between the voltage $\eta(t - \Delta)$ across the capacitance and the noise $\xi(t)$ will be

$$\langle \eta (t-\Delta)\, \xi (t) \rangle = \alpha N_0 e^{-\alpha (t-\Delta)} \int_{-\infty}^{t-\Delta} e^{\alpha x} \delta (t-x)\, dx =$$

$$= \begin{cases} 0 & \text{for } \Delta \geqslant 0, \\ \alpha N_0 e^{-\alpha \Delta} & \text{for } \Delta < 0 \end{cases} \quad \left(\alpha = \frac{1}{RC}\right).$$

If Eqs. (31) are considered, Eq. (29) can be written as

$$\Delta\varphi = -\frac{\omega_0}{A(t)} \int_{-\Delta}^{0} \cos\,[\varphi_0 + \omega_0 t + \omega_0 x + \varphi(t)]\, \xi\,(t+x)\, dx. \tag{32}$$

Because of the small magnitude of $\Delta\varphi$, the random function $\zeta(t)$ can be written in the following form:

$$\zeta(t) = -\xi(t) \sin\,[\omega_0 t + \varphi_0 + \varphi(t-\Delta) + \Delta\varphi] = -\xi(t)\sin\,[\omega_0 t + \varphi_0 + \\ + \varphi(t-\Delta)] - \xi(t)\,\Delta\varphi \cos\,[\omega_0 t + \varphi_0 + \varphi(t-\Delta)]. \tag{33}$$

The mean value of this function is

$$\langle \zeta(t) \rangle = -\langle\langle \xi(t)\, \Delta\varphi \cos\,[\omega_0 t + \varphi_0 + \varphi(t-\Delta)]\rangle\rangle_{\varphi_0}. \tag{34}$$

Using Eq. (32), we can write

$$\langle \zeta(t) \rangle = \frac{\omega_0}{A(t)} \int_{-\Delta}^{0} \langle\langle \xi(t)\, \xi(t+x) \cos\,[\omega_0 t + \omega_0 x + \varphi_0 + \varphi(t)] \cos\,[\omega_0 t + \varphi_0 +$$

$$+ \varphi(t-\Delta)]\rangle\rangle_{\varphi_0} dx = \frac{\omega_0}{2A} \int_{-\Delta}^{0} \left\langle\!\!\left\langle \xi(t)\, \xi(t+x) \left[\cos(\omega_0 x + \Delta\varphi) + \right.\right.\right.$$

$$\left.\left.\left. + \cos 2\left(\omega_0 t + \frac{1}{2}\omega_0 x + \varphi_0 + \varphi(t)\right)\right] \right\rangle\!\!\right\rangle_{\varphi_0} dx =$$

$$= \frac{\omega_0}{2A} \int_{-\Delta}^{0} \langle\langle \xi(t)\, \xi(t+x) \cos(\omega_0 x + \Delta\varphi) \rangle\rangle_{\varphi_0} dx =$$

$$= \frac{\omega_0}{2A} \int_{-\Delta}^{0} \{k_\xi(x) \cos \omega_0 x - \langle\langle \xi(t)\, \xi(t+x)\, \Delta\varphi \rangle\rangle_{\varphi_0}\} \sin \omega_0 x\, dx.$$

For normal processes, all the multidimensional moments of odd order are equal to zero, and consequently,

$$\langle \xi(t_1)\, \xi(t_2)\, \xi(t_3) \rangle = 0. \tag{35}$$

Therefore,

$$\langle \zeta(t) \rangle = \frac{\omega_0}{2A} \int_{-\Delta}^{0} k_\xi(x) \cos \omega_0 x\, dx = \frac{\omega_0}{2A} \int_{-\infty}^{0} k_\xi(\tau) \cos \omega_0 \tau\, d\tau = \frac{\omega_0}{8A} S(f_0). \tag{36}$$

The second equation is written on the basis of the fact that for $\Delta \gg \tau_k$, the equation $k_\xi(\Delta) = 0$ is satisfied, and, consequently, the lower limit of integration can be set equal to $-\infty$.

Let us now find the correlation function of the random process $\zeta(t)$ defined by Eq. (33). Let

$$\zeta_0(t) = \zeta(t) - \langle \zeta(t) \rangle. \tag{37}$$

For the correlation function, we can write

$$k_0(\tau) = \langle \zeta(t)\zeta(t+\tau)\rangle - \langle \zeta(t)\rangle\langle \zeta(t+\tau)\rangle,$$

$$\begin{gathered}
\langle \zeta(t)\zeta(t+\tau)\rangle = \langle\langle \xi(t)\xi(t+\tau)\sin(\omega_0 t + \varphi_0 + \varphi(t-\Delta)) \times \\
\times \sin(\omega_0 t + \omega_0\tau + \varphi_0 + \varphi(t+\tau-\Delta))\rangle\rangle_{\varphi_0} + \\
+ \langle\langle \xi(t)\xi(t+\tau)\Delta\varphi\sin(\omega_0 t + \omega_0\tau + \varphi_0 + \varphi(t+\tau-\Delta))\cos(\omega_0 t + \varphi_0 + \\
+ \varphi(t-\Delta))\rangle\rangle_{\varphi_0} + \langle\langle \xi(t)\xi(t+\tau)\Delta\varphi_\tau\sin(\omega_0 t + \varphi_0 + \varphi(t-\Delta))\cos(\omega_0 t + \omega_0\tau + \\
+ \varphi_0 + \varphi(t+\tau-\Delta))\rangle\rangle_{\varphi_0} + \langle\langle \xi(t)\xi(t+\tau)\Delta\varphi\Delta\varphi_\tau\cos(\omega_0 t + \varphi_0 + \\
+ \varphi(t-\Delta))\cos(\omega_0 t + \omega_0\tau + \varphi_0 + \varphi(t+\tau-\Delta))\rangle\rangle_{\varphi_0},
\end{gathered}$$

$$\begin{gathered}
\langle \zeta(t)\rangle\langle \zeta(t+\tau)\rangle = \frac{\omega_0^2}{A^2}\int\limits_{-\Delta}^{0}\int\limits_{-\Delta}^{0}\langle\langle \xi(t)\xi(t+x)\cos(\omega_0 t + \varphi_0 + \\
+ \varphi(t-\Delta))\cos(\omega_0 t + \omega_0 x + \varphi_0 + \varphi(t))\rangle\rangle_{\varphi_0} \times \\
\times \langle\langle \xi(t+\tau)\xi(t+\tau+y)\cos(\omega_0 t + \omega_0\tau + \varphi_0 + \varphi(t+\tau-\Delta))\cos(\omega_0 t + \omega_0\tau + \\
+ \omega_0 y + \varphi_0 + \varphi(t+\tau))\rangle\rangle_{\varphi_0}\,dx\,dy.
\end{gathered}$$

Of course, we are interested in values of $\tau \lesssim \tau_k$, where $k_\xi(\tau) \neq 0$. It can be seen that for $\tau > \tau_k$ all the terms in these equations become zero. However, for small values of $\tau (\tau \ll \Delta)$, we can write

$$\varphi(t+\tau-\Delta) \simeq \varphi(t-\Delta) \simeq \varphi(t).$$

The harmonic factors in the equation for $<\zeta(t)\zeta(t+\tau)>$ can be regarded as independent of the pure fluctuation term. This makes it possible to take the average over $\xi(t)$ and over the random initial phase φ_0 separately. By then using Eq. (32) and (35), we can see that the second and third terms in the right member are equal to zero.

If the necessary computations are performed (we omit them here because of their length), the following approximate results can be obtained:

$$k_0(\tau) = \frac{1}{2}k_\xi(\tau)\cos\omega_0\tau. \tag{38}$$

Thus, if Eqs. (36) and (37) are taken into account, the simplified equation for the envelope (27) can be written in the following final form:

$$\dot{A} = -\alpha A + \frac{c}{2A} + \omega_0\zeta_0(t), \tag{39}$$

where the random function $\zeta_0(t)$ has the correlation function (38), and

$$c = \frac{1}{4}\omega_0^2 S(f_0). \tag{40}$$

3. SOLUTION OF THE FOKKER-PLANCK EQUATION

It is known [13, 14] that when inequality (30) is satisfied, i.e., for $\tau_c \gg \tau_k$, the random process A(t) defined by Eq. (39) can be regarded as a Markov process, and consequently the Fokker-Planck equation can be applied to it. With regard to the first-order differential equation

$$\dot{y} = F(y, \zeta(t))$$

the Fokker-Planck equation for the probability density has the form

$$\dot{W} = -\frac{\partial}{\partial y}\{[K_1(y) + K'(y)]W\} + \frac{1}{2}\frac{\partial^2}{\partial y^2}[K_2(y)W]. \tag{41}$$

Here,

$$K_1(y) = \langle F(y,\zeta)\rangle;\quad K_2(y) = 2\int\limits_{-\infty}^{0} k(F, F_\tau)\,d\tau;\quad K'(y) = \int\limits_{-\infty}^{0} k\left(\frac{\partial F}{\partial y}, F_\tau\right)d\tau;$$

and $k(F, F_\tau)$ and $k(\frac{\partial F}{\partial y}, F_\tau)$ are the correlation functions of the argument.

The one-dimensional probability density in a stationary state represents a solution of Eq. (41) for W = 0. It is easily seen that it is given by the equation

$$W(y) = \frac{C}{K_2(y)} \exp\left[2 \int \frac{K_1(y)}{K_2(y)} dy\right], \tag{42}$$

where the coefficient C is determined from the normalization conditions for the probability density.

If we apply these equations to the equation with which we are concerned (39), we find

$$\begin{gathered} K_1(A) = -\alpha A + \frac{c}{2A}, \quad K'(y) = 0, \\ K_2(A) = 2\omega_0^2 \int_{-\infty}^{0} k_0(\tau)\, d\tau = \omega_0^2 \int_0^\infty k(\tau) \cos \omega_0 \tau\, d\tau = \frac{1}{4} \omega_0^2 S(f_0) = c. \end{gathered} \tag{43}$$

Therefore, on the basis of Eq. (42), we obtain

$$W(A) = \frac{A}{\sigma^2} \exp\left(-\frac{A^2}{2\sigma^2}\right), \quad A \geqslant 0, \tag{44}$$

where

$$\sigma^2 = \frac{c}{2\alpha} = \frac{1}{4} Q \omega_0 S(f_0). \tag{45}$$

Thus, the one-dimensional steady-state probability density for the envelope of the quasi-harmonic fluctuation formed through the action of wideband noise on a narrowband oscillatory circuit is of the Rayleigh form. This result could have been predicted.

It is known [15] that the two-dimensional probability density for the envelope has the form

$$W_2(A, A_\tau) = \frac{AA_\tau}{\sigma^4(1-\rho^2)} I_0\left(\frac{AA_\tau}{\sigma^2} \frac{\rho}{1-\rho^2}\right) \exp\left[-\frac{A^2 + A_\tau^2}{2\sigma^2(1-\rho^2)}\right], \quad \rho = e^{-\alpha|\tau|}. \tag{46}$$

From the Markov nature of the envelope, it follows that the probability density (44) and (46) fully describe the envelope as a steady-state random process, since they define the transition probability

$$p_2(A_\tau, A) = \frac{W_2(A, A_\tau)}{W(A)} = \frac{A_\tau}{\sigma^2(1-\rho^2)} I_0\left(\frac{AA_\tau}{\sigma^2} \frac{\rho}{1-\rho^2}\right) \exp\left[-\frac{A^2\rho^2 + A_\tau^2}{2\sigma^2(1-\rho^2)}\right]. \tag{47}$$

4. THE AVERAGE TIME OF PASSAGE TO THE BOUNDARY

Suppose that at some initial moment of time t_0 the envelope A(t) assumes a definite value $A(t_0) = A_0$ lying within the interval (a, b), where $a \gg 0$. Let us consider the time $\tau = t - t_0$ in which the function A(t) will first attain the boundary value a or b. For the two cases, the time will be different.

It is known from [13, 16] that the average time $M = \langle \tau \rangle$ which must elapse for either the boundary a or the boundary b to be attained is given by the differential equation

$$\frac{1}{2} K_2(A_0) \frac{d^2M}{dA_0^2} + K_1(A_0) \frac{dM}{dA_0} = -1 \tag{48}$$

with the boundary condition

$$M(a) = 0, \quad M(b) = 0. \tag{49}$$

Here $K_1(A_0)$ and $K_2(A_0)$ are defined by Eqs. (43), in which A must be replaced by A_0. Substituting these values into Eq. (48), we obtain

$$\frac{1}{2} c \frac{d^2 M}{dA_0^2} + \left(-\alpha A_0 + \frac{c}{2A_0}\right)\frac{dM}{dA_0} + 1 = 0. \tag{50}$$

Let us find the average time M_b required for the envelope A(t), which has the value A_0 at t_0, to attain for the first time the value $b > A_0$. For this case, the average time for passage to the upper boundary is given by the following equation, as can easily be seen by verification:

$$M_b(A_0) = \int_{A_0}^{b} \left\{ \int_{0}^{x} \frac{2}{K_2(y)} e^{\varphi(y)} dy \right\} e^{-\varphi(x)} dx, \tag{51}$$

where

$$\varphi(y) = 2\int \frac{K_1(y)}{K_2(y)} dy.$$

Substituting the expressions for K_1 and K_2 from (43) into these equations, and integrating, we obtain

$$M_b(A_0) = \int_{A_0}^{b} \left(e^{\frac{\alpha}{c}x^2} - 1\right)\frac{dx}{\alpha x} = \frac{1}{2\alpha}\int_{\frac{\alpha}{c}A_0^2}^{\frac{\alpha}{c}b^2} (e^z - 1)\frac{dz}{z} =$$

$$= \frac{1}{2\alpha}\left[\mathrm{Ei}\left(\frac{b^2}{2\sigma^2}\right) - \mathrm{Ei}\left(\frac{A_0^2}{2\sigma^2}\right) - 2\ln\frac{b}{A_0}\right], \tag{52}$$

where

$$\mathrm{Ei}(z) = \int_{-\infty}^{z} e^t \frac{dt}{t}$$

is an integral exponential function [17].

This solution (52) satisfies the condition $M_{A_0}(A_0) = M_b(b) = 0$, $M_b(A_0) \geq 0$ and increases as b increases and as $A_0 \geq$ decreases. These conditions follow from the meaning of the problem.

Let us now compute the average time M which is required for the envelope A(t), which has the value A_0 at t_0, to attain the value $a < A_0$ for the first time. In this case, the average time for passage to the "lower" boundary will be given by the equation

$$M_a(A_0) = \int_{a}^{A_0} \left\{ \int_{x}^{\infty} \frac{2}{K_2(y)} e^{\varphi(y)} dy \right\} e^{-\varphi(x)} dx. \tag{51a}$$

After performing the computations, we obtain

$$M_a(A_0) = \frac{1}{\alpha}\ln\frac{A_0}{a}. \tag{52a}$$

It is easily seen that this solution satisfies the fundamental equation (48) and the boundary contion $M_{A_0}(A_0) = M_a(a) = 0$ and $M_a(A_0 \geq$, and that it increases with increasing A_0 and decreasing a. It can be shown that an equation similar to (48) is correct for the variance of the time required for passage to a boundary.

REFERENCES

1. J.N. Pierce. A Markoff envelope process, IRE Trans., 1958, IT-4, 4, 163.
2. C.W. Helstrom, C.T. Isley. Two notes on a Markoff envelope process, IRE Trans., 1959, IT-5, 3, 139.
3. J.N. Pierce, C.T. Isley. Further comments on a Markoff envelope process, IRE Trans., 1959, IT-5, 4, 186.
4. B.V. Gnedenko. Course in Probability Theory. GITTL, 1954.
5. M.C. Wang, G.E. Uhlenbeck. On the theory of the Brownian motion, Rev. of Mod. Phys., 1954, 17, 2-3, 323.
6. M.I. Podgoretskiy. The number of false-alarm pulses. Dokl. AN SSSR, 1952.
7. C.W. Helstrom. The distribution on the number of crossings of gaussian stochastic process, IRE Trans., 1957, IT-3, 4, 232.
8. S.M. Ritov. Fluctuations in self-oscillatory systems of the Thomson type. Zh. Eksp. Teoret. Fiz., 1955, 29, 3, 304.
9. G.S. Gorelik and G.A. Yelkin. The transformation of the fluctuations of the amplitude and the phase of self-oscillations by resonance systems. Radiotekhnika i Elektronika, 1957, 2, 1, 28.
10. V.I. Tikhonov. When a nonsteady-state random process can be replaced by a steady-state process. Zh. Tekh. Fiz., 1956, 26, 9, 2057.
11. V.I. Tikhonov. A method of determining the envelope of quasi-harmonic fluctuations. Radiotekhnika i Elektronika, 1957, 2, 4, 502.
12. I.L. Bershteyn. Fluctuations of the amplitude and phase of a skew oscillator. Izvestiya AN SSSR, 1950, 14, 2, 145.
13. L.S. Pontryagin, A.A. Andronov and A.A. Vitt. The static treatment of dynamic systems. From: Collected Works of A.A. Andronov. Izd. AN SSSR, 1956, 142.
14. P.I. Kuznetsov, R.L. Stratonovich, V.I. Tikhonov. Generalization of the Fokker-Planck equation. Zh. Eksp. Teoret. Fiz., 1954, 26, 2, 187.
15. V.I. Bonimovich. Fluctuation processes in radio-receiving instruments. Izd. Sovetskoye Radio, 1951.
16. A.J.F. Siegert, On the first passage time probability function, Phys. Rev., 1951, 81, 617.
17. E. Yanke and F. Emde. Tables of Functions. GTI. 1958.

Submitted October 24, 1960

THE CHARACTERISTICS OF NONLINEAR ELEMENTS OF FREQUENCY DIVIDERS

I.Kh. Rizvkin

The conditions for the existence or absence of a subharmonic regime are established with regards to the characteristics of a nonlinear element in a frequency divider of sinusoidal oscillations.

INTRODUCTION

It is interesting to establish the condition which must be satisfied by nonlinear elements in an oscillatory circuit for the circuit to definitely function, or on the contrary not function, as a frequency divider of sinusoidal oscillations. The effect of the parameters determined by the line part of the circuit (for instance, the losses and the mistuning) on the conditions for the existence of a subharmonic regime has already been fairly well studied.

The importance of the above conditions from the theoretical point of view are obvious. However, it should be noted that the corresponding results may be useful in purely practical applications as well. First, these results could be effectively used in producing circuits with a synthesized nonlinear element, i.e., with a specially designed element whose characteristics makes it possible to satisfy certain requirements. For example, one of these requirements could be the condition that a definite division band be attained for a given frequency-division coefficient. We know only one attempt of this type [1]. The possibilities of this method are far from exhausted.

On the other hand, a knowledge of the above conditions may be useful in regard to already known divider circuits (the optimal selection of the nonlinear element in its regime, the selection of the corresponding approximation in analysis and computation, etc.). As far as the conditions for the absence of a frequency dividing regime are concerned, they can be used in cases when it is important to suppress all subharmonic oscillations (for instance, in certain circuits with steel structures), as well as in frequency dividers when it is important to prevent the appearance of oscillations of the divided frequency with a division coefficient other than the given one. A complete solution of the problem we have formulated for complex nonlinear circuits is difficult. The following discussion is restricted to two cases of practical importance: the conditions for the existence of a dividing regime in a synchronized self-oscillator; and the conditions for the absence of a subharmonic regime in a fairly general circuit. In both cases, we deal with a system with one degree of freedom.

1. THE CONDITIONS FOR THE EXISTENCE OF A FREQUENCY-DIVIDING REGIME IN A COMBINED SELF-OSCILLATOR AND FREQUENCY DIVIDER

1. To divide the frequency of sinusoidal oscillations, simple self-oscillators of the Thomson type synchronized to a subharmonic are often used. The possibility of obtaining a frequency-dividing regime and the requirement of a wide synchronization band impose certain restrictions on the characteristic of the nonlinear element in the self-oscillator divider. It is convenient to characterize the properties of this element by the spectrum at its output when a sinusoidal force acts in its input (for instance, the spectrum of the anode current of a tube when there is a sinusoidal voltage on the grid). It is well-known that in dividing by a factor of n an important part is played by the properties of the characteristic which produce the n-th harmonic of the output spectrum. These properties determine whether division will take place on the width of the synchronization band (see for instance, [2-6]).

However, as far as we know, there has been no more or less rigorous proof of the fact that the presence of the n-th harmonic in the spectrum of the nonlinear element of an excited self-oscillator is sufficient for frequency dividing. In [4], this condition is regarded as necessary, while in [5], it appears as a sufficient condition, but still no proof of this fact is given. It is only noted that in the absence of the n-th harmonic, the corresponding components of the transconductance becomes zero. In this section, we shall first of all give a proof of the above fact. In the second place, we shall establish the requirements for the phase of the n-th harmonic resulting from the conditions for stability. In addition, we shall show that, in the absence of the n-th harmonic, its role can be played by the 2n-th harmonic of the derivative of the characteristics of a nonlinear element.

Let us note that after we had written this article, it was found that, at least in regard to the part relating to the n-th harmonic, our results could be obtained by considering the approximate simplified equations for the amplitude of the phase given in [6] [Eqs. (2.7) and (2.8)]. Although the author of article [6], which was far more general in nature, did not draw the necessary conclusions, it is clear that, for sufficiently small mistunings, the equation for the phase has a stationary solution, while the nondifferential equation for the amplitude also permits a stationary amplitude. From the stability conditions, the requirement for the sign of the synchronization parameter β follows. This parameter is proportional to the amplitude of the n-th harmonic.

Since, as we have said, the possibility of division does not relate to the n-th harmonic of the self-oscillation exclusively, and no analysis of the problem is given in [6], we decided to retain our entire treatment of the question.

2. We shall confine ourselves to the examination of very simple self-oscillator dividers

described by the well-known equation

$$\ddot{x} + x = \mu\varphi(\dot{x}) + \mu\xi x + \lambda_0 \sin n\tau, \tag{1}$$

where $\varphi(\dot{x})$ is the nonlinear characteristic with which we are concerned, ξ is the mistuning, and $0 < \mu \leq 1$ is a small parameter. We recall that the conditions for the existence of the stationary subharmonic regime

$$x = x_0 + \mu\ldots = u \sin\tau - v\cos\tau + \frac{\lambda_0}{1 - n^2}\sin n\tau + \mu\ldots$$

require the existence of real roots u_0 and v_0 which are not equal to zero simultaneously in the equation

$$U = 0, \tag{2}$$

$$V = 0, \tag{3}$$

where U and V are the sinusoidal and cosinusoidal components respectively of the first harmonic of the function $f(u \cos\tau + v \sin\tau + q \cos n\tau)$, and $q = n\lambda_0/1 - n^2)$. Moreover, for $u = u_0$ and $v = v_0$ it is required that the stability conditions [7] be satisfied:

$$\frac{\partial U}{\partial v} + \frac{\partial V}{\partial u} < 0, \tag{4}$$

$$\frac{\partial(U, V)}{\partial(u, v)} < 0. \tag{5}$$

To simplify our problem, we shall assume that the mistuning ξ and the amplitude of the external force λ_0 are small. Since we are interested only in the theoretical possibility of dividing, this assumption will not restrict the general nature of the problem. It is only necessary that the frequency-dividing regime exist in the finite (though arbitrarily small) region of amplitudes and mistunings. We note that in practice these parameters are connected with the instability of the amplitude and of the frequency of the external force and the self-oscillator, and, thus, these regions are made as large as possible.

3. Suppose that the following conditions are satisfied in the absence of an external force: for real $M = M_0$ we have

$$F(M_0) \equiv \frac{1}{\pi}\int_0^{2\pi} \varphi(M_0 \cos\tau)\cos\tau d\tau = 0, \tag{6}$$

$$\frac{\partial F(M_0)}{\partial M_0} < 0. \tag{7}$$

Then, in system (1), there will be a stable self-oscillatory process, represented by the self-oscillator.* If the self-oscillator is now subject to a small synchronizing force, the energy balance of the system will change insignificantly. Consequently, conditions (2) - (3) can be satisfied in a nonautonomous system.

Indeed, in accordance with the above discussion, let us assume that the mistuning is small, of the order of $\mu(\xi = \mu\xi_0)$, and let us consider that U and V are computed for $\mu = 0$, so that the mistuning disappears from the corresponding equations. Let us note also that, because of the evenness of $\varphi(\dot{x}_0)$, as a function of time for $v = 0$, one of the roots can be zero: $v_0 = 0$. The quantity u_0 can be found from Equation (3):

$$R(u, q) \equiv \frac{1}{\pi}\int_0^{2\pi} \varphi(u_0 \cos\tau + q\cos n\tau)\cos\tau d\tau = 0. \tag{8}$$

---

*It is assumed that the square of the circular frequency of the linearized autonomous system, i.e., the system (1) for $\lambda_0 = 0$, differs from unity by a quantity of the order of μ^2. This is confirmed by the fact that below only mistuning of the order of μ is considered.

If both $\varphi(\dot{x})$ and its derivative are continuous, then

$$R(u, q) = R(u, 0) + O(q). \qquad (9)$$

But from (7) and (8), it follows that R(u, 0) changes its sign for u = M_0. Consequently, for sufficiently small parameters of the external force $|q|$, R(u, q) will change its sign in the same way and the amplitude of the subharmonic u_0 will scarcely differ from the amplitude of the self-oscillations M_0.

4. Let us consider the conditions for stability of the oscillations of the divided frequency. By direct computation, it is easy to establish that for $v_0 = 0$ the derivatives $\partial U/\partial u$ and $\partial V/\partial v$ becomes zero. Then the stability conditions (4) - (5) reduce to the requirements that the two remaining derivatives be negative. But from Equations (7) - (9), it follows that, for $u = u_0$ and $v = v_0$,

$$\frac{\partial V}{\partial u} < 0,$$

if the external force is small. Thus, it remains to establish when $\partial U/\partial v$ is negative. It turns out that this conditions imposes restrictions on the n-th harmonic of the spectrum $\varphi(u_0 \cos \tau)$.

Obviously, for $u = u_0$, $v = v_0 = 0$, we have

$$\frac{\partial U}{\partial v} = \frac{1}{\pi}\int_0^{2\pi} \varphi'(\dot{x}_0) \sin^2 \tau d\tau = \frac{1}{\pi}\int_0^{2\pi} \varphi'(u_0 \cos \tau + q \cos n\tau) \sin^2 \tau \, d\tau,$$

where the prime is used to represent differentiations with respect to $\dot{x}$. Let us rewrite this equation in the form

$$\frac{\partial U}{\partial v} = \frac{1}{\pi u_0}\int_0^{2\pi} \varphi'(u_0 \cos \tau + q \cos n\tau)\,[u_0 \sin \tau + nq \sin n\tau - nq \sin n\tau] \sin \tau \, d\tau =$$

$$= -\frac{1}{\pi u_0}\int_0^{2\pi} \varphi'(u_0 \cos \tau + q \cos n\tau)\,[-u_0 \sin \tau - nq \sin n\tau] \sin \tau \, d\tau -$$

$$- \frac{nq}{\pi u_0}\int_0^{2\pi} \varphi'(u_0 \cos \tau + q \cos n\tau) \sin n\tau \sin \tau \, d\tau$$

and compute the first integral by parts. Then

$$\frac{\partial U}{\partial v} = \frac{1}{\pi u_0}\int_0^{2\pi} \varphi(u_0 \cos \tau + q \cos n\tau) \cos \tau \, d\tau -$$

$$- \frac{nq}{\pi u_0}\int_0^{2\pi} \varphi'(u_0 \cos \tau + q \cos n\tau) \sin n\tau \sin \tau \, d\tau.$$

The first of these two integrals is equal to zero because of (3). If we note that

$$\varphi'(u_0 \cos \tau + q \cos n\tau) = \varphi'(u_0 \cos \tau) + o(q)$$

and compute the second integral, we finally obtain

$$\left.\frac{\partial U}{\partial v}\right|_{\substack{u=u_0 \\ v=v_0=0}} = \frac{n^2 |q|}{\pi u_0^2}\int_0^{2\pi} \varphi(u_0 \cos \tau) \cos n\tau \, d\tau + o(q^2). \qquad (10)$$

Thus, the conditions for stability for sufficiently small $|q|$ will be satisfied in the amplitude of the n-th harmonic in the spectrum $\varphi(u \cos \tau)$ is negative in some neighborhood of the amplitude of free self-oscillations (we recall that $u_0 \simeq M_0$).

5. If the n-th harmonic of the spectrum $\varphi(u \cos \tau)$ is identically equal to zero, then, by considering terms of the order of q^2 in equation (10), we obtain

$$\left.\frac{\partial U}{\partial v}\right|_{\substack{u=u_0\\ v=0}} = -\frac{n^2q^2}{\pi u_0^2}\int_0^{2\pi} \varphi'(u_0 \cos \tau) \cos 2n\tau d\tau + O(q^3),$$

and the stability conditions can again be satisfied. Now the amplitude of the 2n-th harmonic of the derivative of the characteristic $\varphi(\dot{\chi})$ must be positive in the neighborhood of the amplitude of the self-oscillations.

Of course, arbitrary small harmonics of all numbers almost always exist in the spectra with which we are concerned, and thus it would seem that frequency division is always possible. However, since the synchronization bands for small harmonics are also small, the subharmonic process becomes impossible in an actual system whenever the magnitude of a given harmonic component is smaller than some critical value (determined in particular by the instability of the frequency of the self-oscillator). However, all this does not reduce the value of the theoretical results obtained in the above-mentioned works and which we have in part proved and added to in our discussion.

6. Let us note that our results are not based either on the approximation of the nonlinear function of the self-oscillator or on an expansion of this function into a series. It is sufficient only that the first derivatives exist and that they be continuous. This statement also holds for [6].

It is necessary to emphasize that the results we have obtained are generally incorrect in the case of a nonself-oscillating system. For instance, in [7], it is shown that in an incompletely excited system with a cubic characteristic it is impossible to divide the frequency by a factor of 3. Therefore, a special study is necessary to establish the sufficient conditions for frequency division in the case of a nonself-oscillatory system.

The important role of certain harmonics of the spectrum $\varphi(u \cos \tau)$ is explained by the fact that the properties of the characteristic which are responsible for these harmonics generate combination components of the spectrum $\varphi(u \cos \tau + q \cos n\tau)$, which sustain the process of division by n. In the next section, it is shown that in the absence of the n-th and (2n + 1)-th harmonic of the spectrum $\varphi(u \cos \tau)$, division is impossible, and a physical explanation of this fact is given.

2. CONDITIONS FOR THE ABSENCE OF THE FREQUENCY-DIVIDING REGIME

1. It is known that, when Thomson circuits are used, it is possible to suppress the periodic subharmonic regime by increasing the losses and the mistuning. We shall not be concerned with the conditions connected with these parameters, but with the form of the nonlinear form of the circuit. As far as we know, the question of the absence of a subharmonic regime has not been specially considered in this respect. However, in a number of works, for instance [2, 4] important results have been obtained. In particular in considering a simpler system than ours in [4], Korolev obtained an equation from which results can be obtained which are a special case of the results we obtained below. In this work, we deal with a system of more general form than in [2, 4], and we shall use a somewhat different method from the accepted one.

2. Many circuits of practical importance in which subharmonic regimes are observed when acted on by a sinusoidal external force can be described by a quasilinear second-order equation

$$\ddot{x} + x = \mu[\psi(x)\dot{x} + f(x)] + \lambda_0 \sin n\tau. \tag{11}$$

Here ψ and f are analytic functions, for simplicity; and $0 < \mu \ll 1$ is a small parameter. For $f(\chi) = \xi\chi$ where ξ is the mistuning, we obtained the well-known equation for a system with nonlinear losses, which is considered in the preceding section for the self-oscillatory case. When both functions are nonlinear, (11) describes a large number of circuits with a single nonlinear element, [8].

Let us restrict our analysis to circuits characterized by Eq. (11), and let us establish the conditions under which a subharmonic process is impossible.

3. In the physical analysis of processes of frequency division, the following concept is

useful: a harmonic divider is a combined structure represented by an active frequency converter interconnected with an oscillatory system tuned to a frequency close to a subharmonic. For the first component, various systems can be used, for instance, a balanced tube modulator, a diode converter with an amplifier, a nonlinear reactance, a variable line reactance, and so on. The oscillations of the frequency which must be divided and the oscillations shaped in the oscillatory circuit are fed to the input of the converter. The subharmonic regime is sustained in the oscillatory system by the energy from the source of the external source or from a constant power supply, or from both of these. In all cases, the channel through which the energy enters the oscillatory system is represented by the oscillations of a combination frequency arising in the converter. The combination frequencies are made up of the frequency of the natural oscillations of the system and the frequency of the external force. It is these combination components which make the existence of a stationary subharmonic regime possible under certain conditions.

It is natural to expect that, if this "combination mechanism" is disrupted, the process of frequency division will be impossible. A simple formal analysis carried out below confirms this.

The combination frequencies which are generated by the nonlinear elements in the circuit and which can sustain subharmonic oscillations with an angular frequency equal to unity under the action of an external force with an angular frequency n [see (11)] must obviously satisfy the equation

$$|pn - q| = 1,$$

where $p, q = 1, 2, 3, \ldots$. Consequently, the order of the combination $p = q$ is $p(n + 1) \pm 1$. In other words,

$$p + q = n + 2j \tag{12a}$$

or

$$p + q = 2n + 1 + 2j, \tag{12b}$$

where $j = 0, 1, 2, \ldots$.

In accordance with our above discussion, we shall require that the nonlinear characteristics $f(\chi)$ and $\Psi(\chi) = \int \varphi(\chi)\, dx$ prevent the formation of combination frequencies of this order.* It can be easily understood that the absence of combination frequencies on the order of (12) under a biharmonic force is equivalent to the absence of a n-th and (2n + 1)-th harmonics in a spectrum of f and Ψ under a sinusoidal external force. Therefore, we can require that the function $f(A \cos \tau)$ never contains the angular frequency components n and 2n + 1 for any amplitude A.

We shall show that under this condition it is possible to guarantee that there will be no frequency divison by a factor of n.

4. Let us compute the sinusoidal (U) and cosinusoidal (V) components of the first harmonic of the function $\psi(\chi_0)\, \chi_0 + f(\chi_0)$, where

$$x_0 = A \sin(\tau + \theta) + q_0 \sin n\tau = u \sin\tau - v \cos\tau + q_0 \sin n\tau;$$

$q_0 = \lambda_0/(1 - n^2)$; and χ_0 is the "zero" approximation of the subharmonic oscillations for the small-parameter method used below (as in the preceding section).

Computing the integrals

$$\frac{1}{\pi} \int_0^{2\pi} \psi\,[A \sin(\tau + \theta) + q_0 \sin n\tau]\,[A \cos(\tau + \theta) + nq_0 \cos n\tau]\, \frac{\sin\tau}{\cos\tau}\, d\tau,$$

---

*This representation, in which we consider $\varphi(\chi)$ instead of its integral will be made clear later [see Eq. (13)].

by parts, we obtain the equations

$$\begin{gathered} U = -V_{\Psi} + U_{f}, \\ V = U_{\Psi} + V_{f}, \end{gathered} \tag{13}$$

where $\Psi(\chi) = \int \psi(\chi) d\chi$, while the quantities in the right members of Eqs. (13) are the sinusoidal and cosinusoidal components of the function $f(\chi_0)$ and $\Psi(\chi_0)$, which appear in the form of subscripts.

It is easily shown that under the condition imposed above, the following equations hold:

$$\begin{gathered} U_{f} = B_{f} \cos\theta, \quad U_{\Psi} = B_{\Psi} \cos\theta, \\ V_{f} = B_{f} \sin\theta, \quad V_{\Psi} = B_{\Psi} \sin\theta. \end{gathered} \tag{14}$$

Here,

$$B_{f} = \sum_{r=0}^{\infty} \sum_{s=0}^{\infty} \frac{A^{2r+1} q_0^{2s}}{2^{2(r+s)} (r+1)!\, r!\, (s!)^2} \frac{d^{2(r+s)+1}}{dz_0^{2(r+s)+1}} f(z_0); \tag{15}$$

the summation is taken over all r and s for which the corresponding derivatives are not equal to zero, and z_0 represents the "operating point" of the characteristic $f(\chi)$. The expression for B_{Ψ} is obtained by replacing f by Ψ in (15).

Equation (15) is obtained automatically from the equations given in [9] for the amplitude of the first harmonic at the output of a nonlinear element under the action of a biharmonic external force. The computation is simplified in that the combination components leading to the appearance of the first harmonic are absent.

5. Substituting (14) into (13) and equating U and V to zero in accordance with (2) and (3), we find

$$\begin{gathered} -B_{\Psi} \sin\theta + B_{f} \cos\theta = 0, \\ B_{\Psi} \cos\theta + B_{f} \sin\theta = 0, \end{gathered} \tag{16}$$

Hence

$$\tan^2\theta = -1.$$

Therefore, under the conditions given in Section 3, Eqs. (16) do not have the real roots required by the theory of frequency dividing [7]. Real roots exist only in the case when the amplitude $A = A_0$ satisfies simultaneously the two equations

$$\begin{gathered} B_{f} = 0, \\ B_{\Psi} = 0. \end{gathered} \tag{17}$$

However, it can be shown that in this case the stability condition (5) is not satisfied, since, for $u = u_0$ and $v = v_0$,

$$\frac{\partial(U, V)}{\partial(u, v)} = 0. \tag{18}$$

Indeed, direct computation shows that

$$-A \frac{\partial(U, V)}{\partial(u, v)} = \frac{\partial(U, V)}{\partial(A, \theta)}. \tag{19}$$

But from Eqs. (16), it follows that the quantity in the right member of (19) is equal to $B_{\Psi}B'_{\Psi} + B_{f}B'_{f}$ (the prime indicates differentiation with respect to A). Therefore, the roots of Eqs. (17) correspond to an unstable dividing regime, characterized by Eq. (18). In terms of the "simplified" variables u and v, we can say that the singular point (u_0, v_0) is regular.*

6. Thus, if the n-th and (2n + 1)-th harmonics are absent from the spectrum of the functions $f(A \cos \tau)$ and $\Psi(A \cos \tau)$ for all amplitudes A, stable stationary periodic oscillations at a frequency which is a factor 1/n of the input frequency will be unable to exist in a nonlinear circuit, described by Eq. (11). If n is an odd number, the equality of the n-th harmonic to zero implies the equality of the (2n + 1)-th harmonic to zero. If the division factor is even, the corresponding spectrum is limited, at the last possible nonzero harmonic is the (2n - 1)-th harmonic. It is important to note that the absence of the n-th harmonic from the spectrum is still insufficient. We could give examples of frequency division by a factor n in systems in which the n-th harmonic is absent and the (2n + 1)-th harmonic is present. We note that the experiment described in [10] also confirms this conclusion.

REFERENCES

1. W.L. Hughes. Proc. I.R.E., 1953 41, 2, 241
2. V.I. Siforov, Radiotekhnika, 1946, 1, 5, 3.
3. O.A. Tkhorzhevskiy, B.K. Shembel', Zh. Tekh. Fiz. 1957, 7, 2, 215.
4. P.G. Korolev, Trudy, VKIAS, 1956, 53, 172.
5. P.G. Korolev, Radiotekhnika i Elektronika, 1959, 4, 2, 262.
6. R.V. Khokhlov, Vestnik Mosk. Univ., 1954, 8, 51.
7. L.I. Mandel'shtam, N.D. Papaleksi, Zh. Tekh. Fiz., 1932, 2, 7-8, 775.
8. M.P. Zlatev, S.L. Farchy. Onde electr., 1957, 37, 369, 1104.
9. I.V. Basik, Method of determining the current component when a sum of sinusoidal voltages act on a nonlinear system. From: Collection of Scientific Works of the TsNIIS. MS, 1948.
10. K. Schlichting, Z. Angew. Phys., 1957, 9, 9, 458.

Submitted September 14, 1960

---

*Strictly speaking, the concepts presented above only indicate the nonexistence of a subharmonic solution in the zero approximation; physically this means that intensive oscillation of a divided frequency is impossible (since the intensity would preclude a small factor μ). However, the concepts of Section 3 are obviously a good indication of the general character of the results obtained.

SOME PROBLEMS IN THE THEORY OF THE REFRACTION OF MAGNETIC WAVES

V.I. Ivanchikov

This article deals with the problem of the relationship between frequency and angles of incidence in the propagation of electromagnetic waves in plane laminar inhomogeneous media. An equation is established for the angles of incidence in the form of a generalized law of refraction (Snell's law). Examples of the determination of the function of relative refraction (errors) are given for the case of a linear ϵ-profile and for the case of an ϵ-profile of the transition layer of the Epstein type.

It is well-known that when the refraction of electromagnetic waves is treated in terms of rays, the angles of incidence and the angles of refraction are determined on the basis of the law of refraction.

Since the criteria for the validity of geometric optics do not predetermine the closeness of the results of the "ray" theory and the wave theory, the value of computations of these angles in the approximation of geometric optics can be determined only after comparison with experimental results.

The following question naturally arises: since the relationship between the angles of incidence (and consequently the angles of refraction) and the wavelength of the propagating waves are not taken into account in the ray theory, how important is this relationship for practical purposes and how can it be taken into account a priori?

In terms of the concept of physics, it can only be expected that the refraction will be stronger, the greater the change of the phase velocity in the direction of the wave at the wavefront. Thus, the refraction in electromagnetic waves will not be determined simply by the nature of the optical inhomogeneity of the medium and the angle with which the ray enters this medium, but also by the radio wave parameter giving the effective thickness of the medium in wavelengths and the change of the refractive index at the wavefront in the direction of the wave.

In this connection, from the point of view of refraction both the case of propagation of extremely short waves in a large inhomogeneity and the case of propagation of extremely long waves in the presence of a local inhomogeneity are equivalent. In both cases, the refraction is not manifested as strongly as would be the case in inhomogeneities with an effective thickness comparable with the wavelength.

The phenomenon of superrefraction, which results in waveguide conditions of propagation can apparently be considered as an example of the alternation of "selective refraction" and reflection.

As shown by V.A. Fok, for the case of a waveguide on the ground with a given hyperbolic profile (for a reduced refractive index), the "line-of-sight distance" is not only a function of the layer parameters which determine the nature of the transition of the refractive index through a minimum, but also a logarithmic function of the ratio of these parameters to the wavelength [1].

In the present article, waveguide concepts are used in considering the problem of determining the angles of incidence of the line-of-sight distance and the relative refraction of electromagnetic waves which are propagated in plane laminar inhomogeneous media. Let the solution of the wave equation*

---

*Let us note, that Eq. (1) is correct for horizontal wave polarization. A more complex

$$\frac{\partial^2 E}{\partial x^2}+\frac{\partial^2 E}{\partial z^2}+k_0^2\varepsilon(z)E=0, \tag{1}$$

which describes the propagation of an electromagnetic wave in a plane laminar medium, have the form

$$E(x,\ z)=E_0 e^{ik_0px+i\varphi(z)}, \tag{2}$$

where

$$\varphi(z)=\text{arc tan}\frac{\operatorname{Im} Z(z)}{\operatorname{Re} Z(z)}; \tag{3}$$

$Z(z) = Z_0 e^{i\varphi(z)}$ is the integral of the equation

$$\frac{d^2Z}{dz^2}+k_0^2[\varepsilon(z)-p^2]Z=0; \qquad p=\sqrt{\varepsilon_0}\sin\vartheta_0; \tag{4}$$

ϑ_0 is the angle of arrival (incidence) at the "boundary" of contact of the homogeneous and inhomogeneous media.

Let us define the angle of incidence of an electromagnetic wave $P = (x, z)$ as an arbitrary point $\vartheta(z)$. For this, we shall use the fact that the phase wavefront is given by the equation

$$\Phi(x,\ z)=k_0px+\text{arc tan}\frac{\operatorname{Im} Z(z)}{\operatorname{Re} Z(z)}=\text{const}, \tag{5}$$

as a consequence of which

$$\tan\vartheta(z)=-\left(\frac{dz}{dx}\right)_{P(x,\ z)}=\frac{\dfrac{\partial\Phi}{\partial x}}{\dfrac{\partial\Phi}{\partial z}}=\frac{k_0p}{\dfrac{1}{|Z_0|^2}\begin{vmatrix}A(z), & B(z)\\ \dfrac{\partial A}{\partial z}, & \dfrac{\partial B}{\partial z}\end{vmatrix}}, \tag{6}$$

where

$$A(z)=\operatorname{Re} Z(z),$$

$$B(z)=\operatorname{Im} Z(z). \tag{7}$$

Let us consider the function $\Theta\left(z,\ \lambda,\ \frac{d\varepsilon}{dz},\ \vartheta_0\right)$ by means of the equation

$$\frac{1}{|Z_0|^2}\begin{vmatrix}A(z), & B(z)\\ \dfrac{\partial A}{\partial z}, & \dfrac{\partial B}{\partial z}\end{vmatrix}=k_0\sqrt{\varepsilon(z)-p^2}\,[1+\Theta(z)]; \tag{8}$$

then

$$\tan\vartheta(z)=\frac{\sqrt{\varepsilon_0}\sin\vartheta_0}{\sqrt{\varepsilon(z)-\varepsilon_0\sin^2\vartheta_0}\left[1+\Theta\left(z,\ \lambda,\ \dfrac{d\varepsilon}{dz},\ \vartheta_0\right)\right]} \tag{9}$$

---

function, which will in addition to its dielectric constant include its logarithmic gradient, will enter in place of $\epsilon(z)$ in the case of vertical wave polarization. In general $\epsilon(z)$ may be taken to be some effective value of dielectric constant.

and, consequently,

$$\sqrt{[\varepsilon(z)-\varepsilon_0\sin^2\vartheta_0]\left[1+\Theta\left(z,\ \lambda,\frac{d\varepsilon}{dz},\vartheta_0\right)\right]^2+\varepsilon_0\sin^2\vartheta_0}\sin\vartheta(z)= \\ =\sqrt{\varepsilon_0}\sin\vartheta_0. \tag{10}$$

It is seen that, for propagation of a plane electromagnetic wave in a plane laminar inhomogeneous medium, a more general condition must be satisfied by the angles of incidence ϑ_0 and $\vartheta(z)$ than the condition defined by the universally known law of refraction (Snell's law)

$$\sqrt{\varepsilon(z)}\sin\vartheta(z)=\sqrt{\varepsilon_0}\sin\vartheta_0=\mathrm{const}. \tag{11}$$

In the limiting case, namely the case of geometric optics, $\Theta\left(z,\lambda,\frac{d\varepsilon}{dz},\vartheta_0\right)\to 0$ and Eq. (10) reduces to (11), as is shown below.

Thus, the expression under the radical in Eq. (10) can be regarded as an expression for the effective dielectric constant. Consequently, the horizontal range of propagation can be defined as

$$x=p\int_{z_0}^{z}\frac{d\zeta}{\sqrt{\varepsilon_\vartheta(\zeta)-p^2}}=p\int_{z_0}^{z}\frac{d\zeta}{[1+\Theta(\zeta)]\sqrt{\varepsilon(\zeta)-p^2}}. \tag{12}$$

If the range determined in the approximation of geometric optics is denoted

$$x_0=p\int_{z_0}^{z}\frac{d\zeta_0}{\sqrt{\varepsilon(\zeta)-p^2}}, \tag{13}$$

Then,

$$x_0-x=p\int_{z_0}^{z}\frac{\Theta(\zeta)\,d\zeta_0}{[1+\Theta(\zeta)]\sqrt{\varepsilon(\zeta)-p^2}} \tag{14}$$

will characterize the change in the horizontal range of propagation due to the dependence of the angles of incidence on the wavelength.

From (10) and (12), it is seen that the dependence of the angles of incidence (and consequently the angles of refraction) and the horizontal range of propagation on the wavelength of the propagating wave is fully determined by the function $\Theta\left(z,\ \lambda,\ \frac{d\varepsilon}{dz},\ \vartheta_0\right)$. In principle, this function can be determined for all the cases of solution of differential equation (4) which are given in [2]. Its physical meaning can be easily established by considering the difference between the angles of incidence rather than the actual angles,

$$\gamma(z)=\pm[\vartheta_0-\vartheta(z)]. \tag{15}$$

Indeed,

$$\tan\gamma(z)=\pm\frac{\tan\vartheta_0-\tan\vartheta(z)}{1+\tan\vartheta_0\tan\vartheta(z)}=\pm\frac{\left(\frac{dz}{dx}\right)_p-\left(\frac{dz}{dx}\right)_0}{1+\left(\frac{dz}{dx}\right)_p\left(\frac{dz}{dx}\right)_0}. \tag{16}$$

Eliminating tg $\vartheta(z)$ from this equation and using (9), we find

$$\tan\gamma(z)=\pm\frac{\sqrt{\varepsilon_0}\sin\vartheta_0-\sqrt{\varepsilon(z)-\varepsilon_0\sin^2\vartheta_0}\tan\vartheta_0\left[1+\Theta\left(z,\lambda,\frac{d\varepsilon}{dz},\vartheta_0\right)\right]}{\sqrt{\varepsilon(z)-\varepsilon_0\sin^2\vartheta_0}\left[1+\theta\left(z,\lambda,\frac{d\varepsilon}{dz}\vartheta_0\right)\right]+\sqrt{\varepsilon_0}\sin\vartheta_0\,\mathrm{tg}\,\vartheta_0}. \tag{17}$$

For $\Theta = 0$ and $\vartheta_0 \to \pi/2$.

$$\tan \gamma_{0\,\max}(z) = \mp \sqrt{\frac{\varepsilon(z) - \varepsilon_0}{\varepsilon_0}}. \tag{18}$$

For $\Theta \neq 0$ and $\vartheta_0 \to \pi/2$

$$\tan \gamma_{\max}(z) = \mp \sqrt{\frac{\varepsilon(z) - \varepsilon_0}{\varepsilon_0}} \left[1 + \Theta\left(z, \lambda, \frac{d\varepsilon}{dz}, \vartheta_0 = \frac{\pi}{2}\right)\right]; \tag{19}$$

consequently,

$$\tan \gamma_{\max}(z) = \tan \gamma_{0\,\max}(z) \left[1 + \Theta\left(z, \lambda, \frac{d\varepsilon}{dz}, \vartheta_0 = \frac{\pi}{2}\right)\right]. \tag{20}$$

For all cases of propagation in which

$$\tan \gamma_{\max}(z) \simeq \gamma_{\max}(z), \tag{21}$$

$$\tan \gamma_{0\,\max}(z) \simeq \gamma_{0\,\max}(z),$$

$$\Theta\left(z, \lambda, \frac{d\varepsilon}{dz}, \vartheta_0 = \frac{\pi}{2}\right) = \frac{\Delta\gamma(z)}{\gamma_{0\,\max}(z)}. \tag{22}$$

Thus, $\Theta\left(z, \lambda, \frac{d\varepsilon}{dz}, \vartheta_0\right)$ can be called the "relative-refraction function."

Depending on the nature of the ϵ-profile, the relative refraction function Θ may increase monotonically with increasing wavelength, or it may pass through extrema when certain relations hold between the effective thickness of the inhomogeneity, the wavelength, the angle of incidence, and the gradient of the dielectric constant.

For illustration, we give two examples.

1. A linear ϵ-profile. If

$$z < 0 \quad \varepsilon = \text{const} = \varepsilon_1,$$

$$z \geqslant 0 \quad \varepsilon(z) = \varepsilon_1 + az; \; a > 0,$$

then, as known from [2]. In the region $z > 0$

$$Z(z) = cw^{\frac{1}{3}} H^{(1)}_{\frac{1}{3}}(w), \tag{23}$$

where

$$w = \frac{2k_0}{3a} \sqrt{[\varepsilon(z) - p^2]^3}. \tag{24}$$

a) When $w \gg 1$, which corresponds to a case of the slowly changing refractive index, $\left(\frac{d}{k_0} = \frac{1}{2\pi} \frac{d\varepsilon}{dz} \lambda \text{ is small}\right)$, and angles ϑ_0 which are not too close to 90°, it is easily seen that

$$\Theta\left(z, \lambda, \frac{d\varepsilon}{dz}, \vartheta_0\right) \simeq \frac{\delta}{\left(\frac{2k_0}{3a}\right)^2 [az + \varepsilon_1 \cos^2 \vartheta_0]^3 + \delta^2}, \tag{25}$$

where $\delta = 0.07$.

b) When $w \ll 1$, which corresponds to the case of large gradients of the dielectric constant and extremely small angles of incidence, the function of the relative refraction has a more complicated form, namely

$$\Theta\left(z, \lambda, \frac{d\varepsilon}{dz}, \vartheta_0\right) \simeq \frac{\varkappa}{\sqrt{3}\, v\, [4v^4 - 2\varkappa v^3 + \varkappa^2]} - 1, \tag{26}$$

where

$$v = \left(\frac{w}{2}\right)^{\frac{1}{3}} = \left(\frac{k_0}{3a}\right)^{\frac{1}{3}} \sqrt{az + \varepsilon_1 \cos^2 \vartheta_0};$$

$$\varkappa = 2\,\frac{\Gamma\left(\frac{4}{3}\right)}{\Gamma\left(\frac{2}{3}\right)} \simeq \frac{4}{3}. \tag{27}$$

2. Transition region of the Epstein type. Here, as known from [3].

$$\varepsilon(z) = \varepsilon_1 + (\varepsilon_2 - \varepsilon_1)\frac{e^{qz}}{1 + e^{qz}}, \tag{28}$$

where q = 4/L; L being the effective thickness of the layer. For this case, we also have

$$Z(z) = e^{ik_0 z \sqrt{\varepsilon_2 - p^2}}\, F(a - b, - a - b, 1 - 2b; - e^{-qz}); \tag{29}$$

$$a = i\,\frac{\pi}{2}\,\frac{L}{\lambda}\sqrt{\varepsilon_1} \cos \vartheta_0; \quad b = i\,\frac{\pi}{2}\,\frac{L}{\lambda}\sqrt{\varepsilon_2 - p^2} \text{ — parameters }.$$

If we restrict ourselves to the first two terms of the hypergeometric series and perform the computations according to (8), we find

$$\Theta\left(z, \lambda, \frac{d\varepsilon}{dz}, \vartheta_0\right) = \sqrt{\frac{\varepsilon_2 - p^2}{\varepsilon(z) - p^2}\left[1 - \frac{2m}{(1 + 4b_0^2)\,e^{qz} + m^2 e^{-qz} + 2m}\right]} - 1, \tag{30}$$

where

$$0 \leqslant z < \infty;$$

$$m = \left(\frac{\pi}{2}\right)^2 \left(\frac{L}{\lambda}\right)^2 \Delta\varepsilon;$$

$$\Delta\varepsilon = \varepsilon_2 - \varepsilon_1 > 0; \tag{31}$$

$$b_0 = \frac{\pi}{2}\,\frac{L}{\lambda}\sqrt{\varepsilon_2 - \varepsilon_1 \sin^2 \vartheta_0}. \tag{32}$$

If the auxiliary function

$$R\left(z, \frac{L}{\lambda}, \Delta\varepsilon, \vartheta_0\right) = \frac{2m}{(1 + 4b_0^2)\,e^{qz} + m^2 e^{-qz} + 2m}, \tag{33}$$

is used, it can be easily seen that, for $\vartheta_0 = \pi/2$,

$$m = m_{\text{extr}} = e^{\frac{4z}{L}}, \tag{34}$$

and $R\left(z, \frac{L}{\lambda}, \Delta\varepsilon, \vartheta_0\right)$ has a maximum.

Without pausing for a detailed examination of all the consequences which can be deduced from the above examples, let us point out that the case of a Hankel function with a large argument, which made it possible to determine the dependence of the angle of incidence on frequency in the region adjacent to that of geometric optics, provides a vivid illustration of the degeneration of the refraction law (10) in the universally known Snell's law for $d\epsilon/dz$ $\lambda \to 0$.

Let us give the numerical value of the relative refraction Θ for the case of the so-called standard refraction for the purpose of emphasizing the small magnitude of this function relative to its value at the same wavelength for the case of deep subrefraction and "glancing" incidence.

1. Let z = 50 m, $\vartheta_0 = 89°$, $\epsilon_1 = 1.000645$, $\lambda = 4$ m, a - $d\epsilon/dz = -8 \cdot 10^{-8}\,\frac{1}{\text{m}}$ (the case of a

"standard" atmosphere) and $w = \frac{2k_0}{3a}\sqrt{(az + \varepsilon_1 \cos^2 \vartheta_0)^3} \simeq 68$. Thus, we have the case $w \gg 1$. According to (25)

$$\Theta\left(z, \lambda, \frac{d\varepsilon}{dz}, \vartheta_0\right) \simeq \frac{\delta}{w^2} \simeq 10^{-3}\%.$$

2. Let $z = 25$ m; $\vartheta_0 = 90°$, $\lambda = 4$ m, $a = d\epsilon/dz = 4 \cdot 10^{-7} \frac{1}{\text{m}}$ (the case of deep subrefraction) $w = \frac{2k_0}{3a}\sqrt{(az)^3} \simeq 0{,}08$,. Thus, we have the case $w \ll 1$. According to (26)

$$\Theta\left(z, \lambda, \frac{d\varepsilon}{dz}, \vartheta_0 = \frac{\pi}{2}\right) = \frac{\Delta\gamma}{\gamma_0 \max(z)} \simeq \frac{1}{\varkappa\sqrt{3}\,v} - 1 \simeq 26\%.$$

In our opinion, the examples we have given show convincingly that the form of the function for the distribution of the dielectric constant of the medium has a determining effect on the magnitude and nature of radio refraction at small angles of incidence (large zenith angles), as was established previously for the case of a spherically laminar atmosphere in [4] and [5].

Of course, all the equations giving the relationship between the wavelength and the effective parameters of the inhomogeneities for characteristics such as the angles of incidence (and the angles of refraction), the line-of-sight distance and the relative refraction can be easily carried over to the case of elastic waves.

Since several of the cases of refraction of a plane electromagnetic wave in a plane laminar formation are of interest in both applied physics and general physics, it is advisable that they be written up separately.

Conclusion. On the basis of wave concepts, we have considered the problems of determining the angles of incidence, the line-of-sight distance, and the relative refraction of electromagnetic waves when they are propagated in plane laminar inhomogeneous media. We have shown that the dependence of these characteristics on the wavelength of the propagating wave and the effective parameters of the inhomogeneity are fully determined by the relative-refraction function for the given type of ϵ-profile. We have established that the relationship between the angles of incidence is more complicated than the universally known law of refraction (Snell's law). Only in the limiting case, namely the case of geometric optics, where the relative-refraction function tends toward zero, do the angles of incidence cease to depend on frequency and does the refraction law reduce to Snell's law. In conclusion we gave examples of the determination of the relative-refractive function for a linear ϵ-profile and for an ϵ-profile of the transition region of Epstein's type. We also gave the numerical values of the relative refraction for the case of propagation of waves in the range of meter wavelengths under the condition of a "standard" atmosphere and under the condition of deep subrefraction.

REFERENCES

1. V.A. Fok. Approximate formula for the line-of-sight distance for the case of subrefraction. Radiotekhnika i Elektronika, 1956, 1, 5, 560.
2. L.M. Brekhovskikh. Waves in laminar media. Izd. AN SSSR, 1957.
3. P. Epstein. Reflection of waves in an inhomogeneous absorbing medium. Proc. Nat. Acad. Sci. U.S.A., 1930, 16, 627.
4. D.M. Vysokovskiy. Some special features of the calculation of radio refraction. Radiotekhnika i Elektronika. 1956, 1, 3, 274.
5. A.V. Shabel'nikov. The influence of the form of the distribution function of the dielectric constant of air with respect to height on the refraction of radio waves in the lower layers of the atmosphere. Radiotekhnika i Elektronika. 1956, 1, 3, 277.

Laboratory of Radio Physics,
Siberian Institute of Physics and Engineering
Attached to the V.V. Kuybyshev Tomsk
State University

Submitted September 23, 1960

THE ELECTROMAGNETIC FIELD AND THE DISTRIBUTION OF CURRENT ALONG AN INFINITELY LONG UNINSULATED WIRE IN A CONDUCTING MEDIUM

P. P. Pavlov

This is a study of the electromagnetic field, the input impedance, and the current distribution along an infinitely long uninsulated wire in a conducting medium under lumped excitation. The study covers the frequency range from $6 \cdot 10^3$ to $3 \cdot 10^7$ cps, and the cases where the uninsulated wire is placed in sea water, moist soil, and dry soil are considered.

INTRODUCTION

The propagation of electromagnetic waves along an infinitely long wire placed in air is considered by Sommerfeld [1], Noether [2], and Vladimirskiy [3]. The input impedance of such a wire is studied by Kessenikh. Vaynshteyn has considered the classical problem of the excitation of a thin cylindrical conductor of finite length, placed in air, by an outside electromotive force applied at an arbitrary point on the conductor [5].

In practice, segments of an uninsulated cylindrical conductor placed in a conducting medium sometimes serve as radiating elements of an antenna. However, the problem of the electromagnetic field and the distribution of the current along an uninsulated wire placed in a conducting medium has not yet found the treatment it deserves in literature.

1. CURRENT DISTRIBUTION AND INPUT IMPEDANCE OF AN INFINITELY LONG WIRE

Let us express the dependence of the current and the field components on time by e^{-iwt}, and let us define the function Π by the equation

$$E_r = \frac{\partial}{\partial r}\left(\frac{\partial \Pi}{\partial z}\right), \tag{1}$$

Then, from Maxwell's equation for a symmetric field relative to the axis of the wire, we obtain

$$\frac{\partial^2 \Pi}{\partial r^2} + \frac{1}{r}\frac{\partial \Pi}{\partial r} + \frac{\partial^2 \Pi}{\partial z^2} + \omega^2 \mu \varepsilon_k \Pi = 0. \tag{2}$$

Let us write the solution to (2) in the following form

$$\Pi = \int_{-\infty}^{+\infty} A(\gamma)\, Z_0 \left(r\sqrt{k^2 - \gamma^2}\right) e^{i\gamma z}\, d\gamma. \tag{3}$$

To satisfy the principle of radiation, let us assume a solution to Eq. (2) in the conducting medium surrounding an ideal wire in the form

$$\Pi = \int_{-\infty}^{+\infty} A(\gamma)\, H_0^{(1)}(v_3 r)\, e^{i\gamma z}\, d\gamma, \tag{4}$$

where

$$v_3 = \sqrt{k_3^2 - \gamma^2}; \quad k_3 = \frac{2\pi}{\lambda}\sqrt{\varepsilon'_{k_3}}.$$

The field components in the conducting medium are given by the equation

$$E_r = -i\int_{-\infty}^{+\infty} \gamma v_3 A(\gamma)\, H_1^{(1)}(v_3 r)\, e^{i\gamma z}\, d\gamma, \tag{5}$$

$$E_z = \int_{\infty}^{+\infty} v_3^2 A(\gamma)\, H_0^{(1)}(v_3 r)\, e^{i\gamma z}\, d\gamma, \tag{6}$$

$$H_\varphi = -i\omega\varepsilon_{k_3}\int_{-\infty}^{+\infty} v_3 A(\gamma)\, H_1^{(1)}(v_3 r)\, e^{i\gamma z}\, d\gamma. \tag{7}$$

We find the unknown function A (γ) in the boundary condition at the surface of the ideal wire

$$E_{\text{ext}} = -E_z \quad \text{for} \quad r = \rho, \tag{8}$$

where E_{ext} is the intensity of the field of external forces at the surface of the wire. In considering the propagation of electromagnetic waves along a single wire, Vladimirskiy uses Leontovich's boundary conditions

$$E_z + E_{\text{ext}} = \frac{\mu k}{k_\sigma} H_\varphi,$$

where

$$k = \frac{\omega}{c}; \quad k_\sigma = \sqrt{\frac{\omega^2}{c^2}\varepsilon\mu + 4\pi i\mu\sigma}$$

are the wave numbers in a vacuum and in the conductor, respectively. Vladimirskiy assumed the conductivity σ as fairly large and assumed that the depth of penetration of the field into the conductor is much smaller than the radius of the wire. This makes it possible for him to ignore the field inside the conductor (when Leontovich's boundary conditions are assumed to hold at the surface of the cylinder $r = \rho$).

We are interested in the electromagnetic field of an uninsulated wire in the frequency range from $6 \cdot 10^3$ to $3 \cdot 10^7$ cps. At relatively low radio frequencies, the depth of penetration of the field of the conductor may be commensurable with radius. Accordingly, in a rigorous solution of the problem it is necessary to take the field inside the conductor into account. However, if its conductivity is extremely large, it can be regarded as ideal. This makes it possible to avoid mathematical difficulties and to obtain equations which are suitable for analysis and computation.

As in [3], we shall assume that an electromagnetic field of frequency ω is excited by electromotive forces $\mathscr{E}(z)e^{-iwt}$ distributed on the surface of the conductor. For this, we shall assume that $\mathscr{E}(z)$ is directed along the axis of the conductor.

Let us consider the case of a lumped electromotive force, assuming that the intensity of the field of external forces differs from zero only in the segment $0 < z < a$. The emf of the external force is

$$\mathscr{E}_0 = \int_0^a E_{\text{ext}}\, dz.$$

However, the case of radiation in the half-space ($z > 0$) can be obtained in pure form, if an ideally conducting plane is placed perpendicular to the axis of the wire near the point where the emf $\mathscr{E}_0$ is applied. Because of the mirror reflection, it is necessary to set the emf $\mathscr{E} = 2\mathscr{E}_0$ in the equations for the field components in radiation in the half-space.

The intensity of this field E_{ext} produced by the emf of the external source $\mathscr{E}$ can be written in the form of the integral

$$E_{\text{ext}} = \frac{\mathscr{E}}{2\pi}\int_{-\infty}^{+\infty} \frac{\sin\gamma a}{\gamma a}\, e^{i\gamma z}\, d\gamma. \tag{9}$$

Defining

$$K(\gamma) = \frac{\mathscr{E}}{2\pi} \frac{\sin \gamma a}{\gamma a}, \tag{10}$$

we obtain

$$E_{\mathrm{ext}} = \int_{-\infty}^{+\infty} K(\gamma)\, e^{i\gamma z} d\gamma. \tag{11}$$

On the basis of boundary condition (8), we find

$$A(\gamma) = -\frac{K(\gamma)}{v_3^2 H_0^{(1)}(v_3\rho)}. \tag{12}$$

The current in the wire I_z is related to the field component H_φ in the conducting medium at the surface of the wire by the equation

$$I_z = 2\pi\rho H_\varphi. \tag{13}$$

On the basis of (7) and (12) we have for a → 0

$$I_z = i\,\omega\rho\varepsilon_{k_3}\mathscr{E} \int_{-\infty}^{+\infty} \frac{H_1^{(1)}(v_3\rho)}{v_3 H_0^{(1)}(v_3\rho)} e^{i\gamma z}\, d\gamma. \tag{14}$$

The function under the integral is multivalued in the complex plane γ. The branching points are the points $\gamma = \pm k_3$. To restrict ourselves to the consideration of a single branch $z > 0$, we describe our section from the branch point $\gamma = k_3$ to infinity. As a result, the integral reduces to a contour L about the section line connected to the branching point $\gamma = k_3$.

Integral (14) is equal to the integral over the section. Let us perform the substitution

$$k_3 - \gamma = s, \quad d\gamma = -ds.$$

As a result of the substitution, we obtain

$$\int_{L_R} = \underset{(1)}{\int_{-iR}^{-i\rho_1}} + \underset{(2)}{\int_{-i\rho_1}^{-iR}} + \int_{C_{\rho_1}}.$$

As $\rho_1 \to 0$ the integral over the circumference $C\rho_1$ tends to zero. At the first shore

$$s = \tau e^{i\frac{3\pi}{2}}, \qquad v_{31} = \sqrt{\tau e^{i\frac{3\pi}{2}}(2k_3 + i\tau)}.$$

At the second shore

$$s = \tau e^{-i\frac{\pi}{2}}, \quad v_{32} = \sqrt{\tau e^{-i\frac{\pi}{2}}(2k_3 + i\tau)}.$$

Thus, we have

$$J_{L_R} = -ie^{ik_3 z} \int_{\rho_1}^{R} \left\{ \frac{H_1^{(1)}(e^{i\pi} v_{32}\rho)}{e^{i\pi} v_{32} H_0^{(1)}(e^{i\pi} v_{32}\rho)} - \frac{H_1^{(1)}(v_{32}\rho)}{v_{32} H_0^{(1)}(v_{32}\rho)} \right\} e^{-z\tau}\, d\tau. \tag{15}$$

Using the equation

$$H_p^{(1)}(e^{i\pi}z) = -e^{-i\pi p} H_p^{(2)}(z)$$

and letting $\rho_1 \to 0$ and R → ∞, we obtain

$$J_{L_R} = -ie^{ik_3 z} \int_0^\infty \left[\frac{H_1^{(2)}(v_{32}\rho)}{v_{32} H_0^{(2)}(v_{32}\rho)} - \frac{H_1^{(1)}(v_{32}\rho)}{v_{32} H_0^{(1)}(v_{32}\rho)} \right] e^{-z\tau}\, d\tau.$$

Let us restrict the region of integration to values of τ satisfying the inequality

$$|v_{32}|\rho = |\sqrt{-i\tau(2k_3 + i\tau)}|\rho \ll 1 \tag{17}$$

or

$$|\sqrt{-i\tau(2k_3 + i\tau)}| = \frac{1}{\alpha\rho} \quad \text{for } \alpha \gg 1. \tag{18}$$

When inequality (17) holds, we can replace the Hankel function by the first terms of their expansion into series. Dropping all quantities of negligible magnitude, we obtain

$$J_{L_R} = \frac{2}{\pi\rho} e^{ik_3 z} \left\{ \int_0^m \frac{e^{-z\tau}\, d\tau}{v_{32}^2 \left[1 - i\frac{2}{\pi}\ln(v_{32}\rho)\right]} + \int_0^m \frac{e^{-z\tau}\, d\tau}{v_{32}^2 \left[1 + i\frac{2}{\pi}\ln(v_{32}\rho)\right]} \right\} \tag{19}$$

or

$$J_{L_R} = \frac{4\pi}{\rho} e^{ik_3 z} \int_0^m \frac{1}{\{\ln[-i\tau(2k_3 + i\tau)\rho^2]\}^2 + \pi^2} \frac{e^{-z\tau}\, d\tau}{-i\tau(2k_3 + i\tau)}. \tag{20}$$

We find the upper limit of integration m from inequality (17).

Setting

$$k_3 = \frac{2\pi}{\lambda}\sqrt{\overline{\varepsilon'_{k_3}}} = n + ip,$$

we can write (18) in the form

$$\tau^4 + 4p\tau^3 + 4(n^2 + p^2)\tau^2 - \frac{1}{(\alpha\rho)^4} = 0. \tag{21}$$

One of the roots of this equation is the upper integration limit of (20).

Table 1 gives the roots of Eq. (21) computed for sea water, wet soil, and dry soil with $\rho = 2$ mm and $\alpha = 10$.

Frequency f, cps	τ nepers/m		
	sea water $\left(\varepsilon'_3 = 80,\ \sigma_3 = 4\frac{1}{\text{ohm}\cdot\text{m}}\right)$	wet soil $\left((\varepsilon'_3 = 10,\ \sigma_3 = 5\cdot 10^{-2}\frac{1}{\text{ohm}\cdot\text{m}}\right)$	dry soil $\left((\varepsilon'_3 = 4,\ \sigma_3 = 10^{-3}\frac{1}{\text{ohm}\cdot\text{m}}\right)$
$6\cdot 10^3$	49.69125	49.97582	—
$3\cdot 10^4$	49.30699	49.92301	—
$3\cdot 10^5$	47.77654	49.75647	49.9667
$3\cdot 10^6$	42.89065	49.23667	49.9201
$3\cdot 10^7$	28.10280	47.83160	49.8761

Let us write integral (20) in the form of the sum of two integrals:

$$J_{L_R} = \frac{4\pi}{\rho} e^{ik_3 z} \left\{ \int_0^1 \frac{1}{\pi^2 + \{\ln[-i\tau(2k_3 + i\tau)\rho^2]\}^2} \frac{e^{-z\tau} d\tau}{-i\tau(2k_3 + i\tau)} + \int_1^m \frac{1}{\pi^2 + \{\ln[-i\tau(2k_3 + i\tau)\rho^2]\}^2} \frac{e^{-z\tau} d\tau}{-i\tau(2k_3 + i\tau)} \right\}. \tag{22}$$

A study of the integral function has shown that the second integral in Eq. (22) has an extremely small value for z > 1 and that it can be ignored.

For $\tau = 0$, the denominator of the function under the integral in the equation

$$J = \int_0^1 \frac{1}{\pi^2 + \{\ln[-i\tau(2k_3 + i\tau)\rho^2]\}^2} \frac{e^{-z\tau} d\tau}{-i\tau(2k_3 + i\tau)} \tag{23}$$

becomes zero. Consequently, the function under the integral is equal to infinity. To eliminate the point $\tau = 0$, let us divide the region of integration from zero to 1 into two segments with limits from 0 to h and from h to 1. As a result, we can write Eq. (23) in the form

$$J = \int_0^h \frac{1}{\pi^2 + \{\ln[-i\tau(2k_3 + i\tau)\rho^2]\}^2} \frac{e^{-z\tau} d\tau}{-i\tau(2k_3 + i\tau)} + \int_h^1 \frac{1}{\pi^2 + \{\ln[-i\tau(2k_3 + i\tau)\rho^2]\}^2} \frac{e^{-z\tau} d\tau}{-i\tau(2k_3 + i\tau)}. \tag{24}$$

We select the limit of integration h from the inequality

$$|-i2k_3| \gg \tau = h. \tag{25}$$

When inequality (25) holds, it is possible to neglect the quantity τ^2 in the function under the first integral in Eq. (24). On this basis, we can write

$$J_1 = \int\limits_0^h \frac{1}{\pi^2 + \{\ln[-i\tau(2k_3 + i\tau)\rho^2]\}^2} \frac{e^{-z\tau} d\tau}{-i\tau(2k_3 + i\tau)} \simeq$$
$$\simeq -\frac{1}{i2k_3} \int\limits_0^h \frac{e^{-z\tau} d\tau}{\tau[\ln(-i2k_3\rho^2) + \ln\tau]^2}. \tag{26}$$

For h$\ll$1 and finite values of z, which are of practical interest, the exponential function e^{-zt}, can be taken equal to e^{-zh} and carried outside the integral sign.

Writing

$$a = \ln(-i2k_3\rho^2),$$

we can write Eq. (26) in the form

$$J_1 = -\frac{e^{-zh}}{i2k_3} \int\limits_0^h \frac{d\tau}{\tau(a + \ln\tau)^2}. \tag{27}$$

Let us perform the following substitution of variables:

$$\ln\tau = u, \qquad d\ln\tau = du.$$

Consequently, we obtain

$$J_1 = -\frac{e^{-zh}}{i2k_3} \int\limits_{-\infty}^{\ln h} \frac{du}{(a+u)^2} \tag{28}$$

or

$$J_1 = \frac{1}{i2k_3} \frac{e^{-zh}}{a + \ln h}. \tag{29}$$

Substituting the value of a into (29), we have

$$J_1 = \frac{1}{i2k_3} \frac{e^{-zh}}{\ln(-i2k_3\rho^2) + \ln h}. \tag{30}$$

Thus, we can write integral (23) in the form

$$J = \frac{1}{i2k_3} \frac{e^{-zh}}{\ln(-i2k_3\rho^2) + \ln h} +$$
$$+ \int\limits_h^1 \frac{1}{\pi^2 + \{\ln[-i\tau(2k_3 + i\tau)\rho^2]\}^2} \frac{e^{-z\tau} d\tau}{-i\tau(2k_3 + i\tau)}. \tag{31}$$

The equation for the current in the wire has the form

$$I_z = i4\pi\omega\varepsilon_{k_3}\mathcal{E}e^{ik_3 z}\left\{\frac{1}{i2k_3} \frac{e^{-zh}}{\ln(-i2k_3\rho^2) + \ln h} + \right.$$
$$+ \int\limits_h^1 \frac{1}{\pi^2 + \{\ln[-i\tau(2k_3 + i\tau)\rho^2]\}^2} \frac{e^{-z\tau} d\tau}{-i\tau(2k_3 + i\tau)} +$$
$$\left. + \int\limits_1^m \frac{1}{\pi^2 + \{\ln[-i\tau(2k_3 + i\tau)\rho^2]\}^2} \frac{e^{-z\tau} d\tau}{-i\tau(2k_3 + i\tau)}\right\}. \tag{32}$$

For z > 1 the last integral in Eq. (32) can be neglected, since for $z\tau > 1$ the exponential function is small, while the modulus of the denominator of the function under the integral is large.

If we denote

$$F(z) = \frac{1}{i2k_3}\,\frac{e^{-zh}}{\ln(-i2k_3\rho^2) + \ln h} + \int_h^1 \frac{1}{\pi^2 + \{\ln[-i\tau(2k_3 + i\tau)\rho^2]\}^2}\,\frac{e^{-z\tau}\,d\tau}{-i\tau(2k_3 + i\tau)} + \\ + \int_1^m \frac{1}{\pi^2 + \{\ln[-i\tau(2k_3 + i\tau)\rho^2]\}^2}\,\frac{e^{-z\tau}\,d\tau}{-i\tau(2k_3 + i\tau)},$$

we can write Eq. (32) in the form

$$I_z = i4\pi\omega\varepsilon_{k3}\mathscr{E}e^{ik_3z}F(z). \tag{33}$$

Equation (33) was used to compute curves showing the modulus of the current as a function of z, as well as to compute the moduli of the function $e^{ik_3 z}$ and F(z) for an uninsulated wire of radius ρ = 2 mm, placed in sea water, in wet and dry soil. Figures 1, 2 and 3 shows standardized graphs as the moduli: 1 - $|I_z|$; 2 - $|e^{ik_3 z}|$; 3 - $|F(z)|$ for sea water, wet and dry soil, respectively. From the graphs, it can be seen that the function F(z) changes slowly. When an uninsulated wire is placed in sea water or in wet soil, the change of the current over wide range of frequencies is chiefly determined by the rapidly changing function $e^{ik_3 z}$. Obviously in engineering computations, the modulus of the function F(z) can be regarded as an approximately constant coefficient for these media.

In the case where the uninsulated wire is placed in dry soil, the change of the current differs rather considerably from the exponential change of $e^{ik_3 z}$, since the absolute value of the function $e^{ik_3 z}$ changes relatively slowly.

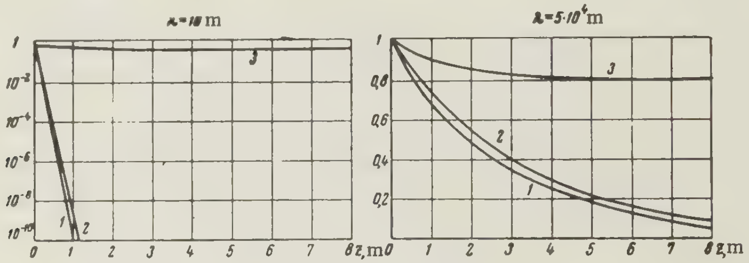

Figure 1.

To determine the power consumed by the source of the external electromotive force, let us compute the current near the point where the electromotive force is applied.

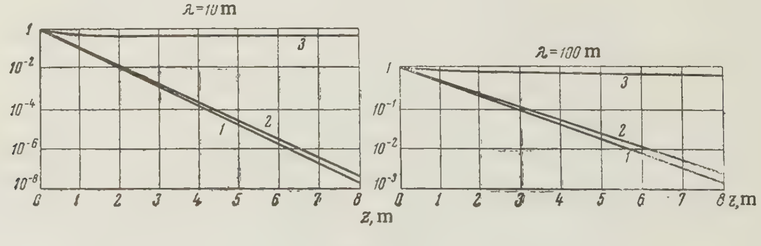

Figure 2.

Taking z = 0 in (32), we obtain

$$I_0 = i4\pi\omega\varepsilon_{k3}\mathscr{E}\left\{\frac{1}{i2k_3}\,\frac{1}{\ln(-i2k_3\rho^2) + \ln h} + \right. \\ + \int_h^1 \frac{1}{\pi^2 + \{\ln[-i\tau(2k_3 + i\tau)\rho^2]\}^2}\,\frac{d\tau}{-i\tau(2k_3 + i\tau)} + \\ \left. + \int_1^m \frac{1}{\pi^2 + \{\ln[-i\tau(2k_3 + i\tau)\rho^2]\}^2}\,\frac{d\tau}{-i\tau(2k_3 + i\tau)}\right\}. \tag{34}$$

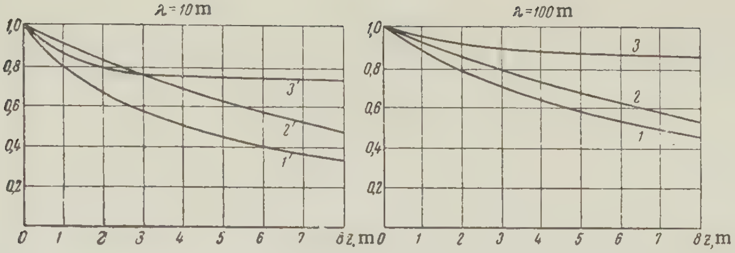

Figure 3.

Since $\mathscr{E} = 2\mathscr{E}_0$, the input impedance of the wire is

$$Z_{\text{in}} = \frac{\mathscr{E}_0}{I_0} = \frac{\mathscr{E}}{2I_0}, \qquad R_{\text{in}} = \frac{\mathscr{E}_0}{\operatorname{Re} I_0} = \frac{\mathscr{E}}{2 \operatorname{Re} I_0},$$

since the given case of the radiation is on one side. When there is radiation on both sides, the same current is obtained when an emf twice as large as 2 $\mathscr{E}_0$ is applied and the input impedance is $2Z_{\text{in}}$. The power consumed by the source of the external emf is

$$P = \frac{1}{2} \mathscr{E}_0 \operatorname{Re} I_0 = \frac{\mathscr{E}_0^2}{2R_{\text{in}}} = \frac{\mathscr{E}^2}{8R_{\text{in}}}.$$

Table 2 gives values of the input impedance of an uninsulated wire of radius ρ = 2 mm.

Frequency f, cps	Input impedance Z_{in}		
	sea water $\left(\varepsilon_s' = 80,\ \sigma_s = 4 \frac{1}{\text{ohm} \cdot \text{m}}\right)$	wet soil $\left(\varepsilon_s' = 10,\ \sigma_s = 5 \cdot 10^{-2} \frac{1}{\text{ohm} \cdot \text{m}}\right)$	dry soil $\left(\varepsilon_s' = 10,\ \sigma_s = 10^{-3} \frac{1}{\text{ohm} \cdot \text{m}}\right)$
$6 \cdot 10^3$	0.16939 — i 0.13166	—	—
$3 \cdot 10^6$	—	14.903 — i 10.765	150.92 — i 53.519
$3 \cdot 10^7$	3.2393 — i 2.3355	41.133 — i 19.066	153.82 — i 30.912

2. THE INTENSITY OF THE ELECTROMAGNETIC FIELD OF THE SPACE WAVE AND THE CHARACTERISTICS OF THE DIRECTIVITY OF AN INFINITELY LONG UNINSULATED WIRE

According to (17) and (12), the field component H_φ of the space wave is given by the equation

$$H_\varphi = i \frac{\omega \varepsilon_{k3} \mathscr{E}}{2\pi} \int_{-\infty}^{+\infty} \frac{H_1^{(1)}(v_3 r)}{v_3 H_0^{(1)}(v_3 \rho)} e^{i\gamma |z|} d\gamma. \tag{35}$$

For large values of r and z, the integral of Eq. (35) can be computed by the saddle-point method.

Using the asymptotic representation of the Hankel function for $r \gg 1$ and $z \gg 1$ we have

$$H_1^{(1)}\left(r\sqrt{k_3^2 - \gamma^2}\right) e^{i\gamma z} = \left(\frac{2}{\pi r \sqrt{k_3^2 - \gamma^2}}\right)^{1/2} e^{i\left(r\sqrt{k_3^2 - \gamma^2} - \frac{\pi}{2} - \frac{\pi}{4}\right)} e^{i\gamma z}. \tag{36}$$

If we compute the derivative of the exponential function (36) and equate it to zero, we have

$$\frac{\gamma_0}{\sqrt{k_3^2 - \gamma^2}} = \frac{z}{r}. \tag{37}$$

Defining

$$\tan\vartheta = \frac{z}{r}, \tag{38}$$

where the angle ϑ is measured from the plane perpendicular to the axis of the wire, we obtain

$$\gamma_0^2(1+\tan^2\vartheta) = k_3^2\tan^2\vartheta. \tag{39}$$

From (39), we find

$$\gamma_0 = \pm k_3 \sin\vartheta. \tag{40}$$

The function $v_3 H_0^{(1)}(v_3\rho)$ of Eq. (35) changes slowly in the neighborhood of the saddle point. It can be carried outside the integral and computed for $\gamma = \gamma_0 = k_3 \sin\vartheta$ for values of $\vartheta \neq \pm \pi/2$, since for $\vartheta = \pm\pi/2$ $\gamma_0 = k_3$, i.e., the function $v_3 = \sqrt{k_3^2 - \gamma_0^2} = 0$.

Consequently (35) can be written in the form

$$H_\varphi = i\frac{\omega\varepsilon_{k3}\mathscr{E}}{2\pi_3}\frac{1}{\sqrt{k_3^2-\gamma_0^2}\,H_0^{(1)}\left(\rho\sqrt{k_3^2-\gamma_0^2}\right)}\left\{\int\limits_{\varepsilon_1 \mathrm{cir}(-k_3\sin\vartheta)} H_1^{(1)}\left(r\sqrt{k_3^2-\gamma^2}\right)e^{i\gamma|z|}d\gamma + \right.$$
$$\left. + \int\limits_{\varepsilon_2 \mathrm{cir}(k_3\sin\vartheta)} H_1^{(1)}\left(r\sqrt{k_3^2-\gamma^2}\right)e^{i\gamma|z|}d\gamma\right\}. \tag{41}$$

Since the function under the integral in Eq. (41) is extremely small at points γ which are distant from the point $\gamma_0 = \pm k_3 \sin\vartheta$, we can change from an integration over segments in the neighborhood of the saddle points to an integration over a contour $\int$ going from $-\infty$ to $+\infty$. As a result, we can write Eq. (41) in the form

$$H_\varphi = i\frac{\omega\varepsilon_{k3}\mathscr{E}}{2\pi}\frac{1}{\sqrt{k_3^2-\gamma_0^2}\,H_0^{(1)}\left(\rho\sqrt{k_3^2-\gamma_0^2}\right)}\int\limits_{-\infty}^{+\infty} H_1^{(1)}\left(r\sqrt{k_3^2-\gamma^2}\right)e^{i\gamma|z|}d\gamma. \tag{42}$$

Considering that, for $\left|\sqrt{k_3^2-\gamma^2}\right| r \gg 1$

we have
$$H_1^{(1)}\left(r\sqrt{k_3^2-\gamma^2}\right) = -iH_0^{(1)}\left(r\sqrt{k_3^2-\gamma^2}\right),$$

$$H_\varphi = \frac{\omega\varepsilon_{k3}\mathscr{E}}{2\pi}\frac{1}{\sqrt{k_3^2-\gamma_0^2}\,H_0^{(1)}\left(\rho\sqrt{k_3^2-\gamma_0^2}\right)}\int\limits_{-\infty}^{+\infty} H_0^{(1)}\left(r\sqrt{k_3^2-\gamma^2}\right)e^{i\gamma|z|}d\gamma. \tag{43}$$

It is known that,

$$\int\limits_{-\infty}^{+\infty} H_0^{(1)}\left(r\sqrt{k_3^2-\gamma^2}\right)e^{i\gamma|z|}d\gamma = -i2\frac{e^{ik_3R}}{R},$$

where $R = \sqrt{r^2+z^2}$.

Consequently, we obtain

$$H_\varphi = -i\frac{\omega\varepsilon_{k3}\mathscr{E}}{\pi}\frac{1}{\sqrt{k_3^2-\gamma_0^2}\,H_0^{(1)}\left(\rho\sqrt{k_3^2-\gamma_0^2}\right)}\frac{e^{ik_3R}}{R}. \tag{44}$$

For small values of the wire gradient ρ, we can replace the Hankel function by the first term of its expansion into a series. Thus, we can write Eq. (44) in the form

$$H_\varphi = -i\frac{\omega\varepsilon_{k3}\mathscr{E}}{\pi}\frac{1}{\sqrt{k_3^2-\gamma_0^2}\left(1-i\frac{2}{\pi}\ln\frac{1{,}12}{\rho\sqrt{k_3^2-\gamma_0^2}}\right)}\frac{e^{ik_3R}}{R}. \tag{45}$$

With Eq. (45) for H_φ, it is easy to find the field component E_r and E_z. Substituting the value of γ_0 into (45), we find

$$H_\varphi = -i\frac{\omega\varepsilon_{k3}\mathscr{E}}{\pi}\frac{1}{k_3\cos\vartheta\left(1-i\frac{2}{\pi}\ln\frac{1{,}12}{\rho k_3\cos\vartheta}\right)}\frac{e^{ik_3R}}{R}. \tag{46}$$

The studies showed that, because of the strong damping, the amplitude of the current in the wire decreases sharply as the coordinate z increases. This makes it possible to replace an infinitely long wire by a wire of finite length. Consequently, for large values of R, the function

$$f(\vartheta) = \frac{1}{\cos\vartheta\left(1 - i\,\frac{2}{\pi}\ln\frac{1{,}12}{\rho k_3 \cos\vartheta}\right)} \tag{47}$$

determines the characteristics of the directivity of a wire of finite length. We note that equation (47) can be used for $0 \leqslant \vartheta < \pi/2$. A study of function of (47) shows that the main part of the electromagnetic energy is concentrated in a cone whose generatrix forms a relatively small angle with the axis of the wire.

The author considers it his pleasant duty to thank L. A. Vaynshteyn for his valuable advice and consideration of the results of this work.

REFERENCES

1. A. Sommerfeld, Ann. der Physik und Chemie, 1899, 67, vol. 2, 233;
   F. Frank, R. Mieses, Differential and Integral Equations of Mathematical Physics II, ONTI, 1937, pp. 925-932.
2. F. Noether, Sov. Phys., 1935, 8, 7.
3. V. V. Vladimirskiy, Izv. AN SSSR, Ser. Fiz. 1944, 8, 3, 139.
4. V. N. Kessenikh, Dokl. AN SSSR, 1940, 27, 6, 558.
5. L. A. Vaynshteyn, Zh. Tekh. Fiz. 1959, 29, 6, 673.

Submitted to the editors 16 August 1960

WAVE PROPAGATION IN NONLINEAR LINES WITH DISPERSION

R. V. Khokhlov

The report is devoted to a study of the process of propagation of electromagnetic waves in nonlinear lines when the phase velocities of the fundamental and second harmonic components of the wave are close to one another while the velocities of the remaining harmonics are remote from them. A lossless line is analyzed in detail, and the role of attenuation in the system is examined. Analysis is performed on the basis of qualitative integration of the differential equations describing the process of parametric interaction of the harmonic components and also on the basis of their analytic solution for individual cases.

INTRODUCTION

Interest in wave processes in lines with nonlinear distributed parameters has increased considerably. This is explained by the possibilities offered by such lines in the creation of new circuits for such devices as low-noise amplifiers and frequency converters. Thus, a number of authors [1-3] have examined in some detail the problems of parametric effects of amplification and frequency conversion in lines whose parameters vary in space and time as a traveling sinusoidal wave. One means of achieving such a change in parameters is the passage of a high-frequency signal ("boost") through the line. However, this high-frequency signal itself may be distorted in the line and the nature of this distortion is a priori unknown.

Another interesting problem closely associated with the process of wave propagation in nonlinear lines is that of frequency multiplication. Interaction of the wave and its harmonics leads to an interchange of energy and, as shown below, under certain conditions almost all the wave energy may be transformed to energy of one of the higher harmonic components. This circumstance may serve as the basis for creation of frequency multipliers.

Thus, the problem of wave propagation in nonlinear lines acquires increasingly greater importance.

It is necessary to distinguish two limiting cases — the case of a high-dispersion line and the case of a nondispersion line.

In the second case the higher harmonic components arising due to nonlinearity of the parameters of the line have the same phase velocity as the fundamental. As a result there is strong interaction between the signal and all of its harmonic components; hence, in propagation along the line there is a definite distribution of energy between these components and the fundamental signal. Consequently, the shape of the signal is distorted and takes the form of a shock wave [4-6].

In the case of the presence of dispersion only a few (in the simplest case, one) higher harmonics of the signal have a propagational velocity close to that of the fundamental component. Interaction is thus achieved only between these components and the fundamental, with the result that there occurs, generally speaking, a difference frequency-energy process.

The present report is devoted to a study of this process in the simplest case, when only one, the second, harmonic of the signal has a phase velocity close to that of the fundamental component. It is of interest to mention that the case under discussion is essentially the space-time analog of the process of parametric interaction between two oscillatory modes of pendulum as analyzed in their time by A. A. Vitt and G. S. Gorelik [7].

1. DERIVATION OF PRINCIPAL EQUATIONS

We shall limit discussion to a slightly nonlinear line in which the nonlinear parameter is the distributed capacitance, so that

$$Q = CU + DU^2, \tag{1}$$

where Q is line charge and U is voltage. Parameter D, characterizing the nonlinearity of the medium, is hereafter considered small.

The difficulty of rigorous statement of the problem of wave propagation in a dispersive medium is well-known. Description by means of ordinary telegraph equations (with standard notation)

$$\frac{\partial I}{\partial z} = -\frac{\partial Q}{\partial t} - GU, \quad \frac{\partial U}{\partial z} = -L\frac{\partial U}{\partial t} \tag{2}$$

or their corollaries

$$\frac{\partial^2 U}{\partial z^2} - L\frac{\partial^2 Q}{\partial t^2} - LG\frac{\partial U}{\partial t} = 0, \tag{3}$$

are, generally speaking, nonuniform, since the parameters L, C, G and D entering into them are functions of frequency ω. Nevertheless, for linear and slightly nonlinear media this relation may be dealt with directly at the level of equations for spectral components or of the shortened equations, respectively, by deriving them without consideration of this relation. Proceeding in this manner, we find that the wave process in the case under discussion is described by the expression

$$U = U_1 \cos[\omega t - \gamma z + \varphi_1] + U_2 \cos[2(\omega t - \gamma z) + \varphi_2], \tag{4}$$

where amplitudes U_1 and U_2 and phases φ_1 and φ_2 are slowly varying functions of coordinate z. The quantity γ is defined from (4) as

$$\gamma = \omega\sqrt{\frac{1}{2}(L_1C_1 + L_2C_2)}, \tag{5}$$

where subscript 1 indicates that the parameter values are taken for frequency ω and subscript 2 indicates that the parameter values are taken for frequency 2ω. It is hereby assumed that a line excited by whatever means at the input is matched at the output. Deriving in the usual manner the shortened equations describing the amplitude and phase behavior, we have

$$\begin{gathered}\dot{U}_1 + \beta_1 U_1 U_2 \sin\Phi + \delta_1 U_1 = 0,\\ 2\dot{\varphi}_1 + \frac{\Delta}{2} + 2\beta_1 U_2 \cos\Phi = 0,\\ \dot{U}_2 - \beta_2 U_1^2 \sin\Phi + \delta_2 U_2 = 0, \quad \dot{\varphi}_2 - \frac{\Delta}{2} + \beta_2 \frac{U_1^2}{U_2}\cos\Phi = 0,\end{gathered} \tag{6}$$

where Φ is the phase difference:

$$\Phi = 2\varphi_1 - \varphi_2; \tag{7}$$

parameter Δ characterizes the phase-velocity mismatch of partial systems:

$$\Delta = \frac{L_1C_1 - L_2C_2}{\gamma}\omega^2; \tag{8}$$

$\beta_{1,2}$ are the coupling coefficients; $\delta_{1,2}$ are the damping coefficients:

$$\beta = \frac{1}{2}\frac{LD\omega^2}{\gamma}; \quad \delta = \frac{1}{2}\frac{LG\omega}{\gamma}. \tag{9}$$

Applying the next-to-last equation in system (6) to the last equation in the same system, we obtain the phase equation

$$\dot{\Phi} + \Delta + \left[2\beta_1 U_2 - \beta_2 \frac{U_1^2}{U_2}\right]\cos\Phi = 0. \tag{10}$$

In the above mentioned sense the shortened equations (6) and (10) are more rigorous then the initial telegraph equations (2). They completely describe the wave propagation process in a dispersive line when the only interacting components are those of the fundamental and the second harmonic.

Equations (6) cannot be solved in closed form in the general case. Nevertheless, analysis of the process on the whole may be performed on the basis of examination of the different limiting cases. The ensuing sections of this report also discuss this problem.

2. QUALITATIVE ANALYSIS IN THE ABSENCE OF DAMPING

In the absence of damping the system of equations (6) and (10) permit qualitative integration in the phase plane. In this integration let us introduce the new variables

$$w = U_1^2, \quad x = U_2 \sin\Phi, \quad y = U_2\cos\Phi. \tag{11}$$

The system of equations (6) and (10) then take the form

$$\dot{w} = -2\beta_1 wx, \quad \dot{x} = \beta_2 w + \Delta y - 2\beta_1 y^2, \quad \dot{y} = -\Delta x + 2\beta_1 xy. \tag{12}$$

It is particularly important to note that the system of equations (12) gives us the first integral, which is in the nature of a law of conservation of energy. This relationship has the following form:

$$\beta_1(x^2 + y^2) + \beta_2 w = \beta_1(x_0^2 + y_0^2) + \beta_2 w_0 = \beta_1 U_0^2. \tag{13}$$

The constants x_0, y_0 and w_0 introduced in (13) represent the input values of x, y and w, while U_0 is the corresponding (in the energy sense) relative amplitude of the second harmonic component. Now, by means of (13), eliminating the value w from the second equation in (12), we arrive at the system

$$\begin{gathered}\dot{x} = \beta_1 U_0^2 + \Delta y - \beta_1 x^2 - 3\beta_1 y^2,\\ \dot{y} = -\Delta x + 2\beta_1 xy.\end{gathered} \tag{14}$$

Dividing one of these equations into the other, we obtain the equation describing the behavior of the integral curves in the plane xy:

$$\frac{dx}{dy} = \frac{\beta_1 U_0^2 + \Delta y - \beta_1 x^2 - 3\beta_1 y^2}{x(2\beta_1 y - \Delta)}. \qquad (15)$$

On the basis of this equation, examining the nature of the existing singular points, we may easily determine the behavior of the integral curves with different parameter ratios. This behavior is represented in Figures 1a, 1b and 1 c for the cases $\triangle = 0$, $|\triangle| < 2\beta_1 U_0$ and $|\triangle| > 2\beta_1 U_0$.

All integral curves reflecting the possible motion within the system are located within a closed integral curve, a circle with radius U_0. The integral curves external to this circle cannot be physically realized since they correspond to states with negative energy of the fundamental component. Even this closed integral curve may be wholly realized only in the case $|\triangle| > 2\beta_1 U_0$ (Figure 1c). Otherwise it passes through two singular saddle points intersected by another integral curve, the straight line $y = \triangle/2\beta_1$, that is, the separatrix (Figures 1a and 1b). Motion (in the limiting case) is represented by that part of the circle delimited by the saddle points and the straight line joining them.

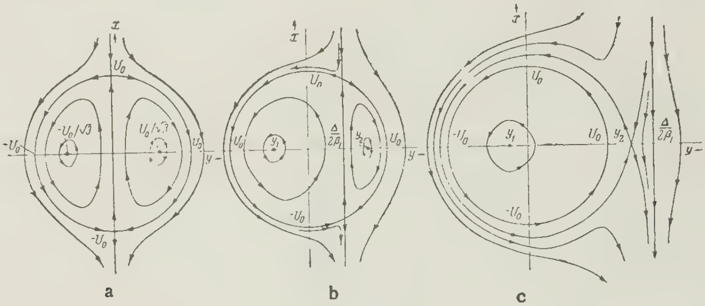

Figure 1

a) Behavior of integral curves of Eq. (15) in the case $\triangle = 0$; b) behavior of integral curves of Eq. (15) in the case $|\triangle| < 2\beta_1 U_0$; c) behavior of integral curves of Eq. (15) in the case $|\triangle| > 2\beta_1 U_0$.

This means that if the system contains a strong wave field of double frequency, in the case $|\triangle| > 2\beta_1 U_0$ it does not have a parametric resonant action on the weak field of the fundamental component. The absence of such action is due to the fact that the phase-velocity mismatch $\triangle$ lies beyond the zone of parametric excitation of the fundamental component. In the region $|\triangle| < 2\beta_1 U_0$ there is parametric interaction of the partial wave systems, with the result that within the system there arise spatial beats between the fundamental and the second harmonic components. These beats are obtained as the result of excitation and build-up of oscillations of fundamental frequency and a corresponding drop in amplitude of the second harmonic. The phase velocities meanwhile vary in such manner that the fundamental component begins to excite the second harmonic, thereby suppressing itself to zero. After this the process is periodically repeated.

With $\triangle = 0$ all the energy of the second harmonic may be transferred to energy of the fundamental component and conversely (that is, full beats may occur). This is associated with the fact that an integral curve, the separatrix, in this case passes through the point $x = 0$, $y = 0$, which corresponds to $U_2 = 0$,

$$U_1 = \sqrt{\frac{\beta_1}{\beta_2}}\, U_0.$$

It must be mentioned that the spatial beats also occur in the case of eccentricity in the ovals of the integral curves (Figure 1c) and are caused by the presence of definite interaction between the systems. However, this interaction is not a resonance phenomenon — the beats have little depth and period.

In the case $|\triangle| < 2\beta_1 U_0$ there are two stable, stationary states in the system, corresponding to singular points of the center node type (Figures 1a and 1b)

$$\begin{aligned} U_2 &= |y_1|, \quad U_1 = \sqrt{\frac{\beta_1}{\beta_2}(U_0^2 - y_1^2)}, \ \cos\Phi = -1, \\ U_2 &= |y_2|, \quad U_1 = \sqrt{\frac{\beta_1}{\beta_2}(U_0^2 - y_2^2)}, \ \cos\Phi = +1, \end{aligned} \qquad (16)$$

where

$$y_{1,2} = \frac{\Delta}{6\beta_1} \pm \sqrt{\frac{U_0^2}{3} + \frac{\Delta^2}{36\beta_1^2}}, \tag{17}$$

representing a synchronous wave process with constant amplitudes of the first and second harmonic components. One of them is cophasal and the other antiphasal. When $\Delta = 0$, in both synchronous states the conveyed available power is distributed over the partial systems so that

$$\beta_2 U_1^2 = 2\beta_1 U_2^2. \tag{18}$$

When $\Delta \neq 0$ this symmetry in power distribution is disturbed. Compared with (18), in one of the synchronous states, the power is predominantly in the fundamental component, and in the other state, the power is predominantly in the second harmonic.

All other possible states of the system are expressed as closed integral curves surrounding two singular points and describing the process of spatial beats around these stationary states.

With sufficiently large mismatch, when $|\Delta| > 2\beta_1 U_0$ (Figure 1c), the state with predominance of power in the second harmonic vanishes and only the synchronous state characterized by predominance of power in the fundamental component remains. It is of interest to note that this remaining state (y_1 in Figure 1c), depending on the sign of mismatch, may be cophasal or antiphasal. If the phase velocity of the fundamental component in the absence of interaction is greater than the velocity of the harmonic, the remaining state is cophasal; if it is less than the harmonic velocity, it is antiphasal.

The other possible states of the system are represented by the closed integral curves which surround the remaining singular point in this case. They describe the oscillations of amplitude and phase about the synchronous state, that is, spatial beats. One of the integral curves passes through the point $x = 0$, $y = 0$ at the phase plane. This trajectory describes the beat state characterizing total transfer of energy of the second harmonic to the first (but not the reverse).

Thus, on the basis of an examination of the phasal behavior of movements in plane xy we may ascertain many of the typical features and characteristics of the system. A number of the characteristics of the system are not determinable by such analysis. The most important of these are the spatial extent and scales of the processes. In order to determine them the next section discusses several cases permitting analytical solution.

3. SCALES OF PROCESSES IN AN UNDAMPED SYSTEM

It is evident that the nonelementary cases permitting analytical solution are limited to those of small amplitude and phase oscillation about synchronous states and to cases of motion along the trajectories $U_2 = U_0$ and $y = \Delta/2\beta_1$. We shall discuss these cases separately, and then use them as the basis for analysis of the spatial characteristics of processes in the general case of undamped systems.

A. Motion along ellipses (close, closed trajectories) surrounding singular points $x = 0$, $y = y_{1,2}$ in the case $|\Delta| < 2\beta_1 U_0$ is evidently harmonic. The equations describing it may easily be obtained by linearizing Eqs. (14) about these points. For trajectories close to points $x = 0$, $y = y_2$ (Figure 1b) we have

$$\dot{x} = -a\eta, \qquad \dot{\eta} = bx, \tag{19}$$

where

$$\eta = y - y_2; \quad a = \sqrt{12\beta_1^2 U_0^2 + \Delta^2}; \qquad b = -\frac{2}{3}\Delta + \frac{1}{3}\sqrt{12\beta_1^2 U_0^2 + \Delta^2}. \tag{20}$$

From this it is evident that the wave number Γ of the spatial beats is defined by the relation

$$\Gamma^2 = ab = \frac{1}{3}(12\beta_1^2 U_0^2 + \Delta^2) - \frac{2}{3}\Delta\sqrt{12\beta_1^2 U_0^2 + \Delta^2}. \tag{21}$$

It is easily verified that in the boundary case, when $|\Delta| = 2\beta_1 U_0$, the wave number vanishes. In cases of near-boundary values the wave number is

$$\Gamma^2 = \frac{1}{2}(4\beta_1^2 U_0^2 - \Delta^2) + \frac{3}{8}(2\beta_1 U_0 - \Delta)^2 + \ldots . \qquad (22)$$

In similar manner, obtaining the expression for the wave number of processes represented by ellipses close to $x = 0$ and $y = y_1$, we have

$$\Gamma^2 = \frac{1}{3}(12\beta_1^2 U_0^2 + \Delta^2) + \frac{2}{3}\Delta\sqrt{12\beta_1^2 U_0^2 + \Delta^2}. \qquad (23)$$

With large values of mismatch $|\Delta| \gg \sqrt{12}\beta_1 U_0$, when the parametric interaction between partial systems is extremely weak,

$$\Gamma \simeq \Delta, \qquad (24)$$

that is, the beating process reduces to simple addition of two waves with the corresponding partial phase velocities.

B. Motion along a limiting trajectory, where $U_2 = U_0$ and $U_1 = 0$, is described by the phase equation

$$\dot{\Phi} + \Delta + 2\beta_1 U_0 \cos\Phi = 0. \qquad (25)$$

This equation is solved in explicit form (for example, see reference [8]). In the case $|\Delta| < 2\beta_1 U_0$ it describes the process of exponential transition from the stationary phase

$$\Phi_c = \arccos\left(\frac{\Delta}{2\beta_1 U_0}\right) \qquad (26)$$

with positive value of sin Φ to the stationary phase with negative value of sin Φ. Although this transition occupies an infinitely greath length z, it occurs chiefly at a length ξ of the order of

$$\xi = \frac{1}{\sqrt{4\beta_1^2 U_0^2 - \Delta^2}}. \qquad (27)$$

The other part of the limiting trajectory in the case $|\Delta| < 2\beta_1 U_0$ is determined by the condition $y = \Delta/2\beta_1$. Inserting it into the first equation of (14), we may obtain

$$\dot{x} = \beta_1\left(U_0^2 - \frac{\Delta^2}{4\beta_1^2}\right) - \beta_1 x^2. \qquad (28)$$

The solution of Eq. (28) has the form

$$x = \sqrt{U_0^2 - \frac{\Delta^2}{4\beta_1^2}}\tanh\beta_1(z - z_0)\sqrt{U_0^2 - \frac{\Delta^2}{4\beta_1^2}}, \qquad (29)$$

where z_0 is the integration constant. It describes the process of exponential transition of the system from the stationary state at circle $U_2 = U_0$ with negative value of sin Φ to the state $U_2 = U_0$ and $\sin\Phi > 0$. As in the case of motion along the arc of a circle, the length of this transition is infinite. However, as in the previous case, it occurs chiefly at a length of the order of that defined in relation (27).

It is of interest to note that in the case $\Delta = 0$ the solution just derived* corresponds to such boundary conditions when only the fundamental component of the wave field exists at the input and the second harmonic is completely absent. It follows from solution (29) that in this case the amplitude of the second harmonic rises monotonically and the amplitude of the fundamental component is entirely suppressed. As a result all the energy transfers to the second harmonic.

As follows from the qualitative examination presented in the preceding section, such a conclusion is not consistent. This is associated with the fact that the trajectory of solution (29) is a separatrix. Where the system converges on the stationary value $U_2 = U_0$, $U_1 = 0$ is not stable. Any small mismatch in phase velocity, fluctuation in amplitude of harmonics at the input, etc. will cause motion to occur along a closed trajectory which describes the spatial beats. The instability is caused by parametric excitation of oscillations of the fundamental component.

---

*Solution (29) in the case $\Delta = 0$ was also derived by B. Old and T. Caino (Stanford University, US). The author takes this opportunity to thank them for their interesting discussion of this solution.

In the case $|\Delta| > 2\beta_1 U_0$ movement along the limiting trajectory $U_2 = 0$ is stable and in this case there is no stationary value of phase (26). The phase has a definite mean increment per spatial period. Cos Φ and sin Φ are periodic functions of distance, wherein the wave number is

$$\Gamma = \sqrt{\Delta^2 - 4\beta_1^2 U_0^2}. \tag{30}$$

On the basis of the above discussion of spatial processes at the limiting trajectories we may draw several conclusions concerning the extent of spatial beats in the general case.

In the case $|\Delta| < 2\beta_1 U_0$ the trajectories immediately surrounding the nodal singular points possess the smallest spatial-beat period of the family of trajectories delimited by separatrices. The wave numbers of the beat process in this case are defined by relations (21) and (23). In transition from trajectory to trajectory from a nodal point toward the separatrix the beat period increases to values of the order of (27) for trajectories near the separatrix. In the immediate vicinity of the separatrix itself the spatial period increases more rapidly, logarithmically approaching infinity with decreasing distance to the separatrix.

The dependence of the beat period on amplitude in the case $|\Delta| > 2\beta_1 U_0$ at trajectories around the nodal singular point is also a monotonically increasing function. In the vicinity of the node the period is defined by relation (23), while at the limiting integral curve it is defined by relation (30).

Thus, it may be considered that the extent of spatial beating has been qualitatively determined in the general case also.

4. INFLUENCE OF POWER DISSIPATION ON PROCESSES IN THE SYSTEM

The foregoing discussion dealt with an undamped system. The general case with consideration of the influence of power dissipation in the system, when the damping coefficients δ_1 and δ_2 differ and are arbitrarily related to coupling coefficients β_1 and β_2, may be analyzed only by means of numerical integration of Eqs. (6) and (10). The analytical basis of this is found in the absence of an energy integral of the type (13). Such an integral exists only in the case where the damping coefficients δ_1 and δ_2 are equal:

$$\delta_1 = \delta_2 = \delta. \tag{31}$$

Then the energy integral takes the form

$$\beta_1 (x^2 + y^2) + \beta_2 w = \beta_1 U_0^2 e^{-2\delta z}. \tag{32}$$

However, even in this case, it is apparent that analysis of system behavior by any means other than on the basis of numerical integration is possible only in the case of complete equality of the partial phase velocities of the fundamental component of the wave field and its second harmonic ($\Delta = 0$). In order to demonstrate this let us examine the equations defining the behavior of a system similar to the equations in (14). They have the form

$$\dot{x} = -\delta x + \Delta y - \beta_1 x^2 - 3\beta_1 y^2 + \beta_1 U_0^2 e^{-2\delta z}, \quad \dot{y} = -\delta y - \Delta x + 2\beta_1 xy. \tag{33}$$

Introducing the new dimensionless amplitudes X and Y according to the relation

$$x = XU_0 e^{-\delta z}, \; y = YU_0 e^{-\delta z} \tag{34}$$

and a new argument, the dimensionless "reduced" distance Z, by means of the relation

$$Z = \frac{2\beta_1 U_0}{\delta}(1 - e^{-\delta z}), \tag{35}$$

we may reduce the system of equations in (33) to the form

$$X' = \frac{\Delta}{2(\beta_1 U_0 - \delta Z)} Y - \frac{1}{2} X^2 - \frac{3}{2} Y^2 + \frac{1}{2}, \quad Y' = -\frac{\Delta}{2(\beta U_{10} - \delta Z)} X + XY, \tag{36}$$

where the dash denotes differentiation over the reduced distance Z.

At first glance the system of equations (36) appears to have the form of the system (14), but it is considerably different. The difference lies in the dependence of the coefficients of the linear terms in the right members on the argument. This prohibits use of the method of qualitative integration at phase plane XY, as was done for the system in (14). The only possible case for analysis is the case of $\Delta = 0$, which we shall now discuss.

In the case $\Delta = 0$, Eqs. (36) take the form

$$2X' = -X^2 - 3Y^2 + 1, \quad Y' = XY, \tag{37}$$

which is the dimensionless form of (14) with $\Delta = 0$. Figure 1a represents the integral curves in this case at plane XY. The period of rotation of the imaging point along the closed integral curves is of the order of unity on the scale of the reduced distance Z.

Let us explain the significance of the relative distance Z [relation (35)].

If the system is undamped ($\delta = 0$), the reduced distance is proportional to true distance from the input of the system, wherein the scale factor is the nonlinearity parameter $\beta_1 U_0$. In this case as long as Z is small, nonlinearity of the system may generally be disregarded. It becomes significant only at values of Z of the order of unity.

In the case $\delta \neq 0$ the relative distance is a nonlinear function of the real distance from the input; with an infinite increase in distance from the input it remains finite. There is a substantial difference in the two cases: $2\beta_1 U_0 \gg \delta$ and the opposite case. The first case corresponds to the condition in which damping has little effect at distances where the nonlinearity is already significant. The relative distance at sufficiently large distances from the input of the system may have an extremely large value. The second case, conversely, is attained when nonlinearity is slight. Parameter Z is then small at any distance from the input.

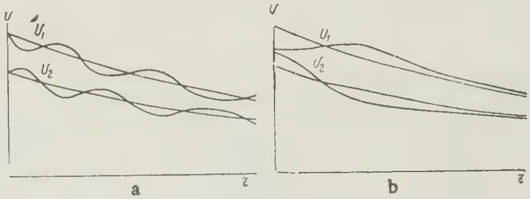

Figure 2. The spatial damped-beat process occurs near values of amplitude which are characteristic of synchronous states:

a) case of small damping $\delta \ll 2\beta_1 U_0$; b) case of considerable damping $\delta > 2\beta_1 U_0$.

Thus, the relative distance Z characterizes the degree of occurrence of nonlinear properties of the system: if it is of the order of unity or greater, there is considerable nonlinearity; if it is small, there is little nonlinearity.

It follows from the above observations that only in the case of $2\beta_1 U_0 \gg \delta$ may the imaging point at phase plane XY describe several revolutions over a closed trajectory, finally approaching a definite point on it characterized by Z_∞:

$$Z_\infty = \frac{2\beta_1 U_0}{\delta}. \tag{38}$$

In the case of considerable damping $\delta \gg 2\beta_1 U_0$ the imaging point completes only a small arc along the trajectory, characterized by the interval Z (38).

In particular, it must be noted that the spatial beat period increases with distance, which is the result of the nonlinear dependence of the reduced distance on the real distance. With sufficiently large damping the second and even the first "period" may extend to infinity (Figure 2b).

In the case under discussion, as in the case of no damping, there exist synchronous states, cophasal and antiphasal, which are characterized by the solutions

$$U_1 = \sqrt{\frac{2\beta_2}{3\beta_1}}\, U_0 e^{-\delta z}, \quad U_2 = \sqrt{\frac{1}{3}}\, U_0 e^{-\delta z} \tag{39}$$

and around which there may occur amplitude and phase oscillations — damped beats (Figure 2).

As in the case of no damping, motion along the integral curves (separatrices) delimiting the possible energy states may be described analytically. One of these curves is characterized by equality of the amplitude of the fundamental component to zero $U_1 = 0$. In this case

$$X^2 + Y^2 = 1 \tag{40}$$

and Eqs. (37) are easily integrated. As a result the amplitudes of the second harmonic component x and y are described by the expressions

$$x = -U_0 e^{-\delta z} \tanh \frac{2\beta_1 U_0}{\delta} (e^{-\delta z_0} - e^{-\delta z}), \quad y = \pm \frac{U_0 e^{-\delta z}}{\cosh \frac{2\beta_1 U_0}{\delta} (e^{-\delta z_0} - e^{-\delta z})}, \tag{41}$$

where z_0 is the distance characterized by passage of amplitude x through zero.

Motion along the other separatrix, the equation of which is

$$Y = 0, \tag{42}$$

may also be described analytically. Inserting (42) into Eq. (37) and integrating, we have

$$x = U_0 e^{-\delta z} \tanh \frac{2\beta_1 U_0}{\delta} (e^{-\delta z_0} - e^{-\delta z}), \quad U_1 = \frac{\sqrt{\frac{\beta_2}{\beta_1}}\, U_0 e^{-\delta z}}{\cosh \frac{2\beta_1 U_0}{\delta} (e^{-\delta z_0} - e^{-\delta z})}. \tag{43}$$

Plots representing the relationships in (41) and (43) are given in Figure 3. The boundary conditions therein are chosen close to the saddle point from which the motion begins.

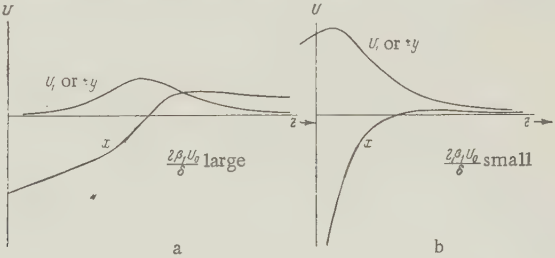

Figure 3. Change in amplitude of harmonic components with distance in the case of motion along separatrices:

a) small damping; b) large damping.

An examination of the curves shows that in the case of small damping (Figure 3a) motion along the separatrix leads to a parametrically unstable state (with $z \to \infty\ |x| > U_1$), whereas in the case of large damping (Figure 3b) motion along the separatrix leads to a stable state and may be achieved in practice.

It follows from the observations of this section that in the general case of different, but small, damping coefficients, damping has little effect at distances of the order of one beat period. Hence, on the basis of a reasonable approximation, it is of interest to analyze the other extreme case, wherein at least one of the damping coefficients is large.

5. CASE OF STRONG DAMPING IN A LINE

Since in practical cases damping at a harmonic frequence is greater than damping of the fundamental component, in this section we shall discuss a case which may be of some interest when the damping coefficient δ_2 is large:

$$\delta_2 \gg \beta_{1,2} U_0, \tag{44}$$

and coefficient δ_1 is small and is of the order of the right-hand term in (44).

In this case the equations [similar to those in (12)] describing the wave processes in the system

$$\dot{w} = -2\delta_1 w - 2\beta_1 w x, \quad \dot{x} = -\delta_2 x + \beta_2 w + \Delta y - 2\beta_1 y^2,$$
$$\dot{y} = -\delta_2 y - \Delta x + 2\beta_1 x y \tag{45}$$

may be simplified and their solutions analyzed. Proceeding to this simplification, we note that the most interesting region of mismatch of phase velocities is of the order of $\triangle \approx \beta_{1,2} U_0$. Turning our attention to this region, in the right-hand sides of the second and third equations of system (45) we may disregard the nonlinear terms and terms which are proportional to $\triangle$. Then we have

$$w = -2\delta_1 w - 2\beta_1 wx, \ \dot{x} = -\delta_2 x + \beta_2 w, \ \dot{y} = -\delta_2 y. \tag{46}$$

In addition, the equation for the y components may be eliminated. This indicates that in the case of large damping at a harmonic frequency parametric correlation of the fundamental component is achieved only with the harmonic component x. The equations describing the wave process are somewhat simplified.

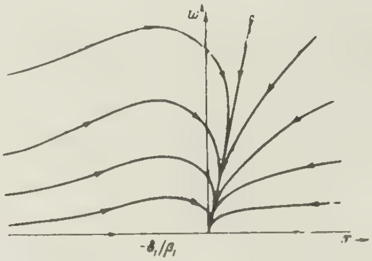

Figure 4. Behavior of integral curves of Eq. (47).

It is simplest of all to analyze the general properties of the solutions of the system of the first two equations in (24) by qualitative integration at plane xw. Dividing one equation into the other, we obtain

$$\frac{dx}{dw} = \frac{\delta_2 x - \beta_2 w}{2w(\delta_1 + \beta_1 x)}. \tag{47}$$

It must be kept in mind that by definition coordinate w can only be positive. The phase patterns of motion are easily plotted from Eq. (47) (Figure 4). All the integral curves flow into a curve characterizing the continuous change with a spatial scale $1/2\ \delta_1$ and the corresponding definite boundary conditions at the input. In order to derive its equation, it is necessary to assume that the change in x is slow and to disregard in the second equation of (46) the term $\dot{x}$ in comparison with $\delta_2 x$. The resulting approximate equation for this integral curve has the form

$$y \simeq \frac{\beta_2}{\delta_2} w. \tag{48}$$

The rate of approach of the imaging points along the fundamental integral curve to the curve of (48) is considerably greater than the rate of change along curve (48) and is characterized by the spatial scale $1/\delta_2$.

From the phase pattern of motions we may establish the general character of interaction of the fundamental and second harmonic components with different boundary motions at the input of the system.

From Figure 4 it is seen that if to the input there are applied a large signal of double frequency and a small signal of fundamental frequency, under certain phase relations ($x_0 < 0$, that is, $\sin \Phi < 0$) this small signal is increased, reaching a maximum at a distance from the input of the order of

$$z_m = \frac{1}{\delta_2} \ln \frac{\beta_1 x_0}{2\delta_1} \tag{49}$$

and then decreases with increasing distance from the input. Let it be mentioned that the maximum possible gain in fundamental component is extremely small and does not exceed a few decibels.

If, on the other hand, we apply the voltage of only the fundamental component at the input of the system, it rapidly excites the second harmonic, which at a distance of the order of

$1/\delta_2$ reaches a maximum of

$$x_m \simeq \frac{\beta_2 w_0}{\delta_2}, \tag{50}$$

and then slowly decreases exponentially with the index $2\delta_1$.

Thus, all possible excitations of components of the wave field occur at distances of the order of $1/\delta_2$ from the input, after which the amplitudes slowly decrease with a specific, characteristic scale change equal to $1 2\delta_1$.

CONCLUSIONS

In the propagation of waves within a highly dispersive line with nonlinear distributed parameters between the different harmonic components parametric coupling occurs. In the case of near synchronism between the fundamental and second harmonic components (which is the subject of this report), this coupling generally leads to spatial energy beats between the components. In the case of equal damping of components there exist distinct synchronous stationary states in which there are no energy beats between the fundamental and second-harmonic components of the wave. There may be one or two such states, depending on the amount of mismatch in the partial phase velocities of the components: with small mismatch there are two and with sufficiently large mismatch there is one. In the case of equality of the partial phase velocities the power conveyed by the fundamental component in both synchronous states is twice as great as the power conveyed by the harmonic.

The presence of two stationary states may be used for the creation of traveling-wave parameters — new memory elements for high-speed computers. Their switching time (from one stationary state to the other) may be substantially decreased in comparison with parametrons of resonant type.

The energy beats occur in the vicinity of values of amplitude and phase characteristic for stationary synchronous states. Power dissipation in the system leads not only to damping of the wave process but also to an increase in the beat period, this increase being proportional to distance from the input. Finally, one of the periods proves to be the last — it extends to infinity. The beat-energy process also occurs in the case of heavy damping, although the beat amplitude therein is small.

REFERENCES

1. P.K. Tien, H. Suhl, A traveling-wave ferromagnetic amplifier, Proc. IRE, 1958, 46, 4, 700.
2. P.K. Tien, Parametric amplification and frequency mixing in propagation circuits, J. Appl. Phys., 1958, 29, 9, 1347.
3. A.L. Cullen, Theory of traveling-wave parametric amplifier, Nature, 1958, 181; 332; Proc. IEE, 1960, 107B, 32, 101.
4. A.V. Gaponov, G.I. Freydman, Toward a theory of shock-excited electromagnetic waves in nonlinear media, Izv. Vuzov MVO SSSR (Radiofizika), 1960, 3, 1, 79.
5. R. Landauer, Parametric amplification along nonlinear transmission lines, J. Appl. Phys., 1960, 31, 3, 479.
6. R.V. Khokhlov, Toward a theory of shock-excited radio waves in nonlinear lines, Radiotekhnika i Elektronika, 1961, 6, 6, 917.
7. A.A. Vitt, G.S. Gorelik, Oscillations of an elastic pendulum as an example of oscillations of two parametrically coupled linear systems, Zh. Tekh. Fiz., 1933, 3, 2-3, 294
8. R.V. Khokhlov, Toward a theory of locking with an external force of small amplitude, Dokl. AN SSSR, 1954, 47, 3, 411.

Submitted to the editors 15 August 1960

CALCULATION OF THE PHASE VELOCITY OF WAVES IN AN ARTIFICIAL METAL DIELECTRIC WHEN THE CURRENT HARMONICS ON THE ELEMENTS OF THE STRUCTURE ARE CONSIDERED

L. S. Benenson

A generalized characteristic equation for the phase velocity of waves in an artificial metal dielectric is derived. This equation is suitable for the general case of an arbitrary distribution of the current on the elements of the structure.

Corrections for the effect of the first current harmonic are computed for the phase velocity of waves in a system of infinitely long rods.

INTRODUCTION

In [1], it is shown that the method of induced emf can be used to compute the phase velocity of waves in an artificial metal dielectric. The characteristic equation is derived and analyzed in [1] on the basis of structures whose elements are thin cylindrical rods. The computation is simplified by assuming that the currents flowing at the surface of the rods have only an actual component and that their distribution is described by a certain real function which remains constant throughout the cross section of the rod. Consequently, the practical applications of Eq. (32) of [1] is restricted to the case of thin rods with relatively large periods of the structure, under which condition this function is justified.

It is desirable to derive a generalized characteristic equation suitable for the general case of an arbitrary current distribution in the rods. This would make it possible, in particular, to establish the limits of the practical applicability of the simple equation (32) in [1]. Let us consider this problem, restricting ourselves, as in [1], to the case of propagation of waves along one of the axes of the structure (this case can be generalized to the case of an arbitrary direction of propagation by means of the method presented in [2]). Thus, instead of considering a three-dimensional structure, we shall be able to deal with an equivalent structure in the form of a one-dimensional lattice placed in a rectangular waveguide with two metal walls and two perfectly permeable walls. The axis of the waveguide coincides with the axis of the lattice, along which the wave propagates (the z-axis; see diagram).

In principle, two methods can be followed in solving this problem. In the first method, the currents flowing on the surface of the elements of the structure are represented in the form of a superposition of orthogonal functions. In general the coefficients of this superposition are unknown. This makes it possible to approximate the arbitrary distribution of the current with any degree of accuracy, depending on the number of approximating functions. Consequently, the phase velocity can be obtained with great accuracy. In the second method, the current distribution in the elements of the structure is assumed to be known and identical to the distribution found from a preliminary solution of a simpler problem. Obviously, this identity of the currents can only be approximate. In reality, in the first method as well, it is necessary to speak of an approximation to the current's distribution, since the characteristic equation can be actually solved when the number of approximating functions is small. Below we shall consider both of these methods.

1. THE CURRENT DISTRIBUTION IN THE ELEMENTS OF THE STRUCTURE IS UNKNOWN BEFOREHAND

In accordance with the above discussion, let us suppose that the currents $\vec{K}$ flowing at the surface of the structure elements are represented by a superposition of real functions Ψ_2 forming a complete orthogonal system on this surface. Then, for the n-th element we can write

$$\vec{K}_n = e^{-ihnL_z} \sum_j a_j \vec{\psi}_j, \tag{1}$$

where L_z is the period of the lattice on the axis of the equivalent waveguide; h is the phase constant of the wave in the structure which must be determined; and a_j is the amplitude of the j-th current harmonic.

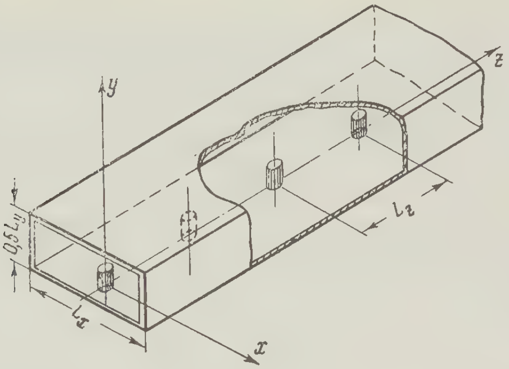

The total field produced by all the elements of the one-dimensional lattice in the equivalent waveguide is

$$\vec{E}\{\vec{K}\} = \sum_n \vec{E}\{\vec{K}_n\} = \sum_{n,\,j} e^{-ihnL_z} a_j \vec{E}_n\{\vec{\psi}_j\}, \tag{2}$$

where $\vec{E}_n\ \vec{\Psi}_j$ represents the field generated by the current $\vec{\Psi}_j$ which is distributed on the n-th element. This field must satisfy the boundary conditions at the surface of the equivalent waveguide.

At the surface s_n of each element of the structure, the following boundary condition is satisfied:

$$\vec{E}_{kac}\{\vec{K}\} = 0. \tag{3}$$

Then, multiplying (3) by $\vec{\Psi}_p$ and integrating over the surface of an arbitrary element of the structure, for example, the zeroth element (i.e., the element near the origin of coordinates), and also taking into account (2), we obtain a system of homogeneous linear equations for the unknown amplitudes a_j:

$$\sum_j a_j \Big(\sum_n e^{-ihnL_z} Z_{0n,\,pj}\Big) = 0, \qquad p = 1, 2, \ldots, \tag{4}$$

where

$$Z_{0n,\,pj} = -\frac{1}{T^2} \int_{s_0} \vec{\psi}_p \vec{E}_n\{\vec{\psi}_j\}\, ds \tag{5}$$

is the impedance which the current $\vec{\Psi}_j$, distributed on the zeroth element (with the surface s_0), encounters as a result of induction by the current $\vec{\Psi}_p$ distributed on the n-th element; and T is a dimensional divisor which is equal to the perimeter of the cross section of the structure element and which is used to make the definition of the induced impedance identical with the generally accepted one. The condition for the existence of nontrivial solutions of system (4) is that the determinant of the system equals zero

$$\begin{vmatrix} A_{00}, & A_{10}, & \dots \\ A_{01}, & A_{11}, & \dots \\ \dots & \dots & \dots \end{vmatrix} = 0, \tag{6a}$$

where

$$A_{pj} = \sum_n e^{-ihnL_z} Z_{0n,\,pj}. \tag{6b}$$

Equation (6a) is the characteristic equation for which we have been looking to determine the phase constant h of the waves in the structure. If the current distribution is described sufficiently well by the function, then (6a) becomes

$$A_{00} \equiv \sum_n e^{-ihnL_z} Z_{0n,\,00} = 0. \tag{7}$$

Equation (7) is the same as (15) obtained in [1]. Equation (6a) thus represents a generalization of (15) to the case of an arbitrary current distribution, unknown beforehand, on the elements of the structure. In general, it is an infinite determinant, since (1) is an infinite series. Since, however, the current distribution of the elements of the structure can be approximated, with sufficient accuracy for practical purposes, by a finite number of functions $\vec{\Psi}_j$ in (1), the determinant (6a) will actually be of second to fourth order, and its solution will present no fundamental difficulties. The solution can be considerably simplified, if it is considered that in the majority of cases, the value $h = h_0$ in the 0-th approximation [when (6a) reduced to (7)] is fairly close to the true value. Thus, it is necessary to use (7) only to compute the correction to h_0. Determinant (6a) can be solved by the method of successive approximations. Expanding (6a) in terms of the elements of the first row (or column) and transposing all the terms except the first to the right side, we write (6a) in the form

$$A_{00}(h) = -\frac{\sum\limits_{k=1}^{N} A_{0k}(h)\, B_{0k}(h)}{B_{00}(h)}. \tag{8}$$

Here B_{ik} is the algebraic complement of the element A_{ik}. We obtain the 0-th approximation $h = h_0$ by solving (8) with the right member discarded, i.e., by solving the equation

$$A_{00}(h) = 0. \tag{9}$$

We find a correction to $h = h_0$ by solving (8) with $h = h_0$ substituted into the right-hand side. Thus, we have the equation

$$A_{00}(h) = -\frac{\sum\limits_{k=1}^{N} A_{0k}(h_0)\, B_{0k}(h_0)}{B_{00}(h_0)}, \tag{10}$$

and so on.

Since the free term in (9) is the quantity $X_{00,00}$ — the radiation reaction of the elements of the structure (see for instance, Eq. (30) in [1]), the solution of Eq. (10) is the same as the solution of (9), but with a corrected value of $X_{00,00}$ equal to

$$X'_{00,\,00} = X_{00,\,00} + \frac{\sum\limits_{k=1}^{N} A_{0k}(h_0)\, B_{0k}(h_0)}{B_{00}(h_0)}. \tag{11}$$

Obviously, if there are detailed graphs of $h_0 = f(X_{00,00})$, we can find h_1 from them and $h_1 = f(X_{00,00})$.

The succeeding approximations are found in an analogous fashion.

For our subsequent analysis of Eq. (6a), let us transform Eq. (6b) to a simpler form. We define

$$f_m^{(j)} = \frac{1}{T} \int\limits_{S_0} \vec{\psi}_j \vec{E}_m \, ds \tag{12}$$

— the total emf produced by the n-th natural wave of equivalent waveguides and acting on the j-th component of the current distribution on the 0-th rod. Let us represent the field excited by the structure element by an expansion in terms of the natural wave of equivalent waveguide:

$$\vec{E}_n\{\vec{\psi}_j\} = \begin{cases} \sum\limits_m C_m^{(nj)} \vec{E}_m, & z > z_n + a, \\ \sum\limits_m C_{-m}^{(nj)} \vec{E}_{-m}, & z < z_n - a, \end{cases} \tag{13}$$

where

$$C_{\pm m}^{(nj)} = \frac{1}{N_m} f_{\mp m}^{(j)} e^{\pm i\gamma_m z_n}; \quad N_m = \int\limits_{S_\perp} \{[\vec{E}_m \vec{H}_{-m}] - [\vec{E}_{-m} \vec{H}_m]\} \vec{i}_z \, dS; \tag{14}$$

z_n is the coordinate of the center of the n-th rod; a is the radius of the rod; S is the cross section of the waveguide; and m is the subsequent (consisting of one or several numbers) indicating the mode of the natural wave (positive). The subscript -m indicates an opposite wave in the m-th mode (for which the propagation constant is $\gamma_{-m} = -\gamma_m$).* Using Eqs. (12) to (14), we obtain for $Z_{0n,pj}$ with $n \neq 0$:

$$Z_{0n,\,pj} = \begin{cases} -\sum\limits_m \frac{1}{N_m} f_{-m}^{(j)} f_m^{(p)} e^{-i\gamma_m |n| L_z}, & n > 0, \\ -\sum\limits_m \frac{1}{N_m} f_m^{(j)} f_{-m}^{(p)} e^{-i\gamma_m |n| L_z}, & n < 0. \end{cases} \tag{15}$$

The quality $Z_{00,pj} = R_{00,pj} + iX_{00,pj}$ cannot be expressed as easily. However, for its real part $R_{00,pj}$, which is equal to twice the mutual radiation power of the currents $\vec{\Psi}_j$ and $\vec{\Psi}_p$, we find, considering (13) and (14)

$$R_{00,\,pj} = \operatorname{Re} \int\limits_{S_{\perp 1} + S_{\perp 2}} [\vec{E}_0\{\vec{\psi}_j\} \vec{H}_0^*\{\vec{\psi}_p\}] \, d\vec{S} = \sum_m \frac{2P_m}{|N_m|^2} \{f_m^{(j)} f_m^{(p)*} + f_{-m}^{(j)} f_{-m}^{(p)*}\}, \tag{16}$$

where $S_{\perp 1}$ and $S_{\perp 2}$ are the cross sections of the equivalent waveguide to the left and to the right of the zeroth element; and $P_m = \frac{1}{2} \int\limits_{S_{\perp 1}} [\vec{E}_m \vec{H}_m^*] \, d\vec{S} = \frac{1}{2} \int\limits_{S_{\perp 2}} [\vec{E}_{-m} \vec{H}_{-m}^*] \, d\vec{S}$ — is the power carried along the axis of the waveguide by the natural waves with a subscript m in the direction z > 0 and with a subscript -m (in the direction z < 0). The summation in Eq. (16) is taken only over the wave which propagates for the given dimensions of the waveguide. Let the wave with ± m be normalized in such a way that for propagating waves

$$\vec{E}_m = \vec{E}_{-m}^*, \quad \vec{H}_m = -\vec{H}_{-m}^*. \tag{17}$$

Then, for these waves,

$$N_m = -4P_m, \quad f_{-m} = f_m^* \tag{18}$$

and

$$R_{00,\,pj} = -\sum_m \frac{1}{2N_m} \{f_m^{(j)} f_{-m}^{(p)} + f_{-m}^{(j)} f_m^{(p)}\}. \tag{19}$$

Using Eqs. (15) and (19) and summing the resulting geometric progressions, we find

$$\begin{aligned} \sum_{n=-\infty}^{\infty} e^{-ihnL_z} Z_{0n,\,pj} = iX_{00,\,pj} + i \sum_{m=0}^{\infty} \Big\{ \frac{f_{-m}^{(j)} f_m^{(p)}}{2N_m} \cot\left(\frac{\gamma_m - h}{2} L_z\right) + \\ + \frac{f_m^{(j)} f_{-m}^{(p)}}{2N_m} \cot\left(\frac{\gamma_m + h}{2} L_z\right) \Big\} + \frac{1}{2} \sum_{m>t} \frac{f_{-m}^{(j)} f_m^{(p)} + f_m^{(j)} f_{-m}^{(p)}}{N_m}, \end{aligned} \tag{20}$$

---

*See [3] (81.01) and [4] (XV.26).

where t is the number of propagating wave modes. The function f can be both even

$$f^{(j)}_{-m} = f^{(j)}_{m}, \tag{21a}$$

and odd

$$f^{(j)}_{-m} = -\, f^{(j)}_{m} \tag{21b}$$

with respect to the z-axis. If $f^{(j)}_{-m}$ and $f^{(p)}_{-m}$ satisfy simultaneously the same condition from (21), Eq. (20) will become

$$\begin{gathered}\sum_{n=-\infty}^{\infty} e^{-ihnL_z} Z_{0n,\,pj} = iX_{00,\,pj} + i \sum_{m=0}^{\infty} \frac{f^{(j)}_{m} f^{(p)}_{-m}}{N_m} \frac{\sin \gamma_m L_z}{\cos hL_z - \cos \gamma_m L_z} + \\ + \sum_{m>t} \frac{f^{(j)}_{m} f^{(p)}_{-m}}{N_m} = \sum_{n=-\infty}^{\infty} e^{-ihnL_z} Z_{0n,\,jp}.\end{gathered} \tag{22a}$$

If on the other hand $f^{(j)}_{-m}$ and $f^{(p)}_{-m}$ satisfy different conditions from (21), then, since $X_{00,pj} = R_{00,pj} = 0$ in this case, we obtain

$$\begin{gathered}\sum_{n=-\infty}^{\infty} e^{-ihnL_z} Z_{0n,\,pj} = -i \sum_{m=0}^{\infty} \frac{f^{(j)}_{m} f^{(p)}_{-m}}{N_m} \frac{\sin hL_z}{\cos hL_z - \cos \gamma_m L_z} = \\ = - \sum_{n=-\infty}^{\infty} e^{-ihnL_z} Z_{0n,\,jp}.\end{gathered} \tag{22b}$$

The element A_{pj} of determinant (6a) will obviously be of the form (22a) for j + p even, and in the form (22b) for j + p odd.

Equations (22) are convenient for practical computations and can be used directly in computing (6a). As can be seen from (22a), the quantities $X_{00,pj}$ the self-reactances and mutual reactances of the current harmonics of the structure elements — will appear in Eq. (6a) as parameters. These quantities are completely determined by the geometry of the structure, and in general, they are known. However, it is possible as in the solution of Eq. (32) in [1], to consider $X_{00,00}$ as an independent parameter. Then, easily solving Eq. (6a) for $X_{00,00}$, we can find $X_{00,00}$ as a function of h. Taking the inverse of this function, we obtain $h = h\,(X_{00,00})$. Since $X_{00,00}$ depends on the geometry of the structure, we can find the relation between the geometry of the structure and h, i.e., the solution of the characteristic equation. As distinguished from the method of successive approximations presented above, this gives an exact solution of (6a) (for a given number of approximating functions Ψ_p).

Let us consider a specific example of a structure consisting of infinite rods parallel to the y-axis. First of all, let us note that, if the current on the structure elements have only y-components (as is precisely the case for infinite rods), the complete system of natural waves in the equivalent waveguide will be described by the Hertzian vector $_e = {}_{ey}\vec{i}_y$. Then, the relationship between the field $\vec{E}_m$ and $\vec{E}_{-m}$ holding in addition to (17) has the form

$$\vec{E}_{-m} = \vec{E}_{-m} e^{2i\gamma_m z} \tag{23}$$

for waves of both the propagating type and the damped types.

Since we are considering the case where the waves in the structure propagate only in the direction of the z-axis, the function Ψ_p must obviously be even with respect to the y- and z-axis. With respect to the x-axis, they can be either even or odd. In the first case, Eq. (21a) holds, while in the second case Eq. (21b) holds.

Let $\Psi_p = \cos p\varphi$ (φ is measured from the x-axis). Setting

$$\Pi_{ey} = \frac{1}{k^2} \cos \frac{2m\pi x}{L_x} e^{-i\gamma_m z},\ E_y = k^2 \Pi_y,\ H_x = -\frac{k\gamma_m}{Z_0} \Pi_y,\ \gamma_m = k \sqrt{1 - \left(\frac{2m\pi}{kL_x}\right)^2}, \tag{24}$$

we find

$$\begin{gathered}\frac{N_m}{N_0} = \frac{\gamma_m}{2k},\ f^{(p)}_{m} = i^{-p} J_p\,(ka) \cos\left(p \arccos \frac{\gamma_m}{k}\right) = i^{-p} J_p\,(ka)\, T_p\left(\frac{\gamma_m}{k}\right), \\ f^{(p)}_{-m} = (-1)^p f^{(p)}_{m},\end{gathered} \tag{25}$$

where $T_p\left(\frac{\gamma_m}{k}\right)$ is Chebyshev's polynomial.

For damped waves, $\gamma_m = -i\alpha_m$, $\alpha_m = k\sqrt{\left(\frac{2m\pi}{kL_x}\right)^2 - 1}$. Using the equation

$$T_p(z) = \frac{1}{2}\{[z + i\sqrt{1 - z^2}]^p + [z - i\sqrt{1 - z^2}]^p\},$$

we find for $f_m^{(p)}$:

$$f_m^{(p)} = \frac{1}{2} J_p(ka)\left\{\left[\sqrt{\left(\frac{\alpha_m}{k}\right)^2 + 1} - 1\frac{\alpha_m}{k}\right]^p + (-1)^p\left[\sqrt{\left(\frac{\alpha_m}{k}\right)^2 + 1} + \frac{\alpha_m}{k}\right]^p\right\}. \tag{26}$$

Suppose that the only propagating wave is a TEM wave for which $\gamma_m = \gamma_0 = k$. In this case, Equation (22) will become, as a result of (25) and (26),

$$\begin{aligned}\sum_{n=-\infty}^{\infty} e^{-ihnL_z} Z_{0n,pj} = iR_{00,00}\Bigg\{&\frac{X_{00,pj}}{R_{00,00}} - (-1)^p \frac{J_j(ka)\,J_p(ka)}{J_0^2(ka)} \times \\ &\times \Bigg[i^{-p-j} \frac{\sin kL_z}{\cos hL_z - \sin kL_z} + \sum_{m\geq 1} \frac{k}{2\alpha_m}\Bigg\{\left[\sqrt{\left(\frac{\alpha_m}{k}\right)^2 + 1} - \frac{\alpha_m}{k}\right]^p + \\ &+ (-1)^p\left[\sqrt{\left(\frac{\alpha_m}{k}\right)^2 + 1} + \frac{\alpha_m}{k}\right]^p\Bigg\}\Bigg\{\left[\sqrt{\left(\frac{\alpha_m}{k}\right)^2 + 1} - \frac{\alpha_m}{k}\right]^j + \\ &+ (-1)^j\left[\sqrt{\left(\frac{\alpha_m}{k}\right)^2 + 1} + \frac{\alpha_m}{k}\right]^j\Bigg\}\left\{1 + \frac{\sinh \alpha_m L_z}{\cos hL_z - \operatorname{ch} \alpha_m L_z}\right\}\Bigg]\Bigg\}\end{aligned} \tag{27a}$$

for p + j even,

$$\begin{aligned}\sum_{n=-\infty}^{\infty} e^{-ihnL_z} Z_{0n,pj} = iR_{00,00}\Bigg\{&i^{p-j} \frac{J_j(ka)\,J_p(ka)}{J_0^2(ka)} \frac{\sin hL_z}{\cos hL_z - \cos kL_z} + \\ &+ i(-1)^p \sum_{m\geq 1} \frac{k}{2\alpha_m}\left\{\left[\sqrt{\left(\frac{\alpha_m}{k}\right)^2 + 1} - \frac{\alpha_m}{k}\right]^p + (-1)^p\left[\sqrt{\left(\frac{\alpha_m}{k}\right)^2 + 1} + \frac{\alpha_m}{k}\right]^p\right\} \times \\ &\times \left\{\left[\sqrt{\left(\frac{\alpha_m}{k}\right)^2 + 1} - \frac{\alpha_m}{k}\right]^j + (-1)^j\left[\sqrt{\left(\frac{\alpha_m}{k}\right)^2 + 1} + \frac{\alpha_m}{k}\right]^j\right\} \frac{\sin hL_z}{\cos hL_z - \cosh \alpha_m L_z}\Bigg\}\end{aligned} \tag{27b}$$

for p + j odd.

2. THE APPROXIMATE DISTRIBUTION OF THE CURRENT ON THE STRUCTURE ELEMENTS IS GIVEN

In this method, it is most natural to give a current distribution which is the same as the current distribution in a single element placed in an equivalent waveguide excited by a TEM wave (or, which is entirely equivalent), the current distribution in an element of a two-dimensional lattice of rods on which a plane wave is incident normally). We shall consider the effect of the walls of the equivalent waveguide on the current distribution in the rod and we shall neglect only the influence of waves of higher modes excited by adjacent (along the waveguide axis) elements of the structure. As before, the current distribution will be of the form of Eq. (1), but the coefficients a(j) must be found beforehand from the system of linear equations of the method of induced emf:

$$\sum_j a_j Z_{00,pj} = \frac{f_0^{(p)}}{T}, \quad p = 0, 1, 2, \ldots, \tag{28}$$

where $Z_{00,pj}$ and $f_0^{(p)}$ are defined by Eqs. (5) and (12). Since the current distribution is now known, the characteristic equation must be obtained in a somewhat different way, namely by multiplying Eq. (3) by $\Psi^* = \sum_p \alpha_p^* \Psi_p$, $\alpha_p = a_p/a_0$, $\alpha_0 = 1$, rather than by individual functions Ψ_p. It can be easily seen that as a result we obtain the equation

$$\sum_{p,j} \alpha_j \alpha_p^* \sum_n e^{-ihnL_z} Z_{0n,pj} = 0, \tag{29}$$

or, using Eq. (22), for the inner sum,

$$\frac{\sin kL_z}{\cos hL_z - \cos kL_z} \sum_{j+p=\text{even}} \alpha_j \alpha_p^* R_{00,pj} = \sum_{j+p=\text{even}} \alpha_j \alpha_p^* (X_{00,pj} + \Delta_1) + \\ + \sum_{j+p=\text{odd}} \alpha_j \alpha_p^* \Delta_2, \tag{30}$$

where

$$\Delta_1 = \sum_{m>1} \frac{f_m^{(j)} f_{-m}^{(p)}}{iN_m} \left\{ 1 + \frac{\sinh \alpha_m L_z}{\cos hL_z - \cosh \alpha_m L_z} \right\}; \\ \Delta_2 = - \sum_{m>0} \frac{f_m^{(j)} f_{-m}^{(p)}}{N_m} \frac{\sin hL_z}{\cos hL_z - \cos \gamma_m L_z}. \tag{31}$$

It can be easily seen that $\sum_{j+p=\text{even}} \alpha_j \alpha_p^* R_{00,pj} \equiv R_{00}$ and $\sum_{j+p=\text{even}} \alpha_j \alpha_p^* X_{00,pj} \equiv X_{00}$ represent the self-resistance (R_{00}) and the self-reactance (X_{00}) of a rod in an equivalent waveguide (or a two-dimensional lattice) for a current distribution $\psi = \sum \alpha_p \psi_p$. Equation (30) can be solved in the same way as Eq. (32) from [1]. In the case of a lattice of infinite rods in which the current distribution is described by equation

$$\psi = 1 + \alpha_1 \cos \varphi, \tag{32}$$

we obtain, in accordance with [5]

$$\alpha_1 = \frac{f_0^{(1)}}{f_0^{(0)}} \frac{Z_{00,00}}{Z_{00,11}}, \quad f_0^{(0)} = J_0(ka), \quad f_{\pm 0}^{(1)} = \mp i J_1(ka), \\ R_{00,00} = -\frac{J_0^2(ka)}{N_{TEM}}, \quad R_{00,11} = -\frac{J_1^2(ka)}{N_{TEM}}, \quad \frac{R_{00,11}}{R_{00,00}} = \frac{J_1^2(ka)}{J_0^2(ka)} \simeq \frac{(ka)^2}{2} \ll 1. \tag{33}$$

The terms with $R_{00,11}$ can be neglected because of their small magnitude, while the remaining correction terms can be transposed to the right side of Eq. (30) to make it easier to use the method of successive approximations.

REFERENCES

1. Ya.N. Fel'd, L.S. Benenson. Calculation of the phase velocities of waves in an artificial metal dielectric. Radiotekhnika i Elektronika, 1959, 4, 3, 417.
2. L.S. Benenson. The phase velocity of waves in an anisotropic artificial metal dielectric for an arbitrary direction of propagation. Radiotekhnika i Elektronika, 1959, 4, 11, 1806.
3. L.A. Vaynshteyn. Electromagnetic Waves. Izd. Sovetskoye Radio, 1957.
4. Ya.N. Fel'd, L.S. Benenson. Antenna Feeder Devices, Part II. Izd. VVIA im. N.E. Zhukovskoy, 1959.
5. L.S. Benenson. Induced impedances of a vibrator in a waveguide. Radiotekhnika i Elektronika, 1961, 6, 6, 926.

Submitted on July 28, 1960

THEORETICAL AND EXPERIMENTAL STUDIES OF HELICAL DIELECTRIC ANTENNAS

V. P. Shestopalov, A. A. Bulgakov, B. M. Bulgakov

The report describes theoretical and experimental studies of helical dielectric antennas. The Kirchhoff integral method is used in determining the radiation patterns of these antennas. Experiments in measurement of radiation patterns and current distribution along helical dielectric antennas are described.

It is shown that the increased delay of waves in a helical dielectric waveguide results in a more highly directive radiation of energy into space. By including a dielectric in the helical antenna it is possible to reduce its geometric dimensions.

INTRODUCTION

Dielectric and helical antennas are well known in microwave techniques as traveling-wave antennas. They are segments of dielectric or helical waveguide along which there may be propagated electromagnetic waves with phase velocity v_Φ less than the velocity of light c in free space. The delay in an infinite dielectric waveguide at high frequencies is defined by the expression

$$\frac{c}{v_\Phi} = \sqrt{\varepsilon},$$

where ϵ is the dielectric constant of the waveguide material. In a helical waveguide the delay at high frequencies has the form

$$\frac{c}{v_\Phi} = \frac{1}{\sin\psi},$$

where ψ is the pitch of the helix.

It is known that the longitudinal dimensions of a helical antenna are of the order of (1-3) λ_0 (where λ_0 is the wavelength in free space) whereas a dielectric antenna has dimensions of the order of (3-7) λ_0.

In a helical dielectric waveguide the delay at high frequencies is defined by the formula

$$\frac{c}{v_\Phi} = \sqrt{\frac{\varepsilon+1}{2}}\,\frac{1}{\sin\psi}.$$

It may be expected that a helical dielectric antenna will possess the properties characteristic both of a helical antenna and a dielectric antenna. In particular, its geometric dimensions with appropriate choice of ϵ and pitch ψ must be less than in a helical antenna and in a dielectric antenna.

1. THEORETICAL INVESTIGATION

In determining the modes which may be propagated in an infinite helical dielectric waveguide let us examine a system consisting of a ribbon helix of radius a. Let δ represent the ribbon width, ψ the pitch of the helix and p its spacing. Within the helix there is a medium with dielectric constant ϵ, and magnetic permeability μ_1; outside the helix there is a medium with ϵ_2 and μ_2.

The dispersion equation of the investigated system is found by solving the boundary-value problem with the following boundary conditions:

$$
\begin{gathered}
E_z^{(1)}\big|_{r=a} = E_z^{(2)}\big|_{r=a}, \quad E_\varphi^{(1)}\big|_{z=a} = E_\varphi^{(2)}\big|_{r=a}, \\
\left(H_z^{(2)} - H_z^{(1)}\right)\big|_{r=a} = j_\varphi, \quad \left(H_\varphi^{(1)} - H_\varphi^{(2)}\right)\big|_{r=a} = j_z,
\end{gathered}
\tag{1}
$$

where superscripts 1 and 2 refer to the regions inside and outside the helix, respectively; j_φ and j_z are the surface current components at the helix. The Fourier components for the longitudinal field components in the first region $(0 \leqslant r \leqslant a)$ may be written in the form

$$
\begin{gathered}
E_{zn}^{(1)} = A_n^{(1)} I_n(\gamma_n r)\, e^{in\varphi} e^{-i\beta_n z} e^{i\omega t}, \\
H_{zn}^{(1)} = B_n^{(1)} I_n(\gamma_n r)\, e^{in\varphi} e^{-i\beta_n z} e^{i\omega t},
\end{gathered}
\tag{2}
$$

and in the second region $(r \leqslant a)$

$$
\begin{gathered}
E_{zn}^{(2)} = A_n^{(2)} K_n(\gamma_n r)\, e^{in\varphi} e^{-i\beta_n z} e^{i\omega t}, \\
H_{zn}^{(2)} = B_n^{(2)} K_n(\gamma_n r)\, e^{in\varphi} e^{-i\beta_n z} e^{i\omega t},
\end{gathered}
\tag{3}
$$

where

$$
\begin{gathered}
\gamma_n^2 = \beta_n^2 - k^2; \quad k = \varepsilon\mu k_0; \quad k_0 = \frac{2\pi}{\lambda_0}; \\
\beta_n a = \beta_0 a + \frac{2\pi a}{p} n = \beta_0 a + n \cot \psi;
\end{gathered}
\tag{4}
$$

$I_n(\gamma_n r)$ and $K_n(\gamma_n r)$ are modified Bessel functions.

Considering that $\gamma_n^{(1)} \simeq \gamma_n^{(2)} = \gamma_n$ and using (1), we find

$$
\begin{gathered}
A_n^{(2)} = -\frac{i}{I_n'} \sqrt{\frac{\mu_2}{\varepsilon_2}} \left(\frac{\gamma_n a}{k_2 a}\right) \frac{j_{zn} - \dfrac{n\beta_n a}{(\gamma_n a)^2} j_{\varphi n}}{\dfrac{\varepsilon_1}{\varepsilon_2} \dfrac{K_n}{I_n} - \dfrac{K_n'}{I_n'}}, \\
A_n^{(1)} = -\frac{i}{I_n'} \sqrt{\frac{\mu_2}{\varepsilon_2}} \left(\frac{\gamma_n a}{k_2 a}\right) \frac{j_{zn} - \dfrac{n\beta_n a}{(\gamma_n a)^2} j_{\varphi n}}{\dfrac{\varepsilon_1}{\varepsilon_2} \dfrac{K_n}{I_n} - \dfrac{K_n'}{I_n'}} \frac{K_n}{I_n}, \\
B_n^{(2)} = \frac{1}{I_n} \frac{j_{\varphi n}}{\dfrac{K_n}{I_n} - \dfrac{\mu_2}{\mu_1} \dfrac{K_n'}{I_n'}}, \\
B_n^{(1)} = \frac{1}{I_n} \frac{\mu_2}{\mu_1} \frac{j_{\varphi n}}{\dfrac{K_n}{I_n} - \dfrac{\mu_2}{\mu_1} \dfrac{K_n'}{I_n'}} \frac{K_n'}{I_n'}.
\end{gathered}
\tag{5}
$$

Here and henceforth the arguments of $\gamma_n a$ of the modified Bessel functions are omitted.

Using the variation method (references [1-4]), which in our case has the form

$$
\sum_{n=-\infty}^{\infty} \left(E_{zn}^* j_{zn} + E_{\varphi n}^* j_{\varphi n}\right)\big|_{r=a} = 0,
\tag{6}
$$

we obtain the dispersion equation

$$
L(\beta) = 0,
\tag{7}
$$

where

$$
\begin{gathered}
L(\beta) = -\sum_{n=-\infty}^{\infty} i j_{sn}^2 \cos\psi \left(\frac{k_2 a}{\gamma_n a}\right) \times \\
\times \left\{ \left(\frac{\gamma_n a}{k_2 a}\right)^2 \left[\operatorname{tg}\psi - \frac{n\beta_n a}{(\gamma_n a)^2}\right]^2 \frac{\dfrac{K_n}{I_n'}}{\dfrac{\varepsilon_1}{\varepsilon_2} \dfrac{K_n}{I_n} - \dfrac{K_n'}{I_n'}} + \frac{\dfrac{K_n'}{I_n'}}{\dfrac{K_n}{I_n} - \dfrac{\mu_2}{\mu_1} \dfrac{K_n'}{I_n'}} \right\}, \\
j_{zn} = j_{sn} \sin\psi; \quad j_{\varphi n} = j_{sn} \cos\psi.
\end{gathered}
\tag{8}
$$

The current distribution at the helix ribbon may be presented in the form

$$j_{\varepsilon n} = \frac{\sin\frac{\Delta n}{2}}{\frac{\Delta n}{2}}, \quad \Delta = \frac{2p}{\pi\delta}. \tag{9}$$

As is known, in $L(\beta)$ the resonance term of an infinite sum and the nonresonnance residue may be isolated. Let us present the nonresonance part of $L(\beta)$ in the form

$$S = 2\left[\left(\frac{\gamma_0 a}{k_2 a}\right)^2 \mathrm{tg}\, 2\psi \frac{1}{\varepsilon_1 + \varepsilon_2} - \frac{1}{\frac{1}{\mu_1} + \frac{1}{\mu_2}}\right] \sin\psi \ln\frac{2}{\Delta}. \tag{10}$$

Subsequent discussion will be limited to the case where $\epsilon_1 = \epsilon$, $\epsilon_2 = 1$, $\mu_2 = \mu_1 = 1$, $k_2a = k_0a$.

Solution of the dispersion equation in the zero-resonance region $(n = 0)$ is determined from the formulas

$$Q(\gamma_0 a) = \mathrm{ctg}^2\psi \frac{(\gamma_0 a) I_1 K_1 + (\gamma_0 a)\sin\psi \ln\frac{2}{\Delta}}{\frac{\frac{K_0}{K_1}}{\varepsilon\frac{K_0}{I_0} + \frac{K_1}{I_1}} + \frac{2}{\varepsilon + 1}(\gamma_0 a)\sin\psi\ln\frac{2}{\Delta}}, \tag{11}$$

$$(\gamma_0 a)^2 = (\beta_0 a)^2 - (k_0 a)^2, \quad k_0 a = \gamma_0 a\sqrt{\frac{1}{Q(\gamma_0 a)}}, \quad \beta_0 a = \gamma_0 a\sqrt{1 + \frac{1}{Q(\gamma_0 a)}}$$

($\gamma_0 a$ must be taken in the limits $0 \leqslant \gamma_0 a \leqslant 0.6$).

In the region of first resonance $(n = -1)$

$$\beta_{-1} a = \frac{-\tau \pm \sqrt{\tau^2 - \rho\sigma}}{\rho}, \quad ka = \sqrt{(\beta_{-1} a)^2 - (\gamma_{-1} a)^2},$$

$$\tau = \mathrm{tg}\,\psi\left(\alpha_\varepsilon + \frac{1}{j_\varepsilon^2}\frac{2}{1+\varepsilon}\sin\psi\ln\frac{2}{\Delta}\right), \quad \rho = \frac{\alpha_\varepsilon}{(\gamma_{-1} a)^2} - \frac{1}{j_\varepsilon^2}\sin\psi\ln\frac{2}{\Delta} + \alpha_m,$$

$$\alpha_\varepsilon = \frac{\varkappa}{\varepsilon + \varkappa\chi}, \quad \alpha_m = -(\gamma_{-1} a) I_1 K_1,$$

$$\sigma = (\gamma_{-1} a)^2 \alpha_\varepsilon \,\mathrm{tg}\,\psi + [(\gamma_{-1} a)^2 \mathrm{tg}\, 2\psi + 1]\frac{1}{j_\varepsilon^2}\frac{2}{1+\varepsilon}\sin\psi\ln\frac{2}{\Delta} +$$

$$+ (\gamma_{-1} a)^2\left[\frac{1}{j_\varepsilon^2}\sin\psi\ln\frac{2}{\Delta} - \alpha_m\right],$$

$$\varkappa = \frac{1}{\frac{I_0}{I_1} - \frac{1}{\gamma_{-1} a}}, \quad \chi = \frac{K_0}{K_1} + \frac{1}{\gamma_{-1} a} \quad (0 \leqslant \gamma_{-1} a \leqslant 0{,}6). \tag{12}$$

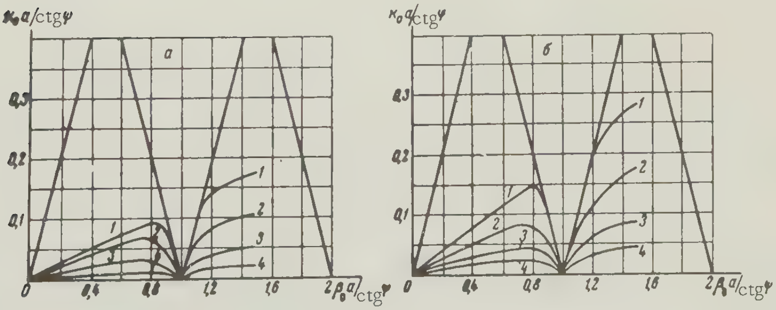

Figure 1. Dispersion curves of helical dielectric waveguide:
a) ctg ψ = 8.42; b) ctg ψ = 5.16; 1) ϵ = 1;
2) ϵ = 4.5; 3) ϵ = 20; 4) ϵ = 81.

Figures 1a and 1b give dispersion curves plotted from (7) - (12). The presence of the dielectric has a strong effect on the phase veloctiy of waves in the helical dielectric waveguide.

2. RADIATION PATTERNS

Let us determine the radiation pattern of a helical dielectric antenna by the Kirchhoff integral method. The $\vec{E}_M$ field in the far zone will be defined as follows:

$$\vec{E}_M = \frac{ie^{-ik_0R}}{k_0R}\int_0^l e^{2\pi iz\left(\frac{\cos\Theta}{\lambda_0}-\frac{1}{\lambda_g}\right)}dz\int_0^{2\pi}\vec{V}(\varphi,\Theta,\Phi)\,d\Phi, \tag{13}$$

where λ_g is the length of the slow wave, R is the distance to the point of observation, Θ and φ are angles in the spherical system of coordinates, Φ is the azimuth angle over the cylindrical surface of the antenna l is the length of the antenna, and V is independent of z. Integrating (13) for z, we obtain the system factor, identical for all traveling-wave antennas,

$$|F_1| = \frac{\sin\left[\frac{k_0a}{2}\frac{l}{a}\left(\frac{\beta_na}{ka}-\cos\Theta\right)\right]}{\frac{k_0a}{2}\frac{l}{a}\left(\frac{\beta_na}{ka}-\cos\Theta\right)}. \tag{14}$$

In our case $\frac{k_0a}{2}\frac{l}{a}$ is small and $|F_1(\Theta)|$ is extremely close to a sine curve.

After calculations similar to those in reference [5], we find the expression for the radiation field in the far zone

$$\vec{F}_2 = \frac{e^{-ik_0R}}{k_0R}\int_0^{2\pi}\vec{V}(\varphi,\Theta,\Phi)\,d\Phi. \tag{15}$$

The field components in the spherical system of coordinates have the form

$$E_R = 0,$$

$$\begin{aligned}E_\Theta = {}&\pi\cos\varphi\Big\{A_n^{(2)}K_n(\gamma_nR)(J_0-J_2)+\sqrt{\frac{\mu_2}{\varepsilon_2}}B_n^{(2)}K_n(\gamma_nR)\cos\Theta(J_0+J_2)-\\&+2i\left[A_n^{(2)}\frac{\omega\varepsilon_2}{\gamma_n}K_n'(\gamma_nR)+iB_n^{(2)}\frac{n\beta_na}{(\gamma_na)^2}K_n(\gamma_nR)\right]J_1\sin(\Theta)\Big\}|F_1(\Theta),\\E_\varphi = {}&\pi\sin\varphi\Big\{A_n^{(2)}K_n(\gamma_nR)\cos\Theta(J_0+J_2)+2i\left[iA_n^{(2)}\frac{n\beta_na}{(\gamma_na)^2}K_n(\gamma_nR)-\right.\\&\left.-B_n^{(2)}\frac{\omega\mu_2}{\gamma_n}K_n'(\gamma_nR)\right]\sin\Theta J_1+\sqrt{\frac{\mu_2}{\varepsilon_2}}B_n^{(2)}K_n(\gamma_nR)(J_0-J_2)\Big\}|F_1(\Theta),\end{aligned} \tag{16}$$

where J_0, J_1 and J_2 are Bessel functions of the first kind with the argument $ka\sin\Theta$.

Figure 2 shows radiation patterns calculated from the formula

$$F = \frac{E_\Theta^2+E_\varphi^2}{\left(E_\Theta^2+E_\varphi^2\right)_{\max}}. \tag{17}$$

For E_Θ^2 $\varphi = 0$, for E_φ^2 $\varphi = \pi/2$. The patterns in Figure 2a, 2b and 2c correspond to n = 0. In the zero resonance state the antenna does not radiate directionally (Figure 2a, ka = 0.361, $\epsilon = 1$, ka/ctg $\psi = 0.07$). The chosen point is located at the boundary of the region of the zeroth and first resonances and for systems with large delay the radiation pattern is directional (Figure 2b, ka = 0.55, $\epsilon = 1$, ka/ctg $\psi = 0.065$; Figure 2c, ka = 0.361, $\epsilon = 4.5$, ka/ctg $\psi = 0.07$). The radiation patterns are symmetrical relative to the antenna axis.

The curves in Figures 2d, 2e, 2f are plotted for $n = -1$, $ka = 0.742$, $\text{ctg}\ \psi = 5.16$. From an examination of the dispersion curves in Figure 1 it is seen that three values of $\beta_0 a$ (or $\beta_{-1} a$) correspond to one value of ka. For Figure 2d $\beta_{-1} a = -1.265$, $\epsilon = 1$ and the delay is greater than unity. For Figure 2e $\beta_{-1} a = -0.88$, $\epsilon = 1$, $v_\Phi \simeq c$. In the first case we have directional radiation and in the second case we have nondirectional radiation. If in the second triangle we chose a point with the same $ka = 0.742$, $\beta_{-1} a = 0.75$, the radiation pattern will be a mirror image of Figure 2e. For Figure 2f $\beta_{-1} a = 1.55$, $\epsilon = 4.5$ and the delay is maximum. The radiation pattern is the narrowest of these last three cases. Figure 2g ($\epsilon = 20$) ($ka = 0.361$, $\text{ctg}\ \psi = 5.16$) show that with an increase in delay the radiation pattern changes from nondirectional to directional with constant $k_0 a = 2\pi a/\lambda_0$. With fixed antenna dimensions an increase in delay corresponds to a shift into the low-frequency region. For the region $n = -1$ the axes of the radiation patterns do not coincide with the axis of the system.

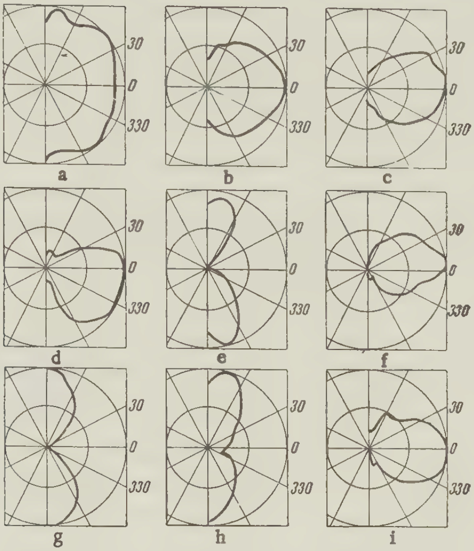

Figure 2. Radiation patterns of helical dielectric antenna, calculated from formulas (16) and (17)

3. PRACTICAL RADIATION PATTERNS AND CURRENT DISTRIBUTION

In order to check the calculation, the radiation patterns and current distribution along the antenna were measured for helics with $\text{ctg}\ \psi = 4.13$, 5.16, 8.42 and with $\epsilon = 1$, 4.5, 20, 81. In all tests the helix dimensions were constant ($l = 14$ cm, $2a = 4.6$ cm) and the wavelength was varied.

Figure 3 shows the block diagram of the measurement setup. RF energy from a GS-12 signal generator was fed through a long line and matching transformer to the antenna. An antenna of waveguide type for wavelengths of 10-25 cm with demountable dipole array and a logarithmic antenna for wavelengths of 19-80 cm were used at the receiving end. The receiving antenna could be rotated about the horizontal axis for plotting the polarization characteristics. The detector was placed directly at the ends of the antenna. The energy was led along a 10 m cable to a sensitive DC galvanometer. The matching and feed devices were a copper tube (approximately 50 cm in length and 30 mm in diameter) which formed a 150 ohm coaxial line with the helix conductor. The central conductor was supported on two discs of organic glass. Into the line there was introduced an RK-50 cable (150 ohms) which was joined with a section of RK-2 cable (100 ohms) approximately 7 cm long and then with a standard cable (75 ohms). An adjustable inductance-type probe was used in plotting the field pattern.

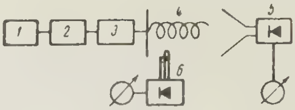

Figure 3. Block diagram of measurement setup: 1, r-f generator; 2, long line; 3, matching device; 4, antenna; 5, receiving antenna; 6 adjustable probe.

Figure 4 shows the results of measurements of a helical antenna with $\epsilon = 1$ and ctg $\psi = 5.16$. These measurements are in excellent agreement with those given in reference [5]. In the region of second resonance (Figure 4a) the reflection coefficients are other than zero. Figures 4b and 4c correspond to the first resonance. A traveling wave

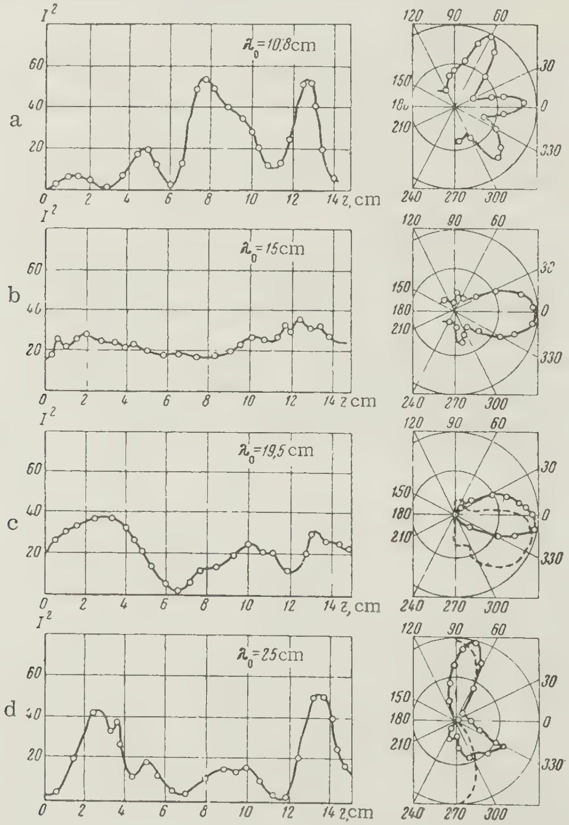

Figure 4. Experimental radiation patterns and current distribution along a helical antenna (ϵ=1, ctg ψ=5.16). The dashed lines indicate theoretical radiation patterns.

was established along the antenna. In regions close to the zeroth resonance standing waves were observed over the entire length of the antenna. The dashed lines in Figure 4 represent the theoretical radiation patterns. The experimental and theoretical curves show excellent coincidence. Here, as subsequently, one of the causes of a certain noncoincidence of the theoretical and experimental curves lies in the fact that in calculating the radiation patterns by the Kirchhoff integral method the metal reflector used in the experiment was not taken into account.

Figures 5 and 6 give the curves of the radiation patterns of helical dielectric antennas for different dielectrics. It is seen from the curves that with directional radiation there are

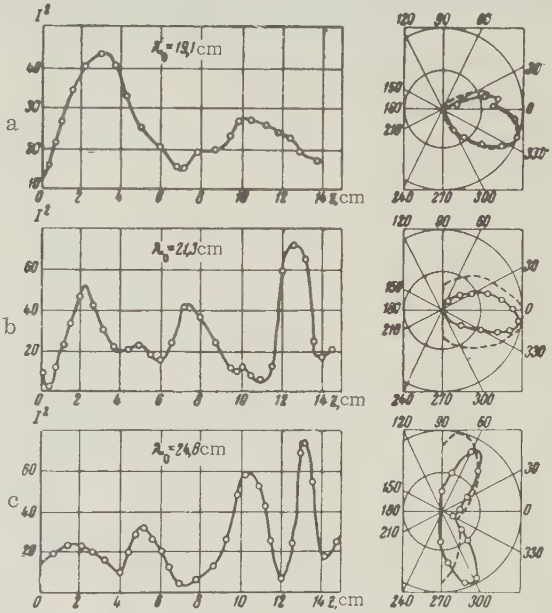

Figure 5. Experimental radiation patterns and current distribution along a helical dielectric antenna ($\epsilon = 4.5$, ctg $\psi = 5.16$): a, b, region of first resonance. Dashed lines indicate theoretical radiation patterns.

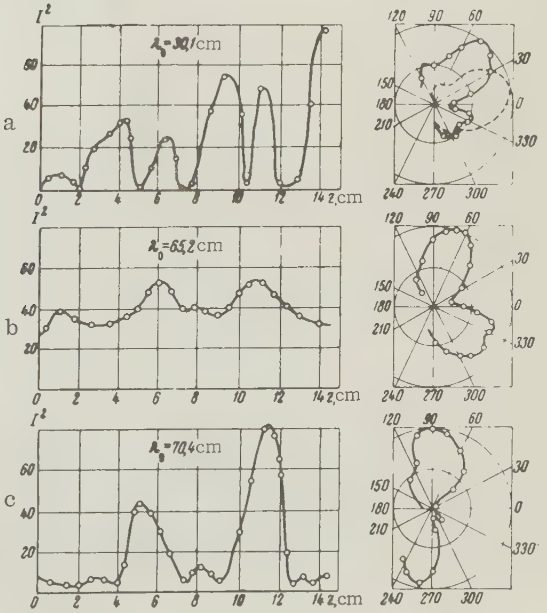

Figure 6. Experimental radiation patterns and current distribution along a helical dielectric antenna ($\epsilon = 20$, ctg $\psi = 8.4$): a, region of first resonance; b, c, region of zeroth resonance. Dashed line indicates theoretical radiation pattern.

traveling and standing waves along the antenna. With fixed antenna dimensions, the greater ϵ, the greater the displacement of directional radiation toward low frequencies. With the introduction of the dielectric a contraction of the range of directional radiation is observed. The radiation patterns coincide in shape with the design patterns; the chief departure is observed in the angles of deviation of the radiation pattern axis from the antenna axis.

Figure 7 presents the results of measurements of a helical dielectric antenna the inner region of which is filled with water. Strong attenuation is observed in the short-wave sector. Figures 7a and 7b correspond to the regions of the third and second resonances. In these regions introduction of the dielectric permits obtaining a direction radiation pattern. In the region of first resonance (Figures 7c and 7d) there is observed displacement of the major maximum of the radiation pattern from the antenna axis. The range of directional radiation is markedly contracted. Figure 7e corresponds to the region of zeroth resonance.

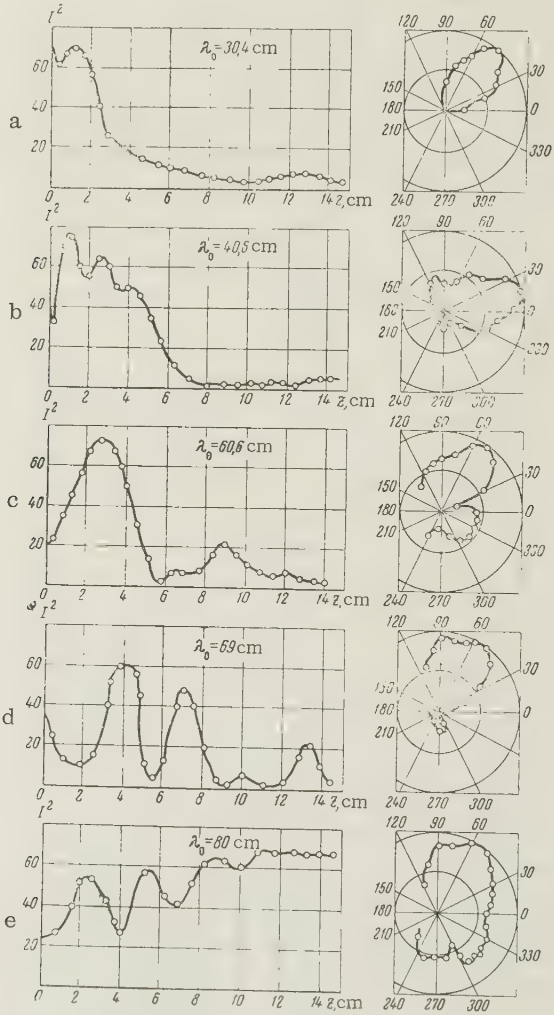

Figure 7. Experimental radiation patterns and current distribution along helical dielectric antenna ($\epsilon = 81$, ctg $\psi = 5.16$): a, b, region of third and second resonances; c, d, region of first resonance; e, region of zeroth resonance.

CONCLUSIONS

Theoretical and experimental investigations of a helical dielectric antenna have shown the following.

1. Introduction of a dielectric into a helical waveguide considerably decreases the phase velocity of electromagnetic waves and increases the delay.
2. An increase in the delay of waves in a helical dielectric waveguide leads to greater directional radiation of energy in space.
3. Introduction of the dielectric shifts the axis of the radiation pattern from the antenna axis. This fact has been verified by experiment, although there is no quantitative coincidence of theory with experiment. Physically, this phenomenon may be explained by the fact that the radiated electromagnetic waves are asymmetrical along the helix azimuth.
4. Introduction of the dielectric into the helical antenna permits a decrease in antenna dimensions by almost $\sqrt{\varepsilon}$ times, but this is accompanied by a decrease in the bandwidth passed by the system.
5. In order to increase the passband in the investigated antenna, instead of a solid dielectric rod within the helix there may be used a laminated dielectric or magnetodielectric medium.

REFERENCES

1. M.Chodorow, E.L.Chu, J. Appl. Phys., 1956, 26, 1, 732.
2. V.P.Shestopalov, L.I.Spol'nik, Zh. Tekh. Fiz. 1960, 30, 1, 3.
3. V.P.Shestopalov, A.A.Bulgakov, Radiotekhnika i Elektronika, 1961, 6, 1, 92.
4. V.P.Shestopalov, S.S.Kal'mykova, Zh. Tekh. Fiz. 1961, 31, 3, 285.

A.M.Gor'kiy State University
at Kharkov

Submitted to the editors 9 July 1960

SPHERICAL TWO-MIRROR ANTENNAS

L. D. Bakhrakh, I. V. Vavilova

The report discusses spherical two-mirror antennas, which permit undistorted scanning of the directivity pattern within a wide sector. Such systems are of great promise for the creation of large antennas (e.g., in radio telescopes).

Two methods for calculation of the profile of a small mirror are presented: (1) by means of focal curves; (2) by the wavefront method. For two-mirror antennas the wavefront method is modified in order to avoid solution of auxiliary differential equations. The optimum relationships between aperture efficiency of a spherical mirror and the dimensions of a small mirror are discussed. The problem of influence of accuracy of installation of the system elements (radiator and small mirror) on the antenna characteristics is analyzed.

INTRODUCTION

Of extreme importance at this time are problems associated with the creation of large mirror antennas in which scanning of the beam is achieved by displacement of small masses.

In this connection much attention is being devoted to spherical mirror antennas in which scanning of the directivity pattern is achieved by displacement of the radiator relative to the center of a spherical surface. Due to symmetry, the surface-utilization factor of the mirror is unchanged (Figure 1). However, the value of the surface-utilization factor of the mirror of a single-mirror spherical antenna depends substantially on the width of the directivity pattern and the angle of scan. This is obvious, since only that part of a spherical mirror may be used in which the reflection-phase errors at the edges do not exceed the allowable values. The calculations for a spherical mirror in which the optimum radiator position was chosen for a given pattern width have shown that with narrow patterns the mirror efficiency is extremely low and increases somewhat with wider patterns.

Figure 2 gives the curve for dependence of the ratio of effective aperture size to sphere diameter D_p/D on width of pattern Ψ. The curve is obtained on the condition that the phase error does not exceed $\lambda/8$ within the limits of the effective aperture.

The curves in Figure 3 show the aperture efficiency $K = D_p/AB$ as a function of total angle of scan for different widths of radiation pattern (designations are given in Figure 1). Let us note that the value of aperture efficiency as given in the figure does not take into account the distribution of amplitudes at the aperture. The disadvantages of a single-mirror spherical system associated with low mirror efficiency in the scan of narrow patterns may be completely eliminated by use of the spherical two-mirror antenna proposed by us in 1951 and described in 1954 (reference [1]).

Recent literature reports on the development of a radio telescope operating on a similar principle [2] and on a variant of the cylindrical canal system [3].

The present report is devoted to the principal problems of calculation and design of a spherical two-mirror system. Special attention is given to problems associated with decreasing the dimensions of the small mirror and to the influence of accuracy of installation of the individual elements of the system on its directivity. These problems may prove to be of extreme importance in designing large antennas, particularly for radio telescopes with high resolution.

In the general case for scan of a radiation pattern of special shape the large mirror may be part of a toroidal surface with a given generatrix and the small mirror may be calculated correspondingly [4]. However, the present report is limited to discussion of spherical two-mirror systems designed for shaping and control of a needle beam.

1. OPERATING PRINCIPLE OF A SPHERICAL TWO-MIRROR SYSTEM

A spherical two-mirror system consists of two mirrors: a large spherical mirror concentrating energy in the principal direction and a small mirror which disperses toward the large mirror the energy incident from the radiator. The small mirror is so calculated that at the aperture of the spherical mirror there is formed a plane wavefront. There is no phase error in the system. Hence, the aperture efficiency and the sector of scan do not depend on the width of the radiation pattern. This is an extremely important factor, giving the spherical two-mirror a distinct advantage over the spherical one-mirror system.

Scan of the radiation pattern in a spherical two-mirror system is achieved by rotating the small mirror along with the radiator relative to the center of the spherical mirror. It is evident that by virtue of symmetry there will be no distortion of the pattern and its maximum will be deflected by the angle of rotation of the small mirror with the radiator (Figure 4).

For a spherical two-mirror system it is important to establish how completely the small mirror and radiator can intercept the beam of rays reflected from the large mirror. It is also important to determine the resulting efficiency of the large mirror and the extent to which the small mirror shadows the rays reflected from the large mirror. In principle the large mirror may be in the form of a hemisphere, but it is not possible to use the entire mirror. In fact, parallel rays striking the spherical mirror are reflected from the latter at different angles φ. In this case, when $2\varphi \leqslant \pi/2$ (the angle between the incident and the reflected ray of the spherical mirror) the small mirror can reflect rays, but when $2\varphi > \pi/2$, one part of the small mirror will shadow the other (Figure 4).

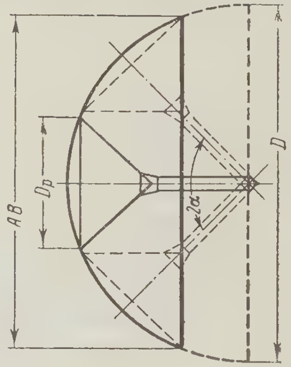

Figure 1. Toward determining the surface-utilization factor of a mirror.

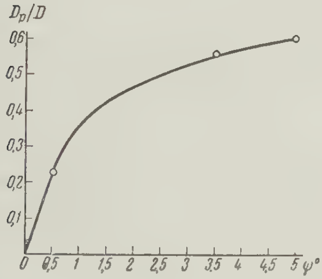

Figure 2. Ratio of aperture to sphere diameter as a function of width of radiation pattern.

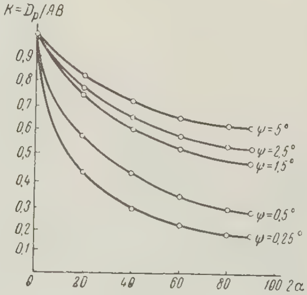

Figure 3. Aperture efficiency as a function of total angle of scan for different widths of radiation pattern

Thus, the maximum effective aperture D_p in a spherical two-mirror system is limited by the side of the inscribed square and is equal to $1.41\ R_0$. It is evident that in the scan of the radiation pattern the entire aperture AB of the mirror must be greater than $1.41\ R_0$.

The aperture AB of a spherical mirror depends on the angle of scan of the pattern 2α (Figure 4).

From geometric considerations it follows that if the effective aperture $D_p = 1.41_0$,

$$AB = \frac{2R_0}{\sqrt{2}}(\sin\alpha + \cos\alpha) \tag{1}$$

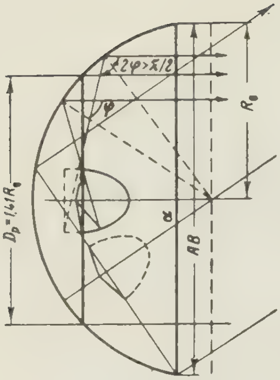

Figure 4. Spherical two-mirror antenna.

and, consequently, the aperture efficiency $K = D_p/AB$ may be determined from

$$K = \frac{1}{\sin\alpha + \cos\alpha}. \tag{2}$$

Figure 5 gives the plot of the function $K = f(2\alpha)$.

It is easily seen that with an increase in the sector of scan (to approximately ± 20°) the aperture efficiency at first drops quite sharply, after which further decrease in aperture efficiency occurs quite slowly.

It is evident that in principle such a system may permit control of the beam not only in one plane but in a solid angle, wherein the maximum possible solid angle is 90° with an aperture efficiency of 0.7, Here the large mirror must be a hemisphere.

If the large spherical mirror is made of a polarized grating in which the conductor is oriented at an angle of 45° (as was done in the toroidal single-mirror antennas in [5 and 6], on the basis of a spherical two-mirror antenna we may construct a system providing control of the beam within the complete solid angle. Calculations show that in such a system an effective aperture of 0.7 D may be obtained.

2. METHODS OF CALCULATING A SPHERICAL TWO-MIRROR SYSTEM

Calculation of a spherical two-mirror system for shaping of a needle-shaped radiation pattern reduces to calculation of the profile of the small mirror, for in this case the latter represents a surface of rotation. In order to solve the problem it is necessary to give the position of the radiator and one of the points of the small mirror profile. The large mirror profile, a circle, is known and the incident wavefront at the large mirror is assumed to be plane.

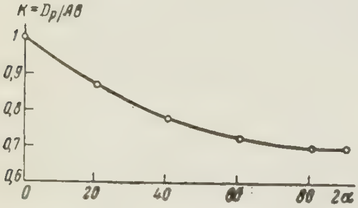

Figure 5. Aperture efficiency as a function of angle of scan of the pattern for $D_p = 1.41\ R_0$.

Calculation of the small mirror profile is best performed by the following two methods: the focal-curve method and the wavefront method.

The first method is an extension of the partial-foci method [7]. "Partial focus" is the conventional term for the point of convergence of rays reflected from a segment of the large mirror. The focal surface in the tridimensional case and the focal curve in the bidimensional case are the locus of the partial foci. We will note that in the case of calculation of two-mirror systems knowledge of the foci surface permits proper selection of initial data for calculation of the small mirror so that its dimensions are close to optimum. In the bidimensional case the focal curves or caustics are evolutes — the locus of centers of curvature of the wavefront. The equation for the focal curve in vector form is

$$\vec{F} = \vec{R} + M\vec{a}_k, \tag{3}$$

where

$$M = \frac{\cos\varphi}{2k_1 - k_2\cos\varphi};$$

k_1 and k_2 are the curvatures of the reflector and the incident wavefront, respectively; φ is the angle of incidence of the wave; $\vec{a}_k$ is the direction of the reflected ray.

It is sometimes convenient to determine the focal curve in parametric form. In the case under discussion this is easily done.

Let parallel rays be incident at the large mirror. Then from Figure 6 we have the relations

$$\left.\begin{aligned}\frac{Y-Y_1}{X-X_1}&=\tan\gamma,\\ \frac{Y-Y_2}{X-X_2}&=\tan\gamma_1,\end{aligned}\right\} \tag{4}$$

$$\left.\begin{aligned}Y_1&=R_0\sin\varphi,\\ X_1&=R_0\cos\varphi,\\ Y_2&=R_0\sin\varphi+R_0\cos\varphi\,d\varphi,\\ X_2&=R_0\cos\varphi-R_0\sin\varphi\,d\varphi,\end{aligned}\right\} \tag{5}$$

$$\operatorname{tg}\gamma_1=\tan\gamma+\frac{2}{\cos^2 2\varphi}. \tag{6}$$

Inserting expressions (5) and (6) into the system of equations in (4) and solving them simultaneously, we obtain the equations for the focal curve

$$\begin{aligned}X&=\cos\varphi\left(1-\frac{\cos 2\varphi}{2}\right),\\ Y&=\sin^3\varphi R_0.\end{aligned} \tag{7}$$

Having found the focal curve and being given a point on the small mirror and the position of the radiator, it is not difficult to plot the profile of the small mirror.

The profile of the small mirror is none other than an envelope of ellipses or hyperbolas, one of the foci of which coincides with the position of the radiator and the second is located on the focal curve at the point of contact of the ray reflected from the large mirror.

If the small mirror is located in front of the focal curve (prefocal region), its profile is described by an envelope of hyperbolas; if it is located in the postfocal region, its profile is described by an envelope of ellipses.

The focal-curve method is extremely convenient in plotting the profile of the small mirror.

The second method of calculation of the small mirror is based on the wavefront method [8], which in turn is based on the widely known work of Hamilton. The essentials of this method are as follows. If any two of three surfaces (the incident wavefront, the reflector and the reflected wavefront) are known, the third surface may be determined. The wavefront method employs vector representation of the surfaces. Let us designate the surface of the incident wavefront as $\vec{X}$, the reflector surface as $\vec{R}$, and the surface of the reflected wavefront as $\vec{Y}$. If, for example, we know $\vec{X}$ and $\vec{R}$, the equation for the third surface $\vec{Y}$ is found from

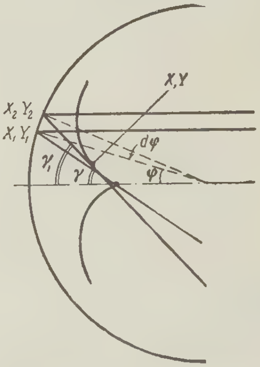

Figure 6. Toward determination of the focal curve.

$$\vec{Y}=\vec{X}-2\vec{\eta}\,[\vec{\eta}\,(\vec{R}-\vec{X})], \tag{8}$$

where $\vec{\eta}$ is the unit normal to the reflector surface.

If $\vec{X}$ and $\vec{Y}$ are known, we can obtain the expression for $\vec{R}$:

$$\vec{R}=\vec{Y}+\vec{\xi}\,\frac{[C^2-(\vec{Y}-\vec{X})^2]}{2\,[C+(\vec{Y}-\vec{X})\,\vec{\xi}]}, \tag{9}$$

where C is the total path of the ray from the incident wavefront to reflected wavefront.

Let us note that the surfaces Y or $\vec{R}$ in the general case are functions of four independent parameters. Thus, $Y=\vec{Y}(u, v, s, t)$, since $\vec{X}=\vec{X}(u, v)$ and $\vec{R}=\vec{R}(s, t)$. Hence, it is necessary to establish the additional relationship between parameters u, v and s, t. It is established from the condition of perpendicularity of the rays and wavefronts by solution of the equations

$$\left.\begin{aligned}(\vec{R}-\vec{X})\,\vec{X}_u=0,\\(\vec{R}-\vec{X})\,\vec{X}_v=0,\end{aligned}\right\} \qquad (10)$$

where $\vec{X}_u$ and $\vec{X}_v$ are partial derivatives for the corresponding parameter. In solving problems by the wavefront method it is desirable that the wavefronts and reflecting surfaces be so chosen as to avoid solution of the equations in (10) wherever possible. With reference to two-mirror calculations (particularly for calculation of the small mirror) the wavefront method has been modified by us so that each point of the surface can be calculated separately. The wavefront method is particularly convenient in those cases where the surface of the large mirror and the incident wavefront may easily be expressed analytically.

Two-mirror antenna calculations deal with two reflecting surfaces and three wavefronts, one of which is intermediate. Application of the wavefront method to the calculation of two-mirror systems consists in judiciously combining procedures wherein the system is first examined as a receiving antenna and, in the final stage, as a transmitting antenna. The small-mirror calculations may be performed with the use of nondifferential vector equations.

In a spherical two-mirror system small-mirror calculations by the wavefront method must be divided into two stages: (1) in receiver operation of the system, the reflected wavefront $\vec{Y}$ is determined for a given plane wavefront $\vec{X}_1$ incident at the large spherical mirror R_L; (2) in transmitter operation, the surface of the small mirror $\vec{R}_S$ is determined for the given spherical wavefront $\vec{X}_2$ incident at the small mirror from the radiator and for the reflected front $\vec{Y}$ as determined from the first stage of calculation.

As was mentioned above, in the case under discussion the small mirror represents a surface of rotation and the problem reduces to determining the profile at the plane. It is more rational to solve the problem by using the polar system of coordinates. The radius of the large mirror is taken as unity.

Then, from Figure 7,

$$\left.\begin{aligned}\vec{R}_b&=\cos\Theta\,\vec{i}+\sin\Theta\,\vec{j},\\\vec{X}_1&=\vec{i}+\sin\Theta\,\vec{j},\\\vec{\eta}&=\cos\Theta\,\vec{i}+\sin\Theta\,\vec{j}.\end{aligned}\right\} \qquad (11)$$

Inserting (11) into (8), we obtain the equation for the reflected wavefront $\vec{Y}$.

$$\begin{aligned}\vec{Y}&=Y_x\vec{i}+Y_y\vec{j},\\Y_x&=[1-2\cos^2\Theta\,(1-\cos\Theta)],\\Y_y&=[\sin\Theta-\sin 2\Theta\,(1-\cos\Theta)].\end{aligned} \qquad (12)$$

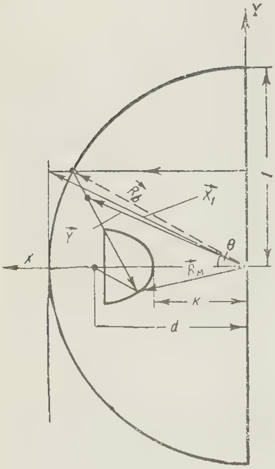

Figure 7. Toward determining the surface of the small mirror.

The spherical wavefront X_2 is conveniently examined directly at the point of location of the radiator, that is,

$$\vec{X}_2=\vec{i}d. \qquad (13)$$

In such examination condition (10) is automatically fulfilled. The unit normal to the reflected front, directed along the reflected ray, is defined as

$$\vec{\xi}=-\cos 2\Theta\,\vec{i}-\sin 2\Theta\,\vec{j}. \qquad (14)$$

Inserting (12), (13) and (14) into expression (9), we obtain the equations for determining the coordinates of the profile of the small mirror:

$$\begin{aligned}R_{xM}&=Y_x-\cos 2\Theta P,\\R_{yM}&=Y_y-\sin 2\Theta P,\end{aligned} \qquad (15)$$

where

$$P=\frac{C^2-[(Y_x-d)^2+Y_y^2]}{2\,[C-\cos 2\Theta\,(Y_x-d)-\sin 2\Theta Y_y]}; \qquad (16)$$

C is the length of path from front $\vec{Y}_1$ to front $\vec{X}_2$. As is seen from Figure 7,

$$C = 1 - 2k + d, \tag{17}$$

where k is the distance from the center of the spherical mirror to the phase center of the radiator.

The equations derived by the wavefront method not only permit relatively simple small-mirror calculation but also permit us to determine the most rational position of system elements as well as the influence of accuracy of installation of the elements on its directivity.

3. SPECIAL ASPECTS IN DESIGNING A SPHERICAL TWO-MIRROR SYSTEM

In designing a spherical two-mirror system it must be kept in mind that the amount of shadowing of the reflected rays from the large mirror by the small mirror is extremely important in obtaining an undistorted radiation pattern. Calculations show that the ratio of the aperture of the small mirror to the value of effective aperture of the large mirror must not exceed 0.25. It should also be kept in mind that the aperture of the small mirror must be less than 4-5 λ, otherwise the calculations by geometric optics become incorrect.

Moreover, it is important that the rays reflected by the small mirror do not undergo reflection from its opposite rim. This condition is always observed if the profile of the small mirror does not intercept the focal curve.

The value of effective aperture D_p in a spherical two-mirror system is closely associated with its geometric dimensions — the position of the aperture of the small mirror R_{xp}, the width of its aperture $2R_{yp}$, the position of the radiator. Formulas (15) for calculation of the small-mirror profile, obtained by the wavefront method, permit us to establish the relation between angle Θ (the sine of which determines the ratio of the effective aperture of the diameter of the large mirror D_p/D) and the values of R_{xp} and R_{yp}.

In effect, for each fixed value of R_{yp} we may calculate from formulas (15) the relation

$$\Theta = f(R_{xp}).$$

In the calculation it must be kept in mind that the profile of the small mirror must not intercept the focal plane as defined in Equation (7). Hence, for each value of R_{yp} we find those extreme values of R_{xp} for which $R_{yp} = y$, where y is the ordinate of the corresponding point on the focal curve. On these assumptions, for a given small-mirror aperture $2R_{yp}$ we obtain the maximum value of effective aperture D_p of the large mirror.

Figure 8 presents the curves for $\Theta = f(R_{xp})$ as calculated with the above consideration. The curves on the right-hand side are for small mirrors located in the prefocal region and the curves on the left-hand side are for small mirrors in the postfocal region. The curves permit us to conclude that with one and the same small-mirror dimensions the greatest ratio of D_p/D is obtained in those cases where the small mirror is located in the postfocal region.

Strictly speaking, the maximum possible effective aperture D_p, equal to 0.707 D ($\Theta = 45°$), is obtained with $R_{xp} = 0.707\ R_0$ and $2R_{yp} = 0.43$ D. However, with a decrease of $2R_{yp}$ to 0.18 D the effective aperture of the large mirror is 0.7 D, that is, it is practically unchanged.

With a decrease in size of the small mirror to $2R_{yp} = 0.05$ D the effective aperture of the large mirror decreases to 0.575 D, that is, by 18%. The above observation refers to mirrors located in the postfocal region.

Figure 9 shows a spherical two-mirror system with small mirrors calculated to provide an effective aperture of 0.7 D (mirror No. 1) and 0.575 D (mirror No. 2).

With a decrease in size of the small mirror the optimum value of R_{xp} also decreases. It is particularly important that this be kept in mind in designing large antennas, since a decrease in dimensions of the steerable part may considerably facilitate construction and reduce cost while the accompanying decrease in aperture efficiency K is insignificant. Figure 10 shows the dependence of decrease in aperture efficiency ΔK on the sector of scan 2α, which dependence is determined by a change in small-mirror aperture size from 0.18 D to 0.05 D. It is seen from the curve that with a sector of scan of 90° the aperture efficiency decreases by 16%.

Choice of the position of the radiator in a spherical two-mirror system is governed by the following considerations.

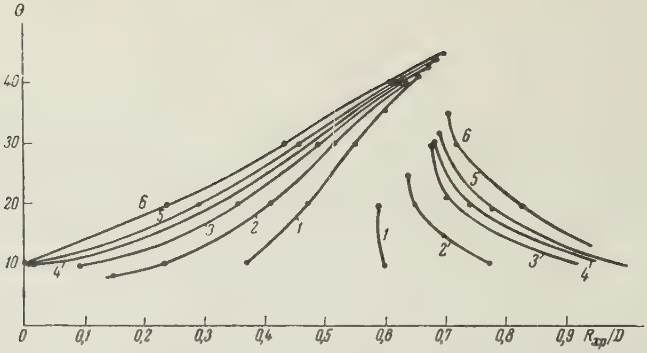

Figure 8. Curves for angle θ as a function of position R_{xp} of small-mirror aperture for different aperture values:

1, $2R_{yp} = 0.05$ D; 2, $2R_{yp} = 0.1$ D; 3, $2R_{yp} = 0.15$ D; 4, $2R_{yp} = 0.18$ D; 5, $2R_{yp} = 0.2$ D; 6, $2R_{yp} = 0.25$ D.

Physical considerations require that in expression (17) $C > 0$. For small mirrors located in the postfocal region $k \leqslant 0.5$. Consequently, in this case $d \leqslant C$. For mirrors located in the prefocal region $k > 0.5$ and $d > C$. It is most advisable to place the radiator near the aperture of the small mirror.

Summing up the above remarks, we may recommend the following sequence in design and calculation of a spherical two-mirror system.

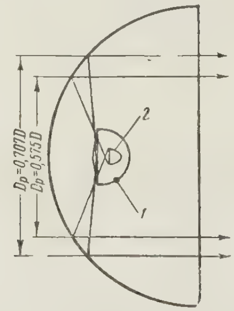

Figure 9. Spherical two-mirror system with small mirrors:

1) Mirror No. 1; 2) mirror No. 2.

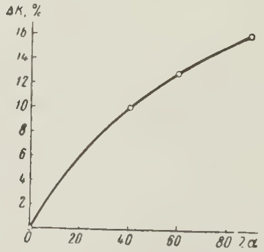

Figure 10. Dependence of decrease in aperture efficiency on sector of scan of directivity pattern.

1. From the curves in Figure 8 select the size of the small mirror (i.e., $2R_{yp}$), select its position R_{xp} and determine the corresponding angle θ the sine of which characterizes the ratio of effective aperture to sphere radius, that is,

$$\sin\theta = \frac{D_p}{D}.$$

2. Assign a position d of the radiator near the small-mirror aperture.
3. Determine the value of C:

$$C = \sqrt{(Y_y - R_{yp})^2 + (Y_x - R_{xp})^2} + \sqrt{R_{yp}^2 + (R_{xp} - d)^2}, \tag{18}$$

where Y_y and Y_x are appropriate points at the reflected wavefront, calculated from formulas (12). For a postfocal system the condition $C > d$ must be fulfilled; for a prefocal system the condition $C < d$ must be fulfilled.

4. Calculate the small-mirror profile from formulas (15).

4. INFLUENCE OF ACCURACY OF INSTALLATION OF INDIVIDUAL ELEMENTS OF THE SYSTEM ON ITS DIRECTIVITY

In designing large spherical two-mirror antennas it is necessary to know the accuracy with which the system elements must be installed, for adjustment of the relative position of elements in a prefabricated antenna structure in a number of cases may prove impossible or at least extremely complex. The establishment of extremely rigid tolerances for relative placement of the system elements may also unduly complicate antenna construction. Hence, it is extremely important to evaluate the degree to which accuracy of installation of the individual elements of the system affects its directivity. This problem may be solved by the wavefront method. This method permits determining the shape of the wavefront at the output of the antenna upon displacement of the radiator and small mirror relative to the design positions.

Calculation of the wavefront is so performed as to establish the correspondence between the aperture points of the large mirror and the wavefront points. Hence, it is not difficult to calculate the curve for phase-error distribution over the antenna aperture, from which we may then directly evaluate the variations in directivity of the system.

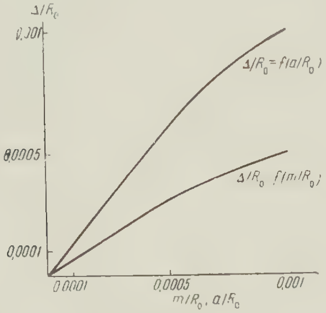

Figure 11. $\triangle/R_0$ as a function of displacement of mirror and radiator.

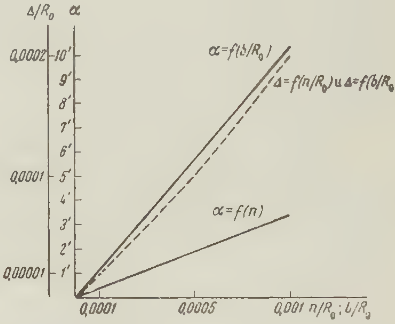

Figure 12. Angle of ray deflection α and phase error $\triangle R_0$ as functions of mirror and radiator displacement.

Let the radiator and small mirror be displaced relative to the design positions.* Then the equation for the wavefront incident from the radiator, in accordance with (13), will have the form

$$\vec{X}_2' = \vec{i}\,(d+m) + \vec{j}n, \tag{19}$$

where m and n are the radiator displacement along the x and y axes, respectively.

With arbitrary displacement the small-mirror coordinates are defined by the expressions

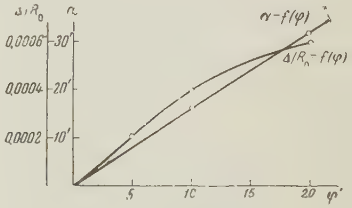

Figure 13. α and $\triangle R_0$ as functions of mirror tilt angle.

$$\begin{aligned} R_{x\text{M}}' &= (R_{x\text{M}} - a)\cos\varphi + (R_{y\text{M}} - b)\sin\varphi, \\ R_{y\text{M}}' &= (a - R_{x\text{M}})\sin\varphi + (R_{y\text{M}} - b)\cos\varphi, \end{aligned} \tag{20}$$

where R_{xs} and R_{ys} are the small-mirror coordinates as calculated from formulas (15); a and b are the mirror displacement along the x and y axes, respectively; φ is the angle of rotation of the mirror about the x-axis.

In determining the wavefront at the antenna output it is convenient to deal with the system in transmitter operation. Using expression (8), it is first necessary to determine the intermediate wavefront $\vec{Y}_1'$ reflected from the displaced small mirror along the incident front $\vec{X}'_2$.

---

*Since we are interested in relatively small displacements, we shall continue to treat the problem as a plane problem.

Then, taking the reflected wavefront $\vec{Y}_1$ as the incident wavefront at the large mirror, from the same expression (8) it is necessary to determine the reflected wavefront $\vec{Y}_2$. We shall not derive the design relations since they are somewhat unwieldy.

Distortions of wavefront Y_2 in the general case depend on several parameters: m, n, a, b, φ. For practical purposes it is of interest to evaluate the influence of each of these parameters separately. An electronic computer was used for calculation of the wavefronts as functions of each of the parameters. On the basis of these calculations curves were plotted (Figures 11, 12, 13) for the dependence of phase error ΔR_0, on change in one or another parameter.

Figure 11 shows the functions $\Delta/R_0 = f(a/R_0)$ and $\Delta/R_0 = f(m/R_0)$, from which it is evident that the tolerance in installation of the mirror along the x-axis must be approximately twice as rigid as for the radiator.

With change in parameters b, n, φ the phase front will not only be distorted but will also be deflected, which leads to displacement of the maximum of the directivity pattern.

Figure 12 shows the angle of ray deflection α as a function of n and b and also shows the phase error relation Δ/R_0, which in the given case characterizes the distortions of the tilted phase front. Finally, Figure 13 presents similar curves for α and Δ/R_0 as functions of the mirror tilt angle φ.

Thus, from the curves in Figures 11, 12 and 13 we may for a given large-mirror size establish the tolerance for installation of the radiator and small-mirror in a spherical two-mirror system.

REFERENCES

1. L.D. Bachrach, Tr. NII MAP, 1954, No. 11 (33).
2. A.K. Head, Nature, 1957, 179, 6.
3. W. Rotman, IRE Trans., 1958, AP-6, 1.
4. I.V. Vavilova, Tr. NII MAP, 1954, No. 11 (33).
5. J.A.C. Jackson, E.C.A. Goodall, Marconi Rev., 1st quarter, 1958, 21, 128, 30.
6. J.M. Flaherty, E. Kadak, IRE Nat. Convention Record, part 1, 1958.
7. L.D. Bachrach, Tr. NII MAP, 1953, No. 3.
8. Kellecher, J. Appl. Phys., 1950, 21, 6, 573

Submitted to the editors 28 October 1960

CALCULATION OF SIDE FLOW IN A LONG WAVEGUIDE LINE

R. F. Matveyev

The report presents calculation of the mean power of side flow arising in a long waveguide line in transmission of pulse signals. The line discontinuities leading to side flow are divided into lumped (located at approximately equal distances) and distributed. These and others are assumed to be random (varying from tube (waveguide) to tube or from line to line).

The waveguide transmission of an H_{01} wave (fundamental mode) is subject to partial conversion into other wave modes (parasitic) at discontinuities of the line. These parasitic waves are again partially converted into the fundamental wave, propagated in the same direction as the initial signal-carrying wave but displaced in time relative to the latter. There also arises a so-called side flow, distorting the effective signal. As was shown in references [2 and 3], if the power of the side flow is small compared with the signal power, it may be considered that the side flow is formed solely as the result of double conversion: fundamental wave → parasitic wave → fundamental wave. Of great importance here for calculation of the flow is the quantity $dg(z)$ — ratio of the amplitude of the parasitic wave formed at a small waveguide discontinuity at segment $(z, z+dz)$ (the z-axis is directed along the waveguide axis) to the amplitude of the fundamental wave at point z. Let $a(z, \theta)$ represent the actual radius of the waveguide (z and θ are cylindrical coordinates) and let a_0 represent the mean value of $a(z, \theta)$. Let us also designate

$$q_p(z) = \frac{1}{\varepsilon_p a_0 \pi} \int_0^{2\pi} [a(z, \theta) - a_0] e^{ip\theta} \, d\theta,$$

where $\varepsilon_0 = 2$; $\varepsilon_p = 1$ for $p > 0$.

The function $q_p(z)$ is resolved to the sum:

$$q_p(z) = q_{1p}(z) + q_{2p}(z),$$

where $q_{1p}(z)$ is a continuous function and $q_{2p}(z)$ is a step function. Jumps in $q_{2p}(z)$ will occur, for example, at points z_1, z_2, ... of the junction of two waveguide tubes. If there are no such joints, we may assume that $q_{2p}(z) \equiv 0$. Then the quantity $dq(z)$ (for the case in which the parasitic wave is an H_{pm} wave) may be presented in the form

$$dq(z) = c_1(p, m)\, dq_{1p}(z) + c_2(p, m)\, dq_{2p}(z), \tag{1}$$

where c_1 and c_2 are constants depending only on the modes of parasitic waves (see reference [2]). Hereafter, for the sake of simplicity, we shall omit the subscripts p and m.

Let us assume that $q_1(z)$ is a stationary, random Gaussian process with the correlation function σ_1^2, $B(z)$ ($B(0) = 1$). We shall assume that jumps in $dq_2(z)$ at discrete points z_1, z_2, ... are independent, identically distributed random quantities with variances equal to σ_2^2. Let us also consider that the quantities $dq_1(x)$ and $dq_2(y)$ are independent for any x and y. Further, as in reference [1], we shall consider that the lumped discontinuities are located at distances of $L + \eta j$ from one another ($j = 1, 2, \ldots$). Here L is the mean length of tube, ηj are random independent quantities with uniform distribution at segment $(-\delta, \delta)$ and $\delta / L \ll 1$.

Let $E_n(z, t)$ represent the side-flow intensity at point z of the waveguide and let $E_0(z)$ represent the amplitude of the fundamental signal-carrying wave at this same point. The probability characteristics of the quantity $E_n(z, t) / E_0(z)$ with consideration of conversion of the fundamental wave into parasitic waves only at lumped discontinuities were calculated in reference [1]. Adopting all of this report's assumptions concerning the mechanism of formation of side flow and the nature of signals traveling along the line, let us calculate the side flow with consideration of the distributed as well as the lumped discontinuities. We shall assume that the effective signal is a population of randomly alternating rectangular pulses and intervals of the same duration τ. The relative frequency of occurrence of a pulse or interval in this population is p or 1-p. Then the side flow $E_n(z,t)$ caused by an infinite sequence of such alternating intervals and pulses may be represented as a sum (compare with references [2] and [3]:

$$E_n(z,\ t) = E_0\,(z) \sum_k \varepsilon_k \int_0^z dq\,(x) \int_x^z \chi_{[0,\tau]} \left(t - k\tau - \frac{z}{v_1} - \theta\,(y - x)\right) \times \\ \times e^{-\beta_1(y-x)} \cos\,[\omega t - \varphi_k - \beta_2\,(y - x)]\,dq\,(y) \tag{2}$$

(the k-th addend represents the side flow caused by passage of the k-th pulse along the waveguide).

Here $\beta_1 = \alpha_n - \alpha_n$ and α_1 are the amplitude-damping factors of the parasitic and fundamental waves; $\beta_2 = h_n - h_1$; h_n and h_1 are the phase constants of the parasitic and fundamental waves; $\theta = \frac{1}{v_n} - \frac{1}{v_1}$; v_n and v_1 are the group velocities of the parasitic and fundamental waves; φ_k is the initial phase of the k-th pulse; quantities $\{\varphi_k\}$ are essentially mutually independent random quantities uniformly distributed at segment $(0, 2\pi)$; ω is the carrier frequency;

$$\chi_{[0,\,\tau]}\,(t) = \begin{cases} 1 \text{ for } t \in (0,\ \tau), \\ 0 \text{ for } t\,\bar{\in}\,(0,\ \tau); \end{cases}$$

ϵ_k are mutually independent random quantities, each equal to unity with probability p and to zero with probability 1-p. In expression (2) the k-th addend will not be identically zero (with fixed z, t), providing k varies within such limits that $0 \leqslant t - k\tau - \frac{z}{v_1} - \theta\,(y - x) \leqslant \tau$, where $x \leqslant y \leqslant z$.

Introducing the new summation lower limit $l = \frac{t - \frac{z}{v_1}}{\tau} - k$ and changing the order of integration in (2), we obtain

$$\frac{E_n\,(z,\ t)}{E_0\,(z)} = A\,(z) \cos \omega\ t + B\,(z) \sin \omega\ t, \tag{3}$$

where

$$\left.\begin{matrix} A\,(z) \\ B\,(z) \end{matrix}\right\} = \sum_{l=1}^{\frac{z\theta}{\tau}} \varepsilon_l \int_{\frac{(l-1)\tau}{\theta}}^{\frac{l\tau}{\theta}} dq\,(y) \int_\theta^y e^{-\beta_1(y-x)} \begin{cases} \cos \\ \sin \end{cases} [\varphi_l + \beta_2\,(y - x)]\,dq\,(x). \tag{4}$$

For subsequent discussion we shall admit the following assumptions:

$$\text{I.}\ \ \beta_1 z \gg 1, \quad \text{II.}\ \beta_1\,z_c \ll 1, \quad \text{III.}\ \ \frac{z\theta}{\tau} \gg 1$$

$$\text{IV.}\ \frac{z_c\,\theta}{\tau} \ll 1, \quad \text{V.}\ \frac{\beta_1^2\,z\delta^2}{L} \ll 1$$

(z_c is the correlation radius of the random process $q_1(z)$).

We shall impose an additional restraint on the process $q_1(z)$. Roughly speaking, it consists in the fact that the random quantities $q_1(z)$ and $q_1(z+z_0)$ become independent with $z_0 \to \infty$ and arbitrary z. Strictly speaking, we assume that $q_1(z)$ is highly random (reference[4]) (this property is possessed in particular by stationary Gaussian processes whose spectral densities are rational fraction functions. Then, from the results given in reference[4] (Theorem 1.1)it follows that with small values of z the quantities A(z) and B(z) are asymptotically normal and, according to the theorem in Section 21 of reference [5], their joint distribution also approaches normal. Since A(z) and B(z) are uncorrelated, with large values of z they may be considered independent. Then the probability characteristics of the ratio $E_n(z,t)/E_0(z)$ are wholly determined by the ensemble averages of quantities A(z) and B(z) (which are equal to zero) and their variances, which are calculated below:

$$M\{A(z)\}^2 = M\{B(z)\}^2 = \frac{p}{2}\sum_{l=1}^{\frac{z}{\tau}} \int\limits_{\frac{(l-1)\tau}{\theta}}^{\frac{l\tau}{\theta}} \int\limits_{\frac{(l-1)\tau}{\theta}}^{\frac{l\tau}{\theta}} \times$$

$$\times \int\limits_0^{y_1}\int\limits_0^{y_2} e^{-\beta_1(y_1+y_2-x_1-x_2)} \cos[\beta_2(y_1-y_2-x_1+x_2)]\, M\{dq(x_1)\,dq(x_2)\,dq(x_3)\,dq(x_4)\} \tag{5}$$

Using equality (1) and the Gaussian property of the process $q_1(z)$, we obtain

$$\begin{aligned} M\{dq(x_1)\,dq(x_2)\,dq(x_3)\,dq(x_4)\} = {} & [(c_1\sigma_1)^4 B''(x_1-x_2)\,B''(y_1-y_2) + \\ & + (c_1\sigma_1)^4 B''(x_1-y_1)\,B''(x_2-y_2) + (c_1\sigma_1)^4 B''(x_1-y_2)\,B''(x_2-y_1)] - \\ & - (c_1c_2\sigma_1\sigma_2)^2 B''(x_1-x_2)\,dx_1\,dx_2\, M\{dq_2(y_1)\,dq_2(y_2)\} - \\ & - (c_1c_2\sigma_1\sigma_2)^2 B''(y_1-y_2)\,dy_1\,dy_2\, M\{dq_2(x_1)\,dq_2(x_2)\} - \\ & - (c_1c_2\sigma_1\sigma_2)^2 B''(x_1-y_2)\,dx_1\,dy_2\, M\{dq_2(x_2)\,dq_2(y_1)\} - \\ & - (c_1c_2\sigma_1\sigma_2)^2 B''(x_2-y_1)\,dx_2\,dy_1\, M\{dq_2(x_1)\,dq_2(y_2)\} + \\ & + (c_2\sigma_2)^4 M\{dq_2(x_1)\,dq_2(x_2)\,dq_2(y_1)\,dq_2(y_2)\}; \end{aligned} \tag{6}$$

$$B''(x) = \frac{d^2}{dx^2}B(x).$$

Correspondingly, sum (5) breaks down into six sums, which we shall designate by $\Sigma_1(z), \ldots, \Sigma_6(z)$ [the first three terms in brackets are equal to $\Sigma_1(z)$ and we take them in the same order as in expression (6)]. Precise calculation of all these sums is extremely complicated and is not necessary. It is quite sufficient to calculate the limits $\frac{\Sigma_k(z)}{z}$ for k=1.6 (here and hereafter, in writing $z \to \infty$ it is to be remembered that z varies within limits determined by assumptions I, III and V).

Using L'Hospital's rule ($\Sigma_1(z) \to \infty$ when $z \to \infty$), we obtain

$$\lim_{z\to\infty}\frac{\Sigma_1(z)}{z} = \frac{p}{2}(c_1\sigma_1)^4\frac{\theta}{\tau}\left\{\int\limits_0^{\tau/\theta} dy_1 \int\limits_0^{\tau/\theta} dy_2 \int\limits_{-\infty}^{y_1}\int\limits_{-\infty}^{y_2} e^{-\beta_1(y_1+y_2-x_1-x_2)} \times\right.$$

$$\times \cos\beta_2(y_1-y_2-x_1+x_2)\,[B''(x_1-x_2)\,B''(y_1-y_2) +$$

$$\left. B''(x_1-y_1)\,B''(x_2-y_2) + B''(x_1-y_2)\,B''(x_2-y_1)]\,dx_2\,dx_1\right\} \equiv J_{11}+J_{12}+J_{13}.$$

Let us calculate the three resulting integrals separately:

$$J_{11} = \frac{p}{2}(c_1\sigma_1)^4\,\frac{\theta}{2\beta_1\tau}\int\limits_0^{\tau/\theta}\left(\frac{\tau}{\theta}-s\right)ds\int\limits_{-\infty}^{\infty} e^{-\beta_1|s-t|}\,B''(t)\,B''(s)\cos\beta_2(s-t)\,dt$$

In virtue of assumption IV

$$J_{11} \simeq \frac{p}{2}(c_1\sigma_1)^4\,\frac{1}{\beta_1}\int\limits_0^{\infty}ds\int\limits_{-\infty}^{\infty} e^{-\beta_1|s-t|}\,B''(t)\,B''(s)\cos\beta_2(s-t)\,dt,$$

$$J_{12} = \frac{p}{2}(c_1\sigma_1)^4\,\frac{\tau}{2\theta}\int\limits_0^{\infty}\int\limits_0^{\infty} e^{-\beta_1(t+s)}\,B''(t)\,B''(s)\cos\beta_2(t-s)\,dt\,ds.$$

In virtue of assumption II

$$J_{12} \simeq \frac{p}{2}(c_1\sigma_1)^4\,\frac{\tau}{\theta}\int\limits_0^{\infty}\int\limits_0^{\infty} B''(t)\,B''(s)\cos\beta_2(t-s)\,ds\,dt =$$

$$\frac{p}{2}(c_1\sigma_1)^4\,\frac{\tau\beta_2^2}{\theta}\left\{\left[\beta_2\int\limits_0^{\infty}B(t)\cos\beta_2 t\,dt\right]^2 + \left[1-\beta_2\int\limits_0^{\infty}B(t)\sin\beta_2 t\,dt\right]^2\right\},$$

$$J_{13} = p\,(c_1\sigma_2)^4\,\frac{\theta}{\tau}\int\limits_0^{\tau/\theta}\left(\frac{\tau}{\theta}-x\right)dx\int\limits_{-x}^{\infty}dt\int\limits_x^{\infty} e^{-\beta_1(t+s)}\,B''(t)\,B''(s)\cos\beta_2(2x+t-s)$$

In virtue of assumptions II and IV

$$J_{13} \simeq p\,(c_1\sigma_1)^4 \int_0^\infty dx \int_{-x}^\infty dt \int_x^\infty B''(t)\,B''(s)\cos\beta_2\,(2x + t - s)\,ds =$$

$$= \frac{p\,(c_1\sigma_1)^4}{\beta_2} \int_0^\infty B''(s)\,ds \int_0^s B''(t)\sin\beta_2\,(s - t)\,dt +$$

$$+ \frac{p\,(c_1\sigma_1)^4}{\beta_2} \int_0^\infty B''(s)\,ds \int_0^\infty B''(t)\sin\beta_2\,(s + t)\,dt.$$

Passing from B''(t) to B(t) in the integrals J_{11} and J_{13}, we finally obtain

$$\lim_{z\to\infty} \frac{\Sigma_1(z)}{z} = p\,(c_1\sigma_1)^4\beta_2^2 \left\{ \frac{\beta_2^2}{2\beta_1} \int_0^\infty B(s)\,ds \int_{-\infty}^\infty e^{-\beta_1|t-s|}B(t)\cos\beta_2\,(s - t)\,dt + \right.$$

$$+ \frac{\tau}{2\theta}\left[\beta_2 \int_0^\infty B(t)\cos\beta_2\,t\,dt\right]^2 + \frac{\tau}{2\theta}\left[1 - \beta_2 \int_0^\infty B(t)\sin\beta_2\,t\,dt\right]^2 +$$

$$\left. + 2\int_0^\infty B^2(t)\,dt + 6\beta_2 \int_0^\infty B(s)\sin\beta_2\,s\,ds \int_0^s B(t)\cos\beta_2\,t\,dt \right\} \equiv F_1. \qquad (7)$$

Let us continue the calculations:

$$\sum\nolimits_6(z) = \frac{p}{2}\,(c_2\sigma_2)^4 \sum_{l=1}^{\frac{z\theta}{\tau}} \; \sum_{j=\frac{(l-1)\tau}{L\theta}}^{\frac{l\tau}{L\theta}} \; \sum_{m=1}^{j-1} e^{-2\beta_1(j-m)L},$$

whence

$$\lim_{z\to\infty} \frac{\Sigma_6(z)}{z} = \frac{p\,(c_2\sigma_2)^4}{4\beta_1 L^2}.$$

When $q_1(z) \equiv 0$ M $\{A(z)\}^2 = \Sigma_6(z)$, which coincides with the result in reference [1].

$$\sum\nolimits_2(z) = \frac{p}{2}\,(c_1c_2\sigma_1\sigma_2)^2 \sum_{l=1}^{\frac{z\theta}{\tau}} \; \sum_{k=\frac{(l-1)\tau}{L\theta}}^{\frac{l\tau}{L\theta}} \int_0^{kL+\sum_1^k \eta_j} e^{-\beta_1\left(2kL + 2\sum_1^k \eta_j - x_1 - x_2\right)} \times$$

$$\cdot\, B''(x_1 - x_2)\cos\beta_2\,(x_1 - x_2)\,dx_2,$$

whence

$$\lim_{z\to\infty} \frac{\Sigma_2(z)}{z} = -\frac{p\,(c_1c_2\sigma_1\sigma_2)^2}{2\beta_1 L}\,\beta_2^2 \int_0^\infty B(t)\cos\beta_2\,t\,dt;$$

$$\sum\nolimits_3(z) = p\,(c_1c_2\sigma_1\sigma_2)^2 \sum_{l=1}^{\frac{z\theta}{\tau}} \int_{\frac{(l-1)\tau}{\theta}}^{\frac{l\tau}{\theta}} dy_1 \int_{\frac{(l-1)\tau}{\theta}}^{y_1} \sum_{k=1}^{y_2/L} e^{-\beta_1\left(y_1 + y_2 - 2kL - 2\sum_1^k \eta_j\right)} \times$$

$$\times B''(y_1 - y_2)\cos\beta_2\,(y_1 - y_2)\,dy_2,$$

by averaging this sum for ηj,

$$\lim_{z\to\infty} \frac{\Sigma_3(z)}{z} = \frac{p\,(c_1c_2\sigma_1\sigma_2)^2\,\theta}{\tau} \times$$

$$\times \int_0^{\tau/\theta} dy_1 \int_0^{y_1} e^{-\beta_1\left(y_1 + y_2 - 2z + \frac{2\tau}{\theta}\right)} \sum_{k=1}^{\frac{y_2 + z - \frac{\tau}{\theta}}{L}} e^{-2\beta_1 kL} M_\eta^k \cos\beta_2\,(y_1 - y_2)\,B''(y_1 - y_2)\,dy_2,$$

$$M_\eta \equiv Me^{-2\beta_1\eta_j} \simeq e^{\frac{2}{3}(\beta_1\delta)^2}.$$

In virtue of assumption V concerning the upper boundary of change in z, $M_\eta^k - 1 \ll 1$ for $k \leqslant z/L$, hence

$$\lim_{z\to\infty}\frac{\Sigma_3(z)}{z} = \frac{p\,(c_1c_2\sigma_1\sigma_2)^2\,\theta}{2\beta_1 L\tau}\int_0^{\tau/\theta} dy_1 \int_0^{y_1} e^{-\beta_1(y_1-y_2)} B''\,(y_1-y_2)\cos\beta_2\,(y_1-y_2)\,dy_2 =$$

$$= -\frac{p\,(c_1c_2\sigma_1\sigma_2)^2}{2\beta_1 L}\,\beta_2^2\int_0^\infty B\,(t)\cos\beta_2\,t\,dt,$$

$$\Sigma_4(z) + \Sigma_5(z) = \frac{p\,(c_1c_2\sigma_1\sigma_2)^2}{2}\sum_{l=1}^{z\theta/\tau}\int_{(l-1)\tau/\theta}^{l\tau/\theta} dy\,\times$$

$$\times\sum_{k=\frac{(l-1)\tau}{L\theta}}^{y/L}\int_0^{kL} e^{-\beta_1(y-x)}\cos\beta_2\Big(2kL + 2\sum_1^k\eta_j - y - x\Big)\,B''\,(y-x)\,dx.$$

Sum $\sum_1^k \eta_j$ with any k, taken over mod 2π, is a random quantity uniformly distributed at segment $(0, 2\pi)$. Averaging this sum for η_j, we thus obtain

$$\Sigma_4(z) = \Sigma_5(z) = 0.$$

Let us write the final expression for the variances of quantities A(z) and B(z) [see (4)]:

$$\lim_{z\to\infty}\frac{M\,\{A\,(z)\}^2}{z} = \lim_{z\to\infty}\frac{M\{B(z)\}^2}{z} = \frac{p\gamma_1^2}{4\beta_1} + F_1 - \frac{p\,(c_1\sigma_1)^4\,\beta_2^2}{\beta_1}\Big[\beta_2\int_0^\infty B\,(t)\cos\beta_2\,t\,dt\Big]^2, \tag{8}$$

where the quantity F_1 is defined by equality (7), while

$$\gamma_1 = \frac{(c_2\sigma_2)^2}{L} + 2\beta_2^2\,(c_1\sigma_1)^2\int_0^\infty B\,(t)\cos\beta_2\,t\,dt. \tag{9}$$

Let us make one simplifying assumption, namely: we shall consider that $z_c\beta_2 \leqslant 1$ (z_c is the correlation radius of the process $q_1\,(z)$).

Physically this is the lower restraint on the spectrum width of $q_1(z)$, since the spectrum width is inversely proportional to z_c. In such a case it is not difficult to prove that in expression (7) the last two addends are several orders of magnitude smaller than the first and hence

$$F_1 \simeq \frac{p\,(c_1\sigma_1)^4\,\beta_2^2}{\beta_1}\left\{\Big[\beta_2\int_0^\infty B\,(t)\cos\beta_2\,t\,dt\Big]^2 + \frac{\beta_1\tau}{2\theta}\Big[1 - \beta_2\int_0^\infty B\,(t)\sin\beta_2\,t\,dt\Big]^2\right\}.$$

Expression (8) is now rewritten as follows:

$$\lim_{z\to\infty}\frac{M\,\{A\,(z)\}^2}{z} = \frac{p}{4\beta_1}\,(\gamma_1^2 + \gamma_2^2). \tag{10}$$

where coefficient γ_1 is defined above and

$$\gamma_2^2 = 2\,(c_1\sigma_1)^4\,\frac{\beta_1\beta_2^2\tau}{\theta}\Big[1 - \beta_2\int_0^\infty B\,(t)\sin\beta_2\,t\,dt\Big]. \tag{11}$$

Let us explain the physical significance of coefficient γ_1. Considering the assumption of statistical independence of losses at the different joints, it is not difficult to see that the quantity $(c_2\sigma_2)^2 z/L$ represents the mean losses in conversion to a parasitic wave only at joints. Let us calculate the conversion losses at distributed discontinuities in a waveguide of length z. In accordance with formula (8) in reference[2], the ratio of parasitic wave amplitude at the end of the line to the fundamental wave amplitude is expressed by the integral

$$\sigma_1\hat{c}_1\int_0^z q_1\,(x)\,e^{-i\beta_2 x}\,dx,$$

where $q_1(x)$ is defined by formula (1) and the constants c_1 from (1) and $\hat{c}_1$ are related by $|c_1 \beta_2| = |\hat{c}_1|$. Thus, the mean conversion loss at distributed discontinuities is

$$\sigma_1^2 |\hat{c}_1|^2 M \left| \int_0^z q_1(x) e^{-i\beta_2 x} dx \right|^2 = 2\beta_2^2 (c_1\sigma_1)^2 \int_0^z (z-x) B(x) \cos\beta_2 x dx.$$

Adding the derived expressions for losses at joints and at distributed discontinuities, referring them to line length z and assuming the limit as z → ∞, we find that the mean linear damping coefficient of thefundamental wave is

$$\frac{(c_2\sigma_2)^2}{L} + 2\beta_2^2 (c_1\sigma_1)^2 \int_0^\infty B(t) \cos\beta_2 t dt = \gamma_1.$$

We will note that this same formula was derived in reference [6] by a slightly different method.

In reference [3] a formula was derived for side flow power relative to signal power $(p_n(z)/p_0(z))$. In our notation this formula is given as follows:

$$\frac{p_n(z)}{p_0(z)} = \frac{pz\gamma_1^2}{2\beta_1}. \qquad (12)$$

The formula was derived with several assumptions concerning the mechanism of generation of side flow: it was assumed that the ratio of power generated at segment $(z, z+\Delta z)$ of the parasitic wave to the signal power at point z is equal to $\gamma, \Delta z$. The above calculation shows that the formula of reference [3] must be replaced by

$$\frac{p_n(z)}{p_0(z)} = \frac{pz}{2\beta_1}(\gamma_1^2 + \gamma_2^2). \qquad (13)$$

The presence of additional coefficient γ_2 is due to the discontinuous nature of the signals transmitted along the line.

Let us note, however, that calculation of side flow from formula (12) is somewhat simpler than from formula (13), since in the latter case it is necessary to know the correlation function B(z) and in the first case it may, in principle, be disregarded. Hence it is of interest to ascertain those cases in which formula (12) may be used, that is, to ascertain when $\gamma_1/\gamma_2 > 1$. From (9) and (11) we obtain (disregarding losses at junctions).

$$\frac{\gamma_1}{\gamma_2} = \sqrt{\frac{2\theta}{\beta_1\tau}} \frac{\left| \beta_2 \int_0^\infty B(t) \cos\beta_2 t dt \right|}{\left| 1 - \beta_2 \int_0^\infty B(t) \sin\beta_2 t dt \right|}. \qquad (14)$$

With $\beta_2 z_c \to 0$ ratio (14) $\frac{\gamma_1}{\gamma_2} = \sqrt{\frac{2\theta}{\beta_1\tau}} \frac{\beta_2 z_c}{1-\beta_2 z_c} \to 0$ with any correlation function. Consequently, formula (12) is incorrect when the correlation radii are small in comparison with β_2 (for example, when $z_c < \frac{1}{\beta_2}\sqrt{\frac{\beta_1\tau}{2\theta}}$). The behavior of the ratio (14) when $1 > \beta_2 z_c > \sqrt{\frac{\beta_1\tau}{2\theta}}$ requires more detailed examination.

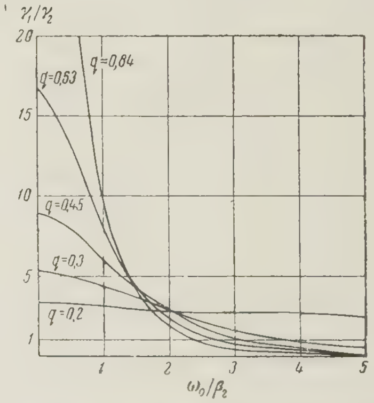

Ratio of coefficients γ_1/γ_2 as a function of ω_0/β_2 at different values of q.

We shall limit discussion to one specific example. Let us take the correlation function.

$$B(z) = \left(1 + \frac{|z|}{z_c}\right) e^{-\frac{|z|}{z_c}} \cos\omega_0 z. \qquad (15)$$

The corresponding spectral density

$$f(\omega) = \int_0^\infty B(z) \cos \omega z dz = \frac{z_c}{[1 + (\omega_0 - \omega)^2 z_c^2]^2} + \frac{z_c}{[1 + (\omega_0 + \omega)^2 z_c^2]^2}. \qquad (16)$$

It is our opinion that the random process $q_1(z)$ with such a correlation function in every case better characterizes discontinuities of the line than processes with correlation functions $B(z) = e^{-\left(\frac{z}{z_c}\right)^2}$ or $B(z) = \sin \Omega z / \Omega z$, since the latter are uniquely defined by their defined by their initual values.

The figure presents curves for ratio γ_1/γ_2 as a function of ω_0/β_2 at different values of $q = \beta_2 z_c$. The calculations were performed on the assumptions: (1) $q_1(z) = q_{11}(z)$; $m = 2$ [see equation (1)]; thus, we refer to the side flow created by the H_{12} wave; (2) waveguide diameter equals 60 mm; (3) the propagated wavelength is 8 mm; (4) $\tau = 5.10^{-9}$ sec. In this $\beta_2 = 0.1$ cm^{-1}; $\beta_2 = 0.1$ cm^{-1}; $\beta_1 = 0.283 \cdot 10^{-5}$ cm^{-1}; $\theta = 45 \cdot 10^{-14}$ sec/cm and assumptions I-V reduce to the following: 3 km $\ll z \ll$ 50,000 km; $z_c \ll$ 100 m; γ_1/γ_2 becomes less than unity when $q \leqslant 0.07$. With such values of q it may be considered that $\gamma_2^2 = \beta_2^2 (c_1\sigma_1)^4 \frac{2\beta_1\tau}{\theta}$.

It is seen from that the closer formula (12) is to formula (13), the greater the wavelength of oscillations of the waveguide axis (the quantity $q_{11}(z)$, as is easily proved, characterizes oscillations of the axis).

REFERENCES

1. V.I. Bunimovich, V.A. Morozov, Concerning the probability of distortion caused by side flow and Gaussian noise, Radiotekhnika i Elektronika, 1959, 4, 10, 1585.
2. B.Z. Katsenelenbaum, V.V. Malin, Formation of side flow in a long waveguide line, Part 2, Radiotekhnika i Elektronika, 1958, 3, 11, 1389.
3. B.Z. Katsenelenbaum, V.V. Malin, Formation of side flow in a long waveguide line, Part 1, Radiotekhnika i Elektronika, 1958, s, 6, 750.
4. V.A. Volkonskiy, Yu.A. Rozanov, Some limit theorems for random functions, Teoriya Veroyatnostey i yeye Primeneniya, 1959, 4, 2, 186.
5. S.N. Bernshteyn, Extension of the limit theorem of probability theory to sum of dependent quantities, Uspekhi Matem. Nauk, 1944, 10, 65.
6. N. Larsen, Die Übertragunseigenschaften von H_{01} -Hohlleitungen mit statisch verteilten Unregelmässigkeiten, Frequenz, 1960, 14, 4, 135.

Submitted to the editors 27 August 1960

SENSITIVITY OF TELEVISION SYSTEMS WITH DIFFERENT SCANNING PARAMETERS*

S. B. Gurevich

In this report a formula is derived for specific and total sensitivity of television systems; the relationship between sensitivity and the amount of transmitted information is examined.

Transmitter sensitivity of a television broadcasting system with a given scanning standard is usually evaluated in the literature as the reciprocal of the scene brightness required to provide an image of satisfactory quality on the screen of the picture tube (references [1, 2, 3]).

This is a somewhat narrow definition, for it only permits comparison of systems with identical scanning parameters and identical requirements for image quality (e.g., television broadcasting systems). If we are to compare the sensitivity of any two television systems, the definition of sensitivity must contain a quantitative factor for image quality (in the absence of nonlinear distortion this factor is expressed as the amount of scene information transmitted by the system) and a factor for the amount of incoming radiated energy per unit of scene information.

The sensitivity of a television system may be increased by increasing the efficiency of conversion of radiant energy into picture signals and by reducing to a minimum the noise-level gain in amplifying the signal. However, this increase in sensitivity is limited by quanta fluctuations in the radiant flux.

In the absence of distortion caused by the nonlinear nature of conversion in monochromatic television systems, the quality of a moving image may be quantitatively determined by the number of image elements N, the number of distinguishable gradations in brightness m and the number of frames (number of transmitted states of the scene) n. In this concept of image quality the camera sensitivity is expressed as the function

$$G_{a} = G(\varepsilon_0, N, m, n), \tag{1}$$

where ϵ_0 is the radiant energy of one element required to create one distinguishable gradation against a background level of $\epsilon = 0$.

Let us derive the relationship between sensitivity and ϵ_0, N, m and n. First we shall consider the single transmission of one element in which only one gradation of nonzero radiant energy is distinguished. The radiant energy characterizing the given element is detectable only when its mean value exceeds its fluctuations by a given factor (k), that is, when $\bar{\epsilon} = k\epsilon_f$. Moreover, it is known (reference [4]) that the radiant energy fluctuation (for radiation whose wavelength is not too long) may be represented in approximate form as

$$\varepsilon_{\Phi} = \sqrt{\overline{\Delta\varepsilon^2}} = \sqrt{\overline{\Delta\mu^2}(h\nu)^2} = \sqrt{\bar{\mu}}h\nu, \tag{2}$$

where $\overline{\Delta\epsilon^2}$ is the variance of the radiant energy; $\bar{\mu}$ is the mean number of quanta corresponding to mean energy $\bar{\epsilon}_0 = \mu h\nu$ (where h is Planck's constant and ν is vrequency or, in the case of nonmonochromatic light, mean frequency). To distinguish one nonzero gradation of radiant energy in a single transmission of a single element it must be assumed that the mean energy is

$$\bar{\varepsilon}_0 = k\varepsilon_{0\Phi} = k\sqrt{\bar{\mu}}h\nu = k^2 h\nu, \tag{3}$$

since

$$\sqrt{\mu} = \frac{\bar{\mu}}{\sqrt{\mu}} = \frac{\bar{\varepsilon}_0}{\varepsilon_{0\Phi}} = k.$$

---

* Paper presented at scientific sessions commemorating "Radio Day" on April 19, 1960 in Leningrad and May 19, 1960 in Moscow.

Let us determine the energy ϵ_m which will permit distinguishing m gradations if a radiant energy of $\overline{\epsilon_0} = k^2 h\nu$ permits transmission of one nonzero graduation. The i-th gradation will be transmitted in the case where the relation

$$\varepsilon_i - \varepsilon_{i-1} = k\sqrt{\overline{\mu_i} + \overline{\mu_{i-1}}\,h\nu} = k\sqrt{(\overline{\varepsilon_i} + \overline{\varepsilon_{i-1}})h\nu}. \tag{4}$$

is satisfied.

As in the case of a single nonzero graduation, the difference between the energies required for transmission of i and i - 1 gradations must be k times greater than the noise energy, which in the given case is the geometric sum of the noise accompanying radiant energies ϵ_i and ϵ_{i-1}. An expression similar to (4) is derived in reference [5].

From Equation (3) it can be shown that condition (4) for any i will be satisfied if

$$\varepsilon_i = \frac{i}{2}(i+1)\,k^2 h\nu, \tag{4a}$$

and consequently the energy ϵ_m required for transmission of m gradations exceeds the energy required for transmission of a single gradation by a factor $l = \frac{m}{2}(m+1)$, that is,

$$\varepsilon_m = \varepsilon_0 \frac{m}{2}(m+1) = \frac{m}{2}(m+1)\,k^2 h\nu. \tag{5}$$

It is easily seen that the number of distinguishable energy gradations m is greater than the numerical value of the ratio of the energy ϵ_m required for the transmission of m gradations to the value k times greater than the noise energy, that is, ψ_m/k (ψ is the signal-to-noise ratio). In effect,

$$m' = \frac{\bar{\varepsilon}_m}{k\varepsilon_{m\Phi}} = \frac{\Phi_m}{k} = \sqrt{\frac{\bar{\varepsilon}_m}{k^2 h\nu}} = \sqrt{\frac{\frac{m}{2}(m+1)\,\bar{\varepsilon}_0}{k^2 h\nu}} = \sqrt{\frac{m}{2}(m+1)} < m,$$

if m > 1. This inequality results from the fact that with the above dependence of fluctuations on signal value the "degrees" of gradation decrease with the signal value.

It is evident that with the necessity for distinguishing m gradations in N elements the transmission of n states of the scene requires an energy not less than

$$\bar{\varepsilon}_{(m,N,n)} = \frac{m}{2}(m+1)\,Nnk^2 h\nu. \tag{6}$$

Considering that the radiation indicator receives only part of the energy radiated by the scene (in the case of isotropic radiation $\alpha = \frac{1}{\frac{\pi D^2}{4}\beta^2\gamma}$ where D is the aperture diameter of the objective projecting the image onto the sensitized surface, β is the angle at which the scene is seen from the objective plane, γ is the radiation absorption coefficient of the objective), we obtain the value for the minimum radiant energy given off by the scene and required for distinguishing m gradations in N elements with n recurrences in the ideal case (in which the camera causes no further deterioration in distinguishability of gradations in these elements):

$$\varepsilon_{\mathrm{sc}(m,N,n)} = \alpha k^2 h\nu \frac{m}{2}(m+1)\,Nn. \tag{7}$$

Actually, there are no ideal cameras and in order to maintain this amount of information concerning the scene it is necessary to increase the amount of energy reaching the camera input. In other words, in order to maintain the required signal-to-noise ratio at the camera output it is necessary to increase the signal-to-noise ratio at the input. Let us introduce the factor

$$\xi = \frac{\psi_{\mathrm{out}}}{\psi_{\mathrm{in}}}, \tag{8}$$

where ψ_{out} is the output signal-to-noise ratio required for transmission of N elements, m gradations and n states of the scene and which would be adequate at the camera input if the system were ideal ($\psi_{\mathrm{out}} = \psi_{\mathrm{in\ id.}}$). Thus, $\psi_{\mathrm{out}} = \bar{\epsilon}_{\mathrm{sc}(m,N,n)}/\sqrt{\bar{\epsilon}_{\mathrm{sc}(m,N,m)} h\nu}$, whereas the input signal-to-noise ratio $\psi_{\mathrm{in}} = \bar{\epsilon}/\sqrt{\bar{\epsilon}\,h\nu}$, where $\bar{\epsilon}$ is the energy which must be delivered to the input of a nonideal system characterized by the coefficient $\xi = \sqrt{\epsilon_{\mathrm{sc}(m,N,n)}/\epsilon}$. This energy is now defined by the expression

$$\bar{\varepsilon} = \frac{\alpha k^2 h\nu}{\xi^2}\frac{m}{2}(m+1)Nn, \tag{9}$$

and the sensitivity

$$G = \frac{1}{\varepsilon} = \frac{\xi^2}{\alpha k^2 h\nu}\cdot\frac{1}{Nn\frac{m}{2}(m+1)}.$$

Let

$$g = \frac{\xi^2}{\alpha k^2 h\nu} \tag{10}$$

and let us refer to it as the specific sensitivity. The specific sensitivity is the reciprocal of the energy which must be radiated by a single element of the scene in order to distinguish at the output of a real system with $\xi = \psi_{out}/\psi_{in}$ a single nonzero gradation of radiant energy.

Quantity G is expressed in terms of g by the relation

$$G = g\frac{1}{\frac{m}{2}(m+1)Nn}. \tag{11}$$

Expression (9), derived for the characteristic of threshold sensitivity of television cameras, permits us to establish the relationship between the energy conveyed from the scene to the camera input and the amount of transmitted information concerning the scene.

It is known (reference [6]) that if m+1 different states are possible in an element (e.g., m nonzero gradations of radiant energy and zero energy) and there are Nn such elements, the number of possible messages is $(m+1)^{Nn}$ and the amount of information contained in this number of possible messages is

$$J = Nn\log_2(m+1). \tag{12}$$

When the number of elements and the number of states of the scene are equal to unity, and when only one nonzero value of brightness (m = 1) can be transmitted, J is also equal to unity.

Comparing expressions (9) and (12), we see that the required radiation energy and the amount of transmitted information are linear functions of the number of elements and the number of transmitted states of the scene. The relationship for the number of gradations is somewhat different. The required radiation energy increases more rapidly than the number of gradations $[\epsilon \sim \frac{m}{2}(m+1)]$, whereas the amount of information increases more slowly than the number of gradations $(J \sim \log_2(m+1))$.

The amount of radiant energy from the scene per unit of information is expressed by the relation

$$\frac{\varepsilon}{J} = \frac{\alpha k^2 h\nu}{\xi^2}\,\frac{m(m+1)}{2}\,\frac{1}{\log_2(m+1)} = \frac{1}{g}\,\frac{m(m+1)}{\log_2(m+1)^2}. \tag{13}$$

When m ≫ 1

$$\frac{\varepsilon}{J} = \frac{1}{g}\,\frac{m^2}{\log_2 m^2}. \tag{13a}$$

It is easily seen that with m = 1 the reciprocal of ϵ/J is equal to g and, consequently, the specific sensitivity may be defined as a quantity inversely proportional to the energy arriving per unit of information.

From the standpoint of increasing the amount of information concerning the scene, it follows from exoressuibs (9), (12) and (13) that it is more convenient to increase the number of elements than to increase the number of gradations.

It must, however, be mentioned that this conclusion refers to the amount of information concerning the scene without reference to the properties of the information receiver. For example, in the transmission of an image an increase in the number of elements beyond $(4\text{-}8)\cdot 10^5$ continues to increase the amount of information concerning the scene in proportion to the number of elements; however, in visual observation these additional elements are not discerned. Moreover, if the number of distinguishable gradations is small (e.g., m < 10), a further increase therein will be perceived by the eye more as a considerable increase in the amount of information concerning the scene than as an increase in the number of elements, hence an identical increase in information concerning the scene proves to be quantitatively nonequivalent.

As another example of the limitations imposed not by the reciever but by the information source we may cite the example of transmission of the intensity distribution of a spectral line. An increase in the number of elements beyond a certain given number (e.g., N = 20-30) may not provide the required additional information due to the limited resolving power of the optical device from which the spectral line is projected to the camera input. On the other hand, an increase in the number of gradations of brightness leads in this case to an increase in accuracy of measurement of intensity of the line at the particular wavelength and hence is of some value.

In the case where there are no limitations in the transmission of information concerning the scene or process and all information has identical value, it is worthwhile to note the advantage (from the standpoint of optimum utilization of energy) of increasing the number of elements rather than the number of distinguishable gradations.

In the transmission of a color image more information is transmitted than in a black-and-white image with the same number of elements. While color, like brightness, is a characteristic of the state of an element of the scene, an increase in the amount of information upon increasing the gradations of brightness in black-and-white television. In order to obtain a color image, it is necessary to obtain from each element information concerning the several values of brightness corresponding to the spectral composition of the radiation emanating from the element, which corresponds to an increase in the number of elements transmitted per frame. Correspondingly, in expressions (9) and (12) we must further introduce the factor ν (for color television the value of ν is usually 2-3 [7]).

From analysis of (9) and (12) with the addition of ν it may be concluded that the introduction of color information is beneficial from the energy standpoint. It increases the amount of information concerning the scene by the factor ν and increases the required radiation energy by the same factor. With an increase in the number of gradations by the factor ν, as we have already seen, the amount of information would be increased by only $\frac{\log_2 \nu m}{\log_2 m}$ times while the required radiation energy is increased by $\frac{\nu}{2}(\nu+1)$ times. In addition, as already noted, an increase in the number of elements by ν times over the number of elements (of the order of $6 \cdot 10^5$) currently found in broadcast television would add little information concerning the scene, whereas an increase by ν times in the amount of information generated in color television presents considerable advantage in visual observation.

REFERENCES

1. G. V. Braude, Fluctuation noise in amplification of television signals and sensitivity of pickup tubes, Tr. Sekissi Televideniva, 1948.
2. A. M. Khalfin, Principles of Television Engineering,Izd. Sovetskoye radio, 1955.
3. S. B. Gurevich, R. A. Ganburg, Sensitivity of television cameras, Tekhnika Kino i Televideniya, 1959, 6, 1.
4. S. I. Vavilov, Microstructure of Light, Izd. AN SSSR, 1950.
5. G. A. Morton, J. E. Ruedy, The intensifier orthicon, Conference proceedings 2nd National Convention on Military Electronics, 1958, pp. 113-117.
6. C. E. Shannon, A mathematical theory of communication, Bell System Techn. J., 1948, 27.
7. V. L. Kreytser, Compatible combined systems of color television, Tekhnika Kino i Televideniya, 1959, 1, 52.

Submitted to editors 28 May 1960

THEORY OF A FLAT-ELECTRODE TRIODE WITH NEGLIGIBLY SMALL GRID-ANODE SPACE CHARGE

Ye. N. Petrov

The report presents a simple approximate method for calculating cathode current in the case of negligibly small grid-anode space charge in a flat-electrode triode.

It is shown that for the case of zero initial velocities of emitted electrons this method provides practically the same accuracy in calculating space-charge current as the widely used method in which the anode of the equivalent diode at the cathode is located in the plane of the triode grid.

1. STATEMENT OF THE PROBLEM OF CALCULATING CATHODE CURRENT IN A FLAT-ELECTRODE TRIODE

The procedure for calculating cathode current of multielectrode vacuum tubes is based on the knowledge that a multigrid tube can be reduced to an equivalent diode.

The cathode current of an equivalent flat-electrode diode is determined [1] from the given electrode configuration (the value F_k for the active surface of the cathode and the space X_{eq} between cathode and anode), the cathode temperature T, the cathode emission I_S and the voltage at the electrodes ($U_{eq.}$ is the anode potential). If F_k, T and I_S are assumed to be common for the multielectrode tube and the equivalent diode, the problem of calculating the cathode current reduces to determining X_{eq} and U_{eq} In V.S. Lukoshkov's work [2] as well as in a number of other works (e.g., [4, 5]) the triode is represented as two series-connected diodes and it is shown that the "hot" cathode field of a flat-electrode triode with ideal grid is the same as the "hot" cathode field of a flat-electrode diode with cathode-anode space X_d equal to the cathode-grid space X_{kg} of the triode and that the anode potential U_d:

$$U_d = \frac{U_g + \varkappa_2 D U_a}{1 + \varkappa_2 D + \varkappa_1 D'}, \qquad (1)$$

where U_g is the grid potential of the triode, U_a is the anode potential of the triode and D and D' are the forward and reverse penetration of the field of the triode from anode to cathode and from cathode to anode, respectively:

$$\varkappa_1 = \frac{E_{\mathrm{I\,hot}}}{E_{\mathrm{I\,cold}}};$$

$$\varkappa_2 = \frac{E_{\mathrm{II\,hot}}}{E_{\mathrm{II\,cold}}};$$

$E_{\mathrm{I\,hot}}$ and $E_{\mathrm{I\,cold}}$ are the "hot" and "cold" field intensities of the triode at the grid surface facing the cathode; $E_{\mathrm{II\,hot}}$ and $E_{\mathrm{II\,cold}}$ are the "hot" and "cold" field intensities of the triode at the grid surface facing the anode.

Quantities U_g and U_a are usually given, while the grid penetration factors D and D' of the triode may be calculated from the given electrode configuration by the usual formulas. Thus, the problem of determining the cathode current of the triode reduces to determining the "hot" parameters $\varkappa_1$ and $\varkappa_2$.

L.V. Shubin made use of the fact that in most cases of practical importance the grid-anode space charge of the triode may be neglected ($\varkappa_2 = 1$). Formula (1) is then simplified:

$$U_d = \frac{U_g + D U_a}{1 + D + \varkappa_1 D'}. \qquad (2)$$

Coefficient $\varkappa_1$ may be determined by considering the Maxwell distribution of initial electron velocities as given in the tables in reference [3]. The value of U_d is found from formula (2) by the method of successive approximations.

2. CONSTRUCTING THE EQUIVALENT DIODE

Proceeding from general formula (1) and the condition $\varkappa_2 = 1$, we may construct the equivalent diode so that calculation of the cathode current of the triode is simplified.

Let us compare our triode with a certain equivalent diode, the anode of which is located in an arbitrary plane parallel to the plane of the triode grid. Knowing $E_{I\,hot}$, let us determine the anode potential U_{eq} of the equivalent diode from the relation

$$U_{eq} = U_d + E_{I\,hot} X_{gx}, \tag{3}$$

where U_d is the effective grid potential (2) of the triode; X_{gx} is the distance from the grid to the anode of the equivalent diode. Thus, with $X_{gx} > 0$ the potential distribution at the grid surface facing the cathode is extrapolated in the grid-anode space. It is evident that

$$U_{eq} = U_d\left(1 + \frac{X_{gx}}{X_{kg}}\varkappa_1\right). \tag{4}$$

Let us so extrapolate the potential (by choice of X_{gx}) that U_{eq} is not a function of hot parameter $\varkappa_1$. In the general case X_{gx} is then a function of $\varkappa_1$. However, we may select such a value of U_{eq} that X_{gx} is not a function of $\varkappa_1$.

That is, let

$$U_{eq} = \frac{U_g + DU_a}{1 + D}.$$

Then relation (4) will yield

$$X_{gx} = X_{kg}\frac{D'}{1 + D}. \tag{5}$$

Thus, the equivalent diode for the given triode has a cathode-anode space

$$X_{eq} = X_{kg}\frac{1 + D + D'}{1 + D} \tag{6}$$

and the anode potential

$$U_{eq} = \frac{U_g + DU_a}{1 + D}. \tag{7}$$

Linear extrapolation of potential distribution of the cold field in the cathode-grid space up to the plane of X_{eq} leads to the same value for U_{eq} (7); that is, the equation

$$U_{d\,cold} + \frac{U_{d\,cold}}{X_{kg}}X_{gx} = U_{d\,hot} + E_{I\,hot}X_{gx}$$

or

$$U_{d\,cold}\left(1 + \frac{X_{gx}}{X_{kg}}\right) = U_{d\,hot}\left(1 + \frac{X_{gx}}{X_{kg}}\varkappa_1\right)$$

is indeterminate relative to $\varkappa_1$ when

$$X_{gx} = X_{kg}\frac{D'}{1 + D}.$$

Thus, for the important special case in which the grid-anode space charge of the triode may be disregarded determination of the space-charge current of the triode (as well as its parameters) is simple, omitting intermediate determination of the tubular coefficient of $\varkappa_1$.

3. EVALUATING RELATIVE ERROR IN METHODS OF CALCULATING SPACE-CHARGE CURRENT IN TRIODE

Simple evaluation of the relative error of the different methods of calculating cathode current of the triode may be performed for the case of zero initial electron velocities. In this case $\varkappa_1 = 4/3$ and, correspondingly,

$$U_{\mathrm{d}} = \frac{U_{\mathrm{g}} + DU_{\mathrm{a}}}{1 + D + \frac{4}{3} D'}, \tag{8}$$

$$I_{\mathrm{d}} = 2{,}33 \cdot 10^{-6} \frac{U_{\mathrm{d}}^{3/2}}{X_{\mathrm{kg}}^2} F_{\text{к}}. \tag{9}$$

Relation (9) is the well-known Childe's law.

Let us apply this law to the equivalent diode:

$$I_{\mathrm{eq}} = 2{,}33 \cdot 10^{-6} \frac{U_{\mathrm{eq}}^{3/2}}{X_{\mathrm{eq}}^2} F_{\text{к}}. \tag{10}$$

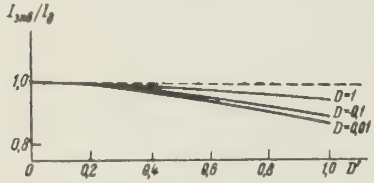

Relative values of space-charge current of triode as calculated by two different methods.

The correctness of one method of equivalence as against the other may be evaluated by means of the relation

$$\frac{I_{\mathrm{eq}}}{I_{\mathrm{d}}} = \frac{U_{\mathrm{eq}}^{3/2} X_{\mathrm{kg}}^2}{U_{\mathrm{d}}^{3/2} X_{\mathrm{eq}}^2}$$

or, using formulas (2), (6) and (7),(2), (6), (7),

$$\frac{I_{\mathrm{eq}}}{I_{\mathrm{d}}} = \frac{\left(1 + \frac{4}{3} \frac{D'}{1+D}\right)^{3/2}}{\left(1 + \frac{D'}{1+D}\right)^2}.$$

It is seen from the figure that for most modern triodes ($D > 0.01$, $D^1 < 0.5$) the divergence of results of calculating the current by the two methods does not exceed several percent.

In the case of a Maxwellian distribution of initial electron velocities $\varkappa_1 \neq 4/3$ and formula (2) becomes somewhat complex, which complicates evaluation of the relative error of methods of calculation in the general from.

In practice, no difference in the values of currents I_d and I_{eq}: is usually detected.

REFERENCES

1. W.R. Ferris, Some characteristics of diodes with oxide-coated cathodes, RCA Rev., 1949, 10, 1, 134.
2. V.S. Lukoshkov, Theoretical fundamentals of calculation of characteristics and parameters of multielectrode vacuum tubes, Candidate's Dissertation, LETI, 1941.
3. L.V. Shubin, Methods of calculating characteristics and parameters of radio tubes, Candidates Dissertation, 1954.
4. F.B. Lewellyn, Inertia of Electrons, translated from 1941 English edition, GTTI, 1946.
5. B.D.H. Tellegen, Physica, 1925, 5, 301.

Submitted to the editors 8 March 1960

NVESTIGATION OF FREQUENCY MULTIPLIER USING THE NONLINEAR CAPACITANCE OF A p-n JUNCTION

V.B. Braginskiy, V.A. Dianova, Ye.R. Mustel'

This report presents the results of an investigation of a microwave frequency multiplier using the nonlinear capacitance of a p-n junction and having a high multiplication factor. Output power is examined as a function of the order of the harmonic, the time constant of the p-n junction of a diode, the input power and fixed diode bias. The amplitude and phase stability of the multiplier are investigated.

Nonlinear active elements as well as nonlinear reactive elements now widely used in the microwave range may serve as the nonlinear element of a frequency multiplier.

If the nonlinear reactive element and associated nonlinear circuits are lossless and the master oscillator is matched only at a frequency f while the load is matched at a frequency nf, it is in principle possible to achieve 100% conversion of power P_f at frequency f to power P_f at frequency nf [1]. At the same time, the conversion losses P_{mf}/P_f of a frequency converter with nonlinear positive resistance in the optimum case may not be less than $1/n^2$ [2, 3].

In recent years a number of works [4, 5, 6] have been devoted to frequency multipliers with the nonlinear capacitance of a p-n junction as the nonlinear reactive element.

Multiplier calculation with consideration of the real diode characteristic in the presence of a large signal presents considerable difficulties and may be performed only by numerical methods for specific cases.

In [5] the efficiency of frequency conversion with a nonlinear resistance (NR diode) and with a nonlinear capacitance (NC diode) for a wideband circuit was compared with the ideal characteristic of diodes and it was shown that the conversion losses of a multiplier with an NC diode increase somewhat less rapidly with increasingly higher order harmonic than the conversion losses of a multiplier with an NR diode.

A double-tuned system was examined in [6] for the small-signal case. The approximate calculations show that with small n, multipliers using a nonlinear capacitance are more efficient than multipliers with a nonlinear resistance. At higher harmonic numbers n the efficiency of multipliers of the first type is lower than that of multipliers of the second type.

In Figure 1, along with theoretical limit values of power-conversion coefficient which may be obtained with an NR diode and NC diode in a tuned system, we present design data from [6]. The value of n at which the multiplier efficiencies are compared (point A in Figure 1) depends on the Q of the nonlinear element and the degree of nonlinearity of the characteristic.

In this report we describe the experimental results of investigation of a frequency multiplier with high multiplication factors (up to $n = 50$). The basic diagram of the multiplier is given in Figure 2. The multiplier is a combination of a 70 ohm coaxial line and a standard coaxial waveguide junction. At a discontinuity there is located a diode 1 whose p-n-junction capacitance is used as the nonlinear element.

Through a fixed attenuator (10-12 db) at the multiplier input there is applied an alternating voltage from an oscillator whose frequency varies from 184 to 600 Mc. The maximum power delivered by the oscillator to the matched load does not exceed 3.5 w.

Coaxial plunger 2 together with the central capacitance of the nonlinear element forms a tank circuit tuned to the frequency of the input signal. Plunger 2 is isolated from the direct component from the outer tube of the coaxial resonator, which is necessary in order to apply fixed bias to the diode.

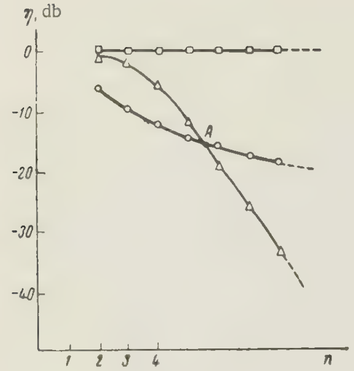

Fig. 1. Conversion losses for: a, ideal NR diode (circles); b, ideal NC diode (squares); c, nonlinear reactance from [6] (triangles).

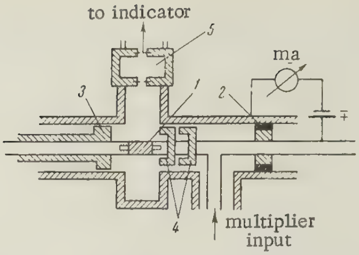

Fig. 2. Basic diagram of multiplier: 1) nonlinear capacitance; 2, 3) coaxial plungers; 4) quarter-wave cups; 5) filter resonator.

The output tank circuit is created by two coaxial plungers 3 and two quarter-wave cups 4, which do not admit the multiplied signal into the input circuit. The output tank circuit is coupled with a reentrant square resonator through an aperture; this resonator serves to filter out the required harmonic.

The Q of the resonator is approximately 200, which provides for attenuation of adjacent harmonics by not less than 20 db. Without the filtering element the adjacent harmonics are five times less than the chosen harmonic.

From the resonator output the signal may be applied to a spectrum analyzer (with special power calibrations) or to a standard wattmeter.

Figure 3 shows the multiplier output power as a function of the harmonic number with a change in input signal frequency (from 184 to 600 Mc), constant frequency of output signal (approximately 9000 Mc) and constant power at the multiplier input. It must be mentioned that the power reaching the diode varied with a change in harmonic. However, this should not have a substantial effect on the relation, since the measurements were performed with sufficient input power for saturation (concerning which see below).

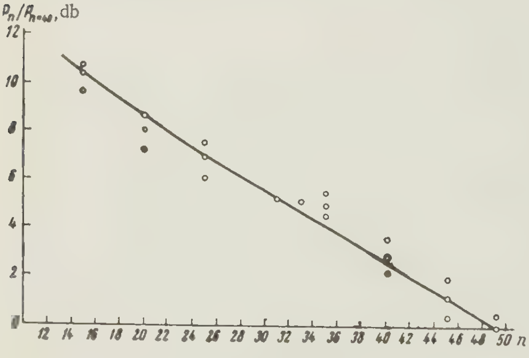

Fig. 3. Multiplier output power as a function of harmonic number.

The ordinate axis in Fig. 3. represents the decibel ratio of output power at the n-th harmonic to the output power at the 49-th harmonic. As is seen from the curve, there occurs a slow drop in output power with the order of the harmonic (approximately 0.3 db per harmonic).

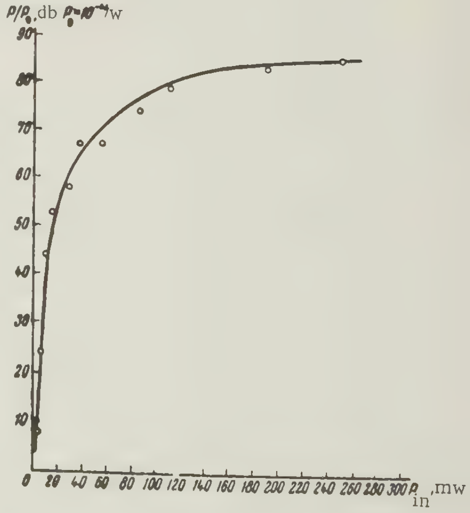

Fig. 4. Output power as a function of multiplier input power.

Figure 4 shows the output power P_{nf} as a function of power P_f applied to the multiplier (n = 36). As is seen from the curve, with P_f = 100-150 mw there occurs a saturation of P_{nf} similar to that observed in [4] at lower multiplication factors. The saturation is associated with creation of an active resistance shunting the capacitance, which arises when the amplitude of the input voltage is greater than the fixed bias or when the doubled amplitude of input voltage is greater than the reverse breakdown voltage. The output power has a clearly defined optimum with a change in fixed bias, blocking the p-n junction of the diode (Fig. 5). With an increase in input power the optimum shifts to the region of large negative bias.

For investigation of phase stability we assemble a setup consisting of two identical multipliers, two unidirectional gates and a measuring line. The signal was applied to the multiplier inputs from a common generator, thereby eliminating signal instability.

A reentrant detector head was used at the same time to check the amplitude stability of one of the multipliers. From the measuring line probe the sum signal from the two multipliers was applied to the detector. In nine hours of continual operation (after a 90 minute warm-up) the amplitude varied by 19 percent. The change in phase shift between multipliers during this same period of time did not exceed 60°.

In investigating the possibility of modulating the output signal, in addition to the fixed bias at the diode, we applied an alternating voltage with a frequency of 10 Mc. Separation of the lines of radiation into several components 10 Mc apart was observed on a spectrum analyzer.

With sufficiently strong modulation and appropriate fixed bias it is possible to redistribute the energy between the central lines and the side components. It is possible to isolate one of the components of the spectrum by using a resonator filter of sufficient Q.

Fig. 6 shows the output power (n = 36) as a function of the time constant of the p-n junction of the diode with approximately identical reverse breakdown voltage (identical saturation power). The figure shows that there is a sharply expressed dependence of the power conversion factor on $\tau = R_S C$.

The maximum observable output power was 2.5 mw (n = 36, $\tau = (R_S C)_{U=-10v} = 0.36 \cdot 10^{-12}$ sec) with an input power of the order of 250 mw.

It is necessary to point out that upon changing multipliers the input power was measured with a wattmeter with matched input. Maximum multiplier power is obtained with a standing-wave ratio of the order of 3.0. This is associated with a shortcoming in multiplier design which does not permit varying the distance between the point of connection of the input cable and the diode.

Thus, upon tuning the input circuit to resonance at the master oscillator frequency, there is a mismatch with the latter and the input power does not exceed 250 mw. This indicates that the conversion loss is not greater than 20 db, which is 11 db better than the minimum conversion loss occurring when using an active nonlinear element with an ideal filtering system at the same harmonic. The resulting power conversion factor and the output power are slightly greater than those obtained in a two-stage multiplier (f_{in} = 218 Mc, f_{out} = 8720 Mc, conversion factor 27 db, output power 2 mw, n = 8·5 = 40) [7].

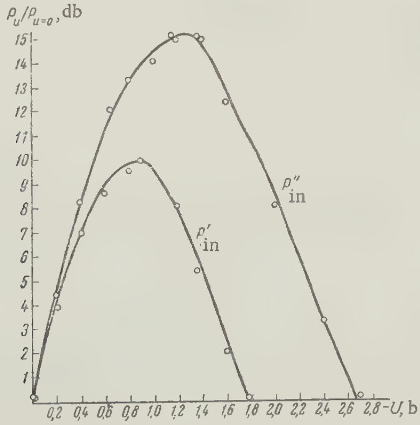

Fig. 5. Output power as a function of fixed bias at diode, $P'_{in} < P''_{in}$.

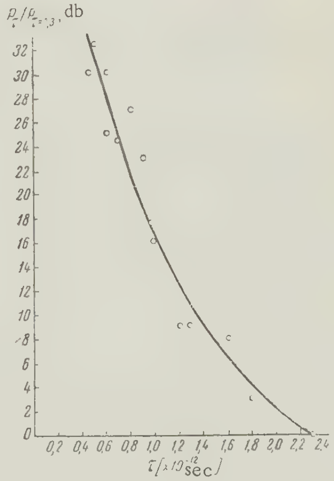

Fig. 6. Output power as a function of time constant of p-n junction.

Such multipliers may be used with success in test equipment and as highly stable local oscillators.

In order to obtain power of the order of 1 mw, it is necessary to use diodes with p-n junction time constant of at least $1 \cdot 10^{-12}$ sec.

In conclusion, the authors wish to thank V.A. Krasilov and V.M. Val'd-Perlov for their assistance in this work.

REFERENCES

1. J.M. Manley, H.E. Rowe. Some general properties of nonlinear elements, Proc. IRE, 1956, 44, 7, 904.
2. C.H. Page. Harmonic generation with ideal rectifiers, Proc. IRE, 1958, 56, 10, 1738.
3. C.H. Page. Frequency conversion with positive nonlinear resistors, J. Res. Nat. Bur. Standards, 1956, 56, 179.
4. Kern, K.N. Chang. Harmonic generation with nonlinear reactances, RCA Rev., 1958, 20, 3, 455.
5. D. Leenov, A. Uhlir, Jr. Generation of harmonics and subharmonics at microwave frequencies with p-n junction diodes, Proc. IRE, 1959, 10, 1724.
6. D.B. Leeson, S. Weinreb. Frequency multiplication with nonlinear capacitors — A circuit analysis, Proc. IRE, 1959, 12, 2076.
7. R. Lowell, M. Kiss. Solid-state microwave power sources using harmonic generation, Proc. IRE, 1960, 7, 1834.

Physics Faculty of the M.V. Lomonosov
Moscow State University
Chair of the Theory of Oscillations

Submitted to the editors
17 November 1960

NONLINEAR NUTATION-TYPE GYROMAGNETIC EFFECTS IN FERRITES*

L.K. Mikhailovskiy, V.P. Makaritshchev, B.P. Pollak and V.A. Fabrikov

We observed experimentally the emergence of natural sinusoidal oscillations of magnetization in a magnetized ferrite sample situation in an IF (30 Mc) tuned circuit and subjected to the action of a transversely polarized microwave field, when the field power exceeded critical value P_{cr}(1-3 watts). A nonlinear region was found to exist in curves of the IF signal power vs. heterodyne power p_h in the mixer circuit at values of p_h, close to P_{cr}. The experimental results are in accord with previously obtained conclusions in the theory of nonlinear gyromagnetic effects connected with nutational oscillations of magnetization in ferrites.

1. STATEMENT OF THE PROBLEM

In a number of papers [1, 2, 3, 4] the effect of mixing two low-power microwave signals was investigated in a magnetized ferrite sample. It was found that the power arising during a mixing of magnetization oscillations at the difference frequency is proportional to the power of each of the interacting microwave signals.

---

*The work was reported at a session of the All-Union, A.S. Popov Scientific-Technical Society of Radio Engineering and Electrocommunication, May 18, 1960.

If P_i, P_s and P_h designate the power of IF (difference) oscillations, signal power and heterodyne power, respectively, then at low values of P_s and P_h there exists a relation between these quantities.

$$P_i = AP_sP_h, \tag{1}$$

where the coefficient of proportionality, A, for the investigated circuits with polycrystalline ferrite samples is of the order of 10^{-3}-10^{-4}/watt, which in the case of heterodyning by klystron, corresponds to a conversion gain ratio of the order of 50 db.

Eq. (1) was first introduced in [1] in an approximation neglecting the inverse action of an IF circuit on the sample. Later in [5] it was shown that under conditions in which the heterodyne power P_h approaches a certain critical value P_{cr}, it is impossible to neglect the field reaction in the calculations. The existence of feedback can lead to the emergence of spontaneous oscillations in the circuit-sample system, if $P_h \geqslant P_{cr}$. The minimum possible value of P_{cr} is inversely proportional to the cube of the ferromagnetic resonant line width ΔH, and for yttrium ferrite single crystals according to calculations it can be rather small (hundreds, tens and even units of a milliwatt).

If the heterodyne power does not exceed P_{cr}, but is close to it, i.e.,

$$P_h \gg (P_{cr} - P_h) > 0$$

then the circuit can be operated as a regenerative amplifier of electromagnetic oscillations excited in the external source circuit. This source, in particular, can be used to create in the sample a microwave signal, the frequency of which is shifted with respect to the heterodyne frequency by an appropriate magnitude [6].

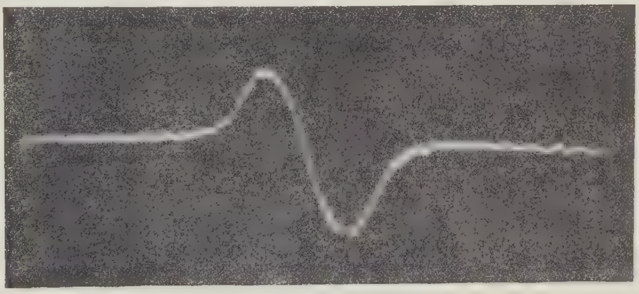

Fig. 1. Oscillogram of the variation of χ''_i of a ferrite sample under the action of a microwave field and of the sinusoidal modulation of the magnetizing field H_0 about the resonant value H_{res}; χ'_i passes from positive values (left-hand side of the figure) through zero at H_0=H_{res} to negative values with a decrease of field H_0 taken from [7].

The amplification is caused by negative impedance in the IF circuit, which arises as a result of the interaction of signals of different frequencies (intermediate and microwave) originating in the ferrite sample via precessing magnetic moments. The dependence of the imaginary part of complex susceptibility $\chi_i = \chi'_i - i\,\chi''_i$, which describes the IF loss f_i, on the magnitude of the static magnetizing field H_0 is illustrated by the oscillogram of Fig. 1, taken from [7]. In the case of H_0 exceeding the field of ferromagnetic resonance H_{res}, $''_i$ is positive which corresponds to absorption of the mean power of an IF signal. When H_0 becomes less than H_{res} however, $'_i$ becomes negative which corresponds to an amplification of the mean power of the IF signal. The oscillogram was recorded on an yttrium ferrite single crystal at a frequency f_i = 8 Mc and a microwave signal power of 5 milliwatts with the aid of a conventional autodyne circuit (IMI-2), applicable for observations of nuclear resonance.

As the heterodyne power approaches the critical value of the conversion gain ratio of a signal, P_i/P_s in the mixer circuit must increase without limit. Eq. (1) must then be generalized to the form

$$P_{\mathrm{i}} = A \frac{P_{\mathrm{s}} P_{\mathrm{h}}}{\left(1 - \frac{P_{\mathrm{h}}}{P_{\mathrm{cr}}}\right)^2} . \tag{2}$$

It is valid only for values $P_h < P_{cr}$. When $P_h = P_{cr}$ the right-hand side of Eq. (2) becomes infinite, corresponding to the advent of natural sinusoidal oscillations in the system, the steady-state amplitude of which can be calculated in a linear approximation with respect to the quantity $(P_h - P_{cr})/P_{cr} > 0$.

The increase in the conversion gain ratio of a ferrite microwave mixer is of great practical significance. The assumed low inherent noise level of ferrite devices makes them a prospect for use in mixer and IF preamplifier circuits. Efficient use of ferrite mixers at microwave frequencies however is possible only if their conversion gain ratio is no worse than in crystal mixers [-(6-8) db].

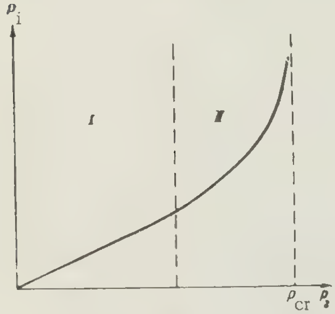

Fig. 2. Theoretical dependence of IF power P_i on heterodyne power P_h at constant signal power P_s:

I — section of linear mixer corresponding to Eq. (1);

II — section of mixer with subsequent IF amplification by the same ferrite sample, Eq. (2).

The nonlinear gyromagnetic properties of ferrites, which provide amplification of IF electromagnetic oscillations and create the possibility of an increase of the conversion gain ratio of ferrite mixers, are connected with emergence of natural nutational oscillations of magnetization in the sample.* The present paper is devoted to an experimental investigation of these effects, theoretically predicted in [5, 6]. The purpose of the investigation was to discover the nonlinear section of the dependence of P_i on P_h in the circuit of two signal microwave mixer (Fig. 2) and the emergence in a ferrite sample placed in an IF tuned circuit, of natural sinusoidal oscillations of magnetization under the action of heterodyne microwave power.

The experiments were carried out in the 3 cm wavelength region, the intermediate frequency was equal to 30 Mc.

2. EXPERIMENTAL EQUIPMENT AND TECHNIQUE OF MEASUREMENT

The investigations were carried out in equipment, a simplified block diagram of which is given in Fig. 3. The microwave signal sources were a (43-I) klystron oscillator, which operates in a pulsed and continuous mode, and a magnetron oscillator operating in the pulsed mode. A ferrite sample with a coil on it was placed in a standard waveguide section at a distance of 6 mm from the narrow waveguide wall. The Q of the tuned circuit formed by the coil shunted by a capacitor equaled 20 at the frequency 30 Mc. The position of the coil turns on the sample was selected in conformity with the maximum IF signal. The static magnetic field was applied parallel to the narrow waveguide wall and corresponded in magnitude to the field of ferromagnetic resonances. The samples were yttrium ferrite single crystals with a ferromagnetic resonance bandwidth of 5-10 oe. The sample shape was almost spherical, and

---

*Nutational oscillation of magnetization is a name for the periodic variation of the angle of uniform precision of magnetic moments of a material around a constant magnetic field H_0 which arises under the action of a transverse microwave magnetic field h.

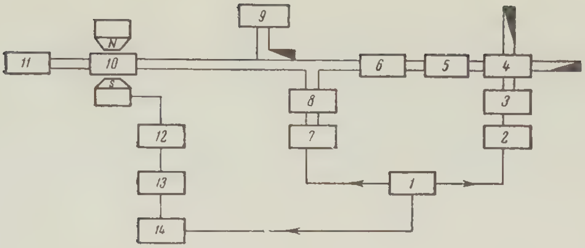

Fig. 3. Block diagram of the equipment:

1 — master pulse generator (synchronizer); 2 — magnetron modulation generator; 3 — magnetron oscillator; 4 — double-T bridge; 5 — cavity resonator, 50-I (disconnected when operating with $\tau = 6$ μsec pulses); 6 — variable attenuator; 7 — klystron oscillator (43-I); 8 — ferrite valve; 9 — microwave power meter; 10 — ferrite mixer; 11 — piston-shorted circuiter or matched load; 12 — 30 Mc preamplifier; 13 — 30 Mc amplifier; 14 — oscilloscope.

its surface was not polished. The signal from the mixer was fed through an IF preamplifier and an IF amplifier to an oscillograph. The total IF signal gain was approximately 10^5. The inherent noise level of the amplifier channel, introduced to the input of the preamplifier was about 5 μv (measured by means of a CG-1). The power supply of the electromagnet and both IF amplifiers was regulated.

The main interferences which had to be avoided in the experiments are the following:

1. Shock perturbation of the circuit containing the ferrite due to a rapid change in the constant component of magnetization of the ferrite in the static field direction which arises under the action of the pulse rise and tail of the heterodyne signal [8].
2. Overheating of the ferrite sample because of thermal scattering of the microwave-field power absorbed by the sample.
3. Direct introduction of the heterodyne modulator pulses into the IF amplifier circuit.

Overheating of the ferrite sample was eliminated during operation of the heterodyne with short-time pulses (1-6 μsec). The effect of shock perturbation and IF amplifier intrusion was reduced by using pulse generator 50-I ($Q = 100,000$) excited by the magnetron oscillator, instead of the magnetron oscillator itself, to directly irradiate the sample.

3. EXPERIMENTAL RESULTS

During the investigation we recorded the IF signal amplitude as a function of heterodyne power for constant microwave signal and the amplitude of natural oscillations originating in the system when $P_h > P_{cr}$ as a function of heterodyne power.* The characteristic curves were taken on the linear region of amplification of both amplifiers. The magnitude of the constant magnetizing field was selected in order to obtain maximum signal on the oscilloscope screen.

Figure 4 presents the dependence of IF power P_i on heterodyne power P_h at a constant microwave power signal level. We applied simultaneously to the sample a signal from the magnetron oscillator through an echo cavity resonator and a signal from the klystron oscillator of length 1 μsec.** Time-retardation of klystron oscillator pulses relative to the magnetron oscillator pulses was chosen, so that their position on an oscilloscope screen would correspond to the average drop of the echo signal from the oscillator. On the experimental curves one may clearly see the nonlinear region which apparently should be ascribed to the superposition of the effect of amplification of the IF signal on the ordinary mixer effect of the two microwave signals. It is impossible to describe the mixer effect in this region by the simple Eq. (1); the generalized Eq. (2) should be used. Curves recorded for cases when $f_S = f_h - \Omega$ and $f_S = f_h + \Omega$ (f_S and f_h are the signal and heterodyne frequencies), do not coincide, the curve for the first case being lower. This effect was not investigated in greater detail.

---

*The measurements were made by V.P. Makarishchev and R.D. Savost'yanova.

**During magnetron operation with pulses of 6 μsec length, the echo cavity resonator was not used. The experimental data obtained in this case confirm the results described below.

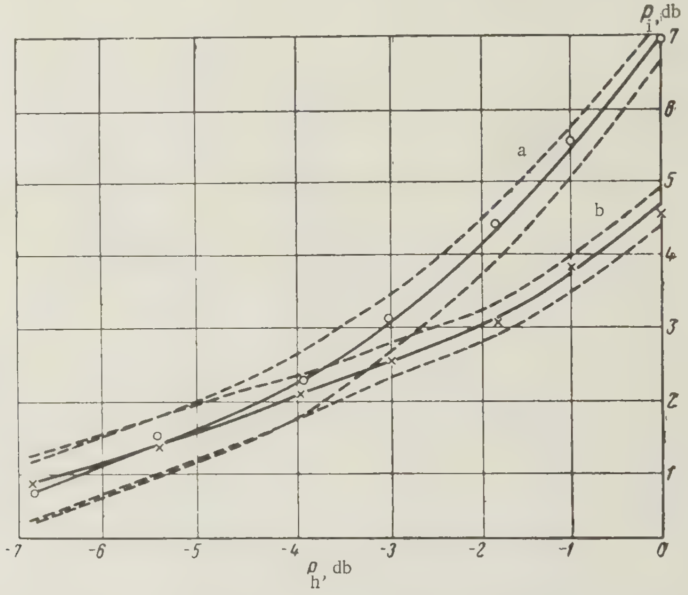

Fig. 4. Experimental dependence of IF power P_i (30 Mc) on heterodyne power P_h at constant signal power P_S: a — f_S = 9400 Mc; f_h = 9370 Mc; b — f_s = 9340 Mc; f_h=9370 Mc.

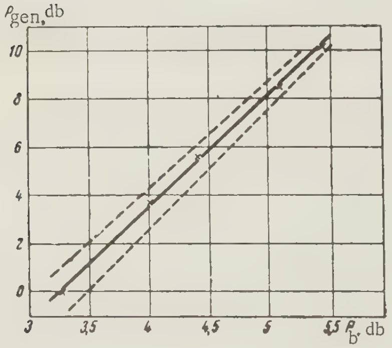

Fig. 5. Experimental dependence of the power of the natural oscillations of magnetization in a ferrite sample at 30 Mc on heterodyne power P_h in the absence of a signal. The dashed curves show the accuracy of measurements.

At heterodyne pulse powers exceeding a certain critical value, close to 1-3 w, we observed a spontaneous emergence of IF oscillations in the circuit. The dependence of the power of these oscillations on heterodyne power, recorded when the klystron oscillator signal was switched on, is shown in Fig. 5.

CONCLUSION

The emergence of natural oscillations of magnetization was observed experimentally in a ferrite sample placed in an IF (30 Mc) tuned circuit, for a transversely polarized microwave field, when the power of this field exceeded a certain value of the order of 1-3 watts. The detected oscillations apparently bears a sinusoidal character and may be identical with relaxation oscillations observed by Weiss in a ferrite sample situated inside a large Q cavity resonator [9].

The existence of a nonlinear region was also discovered on curves of IF signal power versus heterodyne power P_h in a mixer circuit at values of P_h close to P_{cr}. These experimental results are found to accord with the previously obtained conclusions [5, 6] of the theory of nonlinear gyromagnetic effects connected with nutational oscillations of magnetization in ferrites. Final identification of experimentally observed effects become possible after a careful quantitative investigation. The results obtained may be of practical interest in connection with the problem of increasing the efficiency of operation of ferrite mixers of microwave oscillations.

The work was done at the Moscow Energy Institute in the Dept. of Theoretical Radio Engineering. The results were discussed at the K. M. Polivanov seminar, for which the authors take this opportunity to express their sincere gratitude.

REFERENCES

1. V.A. Fabrikov and E.G. Ritter. Nonlinear gyromagnetic properties of ferrites at low microwave power levels, Izvestiya, AN SSSR, 1959, 23, 3, 380.
2. L. Lewin. The efficiency of a ferrite as a microwave mixer, Proc. IEE, 1959, 106, part C, 10, 153.
3. A.L. Mikaelyan and V. Yo. Anton'yants. Microwave mixers using ferrites, Radiotekhnika i Elektronika, 1960, 5, 1, 90.
4. L.K. Mikhailovskiy, B.P. Pollak and V.F. Balakov. Conversion of microwave electromagnetic oscillations in ferrites, Trudy, Third All-Union Conference on Ferrites, Minsk, 1959.
5. V.A. Fabrikov. Conditions of the emergence of natural oscillations of magnetization in a gyromagnetic medium, Radiotekhnika i Elektronika, 1960, 5, 1, 117.
6. V.A. Fabrikov. Efficiency of operation of ferrite elements as microwave mixers in detection circuits, Trudy, Third All-Union Conference on Ferrites, Minsk, 1959.
7. V.A. Fabrikov, V.I. Kozlov, V.T. Kadyeyev and V.D. Kudryavtsev. Experimental investigation on yttrium ferrite single crystals of effect related to nutational oscillations of magnetization of a material under the conditions of ferromagnetic resonance. Theses of reports from the conference on ferromagnetism and antiferromagnetism, Leningrad, May 1961, Izd. AN USSR, 1961.
8. N. Bloembergen, S. Wang. Relaxation effects in para- and ferromagnetic resonance, Phys. Rev., 1954, 93, 1, 72.
9. M.T. Weiss. Microwaves and low-frequency oscillation due to resonance instabilities in ferrites, Phys. Rev. Letters, 1958, 1, 7, 239.

Submitted to editors, 4 July 1960.

PHENOMENA OF MUTUAL COUPLING OF CAVITY RESONATOR AND FERRITE

A. L. Mikaelyan, V. Ya. Anton'yants and Yu. G. Turkov

We investigated phenomena in a cavity resonator with a small ferrite sample. It is shown that the cavity resonator and the magnetized ferrite placed in it form a coupled system analogous to two coupled circuits. We mention cases in which it is necessary to consider these phenomena and we briefly examine several of their practical applications.

INTRODUCTION

In microwave engineering, systems consisting of a cavity resonator with a magnetized ferrite sample are used very frequently. Such systems are employed in ferrite amplifiers, for magnetic retuning of the cavity resonator frequency for measurements of ferrite parameters and other purposes.

In calculations of these systems one usually assumes that the effect of a ferrite reduces to merely changes in the natural frequency and in the Q of an unfilled cavity resonator. Such an assumption is found to be valid not only when the frequency of ferromagnetic resonance differs considerably from the natural frequency of the unfilled cavity resonator, but also if the ferrite possesses appreciable magnetic losses. If these conditions are not fulfilled, however, phenomena of great practical interest occur. It is found that in this case a cavity resonator containing a ferrite behaves like a system of coupled circuits. One of these circuits is the ferrite, in which any type of magnetic oscillations is excited, and the other is the cavity resonator, also excited at one of its natural oscillations. The most interesting phenomena occur in a region where the natural oscillation frequencies of the magnetized ferrite are close to those of the unfilled cavity resonator. An analogous effect of mutual coupling is observed also in acoustical resonant systems (see, for example, [1]).

In the present paper we cite the results of theoretical and experimental studies of the phenomena in a cavity resonator with a magnetic ferrite sample. It is shown that these phenomena must be accounted for when measuring ferrite parameters. We briefly examine several practical applications.

1. DERIVATION OF THE FORMULA

Calculation of the mutual coupling of a cavity resonator and a ferrite can be made by the method of quasi-static approximation, wherein one should consider the frequency dependence of the components of the magnetic permeability tensor of a ferrite.

Let us start with an expression for the natural frequency of cavity resonator and ferrite, written in the following manner:

$$\frac{\omega - \omega_p}{\omega_p} = -\frac{\int\limits_{V_f} \mu_0 \vec{M}\vec{H}_p^* dv + \int\limits_{V_f} (\varepsilon - \varepsilon_0)\vec{E}\vec{E}_p^* dv}{\int\limits_{V_p} (\mu_0 \vec{H}\vec{H}_p^* + \varepsilon_0 \vec{E}\vec{E}_p^*)\, dv}, \qquad (1)$$

where ω_p is the natural frequency of the hollow cavity resonator; $\vec{H}_p$, $\vec{E}_p$ are the magnetic and electric fields in the hollow cavity resonator; $\vec{H}$, $\vec{E}$ are the corresponding fields in the cavity resonator perturbed by a ferrite sample; M is the magnetization of the ferrite; ϵ is the dielectric constant of the dielectric; V_f and V_p are the volumes of the ferrite and cavity resonator respectively.

If the sample is sufficiently small, one may assume that its introduction into a region of the cavity resonator not occupied by a ferrite, does not distort the field. However, the field inside the ferrite and its magnetization may be found from a solution of the static problem which is equivalent to taking into account the demagnetizing-shape factors.

For samples having the shape of an ellipsoid of rotation with symmetry axis parallel to the z-axis, the transverse components of magnetization M are related to the components of the external variable magnetic field H_p in the following manner:

$$M_x = \frac{\chi^e}{\mu_0} H_{px} - j \frac{k^e}{\mu_0} H_{py},$$
$$M_y = j \frac{k^e}{\mu_0} H_{px} + \frac{\chi^e}{\mu_0} H_{py}, \tag{2}$$

where χ^e and k^e, components of the external susceptibility tensor of a ferrite, have the form

$$\frac{\chi^e}{\mu_0} = \frac{\omega_f \omega_M}{\omega_f^2 - \omega^2}, \quad \frac{k^e}{\mu_0} = - \frac{\omega \omega_M}{\omega_f^2 - \omega^2}. \tag{3}$$

Here new notation is introduced:

$$\omega_M = \mu_0 \gamma M_0; \quad \omega_f = \omega_0 - (N_z - N)\, \omega_M; \quad \omega_0 = \mu_0 \gamma H_0; \tag{4}$$

ω_f is the frequency of ferromagnetic resonance, i.e., the natural frequency of a lower type oscillation in the ferrite (uniform precession); H_0, M_0 are the external superimposed magnetizing field and magnetization of the sample (along the z-axis); N_z, N are demagnetizing factors in the z-axis direction and perpendicular to the plane, respectively. Using (2) and (3), we obtain

$$\int\limits_{V_f} \mu_0 \vec{M} \vec{H}_p^* dv = \int\limits_{V_f} \mu_0 \frac{\omega_f \omega_M}{\omega_f^2 - \omega^2} \Big[|H_{px}|^2 + |H_{py}|^2 +$$
$$+ j \frac{\omega}{\omega_f} (H_{py} H_{px}^* - H_{px} H_{py}^*) \Big] dv. \tag{5}$$

Since the frequencies of interest to us are close to the natural frequency of the cavity resonator, at which the properties of the system have a strong frequency dependence, hereafter we will not consider the weak frequency dependence in expressions for the field of a hollow cavity resonator which does not have a resonant character, putting $\omega \simeq \omega_p$.

In addition, for simplicity, we will not consider the influence of dielectric properties of the ferrite, setting $\epsilon = \epsilon_0$. The character of the coupling does not change in this case.

Equation (1) takes the form

$$\frac{\omega - \omega_p}{\omega_f} = - \frac{\omega_M \omega_f}{\omega_f^2 - \omega^2} \frac{I_f}{I_p}, \tag{6}$$

where

$$I_f = \int\limits_{V_f} \mu_0 [|H_{px}|^2 + |H_{py}|^2 + j (H_{py} H_{px}^* - H_{px} H_{py})]\, dv;$$
$$I_p = \int\limits_{V_p} (\mu_0 \vec{H} \vec{H}_p^* + \varepsilon_0 \vec{E} \vec{E}_p^*)\, dv. \tag{7}$$

Assuming that

$$\omega_f^2 - \omega^2 \simeq (\omega_f - \omega)\, 2\omega_f,$$

we obtain from (6)

$$(\omega - \omega_p)(\omega - \omega_f) = \frac{1}{2} \omega_p \omega_M \frac{I_\Phi}{I_p}. \tag{8}$$

In the limiting case when $V_f \to 0$, Equation (8) decomposes into two independent equations $\omega - \omega_p = 0$, $\omega - \omega_f = 0$. The first gives the natural frequency of the hollow cavity resonator, but the second is a well-known expression of Kittel for the frequency of uniform precession in a ferrite spheroid, located in free space. For a sphere of finite dimensions the oscillations in a ferrite and in a cavity no longer are independent. According to their character they are similar to oscillations in coupled circuits.

The solution of Eq. (8) has the form

$$\omega_{1,2} = \frac{1}{2} \left\{ \omega_p + \omega_f \pm \sqrt{(\omega_p - \omega_f)^2 + 2\omega_p \omega_M \frac{I_f}{I_p}} \right\}. \tag{9}$$

Thus, for the frequency of the cavity resonator with a ferrite we obtained two different solutions, determined by the dimensions of the ferrite sample and cavity resonator with the ferrite situated in the cavity resonator, as well as the magnitude of the magnetizing field. This means that the system under consideration close to each resonator type is characterized by two natural frequencies. The corresponding oscillations are no longer pure resonator types of uniform precession, but represent mixed ferrite-cavity resonator oscillation. It should be noted that at no values of the magnetizing field (if losses are absent) do we observe coincidence of the indicated frequencies.

In order to take into account the losses, we set

$$\begin{gathered} \omega = \omega' + j\omega'', \\ \omega_f = \omega_f' + j\omega_f'' = \omega_0 - (N_z - N)\,\omega_M + j\mu_0\gamma\Delta H, \\ \omega_p = \omega_p' + j\omega_p'' = \omega_p' + j\frac{\omega_p'}{2Q}, \end{gathered} \tag{10}$$

where Q is the quality of the hollow cavity resonator and ΔH is the half-width of the resonance curve for the ferrite.

Separating (9) into real and imaginary parts and assuming the losses in the system are sufficiently small, we obtain the basic calculated formulae which determine the complex natural frequencies of the cavity resonator with a ferrite:

$$\begin{gathered} \omega_{1,2}' \simeq \frac{1}{2}\left\{\omega_p' + \omega_f' \pm \sqrt{(\omega_p' - \omega_f')^2 + 2\omega_p'\omega_M \frac{I_f}{I_p}}\right\}, \\ .\ \omega_{1,2}'' \simeq \frac{1}{2}\left\{\omega_p'' + \omega_f'' \pm \frac{(\omega_p'' - \omega_f'')(\omega_p' - \omega_f')}{\sqrt{(\omega_p' - \omega_f')^2 + 2\omega_p'\omega_M \frac{I_f}{I_p}}}\right\}. \end{gathered} \tag{11}$$

2. RECTANGULAR CAVITY RESONATOR WITH A FERRITE SPHERE

The relations obtained are used below for a calculation of the rectangular cavity resonator with H_{mno}-type oscillations, containing a magnetized ferrite sphere (Figure 1).

Such a system is often used in practice and is most convenient for an experimental check of the theoretical results.

The structure of an H_{mno}-type oscillatory field in a rectangular resonator without a ferrite is determined by the expressions

$$E_{pz} = \sin k_{0x}x \sin k_{0y}y,$$

$$H_{px} = j\frac{k_{0y}}{\omega_0\mu_0}\sin k_{0x}x \cos k_{0y}y,$$

$$H_{py} = -j\frac{k_{0x}}{\omega_0\mu_0}\cos k_{0x}x \sin k_{\theta y}y,$$

where

$$k_{0x} = \frac{m\pi}{a}; \qquad k_{0y} = \frac{n\pi}{l};$$

$$k_{0x}^2 + k_{0y}^2 = k_0^2 = \omega^2\varepsilon_0\mu_0;$$

a and l are dimensions of the cavity resonator, shown in Figure 1. For small ferrite samples, which weakly excite the field structure in a cavity resonator, one may assume

$$I_p = \int\limits_{V_p} (\mu_0\vec{H}\vec{H}_p^* + \varepsilon_0\vec{E}\vec{E}_p^*)\,dv \simeq \int\limits_{V_p} (\mu_0\vec{H}_p\vec{H}_p^* + \varepsilon_0\vec{E}_p\vec{E}_p^*)\,dv = 2\varepsilon_0\int\limits_{V_p} |\vec{E}_p|^2\,dv = 2\mu_0\int\limits_{V_p} |\vec{H}_p|^2\,dv. \tag{12}$$

In our case

$$\begin{gathered} I_p = \frac{1}{2}\varepsilon_0 abl = \frac{1}{2}\varepsilon_0 V_p, \\ I_\Phi = \frac{V_f\varepsilon_0}{k_0^2}(k_{0y}^2 \sin^2 k_{0x}x \cos^2 k_{0y}y + k_{0x}^2 \cos^2 k_{0x}x \sin^2 k_{0_\mu}y). \end{gathered} \tag{13}$$

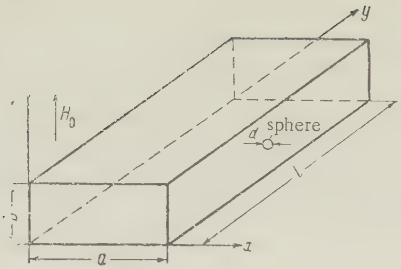

Figure 1. Rectangular cavity resonator with a ferrite sphere

Equations (11) thus take the form

$$\omega'_{1,2} = \frac{1}{2}\left\{\omega'_p + \omega_0 \pm \sqrt{(\omega'_p - \omega_0)^2 + 4\frac{V_f}{V_p}\,\omega_M\omega'_p T(x, y)}\right\},$$
$$\omega''_{1,2} = \frac{1}{2}\left\{\omega''_p + \omega''_f \pm \frac{(\omega''_p - \omega''_f)(\omega'_p - \omega_0)}{\sqrt{(\omega'_p + \omega_0)^2 + 4\frac{V_f}{V_p}\,\omega_M\omega'_p T(x, y)}}\right\}, \tag{14}$$

where

$$T(x, y) = \frac{k_{0y}^2}{k_0^2}\sin^2 k_{0x}x\cos^2 k_{0y}y + \frac{k_{0x}^2}{k_0^2}\cos^2 k_{0x}x\sin^2 k_{0y}y. \tag{15}$$

The dependence of the natural frequencies of the system calculated from Eq. (14) is given in Figure 2 (type H_{160} cavity oscillation, the sphere is situated at the point x = a/2, y = l/2. As may be seen, it is analogous to the well-known Wien graph in radio engineering. Thus, the magnitude of a magnetizing field plays the role of mistuning between the circuits, but the coupling constant is determined by the dimensions of the ferrite sample and its location in the cavity resonator. As the magnitude of the constant magnetic field approaches the value $H_{0p} = \omega_p/\mu_0\gamma$ a transition, as well as an inverse transition of the cavity type oscillations, occurs in the ferrite. The magnitude of H_{0p} represents the constant magnetic field corresponding to the ferromagnetic resonance in the ferrite sphere, at the frequency ω_p. The experimental data given in Figure 2 in the form of individual points are in good agreement with the theoretical results. The greatest discrepancies lie within the limits of the errors of measurement.

Damping of the coupled system $\omega''_{1,2}$ or its equivalent, the half-width of the resonance curves, $\Delta\omega_{1,2} = \omega''_{1,2}$, also changes in a corresponding manner (Figure 3). In proportion to the duration of the cavity resonator oscillation the half-width of its resonance curves changes gradually from $\Delta\omega = \omega''_p = \omega'_p/2Q$ to the value $\Delta\omega = \omega''_f = \mu_0\gamma\Delta H$, corresponding to the half-width of the uniform precession of a ferrite sample (Curve 1). The half-width of the second oscillation curve

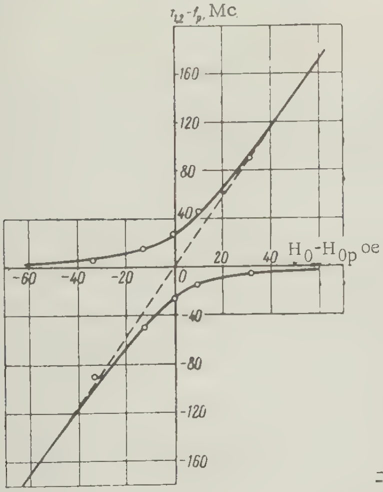

Figure 2

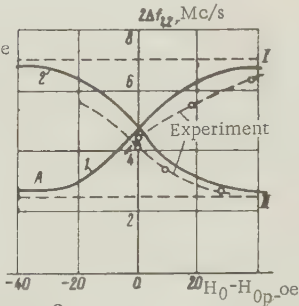

Figure 3

Figure 2. Dependence of the natural frequencies of the coupled system on the magnetizing field (a = 23 mm, b = 10 mm, l = 138 mm, d = 1.24 mm, $4\pi M_0$ = 1700 cps).

Figure 3. Dependence of the sidth of the resonance curves $2\Delta f_{12}$ of the coupled system on the magnetizing field ($2\Delta H$ = 2.5 oe, Q = 3650): I — width of the curve for a ferrite sphere; II — width of the curve for a hollow cavity resonator.

changes from $\Delta\omega = \omega_f''$ to $\Delta\omega = \omega_p''$ (Curve 2). The experimental points on branch A of Curve 1 were not successfully recorded, because at these fields the cavity resonator oscillation, in addition to retuning with uniform precession also interacts with one of the higher mode oscillations of the ferrite sample.

It should be pointed out that the width of the resonance curve of the ferrite cavity resonator coupled system in the steady magnetic field $2\delta H$ differs from the width of the resonance curve of a ferrite $2\Delta H$ which is usually used for the magnetic loss characteristics of a ferrite located in empty space or in a waveguide. It is demonstrated below that the magnitude $2\delta H$ does not remain constant but depends significantly on the operating frequency and parameters of the coupled system.

3. RESONANCE CURVE OF THE COUPLED SYSTEM IN A CONSTANT FIELD

Investigation of a system consisting of a cavity resonator and a ferrite can be simplified if one can use an analogy between this system and the usual coupled circuits which are well investigated in radio engineering (Figure 4). First of all, for a ferrite-cavity resonator it is necessary to introduce the concept of coupling constant. This can be done by comparing the expression for the minimum spread of the coupling frequency in the system under consideration and in the coupled circuits. As follows from (11), the minimum frequency separation equals

$$\omega_1' - \omega_2' = \sqrt{2\omega_p'\omega_M \frac{I_f}{I_p}}. \qquad (16)$$

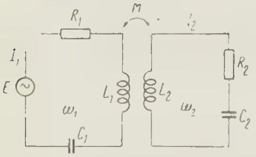

Figure 4. System of coupled circuits.

The corresponding expression for the coupled circuits (for weak coupling) has the form

$$\omega_1' - \omega_2' = K\omega_k', \qquad (17)$$

where K is the coupled constant between the circuits; ω_k' is the natural frequency of each of the circuits.

Comparing (16) and (17), we obtain the expression for the coupling constant of the ferrite-cavity resonator system:

$$K = \sqrt{2\frac{\omega_M}{\omega_p'}\frac{I_f}{I_p}}. \qquad (18)$$

The expressions obtained below for the frequency and attenuation are valid under the condition that the losses in the ferrite and cavity resonator are small. It is well-known from the theory of coupled circuits, however, that the losses can significantly influence the characteristics of the system. Thus, for example, if the damping ratio of the second circuit (Figure 4)

$$d_2 > K, \qquad (19)$$

then, when the natural frequencies of both circuits are equal, the system has a single natural frequency. Carrying out this result to a ferrite-cavity resonator system and identifying the ferrite sample and second circuit, one may find the critical losses in a ferrite, in which there is no retuning of the ferrite and cavity resonator oscillations. Assuming that the damping ratio of the ferrite is

$$d_f = \frac{2\Delta\omega_0}{\omega_f'} = \frac{2\mu_0\gamma\Delta H}{\omega_f'}, \qquad (20)$$

we obtain the critical value

$$\Delta\omega_{0\,cr} = \sqrt{\frac{\omega_M\omega_p'}{2}\frac{I_\Phi}{I_p}}. \qquad (21)$$

Using the analogy with coupled circuits, we now find an expression for the half-width of the resonance curve of the ferrite-cavity system in a constant magnetic field. For two coupled circuits (Figure 4) one can easily obtain an equation of the resonance curve in regard to the tuning of one of the circuits. Thus, for example, the dependence of current I_2 in the second circuit on the mistuning of this circuit can be obtained, using known relations (see, for example, [4])

$$\frac{I_2}{I_{2\max}} = \sqrt{\frac{(K^2+d_1 d_2)^2 + p^2 d_2^2 - \dfrac{K^4 p^2}{p^2+d_1^2}}{(K^2+d_1 d_2)^2 + p^2 d_2^2 - 2K^2 p\xi + (p^2+d_1^2)\,\xi^2}}, \tag{22}$$

where

$$K^2 = \frac{M^2}{L_1 L_2};\ d_1 = \frac{R_1}{\omega_1 L_1};\ d_2 = \frac{R_2}{\omega_2 L_2};\ p = 1 - \frac{\omega_1^2}{\omega^2};\ \xi = 1 - \frac{\omega_2^2}{\omega^2}. \tag{23}$$

The width of the curve, described by Equation (22) at the level 0.7, equals

$$2\Delta\omega_2 \simeq \omega \sqrt{\frac{d_2^2 p^2}{p^2+d_1^2} + \frac{K^2 d_1^2}{(p^2+d_1^2)^2}}. \tag{24}$$

When derivation of this formula it is assumed that

$$K \gg d_1 \sim d_2 \text{ and } \omega \simeq \omega_1 \simeq \omega_2. \tag{25}$$

The expression for the half-width of the resonance curve of the ferrite-cavity resonator at a constant magnetic field δH can be obtained Eq. (24), replacing the natural frequency of the second circuit ω_2 by the natural frequency of the ferrite ω_f. Then $2\Delta\omega_f = 2\mu_0\gamma\delta H$ will correspond to the magnitude $2\Delta\omega_2$. In addition, instead of the magnitudes K_2 and d_2 one should use the corresponding magnitudes determined by Eqs. (18) and (20). After simple transformations we obtain

$$\delta H \simeq \sqrt{\frac{\Delta H^2}{1+\alpha} + \left(\frac{\alpha M_0 \frac{I_f}{I_p} Q}{1+\alpha}\right)^2},$$

where

$$\alpha = \frac{\omega^2}{4Q^2(\omega-\omega_p)^2};\ Q = \frac{1}{d_1}. \tag{26}$$

As we see, the width of the resonance curves change significantly with variation of the oscillator frequency, reaching a maximum when $\omega = \omega_p$:

$$\delta H_{\max} = M_0 Q \frac{I_f}{I_p}. \tag{27}$$

If the resonance indicator is connected, not with the ferrite, but with the cavity resonator (which usually occurs in practice), then the observable resonance curves of the coupled system will be determined by the current I_1, which corresponds to the field in the cavity resonator but not by the current I_2 which determines the magnetization of the ferrite. Using Eq. (23), an expression can be obtained for the modulus of current I_1 [4]:

$$|I_1| = \frac{\dfrac{E}{\omega L_1}\sqrt{\xi^2+d_2^2}}{\sqrt{\xi^2(p^2+d_1^2) - \xi 2k^2 p + p^2 d_2^2 + (K^2+d_1 d_2)^2}}. \tag{28}$$

Differentiating (28) with respect to ξ, we obtain the value of ξ corresponding to the maximum and minimum corrent I_1:

$$\xi = \frac{K^2+2d_1 d_2}{2p} \pm \sqrt{\frac{(K^2+2d_1 d_2)^2}{4p^2} + d_2^2}. \tag{29}$$

The plus sign corresponds to the maximum current, the minus sign to the minimum. The equation of the resonance curve of the coupled system

$$\frac{|I_1|}{|I_{1\max}|} = f(\xi) \tag{30}$$

is obtained by substituting $\xi_{\max}$ into (28).

Several resonance curves calculated from Eq. (30) are given in Figure 5. With a change of oscillator frequency not only the width of the resonance curves but also their shape change.

At sufficiently large mistuning ($p \simeq 10\, d_1$) the resonance curve is almost symmetrical and has a shallow minimum. With a decrease of p, the asymmetry of the resonance curve increases

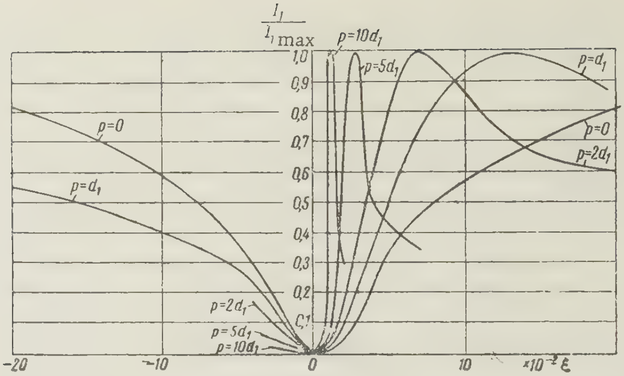

Figure 5. Resonance curves of the ferrite-cavity resonator coupled system with respect to the field ($K = 0.6 \cdot 10^{-2}$, $d_1 = 2.7 \cdot 10^{-4}$, $d_2 = 0$).

and the minimum becomes clearly expressed, the maximum of current I_1 being shifted to the region of large mistuning ξ. When $p = 0$, i.e., when the oscillator frequency ω coincides with the cavity resonator frequency ω_p, the resonance curve is completely "overtuned" and has only a minimum at $\xi = 0$. It can be shown that the width of this curve just as for current I_2 is determined by Eq. (27).

CONCLUSION

This investigation enables us to draw the following conclusions. The cavity resonator and the small ferrite sample placed in it is a coupled system has two natural frequencies—coupling frequencies. The degree of coupling is determined mainly by the ratio of the volumes of the ferrite and cavity resonator as well as the position of the ferrite sample in the cavity resonator. Since the cavity has a multitude of natural frequencies ω_{pn}, then the described phenomena will be observed close to each of these frequencies, the degree of coupling between the ferrite and cavity resonator being determined by the field structure of the corresponding frequency and type of vibration. This is shown in Figure 6, where we were limited to two natural frequencies.

Not only uniform precession, but also other magnetostatic types of oscillations are found to be coupled with natural cavity resonator oscillation. Figure 7 illustrates coupling of the cavity resonator with one of the higher types of oscillations of the ferrite sample. A calculation of these phenomena can also be carried out with the aid of Eq. (1). Thus, instead of Eqs. (2) one should use certain expressions [2] connecting the magnetization and field for the type of oscillation being considered in a ferrite.

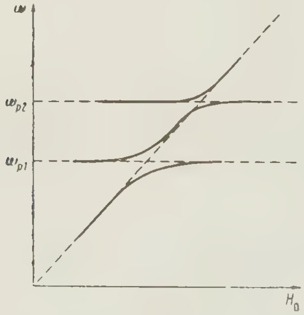

Figure 6. Coupling of two types of oscillations in a cavity resonator with uniform precession.

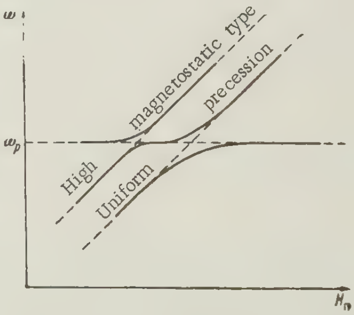

Figure 7. Coupling of two types of oscillations in a ferrite with one of the types of cavity oscillations.

The resonance curve of the ferrite-cavity resonator system in a constant magnetic field may differ strongly from the resonance curve of a ferrite sample located in free space. Its width $2\delta H$ depends not only on the magnetic losses of ferrite but also on the other parameters of the system. Therefore, when measuring ΔH of a ferrite in a cavity resonator, one should observe certain precautions. If the coupling between the ferrite and cavity resonator is more critical, the measurements should be made at frequencies far from the natural frequency of the cavity resonator. In such cases it is more expedient to make measurements in the waveguide.

For a calculation of the ferrite-cavity resonator coupled systems one may also use the eigenfunction method [3], which leads to the same results and a method also used in the present work—the method of small perturbations.

Besides the interaction between a ferrite sample and a cavity resonator mutual coupling of two (or several) closely placed ferrite samples is possible. This is also easily observed experimentally. Moreover, coupling phenomena can be observed when several ferrite samples are placed in the cavity resonator. Thus, the number of resonance peaks of the coupled circuit increases according to the number of samples.

The phenomena considered in the present paper can be used in practice to create a different type of microwave system. The feasibility of efficient frequency retuning of the cavity resonator is perfectly obvious. It is apparent from Figure 2 that the frequency dependence of the magnetizing field is most pronounced in the region where the frequency of ferromagnetic resonance is close to the natural frequency of the cavity resonator. This enables us to obtain appreciable changes of the resonance frequencies with the aid of comparatively small changes of the magnetic field.

In contrast with the known method of retuning of frequency of cavity resonators with the aid of a ferrite, when the small field region is used and it is inexpedient to operate close to the ferromagnetic resonance because of the appreciable decrease of cavity resonator Q, the method we are considering enables us to obtain efficient retuning of the frequency which is not accompanied by an appreciable variation of losses, particularly if we chose $\omega_f'' = \omega_p''$ (see Eq. (14) and Figure 3).

The ferrite-cavity resonator coupled system can be used also as a multifrequency retunable filter. The number of operating frequencies of such a filter depends on the number of ferrite samples placed in the resonator. Small increases of the field, necessary for tuning the natural frequency, enable us to use a coupled system to create fast-acting switches or circuit breakers. Other applications of the properties of a ferrite-cavity resonator coupled system are possible.

The authors express their gratitude to A. A. Pistol'kors for his invaluable remarks.

REFERENCES

1. F. M. Morse, H. Feshbach, Methods of Theoretical Physics, Vol. 2, p. 442 [Russian transl.], IL, 1960.
2. P. C. Fletcher, R. O. Bell, Ferrimagnetic resonance modes in spheres, J. Appl. Phys., 1959, 30, 5, 687.
3. A. L. Mikaelyan, Nonlinear theory of ferrite oscillators, Radiotekhnika i Elektronika 1960, 5, 1, 46.
4. B. P. Aseyev, Fundamentals of Radio Engineering, Svyaz'izdat, 1947.

Submitted to editors 26 July 1960

CALCULATION OF THE POLARIZATION OF AN ALTERNATING MAGNETIC FIELD CORRESPONDING TO EXTREME TRANSITION PROBABILITIES IN ELECTRON PARAMAGNETIC RESONANCE

M. I. Rodak

For electron paramagnetic resonance in a $(K_3(CoCr)(CN)_6$ crystal containing two magnetic complexes, we calculated the alternating magnetic field polarization (both linearly and ellipsoidally polarized), which ensures extremes of the induced transition probability.

INTRODUCTION

As is known, in electron paramagnetic resonance experiments (EPR) it is essential to choose correctly the alternating magnetic field polarization, which determines, to a large extent, the induced transition probability P_{mn} of transition mn proportional to the magnitude $|\vec{h}^*\vec{S}|^2$(see, for example, [1]):

$$P_{mn} \sim |\vec{h}^* \vec{S}|^2 = (h_x^* S_x + h_y^* S_y + h_z^* S_z)(h_x S_x^* + h_y S_y^* + h_z S_z^*), \tag{1}$$

where $\vec{h}$ is a unit complex vector, the components of which are complex directional consines of the inducing magnetic field $\vec{H}(t)$ of amplitude $\vec{H}(t)$ of amplitude $\vec{H}_1$ and frequency ω

$$\vec{H}(t) = \mathrm{Re}\,[H_1 \vec{h} e^{-i\omega t}].$$

In this case $|\vec{h}|^2 = \Sigma h^*_j h_j = 1$, $\vec{h} = \vec{h}_1 + i\vec{h}_2$, $h_j = h_{1j} + ih_{2j}$, $j = x, y, z$, $\vec{h}_1, \vec{h}_2, h_{1j}, h_{2j}$ are real.

Let us remember that a complex $\vec{h}$ corresponds to ellipsoidal polarization of field H(t): the imaginary part lags the real part by a phase angle of $\pi/2$, and the field ellipse circulates in a direction from $\vec{h}_1$ to $\vec{h}_2$; S_{mn} is also a complex vector, the components of which S_x, S_y, S_z are matrix elements of operators of the spin components for the mn transition; in the general case they are complex; $S_j = S_{1j} + iS_{2j}$, $j = x, y, z$. The vector $\vec{S}_{mn}$ and the corresponding ellipse will, henceforth, for brevity, be called, respectively, the "vector spin" and "ellipsoidal spin", omitting the quotes and notation mn in $\vec{S}$.

Thus, the transition probability P_{mn} is proportional to the square modulus of the scalar product of the two complex vectors $\vec{h}$ and $\vec{S}_2$ the extremal properties of which are known [2] and easily formulated in geometrical language. Actually the modulus of the scalar product of a given complex vector $\vec{S}$ and an arbitrary unit complex vector h reaches a maximum, when $\vec{h}$ and $\vec{s}$ are collinear, i.e., both the correspondings ellipses are similar, are identically orientated and circulate in a single direction. Thus,

$$|\vec{h}^*\vec{S}|^2 = |S_x|^2 + |S_y|^2 + |S_z|^2 = S_1^2 + S_2^2,$$

where S_1 and S_2 are the length of the principal semiaxes of the spin ellipsoid. The modulus $|\vec{h}^*\vec{S}|$ reaches minimum (zero), when $\vec{h}$ and $\vec{S}$ are orthogonal, i.e., either:

a) both ellipses are similar, lie in a single plane, but are turned 90° with respect to one another and rotate in opposite direction;

b) the field ellipse degenerates into a straight line perpendicular to the plane of the spin ellipse;

c) $\vec{h}$ represents a linear combination of the vectors described in a) and b).

If we confine ourselves to linearly polarized fields, $|\vec{h}^*\vec{S}|^2$ has extremum values $\bar{\lambda}_1$, $\bar{\lambda}_1$ and $\bar{\lambda}_3$ at orientations $\vec{h}$ in three mutually perpendicular directions-from two principal axes of the spin ellipse and one perpendicular to it; thus $\bar{\lambda}_1 = S_1^2$, $\bar{\lambda}_2 = S_2^2$, $\bar{\lambda}_3 = 0$.

So, the problem of selection of polarization of the alternating magnetic field (unit vector $\vec{h}$ or field ellipse), which makes the probability of the transition under consideration a maximum or zero, leads to a determination of the spin ellipse, i.e., to calculation of the associated transition * of the triplet of matrix elements S_x, S_y, S_z. Thus, we are concerned with crystals, whose unit cell contain only one magnetic group. If, however, the crystal contains several mismatching magnetic groups which correspond generally speaking to different complex vectors $\vec{S}$ (different spin ellipses), the subject of extremal values of the transition probability for the crystal as a whole needs addition consideration.

1. ARRANGEMENT OF THE SPIN ELLIPSES FOR SEVERAL PARTICULAR ORIENTATIONS OF THE STATIC MAGNETIC FIELD.

Let us first point out that for several particular directions of the static magnetic field $\vec{H}_0$ one may predict the arrangement of the spin ellipses, without calculating the matrix elements S_x, S_y, S_z. These directions are connected with the principal axes of magnetic groups [3] (or, in short, with the magnetic axes) x, y, z in which the original system spin Hamiltonian $\hat{\mathscr{H}}$ is usually written.** It is important to remember that the sign of the static magnetic field $\vec{H}_0$ should be chosen in accodance with the selection of a right or left-handed coordinate system (magnetic field is an axial vector) [4]. Let us consider the case when the constant field $\vec{H}_0$ lies in the plane of two magnetic axes (for example, x and y). Then it is easy to demonstrate that for each form the transitions of the spin ellipse is located in a plane perpendicular to plane xy, and its principal axis is directed along the third magnetic axis — the z-axis.

Actually, let us visualize the axis z with respect to the xy plane. A change in the type of axis triplet (from left-to right-hand set, or the reverse) requires a reversal of direction of field $\vec{H}_0$ in space. Let us first use the fact that in an arbitrary, prescribed coordinate system with a sign change of $\vec{H}_0$ the matrix elements S_x, S_y, S_z with accuracy up to general sign***are changed to complex conjugates S_x^*, S_y^*, S_z^*.****which evidently denotes a change in direction of circulation around the spin ellipse. Thus, the sought spin ellipse relative to the two systems of coordinates *with two opposite directions of the z) must be located in like manner, but have opposite directions of circulation, from which our statement follows.

As an example we introduce widely known ruby (Cr^{3+} in corundum Al_2O_2), emerald (Cr^{3+} in $Be_3Al_2Si_6O_{18}$) and other crystals with axially symmetric magnetic properties. In these crystals, usually the z-axis and not the x- or y-axis is directed along the crystallographic axis. Naturally the x- and y-axes are located in the H_0z plane. Calculation [1] confirms that the plane of the spin ellipse and its principal are perpendicular to the H_0z plane. As a consequence we find that if field $\vec{H}_0$ is directed along any of the magnetic axes

---

*If the energy level system is such that coincident transition frequencies exist with different vectors $\vec{S}$, the problem obviously is complicated by the necessity of considering the difference in weights of these various $\vec{S}$ which depends on the experimental conditions.

**The magnetic axes are directed along three mutually perpendicular straight lines, defined experimentally in the general case by the angular variation of the EPR spectrum; thus, both opposing directions along the magnetic axis are equally correct.

***A simultaneous change of sign of all three components of a complex vector, evidently, completely maintains the corresponding ellipse and direction of motion around it, and changes only the origin of calculation of the time of circulation which is not of interest to us.

****For a spin Hamiltonian of sufficiently prevalent from $\hat{\mathscr{H}} = \beta g \vec{H}\vec{\hat{S}} + D\left[\hat{S}_z^2 - \frac{1}{3}S(S+1)\right] + E(\hat{S}_x^2 - \hat{S}_y^2)$ this fact is demonstrated by direct calculation.

(for example, the z-axis), the spin ellipse is either located in a plane perpendicular to field $\vec{H}_0$ and has principal axes along the x- and y-axes, or degenerates into a straight line along $\vec{H}_0$; as an example, ruby is in field $\vec{H}_0$ directed along or perpendicular to the crystallographic axis. Finally, if field $\vec{H}_0$ is directly along the axis of axial symmetry, obviously the spin ellipse lying in a plane perpendicular to the static field is converted into a circle.

2. TRANSITION PROBABILITY FOR A TWO-COMPLEX CRYSTAL

Let us turn to the case of a two-complex crystal. Since both complexes are identically present in the crystal, the transition probability for the crystal as a whole is written in the form of a sum (with weight $\frac{1}{2}$) of two expressions (1) in coordinates x, y z and x', y', z' of magnetic axes of both complexes respectively.

For concreteness, let us consider crystal $K_3Co(CN)_6$ with a paramagnetic ion Cr^{3+} impurity; hereafter we will call it chromium cyanide. In this crystal the two magnetic (y and y') of different complexes are directed along one of the crystallographic axes (c-axis), the magnetic axes x and x^1 symmetrically border upon the b-axis, but the z and z' upon the a-axis [5]. In similar crystals in order to ensure coincidence of EPR spectra from both magnetic complexes, the static magnetic field $\vec{H}_0$ is usually located in the symmetry planes ac or bc. For each of these two cases the direction of the coordinate axes (along the magnetic axes) are chosen of course so that similar axes of different complexes are arranged symmetrically relative to field $\vec{H}_0$. Thus, the projections of $\vec{H}_0$ on coordinate axes x, y, z and x', y', z' respectively are similar, but since one of the coordinate systems is left-handed, and the other right-handed, magnetic field $\vec{H}_0$ has different signs for both complexes which gives the following relation for matrix elements in these two systems

$$S_j = S^*_{j'}, \; j = x, y, z. \tag{2}$$

This means that the spin ellipses of both complexes are located symmetrically relative to planes in which field H_0 lies (planes ac or bc), the directions of circulation being similar for projections of spin ellipses on plane ab and opposite for projections of these ellipses on the symmetry plane (ac or bc, respectively).

Let us confine ourselves to consideration of the case when the field $\vec{H}_0$ is located in plane ac (for plane bc the calculation and results are entirely analogous. Then one may adopt the coordinate systems x, y, z and x', y', z described by the following table of directional cosines [5] (Figure 1), where we set $\xi = 0.104$, $\eta = 0.994$.

	x	y	z
a	ξ	0	η
b	$\pm\eta$	0	$\mp\xi$
c	0	1	0

Reducing the components h_x, h_y, h_x', h_y', h_z' to the crystallographic coordinate system a, b, c and using Eq. (2), we obtain the transition probability for the crystal as a whole in the form

$$\begin{aligned} P_{mn} \sim \frac{1}{2}|\vec{h}^*\vec{S}|^2 + \frac{1}{2}|\vec{h}'^*\vec{S}'|^2 = \\ = f(h_{1a}, h_{2a}, h_{1b}, h_{2b}, h_{1c}, h_{2c}) = \\ = M|h_a|^2 + N|h_b|^2 + \\ + |S_y|^2|h_c|^2 + S(h_{1a}h_{1c} + h_{2a}h_{2c}) + \\ + S'(h_{1b}h_{2c} - h_{1c}h_{2b}) + \\ + S'_{xz}(h_{1b}h_{2a} - h_{1a}h_{2b}), \end{aligned} \tag{3}$$

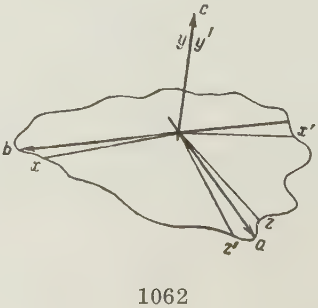

where h_{1j}, h_{2j} ($j = a, b, c$) are respectively the real and imaginary parts of the complex directional cosines of the alternating magnetic field with respect to axes a, b, c;

$$M = \xi^2 |S_x|^2 + \eta^2 |S_z|^2 + \xi\eta S_{xz}; \quad N = \eta^2 |S_x|^2 + \xi^2 |S_z|^2 - \xi\eta S_{xz};$$

$$S = \xi S_{xy} + \eta S_{yz}; \quad S' = \eta S'_{xy} + \xi S'_{yz};$$

$$S_{kl} = S_k S_l^* + S_l S_k^* = 2(S_{1k} S_{1l} + S_{2k} S_{2l});$$

$$S'_{kl} = i(S_k S_l^* - S_l S_k^*) = 2(S_{1k} S_{2l} - S_{2k} S_{1l});$$

$$k, l = x, y, z.$$

3. EXTREMUM CONDITIONS FOR THE TRANSITION PROBABILITY

The problem of determining the polarization of an alternating magnetic field corresponding to extremum values of the transition probability (3) reduces to a search for the complex directional cosines of the field (a group of six numbers h_{1a}, h_{2a}, h_{1b}, h_{2b}, h_{1c}, h_{2c}), corresponding to extremum of quadratic polynomial f on the right-hand side of (3), upon fulfillment of the condition

$$\varphi(h_{1a} \ldots h_{2c}) = h_{1a}^2 + \ldots h_{2c}^2 - 1 = 0. \tag{4}$$

Solving this problem of the search for the relative extremum, in accordance with the method of Lagrangian coefficients, we require the vanishing of all six partial derivatives (of all the components of $\vec{h}$) of the auxiliary function Φ of parameter λ:

$$\Phi = f - \lambda\varphi.$$

From the resulting system of six equations together with coupling condition (4) we obtain λ and then $h_{1a} \ldots h_{2c}$. Equating to zero the determinant of the system gives a sixth-degree equation with three double roots

$$\lambda_1 = 0,$$

$$\lambda_{2,3} = \frac{1}{2}(M + N + |S_y|^2) \pm$$

$$\pm \frac{1}{2}\sqrt{(M + N + |S_y|^2)^2 + S^2 + S'^2 + S'^2_{xz} - 4(MN + M|S_y|^2 + N|S_y|^2)}.$$

We now note that

$$\frac{\partial\Phi}{\partial h_{1a}} h_{1a} + \ldots + \frac{\partial\Phi}{\partial h_{2c}} h_{2c} = 2\Phi - 2\lambda = 0$$

and consequently at the extremum point we have the equality

$$f = \lambda.$$

Thus, with a change of alternating field polarization the magnitude of polynomial f (for brevity we will henceforth call it the transition probability) changes within the limits 0 to λ_2 with an intermediate extremum value λ_3. The unit field ellipses corresponding to the three λ (we will call "extremums") are determined from the subset of there equations (from the initial six) of the form

$$\begin{aligned} 2(M - \lambda) h_{1a} - S'_{xz} h_{2b} + S h_{1c} &= 0, \\ -S'_{xz} h_{1a} + 2(N - \lambda) h_{2b} - S' h_{1c} &= 0, \\ S h_{1a} - S' h_{2b} + 2(|S_y|^2 - \lambda) h_{1c} &= 0, \end{aligned}$$

from which it follows that all three extremum field ellipses are located in planes perpendicular to the symmetry planes ac, and have the b-axis as principal axis. This should be expected, considering the symmetry in the arrangement of the spin ellipses of both complexes and their equivalence.

In the general case, the angles between the planes of three extremum field ellipses like the shape of the ellipses themselves, are extremely diverse; however, as we will see below, in a number of cases the picture simplifies and becomes rather graphic.

First we will indicate a solution of our extremum problem for a linearly polarized alternating field. Since the vector $\vec{h}$ is now real, the problem reduces to the previous one, if we set $h_{2a} = h_{2b} = h_{2c} = 0$ in all the relations. Equating to zero the determinant of the system of the obtained equations gives a cubic equation with roots

$$\bar{\lambda}_1 = N,$$

$$\bar{\lambda}_{2,3} = \frac{1}{2}(M + |S_y|^2) \pm \frac{1}{2}\sqrt{(M - |S_y|^2)^2 + S^2}. \tag{5}$$

These three $\bar{\lambda}$ are extremum values of the transition probability—now already within the limits of linear polarization of the alternating field. Thus, $\bar{\lambda}_1$ corresponds to an alternating magnetic field orientation along the b-axis, and $\bar{\lambda}_2$ and $\bar{\lambda}_3$ to orientations along two mutually perpendicular straight lines in the ac plane, whose equations have respectively the form

$$\frac{h_a}{h_c} = \frac{2(\bar{\lambda}_2 - |S_y|^2)}{S} = \frac{M - |S_y|^2 + \sqrt{(M - |S_y|^2)^2 + S^2}}{S}, \tag{6}$$

$$\frac{h_a}{h_c} = \frac{2(\bar{\lambda}_3 - |S_y|^2)}{S} = -\frac{S}{M - |S_y|^2 + \sqrt{(M - |S_y|^2)^2 + S^2}}. \tag{7}$$

We mention that for chromium cyanide $\bar{\lambda}_3$ is much less than $\bar{\lambda}_1$ and $\bar{\lambda}_2$.

4. SPECIAL CASES IN THE ARRANGEMENT OF SPIN ELLIPSES OF BOTH COMPLEXES

Let us consider two special cases in the mutual arrangement of spin ellipses of both magnetic complexes, we point out beforehand that in chromium cyanide virtually only these cases are realized.

Case A. The spin ellipses of both complexes lie in a single plane perpendicular to plane ac (Figure 2). The necessary and sufficient criterion for this is fulfillment of the condition

$$\bar{\lambda}_3 = 0$$

or

$$4M|S_y|^2 = S^2. \tag{8}$$

Thus, one of the three extreme field ellipses corresponding to the transition probability $\lambda_1 = 0$ degenerates into a straight line described by Eq. (7); this line obviously is perpendicular to the plane containing the original spin ellipses of both complexes. Two other extremum field ellipses lie of course in the latter plane, wherein both principal axes are directed along the b-axis and along a straight line described by Eq. (6). The directions of circulation along these ellipses are opposite, the "maximum" ellipse (corresponding to λ_2) circulating just as the original spin ellipse.

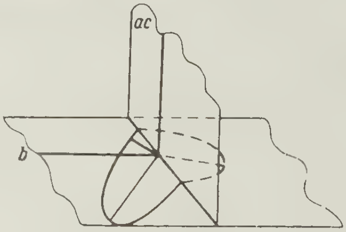

Figure 2

In even more special cases one may also determine the shape of the ellipses. Thus, let the principal axes of the spin ellipses of both complexes diverge from the ac plane by 45°; an indication of this besides Eq. (8) is the additional equality

$$\bar{\lambda}_1 = \bar{\lambda}_2$$

or

$$N = M + |S_y|^2. \tag{9}$$

Thus, both nondegenerating extremum field ellipses change into a circle with positive directions of circulation and with corresponding transition probabilities

$$\lambda_{2,3} = N \pm \frac{1}{2}\sqrt{S'^2 + S'^2_{xz}} = \frac{1}{2}(S_1 \pm S_2)^2.$$

Suppose in the other special case the spin ellipses of both complexes coincide, as indicated, besides Eq. (8), by the additional equality

$$4N(M + |S_y|^2) = S'^2 + S'^2_{xz}. \tag{10}$$

Thus, we evidently return to the case of a one-complex crystal, where

$$\lambda_1 = \lambda_3 = 0,$$

$$\lambda_2 = S_1^2 + S_2^2 = |S_x|^2 + |S_y|^2 + |S_z|^2 = M + N + |S_y|^2.$$

Finally, simultaneous fulfillment of conditions (8), (9) and (10) indicates that the original spin ellipses have coincident circumferences.

We note that in chromium cyanide, case A is accurately realized, when the static magnetic field $\vec{H}_0$ is directed along the C axis (along magnetic axes y and y' of both complexes); see paragraph 1. In addition when S = S' = 0, both spin ellipses lie either in plane ab and their principal axes are directed along axes x and z (x' and z' respectively), or they degenerate into a straight line along the c axis.

Case B. The spin ellipses of both complexes are not known to lie in a single plane, but intersect along the principal axis lying apparently in plane ac (Figure 3). A necessary and sufficient criterion of this is violation of condition (8) and simultaneous fulfillment of the more general condition

$$2S'S'_{xz}(M - |S_y|^2) = S(S'^2_{xz} - S'^2). \qquad (11)$$

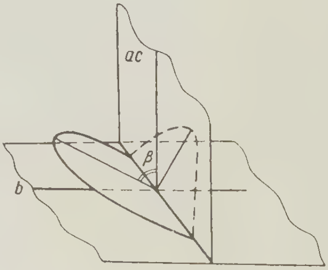

Figure 3

Let the length of the principal axis along which the spin ellipses intersect equal $2S_1$, and the angle between their planes equal 2β. In this case, for a linearly polarized alternating field, the extremum transition probabilities $\bar{\lambda}_1$, $\bar{\lambda}_2$, and $\bar{\lambda}_3$ given by Eqs. (5) equal $S_2^2 \sin^2\beta$, S_1^2, and $S_2^2 \cos^2\beta$ respectively; they are realized when the alternating field is orientated with respect to the b-axis, the straight line intersection of both spin ellipses and with respect to a projection of the second principal semiaxis S_2 of the spin ellipse on the ac plane, that is perpendicular to this straight line. In the general case of elliptical polarization we obtain two extremum field ellipses in a plane passing through the b-axis, and the straight line intersection of the spin ellipses: the maximum field ellipse similar to the projection on this plane of the original spin ellipse and having the same direction of circulation corresponds to the transition probability $\lambda_2 = S_1^2 + S_2^2 \sin^2\beta$; the second field ellipse differing from the first 90° turn in its plane and by a change in direction of circulation gives the transition probability $\lambda_1 = 0$. The third extremum field ellipse degenerates into a straight line perpendicular to the plane of the two extremum ellipses; thus, the transition probability $\lambda_3 = \bar{\lambda}_3$.

In chromium cyanide case B is know to occur when the static field $\vec{H}_0$ is directed along the a-axis*—in the plane of magnetic axes x, z and x', z'. In addition (see Sect. 1) the spin ellipses of both complexes intersect along the y-axis,

$$S = S'_{xz} = 0, \quad \tan^2\beta = \frac{N}{M}, \quad \bar{\lambda}_2 = S_1^2 = |S_y|^2,$$

$$S_2^2 = M + N, \quad \bar{\lambda}_1 = N, \quad \bar{\lambda}_3 = \lambda_3 = M, \quad \lambda_2 = N + |S_y|^2.$$

It is significant that as calculation shows, from condition (8) there follows condition (11), fulfillment of which is a sufficient indication of realization of at least one of the two special cases.

It follows from a calculation for chromium cyanide according to combinations of matrix elements S_i [6] computed on a BESM, that Eq. (11) always holds with good accuracy in this crystal. This means that in chromium cyanide the triplet of extremum field ellipses practically always reduces to a pair of ellipses in a single plane (the second is obtained from the first by 90° rotation and by a change of direction of circulation) and by a straight line perpendicular to this plane. This evidently is to be expected, since the location of the static field $\vec{H}_0$ in the symmetry plane (ac or dc) denotes a divergence by 6 degrees from the plane of the two magnetic axes (yz or yx respectively); see section 1.

Calculations for the other two and multicomplex crystals (for a static magnetic field in the symmetry plane) are more or less analogous to the above. Thus, for instance, in a TiO_2 crystal (rutile) with a Cr^{3+} impurity [7] there exist two magnetic complexes with a common z-axis, turned 90° with respect to one another (thus $\xi = \eta = 45°$) and the computed formulae obtained above with obvious alterations are also applicable in this case.

---

* And also, obviously, along the b-axis, if $\vec{H}_0$ lies in the bc plane.

In the case of an anisotropic g-factor the results remain valid, if everywhere we replace the spin vector $\vec{S}$ by the magnetic moment vector $\vec{\mu}$ whose components μ_x, μ_y, μ_z along the magnetic axes equal g_xS_x, g_yS_y, g_zS_z respectively.

In conclusion I acknowledge the constant interest of M. E. Zhabotinskiy, and also the help and valuable discussions with Ch. M. Briskina and V. F. Zolin.

REFERENCES

1. E. O. Schulz-Dubois, Bell System Techn. J., 1959, 38, 1, 271
2. E. O. Schulz-Dubois, H. E. D. Scovil, R. W. Degrasse, Bell System Techn. J., 1959, 38, 2, 335.
3. K. D. Bowers, J. Owen, Report Prog. Phys., 1955, 18, 304.
4. I. M. Baker, B. Bleaney, K. D. Bowers, Proc. Phys. Soc. B, 1956, 69, pt. 12, 444, 1205.
5. E. Condon, Uspekhi Fiz. Nauk, 1938, 19, 3, 380.
6. Ch. M. Bridkina, V. F. Zolin and M. I. Rodak, Reports on the Paramagnetic Resonance Conference, Kazan 1959.
7. H. I. Gerritsen, S. E. Harrison, H. R. Lewis, I. P. Wittke, Phys. Rev. Letters, 1959, 2, 4, 153.

Submitted to editors 26 July 1960

BRIEF COMMUNICATIONS

CALCULATION OF A MATCHING METALLIC INSERT IN A CIRCULAR WAVEGUIDE

Wang Huan-cho

1. Two circular waveguides with a common axis and different radii are coupled together by a conical junction. An H_{01} wave is incident on the junction. To decrease the amplitude of the nascent wave H_{02} a concentric metallic rod of tapered radius is inserted in the junction. The H_{0n} type waves in the gap between the two coaxial conductors with constant radii a and b are characterized by the longitudinal component of magnetic field

$$H_z = \alpha^2 \cdot U(r, \theta)\, e^{i(\omega t - hz)}. \tag{1}$$

The magnitude of U (r, θ) is determined from the membrane equation

$$\nabla^2 U + \alpha^2 U = 0, \tag{2}$$

where

$$\alpha = \sqrt{k^2 - h^2}; \quad k = \frac{2\pi}{\lambda}; \tag{3}$$

is a root of the transcendental equation

$$J_1(\alpha a) N_1(\alpha b) - J_1(\alpha b) N_1(\alpha a) = 0. \tag{4}$$

From (1) and (2) we obtain

$$H_z(a) = -\alpha^2 A \frac{2}{\pi \alpha a N_1(\alpha a)}, \tag{5}$$

$$H_z(b) = -\alpha^2 A \frac{2}{\pi \alpha b N_1(\alpha b)}. \tag{6}$$

The field components of the H_{01} wave have the form

$$\begin{aligned} E_\theta &= -ik\alpha_1 [A_1 J_1(\alpha_1 r) + B_1 N_1(\alpha_1 r)], \\ H_r &= ih_1\alpha_1 [A_1 J_1(\alpha_1 r) + B_1 N_1(\alpha_1 r)]. \end{aligned} \tag{7}$$

From the normalization condition we obtain the constant A_1 for the H_{01} wave:

$$A_1 = \left[\frac{1}{\pi \alpha_1^2 F_1}\right]^{1/2}, \tag{8}$$

where

$$F_1 = \int_b^a \left[\frac{J_1(\alpha_1 r) N_1(\alpha_1 a) - J_1(\alpha_1 a) N_1(\alpha_1 r)}{N_1(\alpha_1 a)}\right]^2 r\,dr. \tag{9}$$

Analogously the magnitudes of A_2 and F_2 are determined for the H_{02} wave.

In order to determine the field, one must find the wave number. Having found the field, we can then determine the coupling constant between the H_{01} and H_{02} waves in the conical junction.

To find the dependence of wave number h on a in a regular waveguide one must solve Eq. (4). Figures 1 and 2 give the function h = f(a) in mm^{-1} for various values of b for the H_{01} and H_{02} waves. The graphs are calculated for $\lambda = 8$ mm.

2. In a symmetrical waveguide junction with a metallic insert, the coupling coefficient between H_{01} and H_{02} waves is determined by the formula

$$S_{12} = \frac{\pi}{h_2(h_2 - h_1)}\left[a\frac{da}{dz} H_z'(a) H_z^2(a) + b\frac{db}{dz} H_z'(b) H_z^2(b)\right], \tag{10}$$

obtained from Eq. (14), (16) in [1]. Here indices 1 and 2 correspond to the H_{01} and H_{02} waves.

When the H_{01} wave is incident on the junction from the direction of the wide waveguide the amplitude of the parasitic wave H_{02} emerging at the junction is expressed by the formula

$$P = \int_0^L \sqrt{\frac{h_2}{h_1}}\, S_{12} e^{-i\int_0^z (h_1 - h_2)\, dz}\, dz, \tag{11}$$

valid in the absence of a cutoff cross section for the H_{02} wave.

The coupling constants S_{ji} and S_{-ji} which couple the H_{01} and H_{02} waves of both directions, in a waveguide junction with a compensating insert vanish simultaneously. Therefore, if S_{ji} equals zero close to the cutoff cross section, S_{-ji} will equal zero. Thus, as can be shown, the insert will ensure the virtual absence of the H_{02} wave even in that case when a cutoff cross section exists for this wave.

3. For wideband matching of the transmission lines that have different wave impedances, we connect junction devices which represent line sections with variable wave impedances. It is well-known that the reflection coefficient R from the line section with wave impedance $W(\xi)$ equals

$$R = -\frac{1}{2}\int_0^1 \frac{d \ln W(\xi)}{d\xi}\, e^{-i\sigma\xi}\, d\xi, \tag{12}$$

where $\xi = z/L$ and parameter $\sigma = 2kL$ (L is the section length).

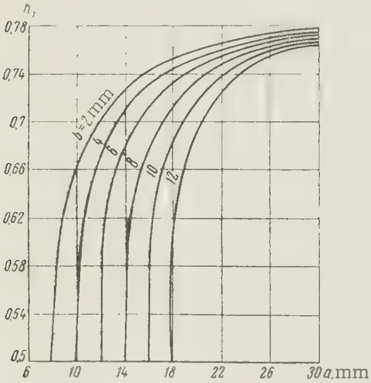

Figure 1. Dependence of h_1 on a for the H_{01} wave

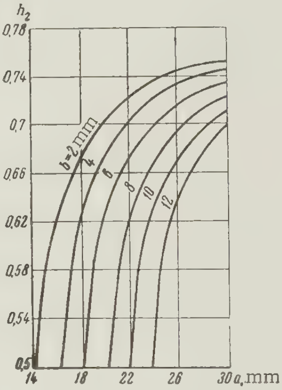

Figure 2. Dependence of h_2 on a for the H_{02} wave

Let us compare Eqs. (11) and (12). We assume that for all z the total coupling constant S_{12} varies so that

$$\sqrt{\frac{h_2}{h_1}}\, S_{12}\, e^{-i\int_0^z (h_1 - h_2)\, dz}\, dz = D\frac{d \ln W(\xi)}{d\xi}\, e^{-i\sigma\xi}\, d\xi. \tag{13}$$

We introduce the new variable ξ in place of z:

$$\xi = \frac{\int_0^z (h_1 - h_2)\, dz}{\int_0^L (h_1 - h_2)\, dz} = \frac{\int_0^z (h_1 - h_2)\, dz}{\sigma} \tag{14}$$

where σ denotes a general phase difference operator:

$$\sigma = \int_0^L (h_1 - h_2)\, dz. \tag{15}$$

Then Eq. (13) takes the form

$$\sqrt{\frac{h_2}{h_1}}\, S_{12}(\xi)\, dz = D\frac{d \ln W(\xi)}{d\xi}\, d\xi \tag{16}$$

and integral (11) becomes identical with (12).

We assume that the change in wave impedance is determined by the function

$$\frac{d\ln W(\xi)}{d\xi}=\sin\pi\xi, \tag{17}$$

adopted from [2] devoted to Eq. (12).

Then from Eqs. (16) and (17) the coupling constant equals

$$S_{12}(\xi)=D\sqrt{\frac{h_1}{h_2}}\sin\pi\xi\frac{d\xi}{dz}. \tag{18}$$

The derivative dξ/dz is defined by

$$\frac{d\xi}{dz}=\frac{1}{\sigma}(h_1-h_2). \tag{19}$$

Functions (18) is close to a maximum at $\sigma \geqslant 2.7\pi$.

4. Substituting Eqs. (5) and (6) into (10) and using Eq. (18), we obtain

$$\frac{A_1A_2}{\pi h_2(h_2-h_1)}\sqrt{\frac{h_2}{h_1}}\left\{\frac{1}{a}\frac{\alpha_1\alpha_2}{N_1(\alpha_1a)N_1(\alpha_2a)}\frac{da}{dz}+\frac{1}{b}\frac{\alpha_1\alpha_2}{N_1(\alpha_1b)N_1(\alpha_2b)}\frac{db}{dz}\right\}= \\ =E\sin\pi\xi\frac{d\xi}{dz}, \tag{20}$$

where E is a new arbitrary constant that can be determined from subsidiary conditions; its method of determination is illustrated below in a numerical example. We determine the shape of the insert b(z) so that when $0 \leqslant \xi \leqslant 1$, $S_{12}(\xi)$ is determined by Eq. (18). Then for b(z) we obtain differential equation (20). When $\xi = 1$ according to (18) $S_{12} = 0$. For the largest z (z > L) we require that S_{12} also equal zero.

This gives for b(z) the equation

$$a\frac{da}{dz}H_z^1(a)H_z^2(a)+ \\ +b\frac{db}{dz}H_z^1(b)H_z^2(b)=0. \tag{21}$$

Substituting (5) and (6) into (21), we obtain

$$\frac{db}{dz}=-\frac{da}{dz}\frac{b}{a}\frac{N_1(\alpha_1b)N_1(\alpha_2b)}{N_1(\alpha_1a)N_1(\alpha_2a)}. \tag{22}$$

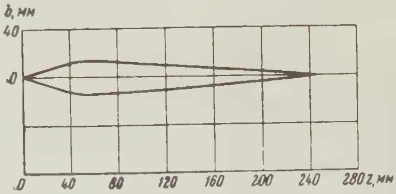

Figure 3. Shape of the metallic insert.

In order to determine the initial part of the insert, one must find the value of db/dz at small b, i.e., under the conditions $b \ll a$, $kb \ll 1$. Thus from Eq. (20) we obtain

$$\frac{db}{dz}=\frac{1{,}27\,Eh_2(h_2-h_1)}{A_1A_2b\alpha_1^2\alpha_2^2}\sqrt{\frac{h_1}{h_2}}\sin\pi\xi\frac{d\xi}{dz}+\frac{1}{1{,}23ab\alpha_1\alpha_2}\frac{da}{dz}. \tag{23}$$

It seems necessary to set up the insert a wide regular waveguide, where da/dz = 0. We will compute z at the point where b = 0. Then for small b

$$b(z)=\left[\frac{Eh_2(h_2-h_1)^3}{A_1A_2\alpha_1^2\alpha_2^2\sigma^2}\sqrt{\frac{h_1}{h_2}}\right]^{1/2}z. \tag{24}$$

5. We cite a numerical example. Let the waveguide whose radius be joined to the cone of the waveguide, which has a = 30 mm, we put the magnitude of da/dz equal to minus 0.1; an H_{01} wave falls from the direction of the wide waveguide. We determine b(z) from point z = 0 in a wide regular waveguide. First b(z) is calculated from Eq. (24), and then from Eq. (20) taking into account (19). The constants A_1 and A_2 vary little with small change of a and b, therefore we use $A_1 = 0.43$, $A_2 = 0.063$ — values obtained from Eq. (8), if we take a = 18 mm and b = 6 mm. E and σ must be chosen in this manner, so that b > 0 for all $0 < \xi < 1$ and so that over this entire range of values, a and b remain such that the junction cross section be larger than the cutoff value for the H_{02} wave. In addition, $\sigma \geqslant 2.7\pi$ should hold.

We calculate several forms of the function b(z) for various values of E and σ. We choose E = −1.5, σ = 3.2 π. In this case when ξ = 1, z = 117.9 mm, we obtain a = 21.1 mm, b = 8.2 mm, i.e., we have conditions at which all the requirements in the calculation are satisfied. At z = 29 mm, i.e., at the origin of the conical junction forming an insert, there is a fracture whose angle equals 7° 50'.

When z ⩾ 117.9 mm we calculate b(z) from Eq. (22) so that $S_{12} = 0$. When z = 217.9 mm we obtain a = 11.1 mm, b = 2.99 mm. Thus the values of zh_2 for an H_{02} wave vanishes (the cutoff cross section for this wave). Finally, when z = 244 mm, we obtain a = 8.5 mm, b = 0. Figure 3 schematically gives the calculated shape of the metallic insert.

The author thanks B.Z. Katsenelenbaum for a statement of the problem and supervision of the work.

REFERENCES

1. B. Z. Katsenelenbaum, Radiotekhnika i Electronika, 1958, 3, 7, 890.
2. J. Willis, N. Sihna, Proc. I. E. E., 1956, 103B, 8, 166.

Submitted to editors 16 December 1960

REQUIREMENTS OF AMPLITUDE AND PHASE STABILITY OF FIELDS IN LINEAR ACCELERATOR CAVITIES

A. P. Fedotov and V. A. Teplyakov

In the case of a projection system for the high-frequency supply of a linear accelerator consisting of several cavity resonators, requirements for stability of the field amplitude and phase in the accelerator cavity resonators are considered. These requirements are determined mainly by the permissible losses of particles in the length of the accelerator. The instability of amplitude and phase of the field disturbs the stability of the longitudinal motion of particles. Radial motion as a rule depends more weakly on the instability of the high-frequency field, and with certain methods of focusing (for example the longitudinal magnetic field) is virtually independent of them.

In the literature, we know of only one paper devoted to this subject. In this paper calculations were made of losses of particles in the accelerator consisting of several dozen cavity resonators, under the assumption of statistical dispersion of the phase of field with respect to planned values. Each cavity resonator has one accelerating gap. Calculation shows that the phase dispersion of the field is 5° in the case of a synchronized phase* of $\varphi = 20°$, and the dispersion of the amplitude of the field is 1-1.5% of the particle loss in the accelerator. Practically, this can be neglected. Such a slight requirement of phase and amplitude of the field is explained by the smallness of the action of the field of the accelerating gaps on the particle, as a consequence of which the statistical deviation of phase from the planned values in the individual cavity resonators compensate one another and the particles do not lose phase stability.

In practice, accelerators more often consist of several long** cavity resonators (see, for example, [2]). In such accelerators the requirements of field amplitude and phase stability are more rigid. The error of the field phase in one long cavity resonator, for instance, cannot compensate the error of field phase of opposite sign in a subsequent long cavity resonator, because in it the particles not entrapped in the region of stable acceleration, irrevocably leave because of acceleration [3,4]. For such acclerartors the dependence of particle loss on the shift of field amplitude and phase in cavity resonators (on the programmed values), can be evaluated by considering the region of stable acceleration of particles in cavity resonator accelerators [3,4].

Let us consider first one long cavity resonator into which bunches of accelerated particles enter whose states in the phase plane uniformly fill the entire region of stable acceleration. With a change of field amplitude and phase in a cavity resonator, this region of stable acceleration is deformed and displaced, and a portion of the particles are outside the region of stable acceleration. We denote by $\varkappa$ the ratio of the current of accelerated particles in the excited mode to the current of accelerated particles. In the case of a calculated field phase in the cavity resonator, the coefficient $\varkappa$ remains equal to unity during an increase of field amplitude u from the calculated value u_0 which corresponds to the synchronized phase φ_{c0}. With a decrease of u from the value u_0 to $u_0 \cos \varphi_{c0}$ [4]

---

* For phase $\varphi = 0$ particle acceleration is a maximum.

** In a long cavity resonator the particles undergo more periods of phase (longitudinal) oscillation. Such a cavity resonator has several accelerating gaps.

$$\varkappa \simeq 1 - \frac{1}{1 - \cos \varphi_{c0}} \cdot \frac{\Delta u}{u_0}, \tag{1}$$

where $\Delta u = u_0 - u$. When $u \leqslant u_0 \cos \varphi_{c0}$ acceleration becomes impossible. It can also be shown that for a constant field amplitude, the dependence of $\varkappa$ on the phase displacement of the field with respect to the programmed $\Delta\varphi$ (within the limits $\pm 3\varphi_{c0}$) is

$$\varkappa \simeq 1 \quad \left|\frac{\Delta\varphi}{3\varphi_{c0}}\right|. \tag{2}$$

We now find the particle loss in N long accelerator cavity resonators with identical regions of stable acceleration for random change of field phase. Let the field amplitudes be calculated. Then, using (2), we obtain the total particle loss in N cavity resonators:

$$1 - \varkappa_N = \frac{\sqrt{N}}{3} \frac{\Delta\varphi}{\varphi_{c0}}. \tag{3}$$

Here $\varkappa_N$ is the coefficient for all N cavity resonators.

The tolerance in the field amplitude is determined from the condition of equivalence of $\Delta u/u$ and $\Delta\varphi/\varphi_{c0}$ (from the point of view of losses), which is found by equating $\varkappa$ in Eqs. (1) and (2)

$$\frac{\Delta u}{u_0} = \frac{1 - \cos \varphi_{c0}}{3} \frac{\Delta\varphi}{\varphi_{c0}}. \tag{4}$$

Thus, the total tolerance is distributed between $\Delta u/u_0$ and $\Delta\varphi/\varphi_{c0}$.

For examples, for three long cavity resonators of a linear accelerator with $\varphi_c = 30°$, giving a loss of 20%, we obtain from (3) a total tolerance of $\Delta\varphi/\varphi_{c0} = 0.35$, which in accordance with (4) can be distributed thus: $\Delta u/u_0 = 1\%$ and $\Delta\varphi \simeq 4°$.

These tolerances are minimal, because we assumed a uniform distribution of particle states in the region of stable acceleration. Indeed with a velocity increase of accelerated particles, their density at the edge of the region of stable acceleration becomes less than at the center. These tolerances ensure the required capture of particles in an accelerator.

The authors thank B. K. Shembel' for valuable advice.

REFERENCES

1. I. L. Zel'manov and A. S. Kompaneyets, Statistical variance of phase in a system of independent cavity resonators, Otchet IKhF AN SSSR, 1953.
2. J. H. Williams et al., Rev. Scient. Instrum., 1958, 29, 6.
3. B. K. Shembel', V. A. Teplyakov, A. P. Fedotov, L. M. Prokunin and A. D. Grishina, Subject of the calculation of a linear accelerator of heavy particles, Reports from the Conference on Charged-Particle Accelerators, Moscow, 1954.
4. A. P. Fedotov, B. K. Shembel', Radiotekhnika i Elektronika, 1961, 6, 1, 108.

Submitted to editors 21 November 1960

EXCITATION OF EVEN HARMONICS DURING FERROMAGNETIC RESONANCE

V. N. Fetina

The subject of excitation of higher harmonic vibrations in an electric tank circuit containing nonlinear reactivity in the form of an induction and sustained voltage, is considered by a number of authors [1-6]. In [2, 3] it was shown that among the possible harmonic components of oscillations excited in a system having a symmetrical and well-defined characteristic of the form

$$F(x) = \alpha x + \beta x^3, \tag{1}$$

even-order oscillations may occur, in particular, with frequency 2ω. Several conclusions[3] regarding this oscillation are of interest, which reduce to the following statements:

1) Oscillations with an appreciable second harmonic exist in a certain narrow frequency region; outside of this region the second harmonic is entirely absent.

2) The region with an appreciable second harmonic corresponds to a rather low frequency of the perturbing force (somewhat greater than $1/2\ \omega$). The resonance of the second harmonic occurs close to this frequency.

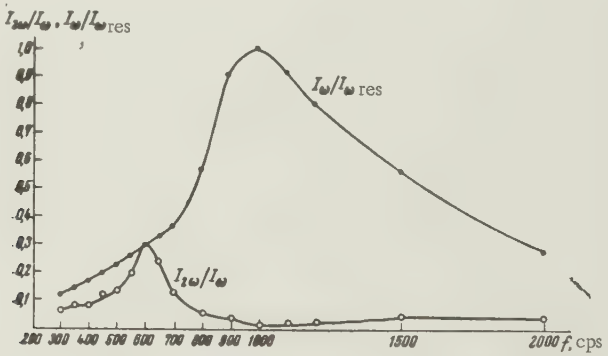

Figure 1. Resonance characteristics of the nonlinear oscillatory circuit at the fundamental frequency and second harmonic.

The subject of the stability of such oscillations was not considered by the authors of [2, 3] and, therefore, there was not sufficient basis for assuming that similar oscillations can actually exist.

The stability of the higher harmonics was investigated in [4]. Its author neglects attenuation in the system; therefore, his derivation concerning the stability of oscillations of frequency 2ω in a dissipative circuit are not stable.

Nevertheless, in a nonlinear tank circuit the even-order harmonic components were observed repeatedly in experiments [1, 4, 5]. The first ones were mentioned in [1]. Without touching upon the possible causes of excitation of these oscillations, the author labelled them anomalous.

An attempt to give a theoretical explanation of the existence of this second harmonic was made in [2]. It was assumed in [5] that the cause of the origin of an even harmonic in a real electric circuit is related to the multivalued (hysteresis) character of the magnetization curve. In the literature at the present time, however, there is no clear physical concept of the mechanism of excitation of even-order higher harmonic oscillations.

The results of our experimental investigation enable us to make certain remarks concerning the mechanism of excitation of higher even-order harmonics. Among the forced oscillations excited in a nonlinear electric tank circuit, even-order higher harmonic oscillations are potentially possible. In the case of a single-valued and symmetrical characteristic of nonlinearity, however, these oscillations must be regarded as unstable. This remark is correct also for a two-valued (hysteresis) symmetric characteristic of a real nonlinear element The case is somewhat different, if this symmetry is violated for one or more reasons. Then an even component appears in the circuit current and resonance occurs in a region predicted by theory [3]. A similar violation of symmetry is possible on account of deviations from sinusoidal behavior of the tank current supply voltage. As a result, the ascending and descending branches of the magnetization curve are no longer identical, and for any amplitude of an external effect a second harmonic resonance arises in the circuit in a specific frequency region.

During observation of this phenomenon the curves shown in Figure 1 can be obtained. The region of excitation of harmonic 2ω and its resonant value are found in accordance with the conclusions drawn in [3] and cited above.

If we compensate the asymmetry of the reversal of the magnetization loop by inducing a small constant bias of the appropriate sign or if we supply the circuit with a more faithfully sinusoidal signal, the second harmonic does not arise for the same conditions and parameters. It appears anew, however, at high amplitudes of external voltage, the even component oscillations 2ω becoming appreciable in amplitude, and their phase is determined by random initial conditions (Figure 2). In this case the stability of even-order higher harmonics, observable at sufficiently large external voltage amplitudes, apparently is caused by a breach of symmetry of reversal of the magnetization loop due to a transient process in the initial period, when the change of magnetic state of the core runs through the particular curves of single-valued magnetization.

Figure 2. Reversal of magnetization loop upon excitation of a second harmonic in the circuit (a, b —different initial phases).

The other possible cause of stability may be the presence in the circuit with a ferromagnetic core of an AC equivalent loss resistance which, as experiment shows, in a certain frequency region (less than ω_{res}) increases linearly with growth of magnetizing field. This can cause the appearance of even harmonics and leads to a resonance.

These considerations, of course, are tentative and require further, more detailed study.

REFERENCES

1. E. Rouelle, Contribution a l'etude experimentale de la ferro-resonance, Rev. gen. electr., 1934, 36, 21, 778.
2. S. I. Pivovarov, Higher harmonics in an electric circuit, containing inductance and capacitance, Elektrichestvo, 1949, 8, 38.
3. A. M. Kats, Biharmonic oscillations of a dissipative nonlinear system caused or maintained by a harmonic excitation force, Priklad. Matem. i Mekhan., 1954, 18, 4 425.
4. T. Hayashi, Forced oscillations in nonlinear systems, transl. from English, Ed. A. I. Lur'ye, IL., 1957.
5. M. D. Karasev and A. M. Sukhov, Even harmonics in a nonlinear tuned circuit with odd nonlinearity, Vestn. Moscow Univ., Ser. Math., Mech., Astron., Physics, Chemistry, 1959, 4, 123.
6. G. R. Rakhimov, Ferroresonance, Izd. AN UkSSR, 1957.

M. V. Lomonosov, Moscow State
Univ., Physics Faculty, Dept. of
Theory of Oscillations.

Submitted to editors 9 March 1961

PHOTOELECTRIC EFFECT IN THE REGION OF SOFT X-RAYS

N. G. Nakhodkin and P. V. Melnik

To interpret curves of the velocity distribution of photoelectrons (extracted by light with quantum energy in the vacuum ultraviolet region), several authors [1] use the concept of energy scattering by excited photoelectrons moving inside solids toward the surface. The motion of these electrons ought to be similar to that of excited secondary electrons [2]. In the quantum energy range of hundreds and thousands of electron volts where the greatest similarity should be observed between the photoelectric effect and secondary emission, no appropriate experimental work is known to us*. Therefore, we attempted to determine the dependence of photocurrent on layer thickness for both a metal and nonmetal. This dependence, as in the case of secondary emission, must characterize the kinetic motion of the excited electrons.

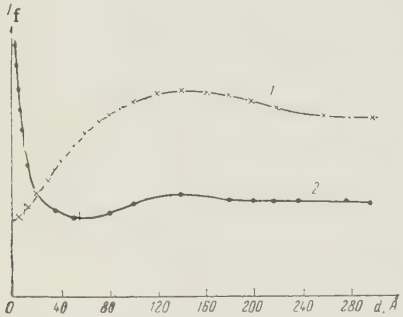

Figure 1. Dependence of the photocurrent in relative units on thickness of the investigated layer: 1—KCl layer on gold substrate; 2—layer of gold on KCl substrate.

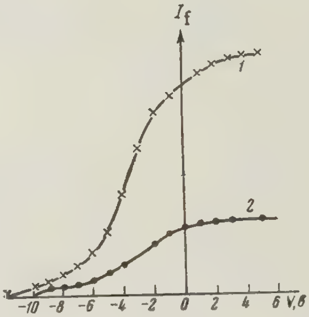

Figure 2. Volt-ampere curves of photocurrent in a retarding field: 1—for a KCl layer; 2—for a gold layer

For the investigation we chose the wedge method proposed by Morgulis [3]. The source of radiation was an x-ray tube and a bent mica crystal adjusted to quantum energies of about 1 kev placed in the same vacuum space as the investigated wedge. The following two systems were selected as objects of investigation: gold wedge on a KCl substrate and a KCl wedge on a gold substrate. The small measured currents, indicating a sufficient conductivity of the relatively thin KCl dielectric layers, did not markedly charge these layers.

Figure 1 shows experimental curves of the variation of photocurrent with growth of thickness of the KCl layer (Curve 1) and of the gold layer (Curve 2). These curves are qualitatively very similar to the broadly peaked curves of secondary emission for cases of heavy substances on light ones and vice versa, which were investigated at length in our secondary emission work [4]. It is difficult to relate the form of experimental curves to the change of conditions for absorption of quanta along layers, since for given wavelengths and normal angles of incidence the coefficients of reflection equal zero, the coefficients of absorption are not large [5], and a marked decrease of radiation (e-fold) sets in at thicknesses greater than necessary for the investigation. One may assume, therefore, that the absorption of radiation over the entire thickness of the investigated layers in the first approximation is uniform. As a result of absorption of quanta x-rays in the bulk of the substance, fast electrons are formed, the probability of formation being larger than for slow ones [5]. The electrons moving in the substance gradually lose their energy and slow electrons are formed, part of which make a basic contribution to the measured photocurrent. The predominance of slow photoelectrons may be detected in the corresponding volt-ampere curves of retardation, measured for a KCl layer (Curve 1 in Figure 2); these curves are similar to analogous curves in the case of secondary emission.

---

* After our work was completed, there appeared a paper by M. A. Rushil, A. P. Lukviska and V. N. Shmelev (Dokl. AN SSSR, 1960, 135, 55) in which the dependence of photocurrent on angle of incidence of quanta (θ) was studied for wavelengths 1.39-13.9 A°. The authors succeeded in interpreting the angular dependence of photocurrent, by assuming that the yield of excited electrons is proportional to $e - \frac{\alpha x}{\cos \theta}$, as in elementary theories of secondary emission.

Thus, the qualitative similarity of the thick curves of secondary emission at primary electron energies of the order of 1000 ev and of the photoelectric effect at quantum energies of the order of 1000 ev is not accidental, because the conditions of motion of fast and slow electrons in these two phenomena must be similar. Therefore, the photoelectronic emission at relatively large quantum energies has many common features with secondary emission at the same primary electron energies and, as in secondary emission, is a bulk phenomenon.

REFERENCES

1. P. I. Lukirskiy, Z. Phys., 1924, 22, 351; Philos. Mag., 1924, 47, 266; J. Dickey, Phys. Rev., 1951, 81, 612; L. Apker, E. Taft, J. Dickey, J. Opt. Soc. America, 1953, 43, 78; H. Hinteregger, Phys. Rev., 1955, 97, 1178; S. Methfessel, Z. Phys., 1957, 147, 442; E. Rudberg, Proc. Roy. Soc. A, 1928, 120, 385.
2. S. I. Pekar, Works of the Conference on Cathode Electronics, Kiev, 1952, pp. 223-224.
3. N. D. Morgulis, Dopovidi Sichnevoy Sesiy AN UkSSR, 1942, 2, 215.
4. N. G. Nakhodkin, V. A. Romanovskiy, Izv. AN SSSR, Ser. Fiz., 1958, 22, 448; Ukr. Fiz. Zh., 1959, 4, 769; Radiotekhnika i Elektronika, 1960, 8, 1275.
5. Handbook of Chemistry and Physics, 1955-1956, 37 ed., p. 2405; H. Robinson, Proc. Roy. Soc. A, 1923, 104, 455; A Bazin, Zh. Eksp. Teoret. Fiz., 1944, 14, 23.

T. G. Shevchenko
Kiev State Univ.

Submitted to editor 7 February 1961

LETTERS TO THE EDITOR

CONCERNING L.P. KUKLEVV AND Yu.P. PZERSKIY'S ARTICLE "COMPARISON OF INTERVAL CODES"

From [1] one may conclude that the problem of decoding interval codes is equivalent to the problem of detecting an n-impulse signal in the presence of noise, when we accept a decision concerning only its presence or absence. It is assumed that the processing takes place at the envelope detector output and that the output noise of the detector is Gaussian. A comparison is made of the noise stability of the two processing methods: a) coincidence method according to the test "n of n"; b) summation method in both cases for nonfluctuation signals and for signals with independent amplitude fluctuations according to the Rayleigh law.

A calculation of the noise stability was carried out with the error sum test, which the authors call the decoding error,

$$p = 0.5\,(1 - \beta_n + \alpha_n),$$

where β_n is the probability of decoding an n-pulse code group in the presence of noise, α_n is the probability of false decoding.

This test is a special case of an ideal observer criterion. It is well-known [2] that in this case (as in many others) the optimum processing is one with respect to an algorithm of the coefficient of likelihood, which in the cases under consideration consists of the following:

a) For nonfluctuating signals the summation is carried out after first making a functional transformation using the law:

$$y = \ln I_0 \left(\frac{EE_c}{\sigma^2} \right)$$

where E is the signal and noise envelope E_c is the signal amplitude; σ^2 is the variance of noise at the detector input. For weak signals this law is quadratic, and for strong signals it is a straight line.

b) For signals with independent pulse fluctuations consisting of a packet, the summation is carried out after first squaring the terms in the bracket. Considering the character of the optimum processing, it is intuitively clear that the summation method without preliminary nonlinear transformations (used by the authors of [1] will have greater noise than the coincidence method. The coincidence method in individual cases, however, is found to be more feasible and, moreover, as correctly noted by the authors of [1], eliminates the possibility of operation for separate random large-amplitude pulses. Therefore, comparison of the noise stability of these methods, generally speaking, is useful.

This comparison must be made, however, only under the condition that the threshold for operation in each method is chosen to be optimum, i.e., ensuring the least total error. The magnitude of the threshold depends on the signal-to-noise ratio, which indicates, by the way, some doubt of the feasibility of applying the ideal observer criterion in practice.

Nevertheless in [1] the optimum threshold value is used only during a study of the coincidence method. The authors write "....the necessity of decoding an n-pulse excludes the possibility of establishing at the output of the summation device an optimum level of limitation", that is, a threshold of operation (quotes are ours).

In the case of detection, the problem of establishing an optimum threshold is entirely analogous in both methods of processing and is solved technically in both cases with equal ease or difficulty. The authors [1] write that in the summation method "the level of amplitude limitation is established, so that only the sum of n pulses exceeds it" (quotes are ours).

This condition is vague, because it is fulfilled only in the absence of noise and for nonfluctuating signals.

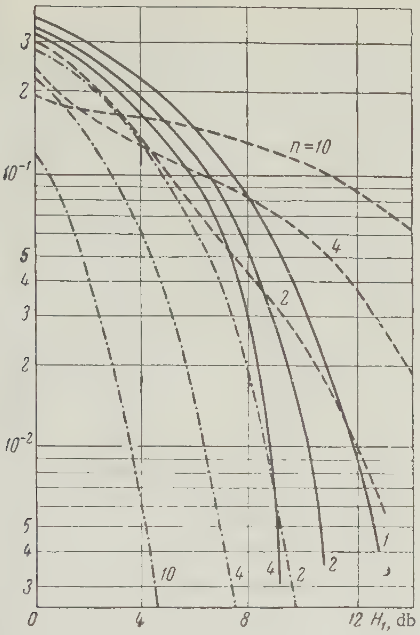

Figure 1 (left). Dependence of decoding error on the power signal-to-noise ratio at the detector input for a regular (nonfluctuating) signal: Solid curves, coincidence method; dashed, summation with optimum threshold.

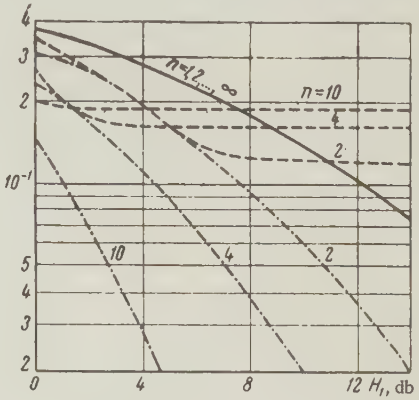

Figure 2 (above). Dependence of decoding error on the power signal-to-noise ratio at the detector for a fluctuating signal: solid lines, coincidence method; dashed, summation method (both are results from [1]); dot-dash, summation method with optimum threshold.

However, in numerical calculations of characteristics of the summation method, in the notation of [1], the threshold value is assumed to equal

$$x_0 = (n - 0{,}5)\left(\sqrt{\frac{\pi}{2}} + k_{\text{п=}} x_{\text{c}}\right)$$

for a nonfluctuating signal and

$$x_0'' = (n - 0{,}5)\sqrt{\frac{\pi}{2}}\sqrt{1 + h^2}$$

for a fluctuating signal.

Use of the nonoptimum threshold during a study of the summation method leads naturally to the fact the noise stability of this method is lower than for the coincidence method, in which the optimum threshold is used, and in the case of fluctuating signals, even decreases with growth of the number of summations.

On the basis of results obtained in this manner, the authors of [1] make a "general derivation of the advantages of the coincidence method over the summation method in the most important cases, when a small decoding error is required" (quotes are ours).

We made calculations of the characteristics of the summation method with use of the optimum threshold. As in [1], a normal approximation was used in this case. The curves plotted from the calculated results are given on graphs borrowed from [1] (Figures 1 and 2).

As expected, at the optimum threshold the summation method always has a larger noise stability than the coincidence method.

Thus, the general conclusion of [1], concerning the larger noise stability of the coincidence method in comparison with the summation method in this problem, which follows from [1], is not correct and can lead to errors by the reader. Complete clarity in this subject could be effected if the authors would explain the considerations which influenced their choice of threshold in the summation method.

REFERENCES

1. L. P. Kuklev and Yu. P. Ozerskiy, Comparison of two methods of decoding interval codes, Radiotekhnika i Elektronika, 1960, 5, 6, 894.
2. W. Peterson, T. Birdsall and W. Foks, Theory of signal detection; Coll. Information theory and its application, translated from English, A. A. Kharkevich, GIFML, 1959, 220.

I. M. Petrov and G. S. Tyslyatskiy

submitted to editors 27 December 1960

ANSWER TO THE LETTER OF I.M. PETROV AND G.S. TYSLYATSKIY

The goal of our paper was a comparison of the noise stability of the summation and coincidence methods when used for signal decoding, transmitted by interval codes. Interval coding includes the transmission of communications in the form of n-identical pulses, differing with respect to the interval between them. Thus, combinations may exist that do not coincide with one another in the magnitude of one such interval.

In our paper we considered the case of processing of a signal, whereby a given code is separated from a background of fluctuation noise and other code combinations. This is the problem of signal decoding.

The necessity of decomposing code combinations that do not coincide with respect to an interval (so-called "neighboring" codes), compels us to choose a threshold of limitation in the summation method, which is exceeded by the sum of n pulses, but not by the sum of n - 1 pulses. Such a choice of threshold creates, for both methods, different conditions in the sense that the passage of any of the signal pulses leads to a loss of signal. Operation of the decoding device only with an n-fold coincidence ensures also a maximum stability of interval codes with respect to random pulse noise, and they are often used for this purpose.

In the absence of noise, the reliability of operation of the decoding device designed in accordance with the summation method, is determined by the stability of the amplitude of the pulse signals and of the threshold of limitation. Therefore, to obtain the maximum likelihood of decoding without a noise threshold it is natural to fix on the middle of an n-step total pulse:

$$U_0 = (n - 0{,}5)\, U_m, \tag{1}$$

where U_0 is the threshold value; U_m is the pulse amplitude in the group. In the presence of fluctuation noise the threshold of limitation for the summation method, according to (1), should be set equal to

$$U_c = (n - 0{,}5)\, U_{mav}, \tag{2}$$

where $U_{m\,av}$ is the mean value of signal and noise at the detector output.

Such a threshold value may not coincide with the optimum value chosen according to the ideal observer criterion which ensures a maximum probability of code detection, i.e., separation of a given code from a background of fluctuation noise only. Therefore, it is perfectly natural that the calculated results of papers using a threshold (2), and of letters using an optimum threshold with respect to detection, do not coincide with one another. The conclusion of the letter concerning the advantage of the method of summation with optimum threshold during detection of a transmitted code, of course, raises no doubts. Simultaneously, the conclusion of the paper remains that, during decoding of an n-pulse interval code, the coincidence method gives better results in case of small errors.

We will analyze the doubts of the authors of the letter concerning the feasibility of applying the ideal observer criterion in practice, caused by the dependence of the optimum threshold value on the signal-to-noise ratio. It should be mentioned, however, that in cases when the signal-to-noise ratio is unknown, the coincidence method may be used to decode a signal, whereas use of the summation method based on knowledge of this ratio is impossible. This is still another advantage of the coincidence method.

The reasons for the objections expounded by I. M. Petrov and G. S. Tyslyatskiy in their letter are first, insufficient clearness in statement of the problem, as a result of which the authors of the letter suppose that the problem of detection of an n-impulse is solved, and not its decoding. Hence, they doubt the validity of the choice of the threshold of limitation for the summation method. Secondly, the authors of the paper in calculating the decoding error estimated only two components of this error, namely, a component of the signal and a component of false passage of noise. This also might suggest the problem of signal detection.

Table 1

Summation method

H_1, **db**	6	10	14	—
x_c	2,83	4,45	7,1	n
p	0,25	0,14	0,03	2
	0,26	0,18	0,07	4

In our case the decoding error has one more component, which takes into account the false passage of two code groups.

The total decoding error equals

$$p = P_s(1-\beta_n) + P_n\alpha_n + \sum_{i=1}^{N-1} P_i\gamma_i, \tag{3}$$

where P_s, P_n and P_i are the a priori probabilities of signal code, pure noise and i-th code, or the weight factors of the corresponding errors, β_n is the probability of false decoding of a signal code; α_n is the probability of false decoding of noise; γ_i is the probability of false decoding of the i-th code; N is the total number of codes.

Equation (3) proves that the result of the comparison may depend on the choice of codes and their a priori distribution probabilities.

On the advice of B. S. Fleyshman the authors of the paper evaluated the influence of the most probable error component from the false transmission of other codes, i.e., errors from the reception of a neighboring code. We considered a special case of an equally probable receiver input of a signal of pure noise and of a neighboring code. Thus,

$$p = \frac{1}{3}(1-\beta_n+\alpha_n+\gamma_1). \tag{4}$$

In the summation method probability γ_i equals the probability of exceeding the threshold of (2) by the sum of (n - 1) choices of signal with noise and a single choice of pure noise. Using the notation of the paper it equals

$$\gamma_1 = 0,5 - \Phi\left[\frac{0,5\,x_c k\text{p}_= - 1,25}{\sqrt{(n-1)\,k^2_{\text{pp}} + 0,43}}\right].$$

In the coincidence method probability γ_i for strong signals approximately equals the probability α of exceeding the threshold by pure noise; therefore,

$$p = \frac{1}{3}(1-\beta^n+\alpha^n+\alpha).$$

The value of the optimum threshold x_{opt} for the coincidence method can be found from the condition $\partial p/\partial x_0 = 0$ which in the case of a constant amplitude signal leads to the following approximate expression for a calculation of threshold with respect to decoding:

$$x_{\text{opt}} \simeq \frac{x_c}{2} - \frac{1}{x_s}\ln\left[\frac{n}{\sqrt{\pi(x_s^2 - 2\ln n)}}\right]. \tag{5}$$

Results of calculation for both methods are given in Tables 1 and 2 showing that upon taking into account the most probable error from a neighboring code, the coincidence method as before has an advantage over the summation method.

Table 3 gives values of the error probability from a neighboring code for both methods, from which it is apparent that the error is less in the coincidence method.

In conclusion we wish to mention that additional calculation carried out by the authors of the letter, together with data from the paper, enable us to compare the efficiency of the summation and coincidence methods for the problem of detection of an n-pulse signal. These calculations

Table 2

Coincidence method

H_1, db	6	10	14	n
x_{opt}	1.7	2.51	3.81	2
	1.42	2.35	3.71	4
p	0.16	0.032	0.0006	2
	0.19	0.044	0.0008	4

Table 3

Error probability

	H_1, db	6	10	14	n
γ_1	Summation method	0.62	0.38	0,08	2
		0.58	0.43	0.18	4
	Coincidence method	0.24	0.043	0.0007	2
		0.36	0.063	0,001	4

may also be of interest to codes with noncoincident intervals, when the choice of threshold of limitation for the summation method is not connected with protection from neighboring codes.

We consider the criticism contained in the letter of I. M. Petrov and G. S. Tyslyatskiy to be useful, because it clarifies a deficiency of our paper and contributed to a more detailed illumination of the subject that arose ther.

We acknowledge the useful advice of B. S. Fleyshman.

L. P. Kuplev and Yu. P. Ozerskiy

Submitted to editors 13 February 1961

ON THE PROBLEM OF THE INFLUENCE OF LIGHT POLARIZATION UPON THE PHOTOEFFECT OF COMPLEX CATHODES

In the paper of Gerlikh and Khora [1] a description was given of the features of photoelectric emission of thin semitransparent Sb-Cs photocathodes operating with reverse illumination. This feature consists in the fact that the yield of such a cathode under these conditions of illumination reveals a dependence of the quantum yield on the state of light polarization inversely established for photoemission in the case of metallic cathodes: a large yield corresponds to an orientation of the electric vector perpendicular to the plane of incidence of a ray (i.e., parallel to the cathode surface).

Interpretations of the results of the author are not given; only the single assumption is expressed that in the case of a Sb-Cs cathode "...there should exist a preferred direction of a photoelectric process of excitation perpendicular to the electric vector" (which appears very artificial to us).

There is a direct confirmation of the truth of the unusual character of the distribution of photoelectrons emitted by a thin Sb-Cs cathode in the case of inverse illumination from the angle of ejection, established by us in [3], if it is assumed as usual that the extraction of photoelectrons occurs in the direction of oscillation of electric field $\vec{E}$. Actually, when working with unpolarized light in the case of normal incidence (our experiments) the electric vector is always parallel to the surface and the existence of maximum electron yield in the direction of $\vec{E}$ should be manifest in the preferential emission of electrons at large angles with respect to the normal. The agreement between our results and the data of Gerlikh and Khora extends even further, however. In both cases a similar dependence on spectral composition is discovered: the effect decreases with a rise in frequency. We assume, therefore, that both effects are an expression of the same feature of photoemission of Sb-Cs layers—the predominance of photoelectron extraction in a layer at appreciable angles to the normal over the entire visible part of the spectrum. We evaluated this angle in accordance with the assumed energy diagram of an Sb-Cs cathode as equal to ~ 25°.

Insufficient data exist for a detailed interpretation of both effects. Thus, in our experiments the effect of polarization of light was not investigated in general, but it was shown that the observable character of the angular distribution is innate only for the case of inverse illumination. In the experiments of Gerlich and Khora the case of direct illumination was not investigated. We will assume, however, that as a first step in this direction one should adopt the assumption already stated by us, viz. that the preferential direction of extraction is the direction of oscillation of vector $\vec{E}$. This allows us not only to explain phenomenologically both effects by the same cause, but also to cease searching for a new explanation of the vector selectivity of photoelectric emission in general.

Regarding the mechanism causing such an angular selectivity of photoelectric emission in the case of an Sb-Cs cathode, it may be of a twofold nature. One reason may be the existence of energetically most-favored directions of photoelectron extraction in the layer thickness from $SbCs_3$ molecules (since the effect is most distinct in the region of small $h\nu$). The other reason may be regarded as the existence of a preferred direction of liberated electrons from the layer. The latter can be associated with the smallest losses as a result of scattering and absorption of electrons in the layer or the minimum reflection from the potential barrier, i.e., with selective transparence of that or another in a specific direction [4]. The opinion on this subject can occur, however, only on the basis of accumulation of sufficient information concerning the energy and crystalline structure of Sb-Cs layers.

REFERENCES

1. P. Gerlikh, K. Khora, Izv. AN SSSR, Ser. Fiz., 1960, 24, 6, 698.
2. Hughes and Du Bridge, Photoelectric Phenomena, GTTI, 1936.
3. N. S. Khlebnikov and E. A. Melamid, Radiotekhnika i Elektronika, 1959, 4, 6, 1008.
4. R. H. Fowler, Proc. Roy. Soc. A, 1930, 128, 123; A. R. Olpin, Phys. Rev., 1931, 38, 1745.

N. S. Klebnikov, A. E. Melamid

Submitted to editor 7 March 1961

RADIO ENGINEERING AND ELECTRONIC PHYSICS

Institute of Radio Engineering and Electronic Physics,
Academy of Sciences of the USSR

EDITORIAL BOARD

Editor-in-Chief: V.A. Kotel'nikov
Associate Editors: D.V. Zernov, Yu.B. Kobzarev

A.I. Berg
B.A. Vvedenskiy
I.S. Gonorovskiy
V.L. Granovskiy
L.A. Zhekulin
N.D. Devyatkov
L.N. Dobretsov
A.N. Kazantsev
S.G. Kalashnikov
P.L. Kapitsa
V.V. Migulin
A.L. Mikaelyan
A.A. Pistol'kors
A.M. Prokhorov
S.M. Rytov
V.I. Siforov
Ya.N. Fel'd
S.E. Khaykin
B.M. Tsarev

Scientific Secretary of Editorial Board: G.A. Bernashevskiy

The English Edition of Radio Engineering and Electronic Physics is mailed to subscribers within 18 weeks after the publication of the original Russian issue.

Russian electronic journals published by the
American Institute of Electrical Engineers
Translated by Royer and Roger, Inc.

	Subscription rates			
	Individuals		Libraries	
	$	£	$	£
Radio Engineering and Electronic Physics	28.50	10	57.00	20
Radio Engineering	14.25	5	28.50	10
Telecommunications	14.25	5	28.50	10

Royer and Roger translates and produces
the following Russian scientific journals:

Biophysics
Entomological Review
Geochemistry
Geodesy and Cartography
Izvestiya, Academy of Sciences of the USSR, Geologic Series
Pavlov Journal of Higher Nervous Activity
Problems of Oncology
Radio Engineering
Radio Engineering and Electronic Physics
Refractories
Sechenov Physiological Journal of the USSR
Soil Science
Telecommunications

Comments and inquiries regarding *Radio Engineering and Electronic Physics* and other translation journals should be sent to:

International Division
Royer and Roger, Inc.

1000 Vermont Avenue, N.W.
Washington 5, D.C.

41 East 28th Street
New York 16, New York

RADIO ENGINEERING AND ELECTRONIC PHYSICS

РАДИОТЕХНИКА И ЭЛЕКТРОНИКА

NUMBER 7 1961

CONTENTS

A.E. Basharinov, Problems in the Statistics of Automatic Pattern Recognition by Multiframe Scanning 917
B.S. Fleyshman, Nonstationary Method for Loading the Memory of a Control Device with Statistical Pattern Recognition 922
V.A. Zyanitskiy, Model of the Memory Loading of a Control Device by the Method of Self-Analysis 929
V.F. Nesteruk, The Theory of Optimal Detection of a Compound Signal with Correlated Noise 934
R.L. Stratonovich, Optimal Reception of a Narrowband Signal of Unknown Frequency on a Background of Noise 942
M.I. Dorman, The Spectrum of an Oscillation whose Frequency Passes through Zero 955
V.I. Tikhonov, The Markov Nature of the Envelope of Quasi-Harmonic Oscillations 961
I.Kh. Rizvkin, The Characteristics of Nonlinear Elements of Frequency Dividers 971
V.I. Ivanchikov, Some Problems in the Theory of the Refraction of Magnetic Waves 979
P.P. Pavlov, The Electromagnetic Field and the Distribution of Current along an Infinitely Long Uninsulated Wire in a Conducting Medium 985
R.V. Khokhlov, Wave Propagation in Nonlinear Lines with Dispersion 993
L.S. Benenson, Calculation of the Phase Velocity of Waves in an Artificial Metal Dielectric when the Current Harmonics on the Elements of the Structure are Considered 1004
V.P. Shestopalov, A.A. Bulgakov, B.M. Bulgakov, Theoretical and Experimental Studies of Helical Dielectric Antennas 1011
L.D. Bakhrakh, I.V. Vavilova, Spherical Two-Mirror Antennas 1020
R.F. Matveyev, Calculation of Side Flow in a Long Waveguide Line 1029
S.B. Gurevich, Sensitivity of Television Systems with Different Scanning Parameters 1036
Ye.N. Petrov, Theory of a Flat-Electrode Triode with Negligibly Small Grid-Anode Space Charge 1040
V.B. Braginskiy, V.A. Dianova, Ye.R. Mustel', Investigation of Frequency Multiplier Using the Nonlinear Capacitance of a p — n Junction 1043
L.K. Mikhailovskiy, et al., Nonlinear Nutation-Type Gyromagnetic Effects in Ferrites 1046
A.L. Mikaelyan, V.Ya. Anton'yants and Yu.G. Turkov, Phenomena of Mutual Coupling of Cavity Resonator and Ferrite 1052
M.I. Rodak, Calculation of the Polarization of an Alternating Magnetic Field Corresponding to Extreme Transition Probabilities in Electron Paramagnetic Resonance 1062

BRIEF COMMUNICATIONS

Wang Huan Cho, Calculation of a Matching Metallic Insert in a Circular Waveguide 1067
A.P. Fedotov and V.A. Teplyakov, Requirements of Amplitude and Phase Stability of Fields in Linear Accelerator Cavities 1070
V.N. Fetina, Excitation of Even Harmonics During Ferromagnetic Resonance . . . 1072
N.G. Nakhodkin and P.V. Melnik, Photoelectric Effect in the Region of Soft X-Rays 1074

LETTERS TO THE EDITOR

Concerning L.P. Kuklev and Yu.P. Ozerskiy's Article "Comparison of Interval Codes", I.M. Petrov and G.S. Tyslyatskiy 1076
Answer to the Letter of I.M. Petrov and G.S. Tyslyatskiy, L.P. Kuklev and Yu.P. Ozerskiy 1080
On the Problem of the Influence of Light Polarization upon the Photoeffect of Complex Cathodes, N.S. Klebnikov and A.E. Melamid 1080